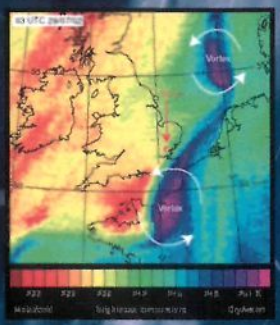

A MATHEMATICAL THEORY OF LARGE-SCALE ATMOSPHERE/OCEAN FLOW

MICHAEL J P CULLEN

Imperial College Press

A MATHEMATICAL THEORY OF LARGE-SCALE ATMOSPHERE/ OCEAN FLOW

This page is intentionally left blank

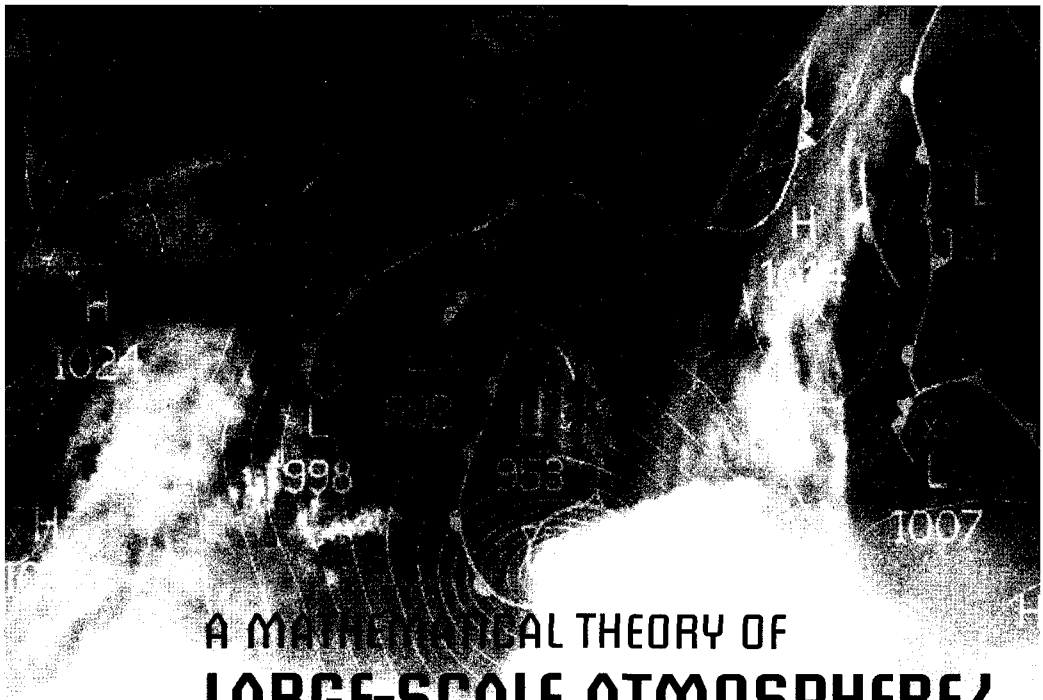

A MATHEMATICAL THEORY OF LARGE-SCALE ATMOSPHERE/ OCEAN FLOW

MICHAEL J P CULLEN
Met Office, UK

ICP
Imperial College Press

Published by

Imperial College Press
57 Shelton Street
Covent Garden
London WC2H 9HE

Distributed by

World Scientific Publishing Co. Pte. Ltd.
5 Toh Tuck Link, Singapore 596224
USA office: 27 Warren Street, Suite 401-402, Hackensack, NJ 07601
UK office: 57 Shelton Street, Covent Garden, London WC2H 9HE

British Library Cataloguing-in-Publication Data
A catalogue record for this book is available from the British Library.

A MATHEMATICAL THEORY OF LARGE-SCALE ATMOSPHERE/OCEAN FLOW

ISBN 1-86094-518-X

Editor: Tjan Kwang Wei

Printed in Singapore by B & JO Enterprise

Dedication

I would like to thank the many people who have inspired this work. In particular James Glimm and Alexandre Chorin, who showed me that nonlinear partial differential equations could be solved and Brian Hoskins for his inspirational work on developing semi-geostrophic theory. I would also like to thank those who collaborated with me on developing this theory over many years. In particular Jim Purser, Glenn Shutts, Simon Chynoweth, Martin Holt, John Norbury, Mike Sewell, Mark Mawson, Rob Douglas and Ian Roulstone. As one who sits between physics and mathematics, I would like to thank the mathematicians who proved the results, Yann Brenier, Jean-David Benamou, Wilfrid Gangbo, Robert McCann, Hamed Maroofi and Misha Feldman.

This page is intentionally left blank

Preface

Accurate extended-range weather predictions are now routinely available for up to a week ahead, and represent a major achievement of the meteorological community over the last 50 years. Underlying it is the highly predictable nature of large-scale atmospheric circulations. Realising it in practice has required a huge investment in computer technology and observing systems, such as satellites. Theoretical work over the last 30 years has emphasised reasons for unpredictability, in particular chaos theory, rather than reasons for predictability. This volume redresses this balance by discussing reasons for the high predictability. These are founded in dynamical meteorological theory developed over 50 years ago, but have been reinforced by exciting recent developments in understanding why some nonlinear systems are much more stable than might be expected. In this volume I first introduce the mathematical model to be used; then describe the mathematical properties of this model; and finally apply the mathematical results to the atmosphere and ocean and relate the predictions of the model to observed behaviour.

Analysis of atmospheric or oceanic circulations directly from the governing equations of dynamics and thermodynamics is difficult because of the 'scale problem'. Theoretical results on the Navier-Stokes equations, for example, concentrate on viscous scales, which are six orders of magnitude smaller than the smallest-scale weather systems. Dynamical meteorologists have addressed this over many years by developing a hierarchy of simplified equations, which represent the behaviour of the atmosphere (or ocean) in particular regimes. These are usually obtained by identifying small parameter(s) characteristic of the regime of interest, and deriving the simplified equations by asymptotic expansion in these parameter(s). Applying these equations to get rigorous mathematical results about the large scale be-

haviour has only been widely attempted over the last 10 years. In order to obtain these results, the steps required are to prove that the simplified equations can be solved, and then to prove there is a solution of the complete equations 'close' to the that of the simplified equations in a suitable sense. The simplified solutions can then be analysed and predictions made about atmosphere/ocean behaviour; subject to the error estimate made above. This procedure is not yet widely followed because of the difficulty in obtaining existence proofs and a posteriori error estimates. More commonly, solutions of the simplified equations are obtained and used subject to the a priori error estimate obtained form the original asymptotic expansion.

This volume is concerned with large-scale atmosphere/ocean flows. The traditional approximations used to describe such flows are based on smallness of the Rossby number, which states that large-scale flows are rotation-dominated, the Froude number, which states that the flow is strongly stratified, and the aspect ratio, which states that the atmosphere is much shallower than the horizontal scale of most weather systems. These lead to the geostrophic approximation, which relates the horizontal wind to the horizontal pressure gradient. The semi-geostrophic equations developed by Hoskins, following earlier work by Eliassen, give a set of simplified equations which is valid on large scales. Their asymptotic validity requires a Lagrangian form of the Rossby number to be small, which means that fluid trajectories cannot curve too sharply. This is appropriate for extra-tropical weather system, including fronts and jet streams which are characterised by a large length-scale in one direction. They are not appropriate for smaller-scale phenomena such as tropical cyclones, which are in a different asymptotic regime.

The analysis of these equations uses results from the theory of the Monge-Kantorovich problem, which has a long history in optimisation theory. There is thus an exciting and fundamental link between the dynamics of atmosphere/ocean flows and many other fields of study, such as economics, probability theory, magnetohydrodynamics and kinetic theory. It also exploits a 'convexity principle' due to Cullen and Purser, which requires that simplified solutions describing large-scale phenomena must be stable to parcel displacements. The convexity property is the basis of proofs of existence of the solutions to the semi-geostrophic equations.

The volume also discusses the application of the semi-geostrophic equations to real flows. An important feature is that the solutions can form fronts, where the solutions are discontinuous in physical space. The formation of fronts does not destroy the predictability of the flow. Cullen and

Roulstone demonstrated that an idealised quasi-periodic solution describing the growth and decay of weather systems, including fronts, remained predictable for more than 30 days. This is a case where the small-scale features are entirely slaved to larger scales. It is also shown that a number of other phenomena can be described. These include the interaction of mountains with the atmospheric circulation, the inland penetration of sea-breezes, the atmospheric response to cumulus convection, and the outcropping of layers of constant density in the ocean. A similar theory for almost axisymmetric flow can describe the eye-wall discontinuity in hurricanes.

More generally, the flow evolution does not exhibit the systematic transfer of energy or enstrophy to small scales characteristic of two- and three-dimensional turbulence. This comes from the constraints on the flow imposed by the convexity condition. The behaviour is reminiscent of that of Hamiltonian systems of ordinary differential equations, which have no attractors and thus describe non-periodic solutions with stable statistics but which can never converge to steady states or periodic orbits. This behaviour can be applied to the real atmosphere, subject to the limitations of the semi-geostrophic approximation. Studies of the accuracy of the approximation in idealised cases suggest that the solutions are reasonably accurate on the scale of developing weather systems for about 6 days. The theory thus suggests that the large scale circulation of the atmosphere is non-turbulent, and that anomalous circulation patterns can persist for long periods. Smaller-scale flow is certainly turbulent, but cannot be described by semi-geostrophic theory. These results thus underpin the ability of operational models to predict large-scale weather patterns a week ahead, and encourages attempts to extend this for longer periods. Thus this theory is an essential counterbalance to chaos theory, which demonstrates how predictability can be lost in nonlinear systems.

M. J. P. Cullen

This page is intentionally left blank

Contents

Chapter 1

Introduction

Accurate extended-range weather predictions are now routinely available for up to a week ahead, and represent a major scientific achievement of the meteorological community over the last 50 years. Figure 1.1 shows the remarkable improvement in the standard of forecasts in the Northern hemisphere over the last 25 years, as measured by the root mean square error difference between forecasts of the height of the 500hpa pressure surface (about 5km above the Earth's surface) and the observations. Three day forecasts today are as accurate as one day forecasts in the late 1970s.

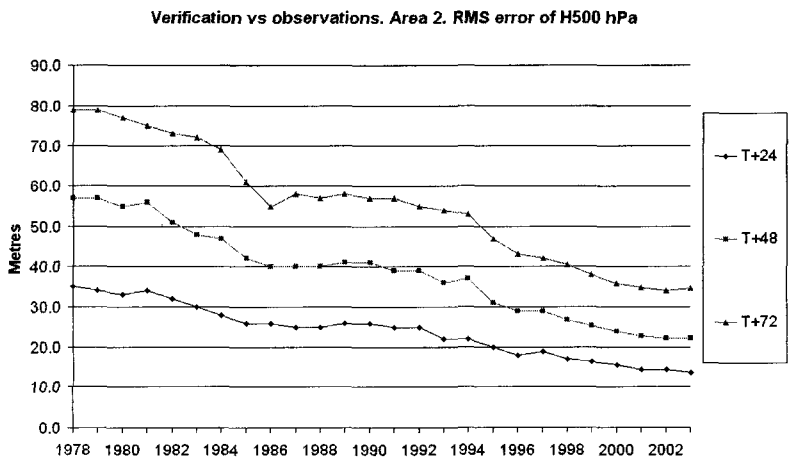

Fig. 1.1 Root mean square errors for forecasts of the height of the 500hpa pressure surface over the North Atlantic and Europe compared with observations. Bottom curve: 24 hour forecasts, middle curve: 48 hour forecasts, top curve: 72 hour forecasts. Source Met Office.

Though it is inconceivable that weather forecasting will ever reach the standard of tidal predictions, where predictions for years ahead can be readily purchased, the standard of weather forecasting indicates that the atmosphere is a highly predictable system. This is a major driver behind a current international research programme, called THORPEX, [Shapiro and Thorpe (2004)], which aims to extend the range of useful predictions to two weeks ahead. Statistical models, e.g. [Winkler et al. (2001)], suggest that such predictions may be achievable.

This runs counter to the popular conception of weather forecasting as a very empirical exercise, and to the widespread belief in 'chaos' theory and the 'butterfly effect'. Though it is undoubtedly true that there are limitations of the predictability of weather, and chaos theory can help us understand them; an important scientific question is to understand why the level of predictability is so high. This book is concerned with providing such an explanation. Realising this predictability in everyday forecasts has required a huge investment in computers and weather observations, particularly satellites. It has also involved the construction of computer models, involving hundreds of thousands of lines of code, which interpret the observations and make the predictions. This book is not concerned with describing how this is done, but only with why it is so successful.

Operational weather forecasting methods are based on the realisation that the atmosphere obeys the fundamental laws of fluid mechanics and thermodynamics; just like any other fluid system. It was L.F.Richardson in 1915 who made the apparently outrageous proposal that the weather could be predicted by simply writing down the fundamental equations, and solving them in a very crude discrete fashion by replacing continuously varying physical variables by values on a discrete grid, [Richardson (1922)]. His ideas could not be pursed in a useful way till the development of computers from the 1940s onwards. However, essentially his method is still used. The computer models solve the basic universal laws of fluid mechanics and thermodynamics, and represent physical quantities by their values on a discrete grid.

Richardson's method does not regard the atmosphere as any different from any other fluid system. It gives no idea of whether it is likely to be successful or not. Understanding whether the weather is likely to be predictable requires a large-scale view of the problem which can explain why the atmosphere contains depressions and anticyclones, and why the weather in the tropics is different from that the extra-tropics. Such understanding was developed by dynamical meteorologists, independently of Richardson's

proposal for operational weather forecasting . In the early 1950s, [Charney, Fjortoft and von Neumann (1950)] developed sets of equations which were specific to the large-scale problem, and used them in the first ever numerical forecast. While, within the next 10 years, actual predictions were being made using the fundamental equations following Richardson's approach, it is the work of Charney and other dynamical meteorologists that underpins the study of why the weather is so predictable.

Theoretical work over the last 30 years has emphasised reasons for unpredictability, in particular chaos theory, rather than reasons for predictability. There are two main contributors to unpredictability. One is the uncertainty in important physical processes in the atmosphere. An example is the formation of ice crystals of different shapes in cirrus cloud, and the large difference in the interaction of crystals of different shapes with the sun's radiation. This is a significant cause of uncertainty, particularly in simulations of climate change. This book, however, is concerned with the dynamical limitations on predictability. These arise because the atmosphere contains motions on all scales; from the large-scale jet-streams associated with changes of weather type over periods of weeks to the small-scale gusts that anyone can observe when going outside on a windy day. An example is shown in the satellite picture in Figure 1.2. This shows several

Fig. 1.2 Infra-red satellite picture for 00UTC on 27 October 2004. ©2004 EUMETSAT.

large-scale cloud bands associated with weather systems. These include an intense low pressure system to the south west of the British Isles and another extended band of cloud extending south-west to north-east to the east of it. This band extends for several thousand kilometres. It is associated with a weather front, which is associated with a change of air mass. There is a smaller scale low pressure system to the north of the main system, and another independent weather system further west over the Atlantic. There are also many very small-scale details, such as the low level (darker) cloud patterns over the Atlantic to the south-west of the main weather system. Figure 1.3 shows a weather chart corresponding to the same time as the

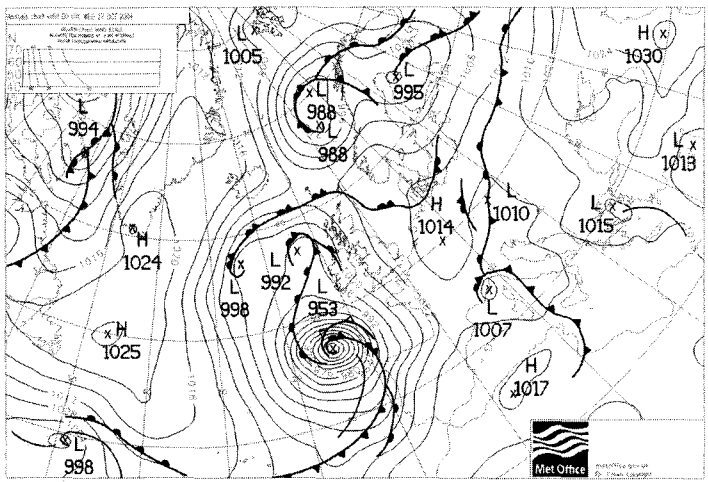

Fig. 1.3 Analysis of mean sea level pressure and rainfall for 00 UTC on 27 October 2004. Source: Met Office. ©Crown copyright 2005 Published by the Met Office.

picture in the same form as appears in the media. The chart shows contours of atmospheric pressure corrected to mean sea level, together with weather fronts. The low pressure system to the south west of the British Isles is clearly seen, as are the system further west over the Atlantic, the smaller system to the north, and the extended weather fronts over Europe. The chart shows only the large-scale structures, but gives no idea of the small-scale fluctuations that are also present. Figure 1.4 shows a plot of wind speed against time from an automatic wind recorder. There is a very large jump in wind speed over a few minutes. The actual change was probably

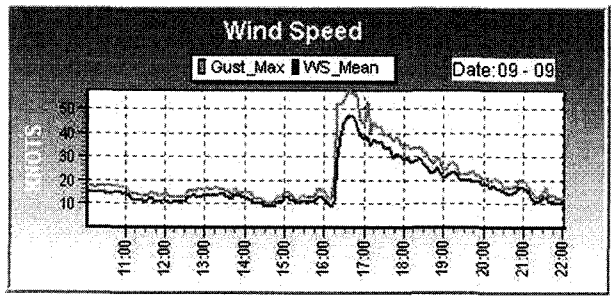

Fig. 1.4 Wind speed (knots) measured at Chichester bar, 9 September 2002. Source: CHIMET support group, Chichester Harbour Conservancy.

faster than the resolution of the available data. In addition, there are small scale fluctuations on the shortest time-scale resolved in the plot. This illustrates that the 'large-scale' flow can have almost discontinuous behaviour as well as the ubiquitous nature of the small-scale fluctuations.

Lorenz encapsulated the existence of motions on a wide range of scales in the atmosphere into a theory of predictability, [Lorenz (1963)]. This uses the idea that each type of motion has a characteristic time-scale, and that it will only be predictable for a few multiples of that time-scale. Thus local gusts of wind will only be predictable for a few seconds. Since different scales of motion are not independent, loss of predictability at small scales will lead (the butterfly effect) to a loss of predictability at large scales. It has been realised for many years that this dynamical argument based on turbulence theory is too simplistic. In 1967, G.D.Robinson published an estimate that this would prevent the weather being forecast for more than one day ahead; while it is now possible to forecast a week ahead on most occasions. The reasons for the higher predictability even then being achieved in practice were sought in the idea of 'large-scale control'. This means that the large scale motions in the atmosphere, such as those shown in Fig. 1.3, evolve in a way that is insensitive to the small scale details. Statistical information about the small-scale flow can be found by applying various diagnostic rules, given the large-scale circulation. Manual forecasting has used such rules for many years, [Met Office (1975)]. In the 1970s, this idea was formalised by the recognition that the large-scale flow was approximately two-dimensional, rather than three-dimensional. Research studies demonstrated that two-dimensional flow has a much higher inherent predictability than general three-dimensional flow, [Charney (1971);

Leith and Kraichnan (1972)].

Though the ideas of two-dimensional turbulence help to explain the higher predictability of the atmosphere, they suggest that in an unforced flow all the energy will migrate to the largest scales. It is then difficult to explain the long-lived disturbances to the atmospheric circulation that lead to persistent spells of anomalous weather. Observed behaviour is in fact statistically very steady. A weather map on one day is qualitatively very like the one on the next day, as seen in Fig. 1.5 which shows a sequence of weather maps over the North Atlantic for a month. The usual explanation is that this steady state is a balance between forcing and dissipation. However, it would better fit the facts if the natural dynamics of large-scale flows was 'non-turbulent', with no systematic migration of energy to larger or smaller scales. Superposed on this statistically steady dynamics are slow changes in qualitative behaviour from season to season. For instance, in the Northern hemisphere, the stronger equator to pole temperature gradient in winter means that depressions are more intense and faster moving.

This volume demonstrates that both the high predictability and the statistical steadiness can be encapsulated in a mathematical theory based on the *semi-geostrophic* equations introduced by [Eliassen (1949)] and [Hoskins (1975)]. The analysis of these equations exploits exciting recent developments in understanding why some nonlinear systems are much more stable than might be expected. In particular, it explains why coherent discontinuous structures, such as the weather fronts shown in Figs. 1.2 and 1.3, can be considered as part of the 'large-scale' flow. In addition, the theory shows that many observed phenomena in the atmosphere can be understood as a small-scale response to large-scale forcing in line with forecasting experience. The theory works by showing that the semi-geostrophic equations are both a good approximation to the fundamental laws of fluid dynamics and thermodynamics on large scales, and also that they can be solved to give purely large-scale solutions. Such solutions are often referred to as a *slow manifold.* While it has sometimes been speculated that an exact slow manifold might exist, which would allow large-scale flows to be predicted independently of other motions; it is clear from much research that this is not the case, e.g. [Lorenz (1992)], [Ford et al. (2000)]. What can be proved, however, is that slow manifolds can be constructed and that a solution of the complete equations can be found within a certain distance of the slow manifold. This distance can be estimated. In this book, solutions of the complete equations are shown to be sufficiently close to

the semi-geostrophic solutions that much of the high predictability of the semi-geostrophic system is inherited by the complete equations. This can explain the current success of weather forecasts. It also suggests that the efforts in THORPEX to extend weather forecasts to two weeks ahead are well worth pursuing.

This volume first sets out the fundamental equations. It then briefly reviews the choices of asymptotic regime, and associated choices of governing parameters, that are relevant to large-scale weather systems. This topic is the main topic of most dynamical meteorology and geophysical fluid dynamics textbooks; and these, such as [Pedlosky (1987)], should be consulted for a more detailed and comprehensive treatment. The general equations can then be approximated by simplified equations which are accurate on large scales and only describe large-scale flows. In order to establish a slow manifold, these simplified equations have to be proved to have a solution for sufficiently long times to describe the phenomena of interest. Many simplified equations developed by meteorologists for this purpose cannot be solved for long enough times to allow them to be used in this way. In this book, novel mathematical ideas are used to prove the semi-geostrophic system can be solved for sufficiently long times. The proofs require ideas originally developed in probability and statistics, [Kantorovich (1942)]. They rely also on a stability principle which is geometrically equivalent to a convexity principle. Physically, the principle states that the solutions, if substituted into the complete fluid equations, would be stable to fast-growing perturbations. This is an essential requirement if the semi-geostrophic solutions are to represent large scale solutions of the complete equations. Analytically, the convexity condition makes the solutions very insensitive to perturbations, which is the reason for their high predictability. It is also essential to the proof of existence of solutions, since it prevents the solutions oscillating on arbitrarily small scales. Such oscillations are characteristic of turbulence, and have so far made a rigorous mathematical treatment of turbulence impossible. The convexity principle states that semi-geostrophic solutions are non-turbulent, and thus can explain the observed statistical steadiness of atmospheric disturbances.

It turns out that, at least in the current state of knowledge, the semi-geostrophic system is the most general system which can define a slow manifold. However, the semi-geostrophic system is only accurate on scales large enough for the solutions to be dominated by the earth's rotation, and restricts the solutions to the weather systems familiar from middle latitude weather maps such as Fig. 1.3 and to quasi-steady tropical circulations

driven by spatially varying heat sources. All the smaller-scale waves and turbulence are excluded. It is an open challenge to find more accurate systems of equations which can be solved for sufficiently long times to define a slow manifold. Nevertheless, we illustrate that the resulting solutions are sufficiently close to reality to explain many well-observed phenomena; such as the drag on the atmosphere exerted by large-scale mountain ranges, the differing inland penetration of sea breeze circulations at different latitudes, and the fact that tropical cyclones cannot normally be generated close to the equator. Thus it is reasonable to suggest that the high predictability of semi-geostrophic solutions underpins the observed predictability of real weather.

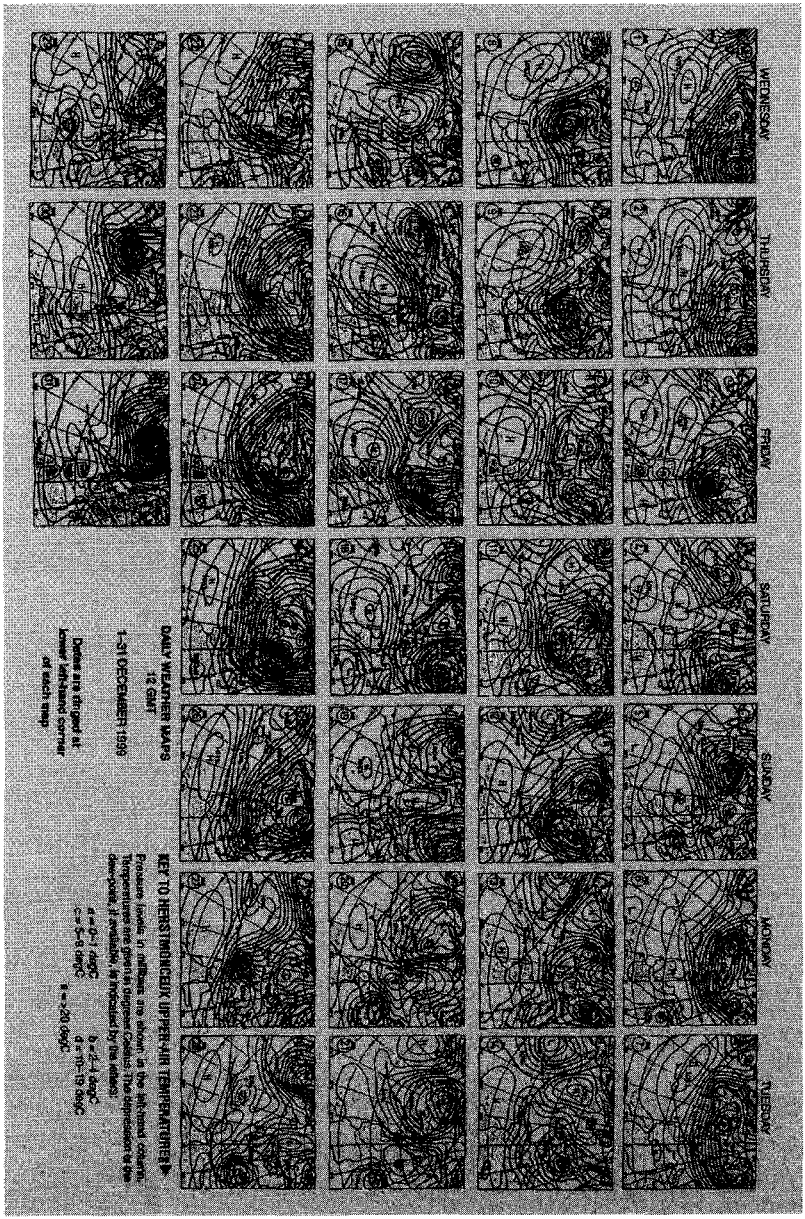

Fig. 1.5 Daily weather maps from 1-28 February 2002. Dates are ringed at lower left corner of each map. Maps are of pressure reduced to mean sea-level with contour interval of 4hpa. Source: *Weather Log*, ©Royal Meteorological Society, Reading, U.K.

This page is intentionally left blank

Chapter 2

The governing equations and asymptotic approximations to them

2.1 The governing equations

The starting point is the traditional one, that recognises that the atmosphere can be regarded as a fluid continuum, and obeys the basic physical laws of dynamics and thermodynamics. This was the basis of Richardson's proposal. It is remarkable how these basic equations, which were formulated many years ago, have stood the test of increasingly sophisticated computer solution and experimental verification. The study of fluid dynamics recognises that fluids exhibit a wide range of different behaviour under different circumstances. This study is facilitated by writing the equations in particular forms, and studying various approximations to them. Thus, in studying the atmosphere, it is convenient to rewrite the basic equations in ways which are different from those used in other applications of fluid dynamics. Various 'traditional' simplifications of the problem are also made which are used in practical applications and do not appear to have a significant effect on the results. The treatment given here is sufficient to explain and justify the large-scale theory described in the rest of the book. Much greater detail is given on the properties of the basic equations and the justification for the traditional approximations in textbooks such as [Pedlosky (1987)], [Gill (1982)] and [Holton (1992)].

The Earth is assumed to rotate with angular velocity Ω on an axis through the coordinate poles. The acceleration due to gravity and the centrifugal acceleration due to the Earth's rotation are combined, and act normally to geopotential surfaces.. We then approximate the geopotential surfaces by spherical surfaces. The equations are defined in spherical polar coordinates (λ, ϕ, r), with origin at the centre of the Earth. The Earth's surface is then assumed to be a spherical surface with radius a with pertur-

bations due to orography. It is defined by the equation $r = r_0(\lambda, \phi)$. The combined gravitational and centrifugal acceleration are assumed to be towards the origin, with a constant magnitude g. The atmosphere is assumed to consist of a compressible ideal gas with pressure, density and temperature p, ρ, T which are functions of position and time. It contains a mixing ratio q of water vapour. It moves with a vector velocity $\mathbf{u} = (u, v, w)$. The evolution is described by the compressible Navier-Stokes equations, the first law of thermodynamics and the equation of state for an ideal gas, all written in a frame of reference rotating with the Earth's angular velocity. These are

$$\begin{aligned} \frac{\mathrm{D}\mathbf{u}}{\mathrm{D}t} + 2\Omega \times \mathbf{u} + \frac{1}{\rho}\nabla p + g\hat{\mathbf{r}} &= \nu \nabla^2 \mathbf{u}, \\ \frac{\partial \rho}{\partial t} + \nabla \cdot (\rho \mathbf{u}) &= 0, \\ C_v \frac{\mathrm{D}T}{\mathrm{D}t} - \frac{RT}{\rho}\frac{\mathrm{D}\rho}{\mathrm{D}t} &= \kappa_h \nabla^2 T + S_h + LP, \\ \frac{\mathrm{D}q}{\mathrm{D}t} &= \kappa_q \nabla^2 q + S_q - P, \\ p &= \rho R T. \end{aligned} \tag{2.1}$$

Here $\mathrm{D}/\mathrm{D}t$ is the Lagrangian derivative $\partial/\partial t + \mathbf{u} \cdot \nabla$ and $\hat{\mathbf{r}}$ is a unit vector in the radial direction. R is the gas constant and C_v the specific heat of air at constant volume, assumed to take the same value everywhere. ν is the kinematic viscosity, also assumed constant. S_h and S_q are the total heat and moisture sources. P is the rate of conversion of water vapour to liquid water or ice, with L the associated latent heat. $\rho\kappa_h$ and κ_q are the thermal conductivity and moisture diffusivity, both assumed constant. Most of these constant coefficient assumptions are not made in operational weather forecasting and climate prediction models, which include a detailed description of atmospheric composition and cloud physics, with the necessary extra complexity in the equations. This extra sophistication is not required for the purposes of this book.

These equations form a system of seven equations for the unknowns $(\mathbf{u}, p, \rho, T, q)$. The obvious physical boundary conditions are that $\mathbf{u} = 0$ at $r = r_0$ and that $p, \rho \to 0$ as $r \to \infty$. While the no-slip condition at the Earth's surface is standard, the issue of the correct mathematical upper boundary condition for an unbounded atmosphere is open.

In the absence of dissipation and source terms, so that the right hand

side terms of the first four equations of (2.1) vanish, equations (2.1) solved in a closed time-independent region Γ with boundary conditions $\mathbf{u} \cdot \mathbf{n} = 0$, where $\mathbf{n}$ is a vector pointing outward from the boundary, conserve the energy integral

$$E = \int_\Gamma \rho \left(\frac{1}{2}(u^2 + v^2 + w^2) + C_v T + gr \right) r^2 \cos\phi \mathrm{d}\lambda \mathrm{d}\phi \mathrm{d}r. \tag{2.2}$$

The requirement that the upper boundary be rigid can be removed by reformulating the equations in 'mass' coordinates, [Wood and Staniforth (2003)].

It is convenient to rewrite the first law of thermodynamics in terms of the potential temperature $\theta = T(p/p_{ref})^{-R/C_p} \equiv T/\Pi$, where C_p is the specific heat of air at constant pressure, assumed to have the same value everywhere, p_{ref} is a constant reference pressure equal to a typical pressure at the Earth's surface, and Π is the Exner pressure. This gives, noting $R = C_p - C_v$,

$$\frac{\mathrm{D}\theta}{\mathrm{D}t} = \frac{1}{C_p \Pi}(\kappa_h \nabla^2 T + S_h + LP). \tag{2.3}$$

This form of the equation is particularly useful in situations where the right hand side terms can be neglected. We can also rewrite the momentum equations by using the definition of θ and the equation of state (the last equation of (2.1)). After some algebraic manipulations we obtain

$$\frac{\mathrm{D}\mathbf{u}}{\mathrm{D}t} + 2\Omega \times \mathbf{u} + C_p \theta \nabla \Pi + g\hat{\mathbf{r}} = \nu \nabla^2 \mathbf{u}. \tag{2.4}$$

In the absence of dissipation and source terms, equations (2.1) imply a conservation law for the *Ertel potential vorticity*

$$\mathcal{Q} = \frac{1}{\rho}(\nabla \times \mathbf{u} + 2\Omega) \cdot \nabla\theta \tag{2.5}$$

in the form

$$\frac{\mathrm{D}\mathcal{Q}}{\mathrm{D}t} = 0. \tag{2.6}$$

2.2 Key asymptotic regimes

This book is concerned with the large-scale flow of the atmosphere. 'Large-scale' refers to the horizontal dimension. In this section we identify flow parameters which are small for large-scale flow. The first step is to recognise that the acceleration due to gravity, g, is much larger than the acceleration of the air in a weather system. However, this acceleration is largely compensated by a vertical pressure gradient. We therefore define a time-independent reference state at rest, which satisfies equations (2.1), with uniform potential temperature θ_0 and with pressure p_0 and density ρ_0 depending only on the radial coordinate. This is given by an Exner pressure $\Pi_0(r)$ satisfying

$$\begin{aligned} C_p\theta_0\frac{\mathrm{d}\Pi_0}{\mathrm{d}r} + g &= 0, \\ \theta_0 &= \text{constant}, \\ \Pi &= 1 \text{ at } r = a. \end{aligned} \tag{2.7}$$

Subtract this state from (2.4). The equation becomes

$$\frac{\mathrm{D}\mathbf{u}}{\mathrm{D}t} + 2\Omega \times \mathbf{u} + C_p\theta\nabla\Pi' - g\frac{\theta'}{\theta_0}\hat{\mathbf{r}} = \nu\nabla^2\mathbf{u} \tag{2.8}$$

where $\theta' = \theta - \theta_0$.

The next step is to recognise that the atmosphere is 'shallow'. About 90% of the mass of the atmosphere is contained in the lowest 15km, which is much smaller than the radius of the earth. However, depressions and anticyclones have a much larger scale than this, so the aspect ratio H/L, where H and L are respectively vertical and horizontal scales, is much less than 1. It is then recognised that in large-scale flows the vertical and horizontal velocities have a similar time-scale, so that $W/U \simeq H/L$, where W and U are typical vertical and horizontal velocities. Under these conditions it can be shown that only the horizontal components of the Coriolis force $2\Omega \times \mathbf{u}$ need be considered, and that the radial coordinate r can be replaced by a wherever it appears undifferentiated. This approximation is discussed in detail by [White et al. (2005)]. The result is that the components of the Coriolis force can be written as $(-fv, fu, 0)$ where the Coriolis parameter $f = 2\Omega\sin\phi$. The shallow atmosphere approximation is very accurate, and is used in many operational weather forecasting and climate models.

The next step is to identify large-scale flow as hydrostatic. In the vertical component of equation (2.8), the term $g\theta'/\theta_0$ is typically about 1ms^{-2}, since the horizontal variations of θ are typically about 10% of the mean value. Since horizontal and vertical velocities have similar time-scales, $\mathrm{D}w/\mathrm{D}t \simeq (H/L)\mathrm{D}u/\mathrm{D}t$. A typical aspect ratio for large-scale flows is 0.01. Thus if $\mathrm{D}w/\mathrm{D}t \simeq 1\text{ms}^{-2}$, $\mathrm{D}u/\mathrm{D}t \simeq 100\text{ms}^{-2}$. This is far larger than observed. The implication is that the vertical component of equation (2.8) can be replaced by a statement of hydrostatic balance.

$$C_p\theta\frac{\partial\Pi'}{\partial r} - g\frac{\theta'}{\theta_0} = 0. \tag{2.9}$$

This approximation is very accurate on large scales, and is used in many weather forecasting and climate models.

The hydrostatic relation (2.9) and the equation of state together give two constraints between the thermodynamic variables Π, ρ and θ. Consistency of the separate evolution equations for ρ and θ yields 'Richardson's equation', see [White (2002)]:

$$\gamma\frac{\partial}{\partial r}\left\{p\left(\frac{\partial w}{\partial r} + \nabla_r\cdot\mathbf{u} - \frac{1}{C_p\Pi}(\kappa_h\nabla^2 T + S_h + LP)\right)\right\} = \frac{\partial p}{\partial r}\nabla_r\cdot\mathbf{u} - \frac{\partial\mathbf{u}}{\partial r}\cdot\nabla_r p. \tag{2.10}$$

In this equation $\gamma = C_p/C_v$ and ∇_r indicates derivatives taken at constant r, i.e. horizontal derivatives. Thus

$$\nabla_r\cdot\mathbf{u} = \frac{1}{a\cos\phi}\left(\frac{\partial u}{\partial\lambda} + \frac{\partial(v\cos\phi)}{\partial\phi}\right)$$

and

$$\nabla_r p = \left(\frac{1}{a\cos\phi}\frac{\partial p}{\partial\lambda}, \frac{1}{a}\frac{\partial p}{\partial\phi}\right).$$

We now classify the various types of flow further. The hydrostatic approximation means that there is no explicit evolution equation for w. The next step is to deduce such an equation from the other equations. The horizontal momentum equations and the thermodynamic equation can be rewritten as

$$\begin{aligned} \frac{\partial u}{\partial t} - fv + \frac{C_p\theta}{a\cos\phi}\frac{\partial \Pi'}{\partial \lambda} &= A_1, \\ \frac{\partial v}{\partial t} + fu + \frac{C_p\theta}{a}\frac{\partial \Pi'}{\partial \phi} &= A_2, \\ \frac{\partial \theta}{\partial t} + w\frac{\partial \theta}{\partial r} &= A_3. \end{aligned} \tag{2.11}$$

where A_1, A_2 and A_3 represent all the remaining terms. The set of equations is completed by the diagnostic equations (2.9), (2.10) and the equation of state. The choice of terms retained on the left hand side of equations (2.11) is made because these will turn out to be the most important terms in the asymptotic regimes in which we are interested.

The first two of equations (2.11) can be combined into an equation for the evolution of the horizontal divergence. The terms resulting from differentiating f and θ are transferred to the right hand side:

$$\frac{\partial}{\partial t}\nabla_r \cdot \mathbf{u} - \frac{f}{a\cos\phi}\left(\frac{\partial v}{\partial \lambda} - \frac{\partial}{\partial \phi}(u\cos\phi)\right) + C_p\theta\nabla_r^2\Pi' = A_4. \tag{2.12}$$

Here $\nabla_r^2 \equiv \nabla_r\cdot(\nabla_r)$. Now calculate the second time derivative, substituting for $\partial u/\partial t$ and $\partial v/\partial t$ using the first two equations of (2.11), and again transferring some terms to the right hand side:

$$\frac{\partial^2}{\partial t^2}(\nabla_r \cdot \mathbf{u}) + f^2\nabla_r \cdot \mathbf{u} + C_p\theta\nabla_r^2\frac{\partial \Pi'}{\partial t} = A_5. \tag{2.13}$$

The final step is to differentiate with respect to r, to use the hydrostatic relation in the form $C_p\theta\partial\Pi/\partial r + g = 0$ to substitute for $\partial^2\Pi'/\partial r\partial t$ in terms of $\partial\theta/\partial t$, and to use the third equation of (2.11) for $\partial\theta/\partial t$. This gives

$$\frac{\partial^2}{\partial t^2}\left(\frac{\partial}{\partial r}(\nabla_r \cdot \mathbf{u})\right) + f^2\frac{\partial}{\partial r}(\nabla_r \cdot \mathbf{u}) + N^2\nabla_r^2 w = A_6 \tag{2.14}$$

where the Brunt-Väisälä frequency $N = \sqrt{\frac{g}{\theta}\frac{\partial\theta}{\partial r}}$. Using (2.10) it is possible to eliminate w in favour of $\nabla_r \cdot \mathbf{u}$, thus obtaining a second order wave equation for the horizontal divergence $\Delta = \nabla_r \cdot \mathbf{u}$. It takes the generic form

$$\frac{\partial^2\Delta}{\partial t^2} + \mathbf{L}\Delta = A \tag{2.15}$$

where $\mathbf{L}$ is a positive definite linear operator.

If $\mathbf{L}\Delta$ is larger than the right hand side terms A, then equation (2.15) describes linear inertia-gravity waves. If $\mathbf{L}\Delta$ and A are of similar magnitude, and the natural frequencies of the waves are large compared with those contained in A, then the response to the 'forcing' terms A can be expressed as the 'slow' equation

$$\mathbf{L}\Delta = A. \tag{2.16}$$

It is therefore important to identify circumstances under which $\mathbf{L}$ is large. The definition of $\mathbf{L}$ is implicit in equation (2.14). Assume a time-scale $L/U = H/W$ as above, and from (2.10) assume that $\Delta \simeq w/H$. The first term in (2.14) has magnitude $(U/L)^2\Delta/H$, the second term has magnitude $f^2\Delta/H$ and the third term has magnitude $N^2L^{-2}H\Delta$. Then the slow dynamics expressed by (2.16) are valid if either the Rossby number $Ro = U/(fL)$ or the Froude number $Fr = U/(NH)$ is small. This book is concerned only with such cases. Much more detailed presentations of these arguments are given in the articles contained in [Norbury and Roulstone (2002)].

In the atmosphere a typical horizontal wind speed is 10ms^{-1}, while a maximum value is about 100ms^{-1}. A mid-latitude value of f is 10^{-4}s^{-1}. Thus the Rossby number is small for horizontal scales much greater than 100km. Weather systems of the type shown in Fig. 1.3 have a substantially larger scale than this, so we can expect to describe them by a set of equations which assumes a small Rossby number. A typical value of N in the troposphere (the lowest 10km of the atmosphere) is 10^{-2}s^{-1}. The Froude number will be small for vertical scales greater than 1km. Most weather systems extend over the full depth of the troposphere, so should be well described by equations assuming a small Froude number. A key parameter is the ratio of the Rossby and Froude numbers. We define the L for which $Ro = Fr$ as the *Rossby radius of deformation* $L_R = NH/f$. Another way of expressing the distinction is whether the aspect ratio H/L is greater or less than f/N. In the troposphere this ratio is about 10^{-2}, consistent with our original assumption that it is much less than unity. If $H/L < f/N$, then $Ro < Fr$, and we can say that the flow is rotation dominated. If $H/L > f/N$ the flow is stratification dominated.

2.3 Derivation of the semi-geostrophic approximation

In this book we use the semi-geostrophic equations to describe the large-scale flow of the atmosphere. These are used because they are a valid approximation to the governing equations (2.1) on large (horizontal) scales and because they can be solved for sufficiently large times to be able to describe the behavior of weather systems. They assume rotation dominated flow, so require that the time-scale of the flow is larger than f^{-1} which is $(2\Omega \sin\phi)^{-1}$. It is important to note at the outset that this time-scale is quite long, it corresponds to a period of 12 hours at the poles and becomes much greater as the equator is approached. Thus the semi-geostrophic model is a rather coarse approximation to the real flow, all the small-scale detail visible in Fig. 1.2 will be absent.

The starting point is the shallow atmosphere hydrostatic equation system derived above, which is very accurate on large horizontal scales. For convenience, it is summarised below:

$$
\begin{aligned}
\frac{\mathrm{D}u}{\mathrm{D}t} - \frac{uv\tan\phi}{a} - fv + \frac{C_p\theta}{a\cos\phi}\frac{\partial \Pi'}{\partial \lambda} &= \nu\nabla^2 u, \\
\frac{\mathrm{D}v}{\mathrm{D}t} + \frac{u^2\tan\phi}{a} + fu + \frac{C_p\theta}{a}\frac{\partial \Pi'}{\partial \phi} &= \nu\nabla^2 v, \\
\frac{\mathrm{D}\theta}{\mathrm{D}t} &= \frac{1}{C_p\Pi}(\kappa_h\nabla^2 T + S_h + LP), \\
\frac{\mathrm{D}q}{\mathrm{D}t} &= \kappa_q\nabla^2 q + S_q - P, \\
C_p\theta\frac{\partial \Pi'}{\partial r} - g\frac{\theta'}{\theta_0} &= 0, \\
p &= \rho RT, \\
\gamma\frac{\partial}{\partial r}\left\{p\left(\frac{\partial w}{\partial r} + \nabla_r\cdot\mathbf{u} - \frac{1}{C_pT}(\kappa_h\nabla^2 T + S_h + LP)\right)\right\} &= \\
\frac{\partial p}{\partial r}\nabla_r\cdot\mathbf{u} - \frac{\partial \mathbf{u}}{\partial r}\cdot\nabla_r p.
\end{aligned}
\tag{2.17}
$$

In conditions where the Rossby number is small, the acceleration term in the horizontal momentum equations is small compared to the Coriolis

terms $-fv$ and fu. We define the *geostrophic wind* (u_g, v_g) by setting

$$-fv_g + \frac{C_p\theta}{a\cos\phi}\frac{\partial\Pi'}{\partial\lambda} = 0, \qquad (2.18)$$
$$fu_g + \frac{C_p\theta}{a}\frac{\partial\Pi'}{\partial\phi} = 0.$$

If the Rossby number is small, the horizontal wind will be close to its geostrophic value.

The semi-geostrophic equations are now derived as in [Hoskins (1975)] by making the geostrophic momentum approximation in (2.17). This consists of replacing the horizontal momentum by its geostrophic value. Thus the first two equations of (2.17) are replaced by

$$\frac{\mathrm{D}u_g}{\mathrm{D}t} - \frac{uv_g\tan\phi}{a} - fv + \frac{C_p\theta}{a\cos\phi}\frac{\partial\Pi'}{\partial\lambda} = \nu\nabla^2 u, \qquad (2.19)$$
$$\frac{\mathrm{D}v_g}{\mathrm{D}t} + \frac{uu_g\tan\phi}{a} + fu + \frac{C_p\theta}{a}\frac{\partial\Pi'}{\partial\phi} = \nu\nabla^2 v.$$

The remaining equations in (2.17) are not approximated. In the absence of dissipation and source terms, and with the boundary conditions $\mathbf{u}\cdot\mathbf{n} = 0$ on the boundary of Γ, the semi-geostrophic equations can be shown to conserve the energy integral

$$E_g = \int_\Gamma \rho\left(\frac{1}{2}(u_g^2 + v_g^2) + C_vT + gr\right)a^2\cos\phi\,\mathrm{d}\lambda\mathrm{d}\phi\mathrm{d}r. \qquad (2.20)$$

The shallow atmosphere semi-geostrophic equations as derived here do not have an exact potential vorticity conservation law of the form (2.6). We will see later that such a conservation law does hold for the deep atmosphere version of the equations.

Much of this book is taken up with analysing the semi-geostrophic equations. However, some key points are noted at the outset:

(i) The only approximations made are to the horizontal momentum. We will see that this ensures large-scale validity. In [Hoskins (1975)] additional approximations are made. These are not valid on large scales, but allow the equations to be solved relatively easily. We will use these additional approximations to illustrate various aspects of the behaviour of the solutions.

(ii) It appears strange that only the horizontal momentum is approximated, not the trajectory. This choice retains energetic consistency, which is essential in proving that the equations can be solved for large times.

(iii) It is possible to make the geostrophic momentum approximation without making the shallow atmosphere approximation. This option will be discussed in section 4.2.

(iv) The solutions will only make sense if the horizontal pressure gradient $\nabla_r \Pi'$ goes to zero at the equator. Otherwise the geostrophic wind cannot be defined. We will demonstrate the existence of solutions which satisfy this constraint in section 4.3.

(v) The assumption made is that $D\mathbf{u}_r/Dt \ll f\hat{\mathbf{r}} \times \mathbf{u}_r$, where $\mathbf{u}_r = (u, v, 0)$. We refer to this condition as stating that the Lagrangian Rossby number Ro_L is small. It only controls the component of $D\mathbf{u}_r/Dt$ normal to $\mathbf{u}_r$. It thus requires the rate of change of horizontal wind direction to be much less than f but does not restrict the rate of change of magnitude.

It is important to recognise that the condition that Ro_L is small is less restrictive than the condition that the Rossby number $Ro = U/fL$ is small. Using a mid-latitude value of $f{=}10^{-4}\mathrm{s}^{-1}$, a value $Ro_L = 0.1$ means that a trajectory cannot change its direction by more than an angle of $\pi/4$ in 24 hours. Figure 2.1 shows some typical trajectories from a weather forecasting model. The period chosen was a stormy winter period with rapidly moving weather systems. The high level trajectories therefore cover a great distance in four days. We see that most of the trajectories do not change direction by an angle of $\pi/4$ in 24 hours (two marked points in Fig. 2.1). However, the trajectory starting furthest west does change direction faster than this off the Californian coast, and the lowest level trajectory (the solid line) changes direction sharply as it crosses the Rockies.

Semi-geostrophic theory can therefore be used for (almost) straight flows, possibly with small scales in the direction normal to the wind direction. The Rossby number based on the cross-wind scale would then be large. A jet-stream in the atmosphere is an example of this case. Semi-geostrophic theory can also be used for large-scale flows where both components of $D\mathbf{u}_r/Dt$ are small and Ro even based on the smallest length scale is small.

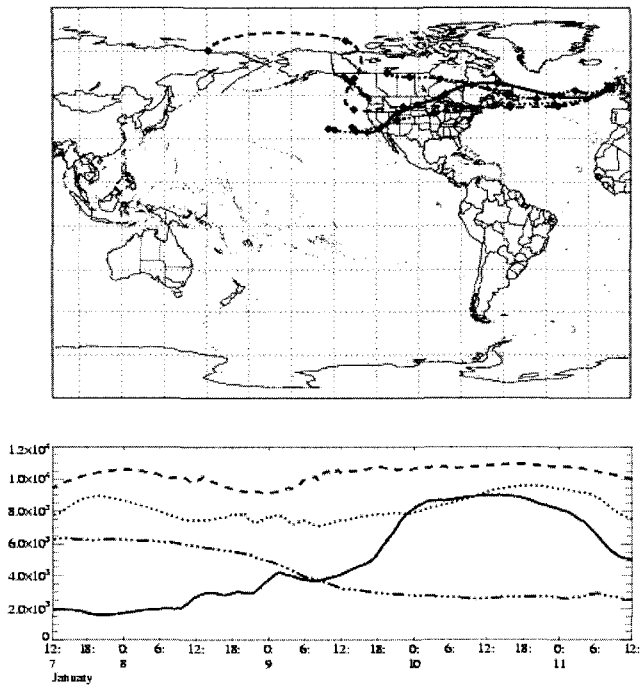

Fig. 2.1 Top: back trajectories from Mace Head for 12UTC on 11 January 2005. The total time covered is 96 hours, with points marked at 12 hour intervals. The trajectories were computed from 3-hourly data. Bottom: the vertical position of the trajectories (m). Source: Atmospheric Dispersion Group, Met Office. ©Crown copyright 2005 Published by the Met Office.

2.4 Various approximations to the shallow water equations

2.4.1 *The shallow water equations*

In this section we place the semi-geostrophic approximation in context by comparing it to other commonly used approximate systems of equations. We do this by applying the approximations to a simpler system of basic equations which is more amenable to analysis, the equations for long waves on shallow water in a rotating frame of reference. This system can be regarded as a set of equations for the vertically averaged flow of the atmosphere. It is relevant because of the assumption of small aspect ratio. We consider only the case of plane geometry since the aim is to illustrate concepts rather than derive results directly applicable to the real system.

The equations are written as

$$\begin{aligned} \frac{\mathrm{D}u}{\mathrm{D}t} + g\frac{\partial h}{\partial x} - fv = 0, \\ \frac{\mathrm{D}v}{\mathrm{D}t} + g\frac{\partial h}{\partial y} + fu = 0, \\ \frac{\partial h}{\partial t} + \nabla \cdot (h\mathbf{u}) = 0. \end{aligned} \tag{2.21}$$

Here $\mathbf{u} = (u, v)$ is the velocity vector and h is the fluid depth. f is the Coriolis parameter which is in general a function of position. The equations are to be solved in a closed region $\Gamma \in \mathcal{R}^2$ with boundary conditions $\mathbf{u} \cdot \mathbf{n} = 0$. These equations then conserve the energy integral

$$E = \frac{1}{2}\int_{\Gamma} \left(h(u^2 + v^2) + gh^2\right) \mathrm{d}x\mathrm{d}y. \tag{2.22}$$

Define the potential vorticity

$$\mathcal{Q} = \frac{\zeta + f}{h} \tag{2.23}$$

where

$$\zeta = \frac{\partial v}{\partial x} - \frac{\partial u}{\partial y}. \tag{2.24}$$

Then $\mathcal{Q}$ satisfies the conservation law

$$\frac{\mathrm{D}\mathcal{Q}}{\mathrm{D}t} = 0. \tag{2.25}$$

2.4.2 *Key parameters*

The first step in understanding the solutions is to find analytic solutions for the special case where the equations describe small perturbations about a state of rest and the effect of rotation takes a simple form. Much more extensive analyses of this type can be found in [Gill (1982)]. For this purpose we temporarily use periodic boundary conditions and assume that f is a constant. We note that the state $u = v = 0, h = H$, where H is a constant, satisfies (2.21). Then seek a general solution $u = u', v = v', h = H + h'$. We assume that all primed quantities are small, so that all the terms linear in the primed quantities have to satisfy the equations on their own. Thus

we obtain

$$\begin{aligned} \frac{\partial u'}{\partial t} + g\frac{\partial h'}{\partial x} - fv' &= 0, \\ \frac{\partial v'}{\partial t} + g\frac{\partial h'}{\partial y} + fu' &= 0, \\ \frac{\partial h'}{\partial t} + \frac{\partial}{\partial x}(Hu') + \frac{\partial}{\partial y}(Hv') &= 0. \end{aligned} \tag{2.26}$$

Seek solutions of (2.21) of the form $u' = \hat{u}\exp i\,(kx + ly - \omega t), v' = \hat{v}\exp i\,(kx + ly - \omega t), h' = \hat{h}\exp i\,(kx + ly - \omega t)$. Equations (2.21) can then be rewritten as

$$\begin{pmatrix} -i\omega & -f & gik \\ f & -i\omega & gil \\ ikH & ilH & -i\omega \end{pmatrix} \begin{pmatrix} \hat{u} \\ \hat{v} \\ \hat{h} \end{pmatrix} = 0. \tag{2.27}$$

Equations (2.26) have the trivial solution $\hat{u} = \hat{v} = \hat{h} = 0$. Non-trivial solutions are only possible if the determinant

$$\begin{vmatrix} -i\omega & -f & gik \\ f & -i\omega & gil \\ ikH & ilH & -i\omega \end{vmatrix} = 0. \tag{2.28}$$

This reduces to the cubic equation

$$i\omega\left(-\omega^2 + gH\left(k^2 + l^2\right) + f^2\right) = 0 \tag{2.29}$$

which has roots

$$\begin{aligned} \omega &= 0 \\ &= \pm\sqrt{gH\left(k^2 + l^2\right) + f^2}. \end{aligned} \tag{2.30}$$

These roots represent the eigenvalues of the matrix

$$\begin{pmatrix} 0 & -f & gik \\ f & 0 & gil \\ ikH & ilH & 0 \end{pmatrix} \tag{2.31}$$

derived from the left hand side of (2.27). The nature of the roots can be further studied by examining the associated eigenfunctions. The eigenfunction

associated with $\omega = 0$ takes the form

$$\begin{pmatrix} \hat{u} \\ \hat{v} \\ \hat{h} \end{pmatrix} = \alpha \begin{pmatrix} -gil \\ gik \\ f \end{pmatrix} \tag{2.32}$$

where α is a constant. This eigenfunction is both geostrophic, satisfying

$$g\frac{\partial h'}{\partial x} - fv' = 0, g\frac{\partial h'}{\partial y} + fu' = 0 \tag{2.33}$$

and non-divergent, satisfying

$$\frac{\partial}{\partial x}(Hu') + \frac{\partial}{\partial y}(Hv') = 0. \tag{2.34}$$

This solution represents a *Rossby* wave. While at the level of this approximation, such a solution is a steady state, and thus not very interesting; it forms the basis of a description of the large-scale motions studied in this book, which are observed to be close to geostrophic, and other important classes of motions which are almost non-divergent.

The eigenfunctions associated with the other eigenvalues are

$$\begin{pmatrix} \hat{u} \\ \hat{v} \\ \hat{h} \end{pmatrix} = \alpha \begin{pmatrix} gk\varpi - gilf \\ -gl\varpi - gikf \\ gH\left(k^2 + l^2\right) \end{pmatrix} \tag{2.35}$$

where

$$\varpi = \sqrt{gH\left(k^2 + l^2\right) + f^2} \tag{2.36}$$

and α is a constant. These eigenfunctions are neither geostrophic nor non-divergent, and represent inertia-gravity waves. The eigenvalues $\pm\varpi$ are the shallow water equivalent of the eigenvalues of the linear operator $\mathbf{L}$ derived in equation (2.16) in section 2.2.

The inertia-gravity wave frequency ϖ is made up of two terms. The first (which describes pure gravity waves) is independent of rotation and depends on the mean depth H. The associated phase speed (calculated by first setting $f = 0$) is $\sqrt{gH}$. It is thus large for large mean depths. The second term (which describes pure inertia waves) always has a frequency f, so the phase speed depends on the horizontal wavelength, being large for large wavelengths. The two terms are equal if

$$1/\sqrt{(k^2 + l^2)} = \sqrt{(gH)}/f \equiv L_R. \tag{2.37}$$

L_R is the Rossby radius of deformation for shallow water flow.

This behaviour links directly to the three-dimensional case analysed in section 2.2. If U is a typical flow speed, the inertia-gravity wave speed is faster than U if either the Froude number $U/\sqrt{gH}$ or the Rossby number $Ro = U/fL$, where L is the length scale, is small. The two conditions coincide if $L = L_R$. The first case is the shallow water analogue of stratification dominated flow and applies for $L < L_R$. The second case corresponds to rotation dominated flow and applies for $L > L_R$. Experiments in the 1950s, when the shallow water equations were used to forecast the evolution of the 500hpa pressure surface, showed that the best match to observations was obtained when H was set to 2000m, corresponding to L_R =1400km ([Reiser (2000)], p.65). This scale corresponds to a wavelength of about a quarter of the circumference of the Earth in middle latitudes.

An important application of this linear analysis is to extract the Rossby wave solution from general data (u, v, h). This is called solving the 'Rossby adjustment' problem. Write $u' = \check{u}(t) \exp i\,(kx + ly), v' = \check{v}(t) \exp i\,(kx + ly), h' = \check{h}(t) \exp i\,(kx + ly)$. The system of equations (2.26) can be rewritten as

$$\frac{\partial}{\partial t} \begin{pmatrix} \check{u} \\ \check{v} \\ \check{h} \end{pmatrix} + \mathbf{L} \begin{pmatrix} \check{u} \\ \check{v} \\ \check{h} \end{pmatrix} = 0. \tag{2.38}$$

Let $\mathbf{E}$ be the matrix whose columns are the eigenfunctions of $\mathbf{L}$ calculated above. Then a general state vector $\check{\mathbf{x}} = \begin{pmatrix} \check{u} \\ \check{v} \\ \check{h} \end{pmatrix}$ can be projected on to a basis of eigenfunctions by setting

$$\tilde{\mathbf{x}} = \mathbf{E}^{-1} \check{\mathbf{x}}. \tag{2.39}$$

The Rossby wave component $\tilde{\mathbf{x}}_0$ is isolated by setting the second and third components of $\tilde{\mathbf{x}}$ to zero. The result can be projected back to its representation in physical variables by multiplying by $\mathbf{E}$. This can be shown to give

$$\check{\mathbf{x}}_0 = \begin{pmatrix} \check{u}_0 \\ \check{v}_0 \\ \check{h}_0 \end{pmatrix} = \frac{\left(\left(-il\check{u} + ik\check{v}\right) H - f\check{h}\right)}{\varpi^2} \begin{pmatrix} -gil \\ gik \\ f \end{pmatrix}. \tag{2.40}$$

The numerator that appears on the right hand side of (2.40) can be written

in terms of the original perturbation variables as

$$\mathcal{Q}' = \left(-\frac{\partial u'}{\partial y} + \frac{\partial v'}{\partial x}\right) H - fh' \tag{2.41}$$

where $\mathcal{Q}'$ can be shown to be the linearised perturbation to the potential vorticity defined in (2.23). Substituting (2.41) into (2.26) gives

$$\frac{\partial \mathcal{Q}'}{\partial t} = 0, \tag{2.42}$$

which is the linearisation of equation (2.25). Using the definition of ϖ^2, the calculation expressed by equation (2.40) can be expressed as first calculating h' from

$$-gH\nabla^2 h' + f^2 h' = f\mathcal{Q}', \tag{2.43}$$

and then calculating u' and v' from h' using the geostrophic relation. This is a simple form of *potential vorticity inversion* where all the flow variables can be derived from the potential vorticity together with diagnostic relations between the variables. In the nonlinear case, we will often write the slow solutions corresponding to Rossby waves in the form of an evolution equation for potential vorticity, together with diagnostic equations allowing the other variables to be calculated. This method was first introduced systematically by [Hoskins et al. (1985)].

2.4.3 *General equations for slow solutions*

We now revert to the original problem as set out in section 2.4.1. Thus the Coriolis parameter f can be a function of position, and the equations are solved in a closed region Γ with $\mathbf{u} \cdot \mathbf{n} = 0$ on the boundary. We seek systems of equations which approximate (2.21) when the flow speed U is small compared with the inertia-gravity wave speed deduced from (2.36). This presentation follows [McWilliams et al. (1999)]. There are many other versions of this type of analysis in the literature, for instance see [Warn et al. (1995)], [Lynch(1989)], [Holm (1996)] and [Mohebalhojeh and Dritschel (2001)].

We assume a time-scale $T \gg \varpi^{-1}$. As in section 2.2, assume that $U/L = T$. Then we use the ratio of the flow speed to the inertia-gravity wave speed:

$$\varepsilon \equiv \frac{U\sqrt{k^2 + l^2}}{\sqrt{gH(k^2 + l^2) + f^2}} \tag{2.44}$$

as the small parameter. Note that

$$\varepsilon = \frac{1}{\sqrt{Fr^{-2} + Ro^{-2}}}. \tag{2.45}$$

Thus $\varepsilon \ll 1$ if either $Fr \ll 1$ or $Ro \ll 1$. Using the condition $\varepsilon \ll 1$ yields a set of approximate equations which are valid whenever there is a clear scale separation between the flow speed and the inertia-gravity wave speed. Rewrite equations (2.21) in terms of the vorticity (2.24) and the divergence

$$\Delta = \frac{\partial u}{\partial x} + \frac{\partial v}{\partial y} \tag{2.46}$$

giving

$$\begin{aligned} \frac{\partial \zeta}{\partial t} + u\frac{\partial(\zeta+f)}{\partial x} + v\frac{\partial(\zeta+f)}{\partial y} + (\zeta+f)\Delta = 0, \\ \frac{\partial \Delta}{\partial t} + u\frac{\partial \Delta}{\partial x} + v\frac{\partial \Delta}{\partial y} + D^2 - 2J(u,v) \\ +g\nabla^2 h - \nabla\cdot(fv, -fu) = 0, \\ \frac{\partial h}{\partial t} + u\frac{\partial h}{\partial x} + v\frac{\partial h}{\partial y} + h\Delta = 0, \end{aligned} \tag{2.47}$$

where $J(u,v) = \frac{\partial u}{\partial x}\frac{\partial v}{\partial y} - \frac{\partial u}{\partial y}\frac{\partial v}{\partial x}$. Differentiating the second of these equations with respect to time and substituting the first and third equation gives

$$\begin{aligned} \frac{\partial^2 \Delta}{\partial t^2} + \left(-gh\nabla^2\Delta + f(\zeta+f)\Delta\right) = g\Delta\nabla^2 h + 2g\nabla\Delta\nabla h + \\ gh\nabla^2(\mathbf{u}\cdot\nabla h) - f\mathbf{u}\cdot\nabla(\zeta+2f) + 2\frac{\partial}{\partial t}J(u,v) + \text{remainder} \end{aligned} \tag{2.48}$$

In this equation the ratio of the magnitude of the first two terms is exactly the square of the ratio of the actual frequency to the inertia-gravity wave frequency ϖ and is thus equal to ε^2. Equation (2.48) can then be approximated by the diagnostic equation obtained by omitting the first term. Since we have assumed that $U/L = T$, it can be shown that it is also consistent to neglect the first two terms on the right hand side and the terms in 'remainder' and approximate (2.48) by

$$\begin{aligned} \left(-gh\nabla^2\Delta + f(\zeta+f)\Delta\right) = \\ gh\nabla^2(\mathbf{u}_a\cdot\nabla h) - f\mathbf{u}_a\cdot\nabla(\zeta+2f) + 2\frac{\partial}{\partial t}J(u_a, v_a) \end{aligned} \tag{2.49}$$

where $\mathbf{u}_a = (u_a, v_a)$ is the rotational part of (u, v) satisfying

$$\begin{aligned} \frac{\partial v_a}{\partial x} - \frac{\partial u_a}{\partial y} &= \zeta, \\ \frac{\partial u_a}{\partial x} + \frac{\partial v_a}{\partial y} &= 0. \end{aligned} \tag{2.50}$$

We can write (u_a, v_a) in terms of a stream-function ψ, so that $u_a = -\partial\psi/\partial y, v_a = \partial\psi/\partial x$. The use of (2.49) implies that the second equation of (2.47) has been approximated by

$$-2J\left(\frac{\partial\psi}{\partial x}, \frac{\partial\psi}{\partial y}\right) + g\nabla^2 h - \nabla \cdot f\nabla\psi = 0. \tag{2.51}$$

We can then form a complete prognostic system by replacing the second equation of (2.47) by (2.51). The resulting equations are called the *nonlinear balance shallow water equations.* Slightly different versions of these appear in the various references cited above. The potential vorticity equation (2.25) is not changed by this approximation. (2.51) and (2.49) are a nonlinear generalisation of the geostrophic and non-divergent conditions (2.33) and (2.34) satisfied by linear Rossby waves. The potential vorticity equation (2.25) has already been shown to be a nonlinear generalisation of equation (2.42) which governs the evolution of linear Rossby waves.

Following [McWilliams et al. (1999)], the nonlinear balance equations can be written as

$$\begin{pmatrix} F & 1 & 0 \\ 0 & \nabla^2 & -M \\ G & 0 & \nabla^2 \end{pmatrix} \begin{pmatrix} \chi \\ \partial h/\partial t \\ \partial\psi/\partial t \end{pmatrix} = \begin{pmatrix} -J(\psi, h) \\ 0 \\ -J(\psi, \zeta + f) \end{pmatrix} \tag{2.52}$$

where

$$\begin{aligned} \nabla^2\chi &= \Delta, \\ F &= \nabla \cdot (h\nabla), \\ M = \nabla \cdot (f\nabla) + 2\left(\frac{\partial^2\psi}{\partial x^2}\frac{\partial^2}{\partial y^2} + \frac{\partial^2\psi}{\partial y^2}\frac{\partial^2}{\partial x^2}\right) &- 2\frac{\partial^2\psi}{\partial x\partial y}\frac{\partial^2}{\partial x\partial y}, \\ G &= \nabla \cdot ((\zeta + f)\nabla). \end{aligned} \tag{2.53}$$

Write (2.52) symbolically as

$$\mathbf{M}\mathbf{u} = \mathbf{A}. \tag{2.54}$$

As discussed in [McWilliams et al. (1999)], we expect equation (2.54) to be solvable if $\mathbf{M}$ is elliptic or degenerate elliptic. It is unlikely to be solvable if $\mathbf{M}$ is hyperbolic. It can be shown that the necessary conditions are

(i) h does not change sign.
(ii) $\zeta + f$ does not change sign.
(iii)

$$(\zeta + f)^2 - \left(\frac{\partial \psi^2}{\partial x^2} - \frac{\partial \psi^2}{\partial y^2}\right)^2 - 4\left(\frac{\partial^2 \psi}{\partial x \partial y}\right)^2 > 0. \qquad (2.55)$$

Though the first two of these conditions are ensured by potential vorticity conservation and the inherent positivity of h, condition (2.55) is not related to a constant of the motion, and spontaneous violations are to be expected. Computations, [McWilliams and Yavneh (1998)], show that these do indeed occur. If the initial data has small Rossby number, the velocity gradients have magnitude $U/L \ll f$ and condition (2.55) will be satisfied. If the initial data has small Froude number but large Rossby number, (2.55) may not be satisfied. We will also see in the following subsections that flow-dependent solvability conditions, such as these, are unavoidable for approximations to the shallow water equations valid on scales greater than L_R. The difficulty caused by condition (2.55) in the case where $Fr \ll 1$, $Ro = \mathrm{O}(1)$ is a result of trying to use the same set of simplified equations in both the asymptotic regimes $Fr \ll 1$ and $Ro \ll 1$.

For these equations to be a useful approximation, they have to be solvable for a time comparable to the time-scale of the phenomena being modelled. Condition (2.55) means that the velocity gradients U/L have to be restricted in the initial data. If Ro is small and comparable to or less than Fr we have $U/L \ll f \simeq \varpi$. The worst likely case is that two fluid particles initially separated by a distance L and with initial relative velocity U will come close together. This will take a time at least $L/U = Ro^{-1} f^{-1} \simeq \varepsilon^{-1} \varpi^{-1}$. Thus it is likely that equation (2.54) can be solved for a time $\mathrm{O}(\varepsilon^{-1} \varpi^{-1})$ provided that $Ro = \mathrm{O}(\varepsilon)$ in the initial data. However, this in itself is not long enough for the solutions to be useful. For instance, the condition $Ro = 0.1$ means that the fluid velocity cannot change by more than $10\mathrm{ms}^{-1}$ over a distance of 1000km in mid-latitudes. If ε is small because Fr rather than Ro is small, the velocity gradients are not constrained and no estimate can be made in this way.

It is therefore necessary to exploit the structure of the equations to prove a better estimate. This has not been achieved for equations (2.54),

though it has been achieved for the simpler equations discussed in the following sections. Several of the difficulties are discussed by [McIntyre and Roulstone (2002)]. The effect is that it appears not to be possible to prove the existence of a slow manifold which is accurate to more than leading order in ε and is uniformly accurate for small ε. This is consistent with the observed endemic nature of small-scale waves in the atmosphere, as illustrated in in Figs. 1.2 and 1.4.

In order to find simplified models which can be solved for long enough times to be useful, we therefore split the cases where $\varepsilon \ll 1$ into the separate cases $Fr < Ro$, $Fr \ll 1$, $Fr = Ro \ll 1$ and $Ro < Fr$, $Ro \ll 1$. As shown in section 2.4.2, these cases correspond to length scales $L < L_R$, $L = L_R$ and $L > L_R$ respectively. The difficulty caused by condition (2.55) in the case of small Fr is avoided by using a system of equations in this asymptotic regime which is based on a constant coefficient elliptic problem. Flow-dependent solvability conditions which require restrictions on the velocity gradients then no longer arise. Flow-dependent conditions are required for the solvability of systems of equations valid for scales larger than L_R, but it is now consistent to restrict the velocity gradients in the initial data. We will show that by limiting the validity of the equations to small Ro, solvability can be proved for arbitrarily large times. We consider each case in turn in the following subsections.

2.4.4 *Slow solutions on small scales*

In this section we assume $Fr \ll 1$ and $Fr < Ro$, so $L < L_R$ and L can thus be as small as desired. There is no assumption about the maximum size of Ro, so the first two equations of (2.21) cannot be approximated. Therefore $g\nabla h$ can be of similar magnitude to $\mathrm{D}\mathbf{u}/\mathrm{D}t$. If H is the characteristic scale of h, this means that $U^2/L \simeq gH/L$, which would mean that $Fr = \mathrm{O}(1)$. The assumption $Fr \ll 1$ can only be achieved by assuming that the mean value of h is much greater than the amplitude of variations of h, so that $\nabla h \simeq Fr^2 H/L$. Write the third equation of (2.21) as

$$\frac{\partial h}{\partial t} + \mathbf{u} \cdot \nabla h + h\Delta = 0. \tag{2.56}$$

The discussion above shows that the last term on the left hand side must be much larger than the other two unless $\Delta = \mathrm{O}(Fr^2 U/L)$. An appropriate asymptotic approximation to (2.47) is therefore to set $\Delta = 0$, giving

$$\begin{aligned} \frac{\partial \zeta}{\partial t} + u\frac{\partial(\zeta+f)}{\partial x} + v\frac{\partial(\zeta+f)}{\partial y} &= 0, \\ -2J(u,v) + g\nabla^2 h - \nabla\cdot(fv,-fu) &= 0, \\ \Delta &= 0. \end{aligned} \tag{2.57}$$

According to the discussion above, we expect the error in this approximation to be $O(Fr^2)$. The equations are still to be solved in a closed region $\Gamma \in \mathcal{R}^2$ with boundary conditions $\mathbf{u}\cdot\mathbf{n} = 0$.

Equations (2.57) are precisely the equations for two-dimensional incompressible flow in a rotating frame of reference. They conserve the energy integral

$$\int_\Gamma \left(\frac{1}{2}(u^2+v^2)\right) \mathrm{d}x\mathrm{d}y. \tag{2.58}$$

This represents purely kinetic energy, which is consistent with the fact that the energy of disturbances in shallow water solutions with $Fr \ll 1$, $Fr < Ro$ is primarily kinetic rather than potential ([Gill (1982)], p.206). The depth h is purely diagnostic, and plays no role in the solution. The role of potential vorticity is played by the absolute vorticity $\zeta + f$. The first equation of (2.57) is thus the equivalent in this asymptotic regime of the general equation (2.25). This is to be expected, since variations in the potential vorticity $Q = (\zeta+f)/h$ will be dominated by variations in $\zeta + f$ under the conditions that variations in h are much smaller than the mean value of h. An example is shown in Fig. 2.2. The mean depth of the fluid has been chosen so that $L_R = 2148$km, corresponding to a wavelength of about 13500km. Most of the variations in h shown in Fig. 2.2 are on a smaller scale than this. It is seen that the scales of the variations in Q are much smaller than the scales of variation in h.

In equation (2.57) the vorticity is transported by the velocity u, v. We now have to calculate the velocity from the vorticity. The condition $\Delta = 0$ means that we can write

$$\mathrm{u} = -\frac{\partial \psi}{\partial \mathrm{y}}, \mathrm{v} = \frac{\partial \psi}{\partial \mathrm{x}}, \qquad \nabla^2\psi = \zeta. \tag{2.59}$$

The boundary conditions applied to (2.57) imply that ψ is constant on the boundaries of Γ, so we can solve the Poisson equation for ψ and calculate the velocity from it. The depth h can then be calculated from the second

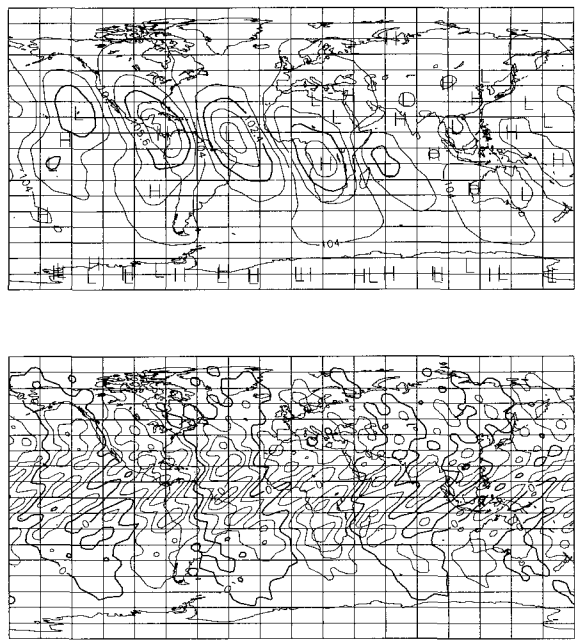

Fig. 2.2 Top: Example depth field with $gh_0 = 10^5 \mathrm{ms}^{-2}\mathrm{s}^{-2}$. Units 100m, contour interval 80m. Bottom: Potential vorticity, units $(\mathrm{ms})^{-1}$, contour interval 0.3×10^{-9}. From [Cullen (2002)]. ©Royal Meteorological Society, Reading, U.K.

equation in (2.57). Note that we now have constant coefficient elliptic equations to solve, unlike the variable coefficient problem of section 2.4.3. Thus no solvability conditions arise.

It is possible to prove that, given suitable initial data, equations (2.57) can be solved uniquely for all finite times. The solutions remain as smooth as the initial data. Equations (2.57) thus define a slow manifold. These theorems are reviewed by [Chemin (2000)]. The proofs exploit the fact that the vorticity is bounded by its initial values. Provided that fluid trajectories can be shown to retain their identity, advecting the vorticity can only rearrange its values, but cannot create new ones. Fluid trajectories can be proved to retain their identity if the velocity is be smooth enough. This means that the velocity gradients, assumed bounded in the initial data, have to be controlled. Classical results quoted by [Chemin (2000)]

state that, if ζ is bounded above and below, and because $\Delta = 0$, the velocity gradient norm

$$\left(\int_0^1 \int_0^1 \left((\nabla u)^2 + (\nabla v)^2 \right) \mathrm{d}x\mathrm{d}y \right)^{\frac{1}{2}} \tag{2.60}$$

is bounded uniformly in time. However, the maximum value of the velocity gradients, measured by

$$\left| \frac{\partial u}{\partial x} \right| + \left| \frac{\partial u}{\partial y} \right| + \left| \frac{\partial v}{\partial x} \right| + \left| \frac{\partial v}{\partial y} \right|, \tag{2.61}$$

cannot be determined without also knowing the vorticity gradients. The main task in the proof is thus to estimate the growth of the vorticity gradients, assuming they are bounded in the initial data.

It is also possible to prove that solutions of the shallow water equations converge to those of equation (2.57) as $Fr \to 0$. This is a special case of the result that the equations for incompressible flow are a limit of those for compressible flow, see [Majda (1984)]. In this asymptotic regime we can assume that the gravity waves are governed by a linear equation with constant coefficients, giving a wave speed $\sqrt{gH}$. The constant coefficients are essential to the proof. The techniques of Klainerman and Majda, [Majda (1984)], chapter 2, can then be used to derive the necessary estimates. In section 6.5 we will see that the qualitative behaviour exhibited by (2.57) is also exhibited by the shallow water equations (2.21) for initial data satisfying $L < L_R$.

2.4.5 *Quasi-geostrophic solutions*

In this section we assume $Fr = Ro \ll 1$. This is the traditional scaling introduced by [Charney (1948)]. It is derived and analysed in detail in [Pedlosky (1987)]. The mathematical properties of the resulting quasi-geostrophic shallow water equations have been analysed by, for instance, [Babin et al. (1999)], [Bourgeois and Beale (1994)] and [Majda (2003)].

The assumption $Ro \ll 1$ means that the first two equations in (2.21) can be approximated by

$$\begin{aligned} g\frac{\partial h}{\partial x} - fv &= 0, \\ g\frac{\partial h}{\partial y} + fu &= 0. \end{aligned} \tag{2.62}$$

Equation (2.62) states that $fU \simeq gH/L$. The assumption $Fr = Ro$ means that $L \simeq \sqrt{gH}/f$, so that $U \simeq \sqrt{gH}$. This contradicts the assumption $Fr \ll 1$. This contradiction can be resolved, as in section 2.4.4, by assuming that the mean value of h, h_0, is large so that $\nabla h \simeq FrH/L$. The third equation of (2.21) can then again be approximated by $\Delta = 0$, but now the estimate is $\Delta \simeq FrU/L$, so the approximation will only be first order accurate in Fr and Ro.

There are now two immediate difficulties. The first is that (2.62) and $\Delta = 0$ contain no prognostic information, the well-known geostrophic degeneracy. The second is that, if f is a function of position, the equations are contradictory because $\mathbf{u}$ derived from (2.62) does not satisfy $\Delta = 0$. The resolution is to go to the next order terms. Thus we define the geostrophic wind by

$$\begin{aligned} g\frac{\partial h}{\partial x} - f_0 v_g &= 0, \\ g\frac{\partial h}{\partial y} + f_0 u_g &= 0, \end{aligned} \tag{2.63}$$

where f_0 is a constant, representative, value of f. Then $\nabla \cdot \mathbf{u}_g = 0$. The ageostrophic wind $\mathbf{u} - \mathbf{u_g}$ is assumed to be much less than $\mathbf{u_g}$. The vorticity is thus approximated by its geostrophic value, but as $\nabla \cdot \mathbf{u}_g = 0$, the divergence is entirely ageostrophic. We use the vorticity- divergence form (2.47) of the shallow water equations. The first two equations are approximated by

$$\begin{aligned} \frac{\partial \zeta_g}{\partial t} + u_g\frac{\partial(\zeta_g + f)}{\partial x} + v_g\frac{\partial(\zeta_g + f)}{\partial y} + f_0\Delta &= 0, \\ g\nabla^2 h - f_0\zeta_g &= 0, \end{aligned} \tag{2.64}$$

and the third equation by

$$\frac{\partial h}{\partial t} + h_0\Delta = 0, \tag{2.65}$$

noting that $\mathbf{u}_g \cdot \nabla h$ vanishes identically.

The equations are again to be solved in a closed region $\Gamma \in \mathbb{R}^2$ with boundary conditions $\mathbf{u} \cdot \mathbf{n} = 0$. It is necessary to apply this condition to the geostrophic windand divergent wind separately. The first of these conditions implies that h has to be constant along the boundary. It can then

be shown that the energy integral

$$\int_\Gamma h_0 \left(\frac{1}{2}(u_g^2 + v_g^2) + gh \right) \mathrm{d}x\mathrm{d}y \tag{2.66}$$

is conserved. Equations (2.64) and (2.65) also conserve the quasi-geostrophic potential vorticity

$$\mathcal{Q}_g = h_0(\zeta_g + f) - f_0(h - h_0). \tag{2.67}$$

The latter quantity is an approximation to the potential vorticity (2.23) valid under the assumptions $Ro \ll 1, Fr \ll 1$. It is identical to the potential vorticity (2.41) of the linearised equations. It obeys the conservation law

$$\frac{\partial \mathcal{Q}_g}{\partial t} + u_g \frac{\partial \mathcal{Q}_g}{\partial x} + v_g \frac{\partial \mathcal{Q}_g}{\partial y} = 0. \tag{2.68}$$

It is easy to see that these approximations are unsuitable for large-scale flow, since the replacement of f by f_0 in (2.63) will only be acceptable in a fairly small region around the latitude used to define f_0. This led to the failure of the quasi-geostrophic equations as a basis for numerical weather forecasting as early as the 1950s, [Phillips (2000)]. At that time computers were very crude, and the resolution of models was far short of that necessary to expose the small-scale limitations of quasi-geostrophic theory. However, they have proved very useful for understanding the processes governing the evolution of extra-tropical weather systems, where quantitative accuracy is not required, [Pedlosky (1987)].

The solutions of equations (2.64) and (2.65) can be found by a method analogous to that for two-dimensional incompressible flow as described in section 2.4.4. The first step is to define an inversion procedure for calculating h, u and v from $\mathcal{Q}_g$. Using (2.63) and (2.67) gives

$$h_0 f_0^{-1} g \nabla^2 h - f_0 h = \mathcal{Q}_g - f h_0 - f_0 h_0. \tag{2.69}$$

This is an constant coefficient elliptic equation for h. It can be solved using the boundary condition that h is constant along the boundary. $\mathbf{u}_g$ can then be calculated from (2.63). This is sufficient for the equations to be advanced in time. However, the boundary condition on h is unphysical. If normal derivative (Neumann) boundary conditions on h are used instead, these imply that the geostrophic wind parallel to the boundary is prescribed. This is also unphysical. As a result, the equations are often solved with periodic boundary conditions. The solution procedure is then analogous to

that in section 2.4.4. Given bounded q_g, equation (2.69) is solved for h and $\mathbf{u}_g$ calculated from (2.63). The solution can then be advanced in time.

If the initial data are geostrophic, and sufficiently smooth, the solutions of the shallow water equations can be proved to converge to those of (2.64) and (2.65) on that time interval, [Majda (2003)], pp. 73 *et seq.*. The fact that the inertia-gravity waves are again governed by a linear equation with constant coefficients, so that the frequency ϖ is a constant $\sqrt{gh_0(k^2+l^2)+f_0^2}$ is essential. The solutions of the shallow water equations can also be analysed in this limit for initial data with large inertia-gravity waves. This involves averaging over inertia-gravity wave periods, and showing that the averaged solution satisfies (2.64) and (2.65) plus an error term which can be estimated. Such methods are described in [Majda (2003)], chapter 8, and [Babin et al. (1999)]. It is again crucial that the inertia-gravity waves can be described by a linear equation with constant coefficients. Since more results of this type have been obtained for the three dimensional case, a representative set is given in that context in section 2.5.5.

The divergence Δ does not need to be calculated to advance the solution in time. If it is required, it can be found by differentiating the second equation of (2.64) with respect to time and eliminating the time derivatives from (2.64) and (2.65) to give the *quasi-geostrophic omega equation*:

$$gh_0\nabla^2\Delta - f_0^2\Delta = f_0\mathbf{u_g}\cdot\nabla(\zeta_g + f). \tag{2.70}$$

The boundary conditions on the divergent velocity yield Neumann boundary conditions for the velocity potential χ, where $\nabla^2\chi = \Delta$. However, if equation (2.70) is written in terms of χ, it becomes fourth order and requires additional boundary conditions.

2.4.6 *Slow solutions on large scales*

Now consider the case $Ro \ll 1$, with $Ro < Fr$ and no assumption about the maximum size of Fr. This corresponds to horizontal scales larger than L_R. The assumption $Ro \ll 1$ means that the first two equations of (2.21) can again be approximated by (2.62). As in section 2.4.5, this means that $fU \simeq gH/L$. Thus $U^2/gH \simeq U/fL$, so we require $Fr = \sqrt{Ro}$. We thus cannot make any assumptions about the size of the terms in the third equation in (2.21) without incurring an error $O(\sqrt{Ro})$. A first approximation to (2.21)

in this case is therefore:

$$\begin{aligned} g\frac{\partial h}{\partial x} - fv &= 0, \\ g\frac{\partial h}{\partial y} + fu &= 0, \\ \frac{\partial h}{\partial t} + \frac{\partial}{\partial x}(hu) + \frac{\partial}{\partial y}(hv) &= 0. \end{aligned} \tag{2.71}$$

Substituting the first two equations into the third gives

$$\frac{\partial h}{\partial t} + h\left(\frac{\partial u}{\partial x} + \frac{\partial v}{\partial y}\right) = 0. \tag{2.72}$$

These equations are the 'Type 2' equations for geostrophic flow, described by [Phillips (1963)].

If f is constant, then $\frac{\partial u}{\partial x} + \frac{\partial v}{\partial y}$ vanishes, and the equations simply say that any choice of h can be specified, and gives a steady state. The boundary conditions on u and v imply that h is constant on the boundaries. To illustrate non-trivial solutions, we therefore make the beta-plane assumption $f = f_0 + \beta y$ with f_0 and β constant, then

$$\frac{\partial h}{\partial t} - \frac{\beta h}{f^2} g \frac{\partial h}{\partial x} = 0. \tag{2.73}$$

This is 'Burger's equation', which is well-known to give discontinuous solutions in finite time for all but constant initial data. Given that the equation was derived on the assumption of large-scale behaviour, it is inappropriate to try and find a continuation of the solution past this point; so the model does not define a slow manifold. It is, nevertheless, used in ocean circulation studies since the limitations are less severe when the equivalent approximations are made in the three-dimensional case described in section 2.5.6. It is then referred to as the 'planetary geostrophic' model.

A more useful set of limiting equations for large-scale shallow water flow are obtained by seeking a more accurate approximation. As in the quasi-geostrophic case, first define the geostrophic wind:

$$\begin{aligned} g\frac{\partial h}{\partial x} - fv_g &= 0, \\ g\frac{\partial h}{\partial y} + fu_g &= 0. \end{aligned} \tag{2.74}$$

Note that the true value of f is used, rather than a constant as in equation (2.63). As in section 2.3 we replace the momentum (u, v) by (u_g, v_g) in the

acceleration terms of (2.21). This yields the semi-geostrophic approximation

$$\begin{aligned} \frac{\partial u_g}{\partial t} + u\frac{\partial u_g}{\partial x} + v\frac{\partial u_g}{\partial y} + g\frac{\partial h}{\partial x} - fv = 0, \\ \frac{\partial v_g}{\partial t} + u\frac{\partial v_g}{\partial x} + v\frac{\partial v_g}{\partial y} + g\frac{\partial h}{\partial y} + fu = 0, \\ \frac{\partial h}{\partial t} + \frac{\partial}{\partial x}(hu) + \frac{\partial}{\partial y}(hv) = 0. \end{aligned} \tag{2.75}$$

The equations are again solved in a region Γ with $\mathbf{u}\cdot\mathbf{n} = \mathbf{0}$ on the boundary. They then conserve the energy integral:

$$\int_\Gamma \left(\frac{1}{2}h\left(u_g^2 + v_g^2\right) + \frac{1}{2}gh^2 \right) \mathrm{d}x\mathrm{d}y. \tag{2.76}$$

Comparing (2.76) to the shallow water energy integral (2.22) shows that the kinetic energy has been approximated by its geostrophic value, but the potential energy has not been approximated. This is consistent with the fact that, for $L > L_R$, the energy of disturbances is primarily potential energy.

The proof of energy conservation exploits the point made in section 2.3 that only the momentum is approximated, not the trajectory. The boundary conditions can thus be applied apply only to the trajectory, not the momentum, expressing the fact that no fluid can enter or leave Γ. No boundary conditions need to be applied to h. This can be contrasted with the need to apply boundary conditions to the geostrophic wind in the quasi-geostrophic equations. As well as enabling energy conservation, this will be important in the analysis in subsequent sections.

We can study the behaviour of equations (2.75) by first rearranging them into a single equation for the evolution of h, in the manner of [Schubert (1985)]. The first two equations can be rewritten as

$$\begin{aligned} \mathbf{Q}\begin{pmatrix} u \\ v \end{pmatrix} + g\frac{\partial}{\partial t}\nabla h = fg\begin{pmatrix} -\frac{\partial h}{\partial y} \\ \frac{\partial h}{\partial x} \end{pmatrix}, \\ \mathbf{Q} = \begin{pmatrix} f^2 + f\frac{\partial v_g}{\partial x} & f\frac{\partial v_g}{\partial y} \\ -f\frac{\partial u_g}{\partial x} & f^2 - f\frac{\partial u_g}{\partial y} \end{pmatrix}. \end{aligned} \tag{2.77}$$

Use of the third equation then gives

$$\frac{\partial h}{\partial t} - \nabla\cdot h\mathbf{Q}^{-1}g\frac{\partial}{\partial t}\nabla h = -\nabla\cdot h\mathbf{Q}^{-1}fg\begin{pmatrix} -\frac{\partial h}{\partial y} \\ \frac{\partial h}{\partial x} \end{pmatrix}. \tag{2.78}$$

This equation is elliptic if $\mathbf{Q}$ is positive definite. It has flow-dependent coefficients, as always occurs for approximations valid for $L > L_R$. Applying the boundary condition $\mathbf{u} \cdot \mathbf{n} = 0$ to the first equation of (2.77) multiplied by $\mathbf{Q}^{-1}$ yields the boundary condition

$$\mathbf{Q}^{-1}\nabla\left(\frac{\partial h}{\partial t}\right) \cdot \mathbf{n} = \mathbf{Q}^{-1}\begin{pmatrix} -\frac{\partial h}{\partial y} \\ \frac{\partial h}{\partial x} \end{pmatrix} \cdot \mathbf{n} \tag{2.79}$$

to $\frac{\partial h}{\partial t}$. Provided $\mathbf{Q}$ is positive definite, this gives a Neumann-type boundary condition for equation (2.78).

In the special case of constant f, [Hoskins (1975)] showed that equations (2.75) conserve the potential vorticity

$$\mathcal{Q}_{sg} = \left\{ f^2 + f\left(\frac{\partial v_g}{\partial x} - \frac{\partial u_g}{\partial y}\right) + \frac{\partial u_g}{\partial x}\frac{\partial v_g}{\partial y} - \frac{\partial v_g}{\partial x}\frac{\partial u_g}{\partial y} \right\} / h \tag{2.80}$$

in the sense that

$$\frac{\partial \mathcal{Q}_{sg}}{\partial t} + \mathbf{u} \cdot \nabla \mathcal{Q}_{sg} = 0. \tag{2.81}$$

It is easy to see that $\mathcal{Q}_{sg} = \det\mathbf{Q}$. Thus, given initial data with positive definite $\mathbf{Q}$, we can expect $\mathbf{Q}$ to remain positive definite and equation (2.78) to be solvable. Rigorous results to this effect will be given in section 3.5. If f is not constant, there is no conserved potential vorticity in the sense of (2.81) and the proof of solvability is more difficult. A formal argument proving solvability in this case is given in section 4.3. Assuming this can be made rigorous, the semi-geostrophic system will define a slow manifold. This robust solvability contrasts with the nonlinear balance equations studied in section 2.4.3. However, it is achieved at the price of being accurate in a much more restricted asymptotic regime. Only limited results proving that semi-geostrophic solutions are the limit of shallow water solutions have been obtained so far. These are discussed in section 5.1. The difficulty is that the fast waves can no longer be described by a constant coefficient problem, so the averaging techniques discussed in sections 2.4.4 and 2.4.5 cannot be used.

The semi-geostrophic potential vorticity (2.80) is approximately f times the potential vorticity (2.23). Thus it is positive in both hemispheres if $\mathbf{Q}$ is positive definite. The potential vorticity (2.23) will typically change sign across the equator. To derive (2.80) from (2.23) the vorticity is approximated, but the depth dependence is not. Since, on scales greater than L_R, variations in potential vorticity reflect variations in h rather than in

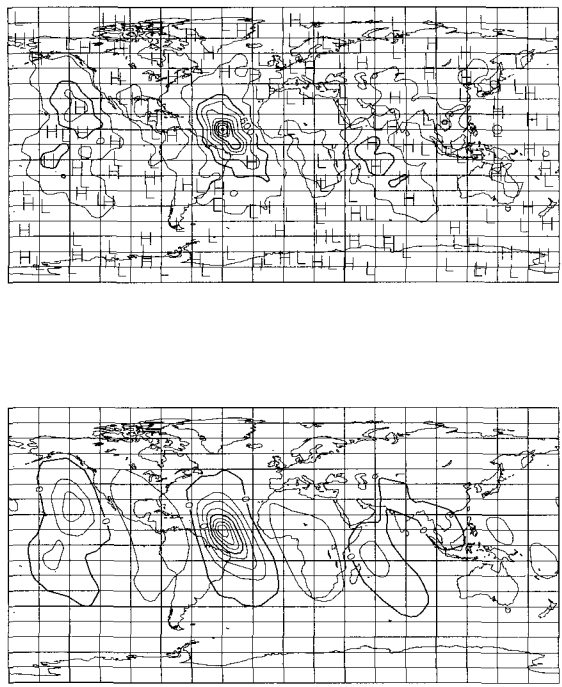

Fig. 2.3 Potential vorticities using depth field from Fig. 2.2 but with $gh_0 = 5000\text{ms}^{-2}\text{s}^{-2}$. Top: Potential vorticity, units $(\text{ms})^{-1}$, contour interval 0.8×10^{-7}. Bottom: Semi-geostrophic potential vorticity, units $10^{-13}(\text{ms})^{-1}\text{s}^{-2}$, contour interval 150.0. From [Cullen (2002)]. ©Royal Meteorological Society, Reading, U.K.

ζ it is appropriate that the depth dependence is not approximated in the definition of $\mathcal{Q}_{sg}$. The approximation to the vorticity is the replacement of ζ by its geostrophic value, plus an extra term. However, this extra term does not make the approximation more accurate, but actually the reverse, [McIntyre and Roulstone (2002)].

These points are illustrated in Fig. 2.3. The same depth field is used as in Fig. 2.2, but the mean value of h is decreased to give L_R=480km, corresponding to a wavelength of about 3000km. Most of the variations in h are on larger scales than this. We see that the potential vorticity distribution is rather similar to the h field shown in Fig. 2.2, and very different from the potential vorticity shown in Fig. 2.2. The semi-geostrophic approximation to it shown in the lower panel of Fig. 2.3 is quite accurate.

2.5 Various approximations to the three-dimensional hydrostatic Boussinesq equations

2.5.1 *The hydrostatic Boussinesq equations*

In order to illustrate how the semi-geostrophic system defined in section 2.3 relates to other approximate systems of equations for the three-dimensional atmosphere, we use a simplification of the shallow atmosphere hydrostatic equations (2.17). We remove all the dissipation and source terms. The hydrostatic relation ensures that Π' is a monotonic function of z, so that the equations can be rewritten with pressure as a vertical coordinate. Following [Hoskins (1975)], define

$$z = \left(1 - \left(\frac{p}{p_{ref}}\right)^{\frac{\gamma-1}{\gamma}}\right) H_s \tag{2.82}$$

where the scale height $H_s = \frac{\gamma p_{ref}}{\rho_{ref} g(\gamma-1)}$, p_{ref} is the reference pressure used in section 2.1, and ρ_{ref} is calculated from p_{ref} and the potential temperature θ_0 used to define the reference state (2.7). z is a function of pressure, defined as the height at which a given pressure is reached in the reference atmosphere defined by (2.7). It is shown by Hoskins that the continuity equation then reduces to $\nabla \cdot (\xi(z)\mathbf{u}) = 0$, where $\xi(z)$ is a function depending on the reference state. The Boussinesq approximation is to set $\xi(z) = 1$, which assumes that fluid particles do not change their pressure very fast following the motion. The equations are solved in a region $\Gamma \in \mathbb{R}^3$ with boundary conditions $\mathbf{u} \cdot \mathbf{n} = 0$. In particular, this implies that the upper and lower boundary conditions are applied on constant pressure surfaces. These features, together with the Boussinesq approximation, are idealisations which will not be accurate at large scales but which aid analysis and are useful for illustrative purposes. Quantitative justification is given by [Hoskins (1982)].

The equations are written in Cartesian coordinates (x, y, z) with z hav-

ing the meaning defined in (2.82). They are

$$\begin{aligned} \frac{\mathrm{D}u}{\mathrm{D}t} - fv + \frac{\partial \varphi}{\partial x} &= 0, \\ \frac{\mathrm{D}v}{\mathrm{D}t} + fu + \frac{\partial \varphi}{\partial y} &= 0, \\ \frac{\mathrm{D}\theta'}{\mathrm{D}t} &= 0, \\ \frac{\partial \varphi}{\partial z} - g\frac{\theta'}{\theta_0} &= 0, \\ \nabla \cdot \mathbf{u} &= 0. \end{aligned} \tag{2.83}$$

φ is a form of geopotential, with units $\mathrm{m}^2\mathrm{s}^{-2}$. Equations (2.83) conserve the energy integral

$$E = \int_\Gamma \left(\frac{1}{2}(u^2 + v^2) - g\theta' z/\theta_0 \right) \mathrm{d}x\mathrm{d}y\mathrm{d}z. \tag{2.84}$$

They also conserve the potential vorticity

$$\mathcal{Q} = (\Xi + (0, 0, f)) \cdot \nabla\theta' \tag{2.85}$$

in the sense that $\mathrm{D}\mathcal{Q}/\mathrm{D}t = 0$. Ξ is defined by

$$\Xi = \left(-\frac{\partial v}{\partial z}, \frac{\partial u}{\partial z}, \frac{\partial v}{\partial x} - \frac{\partial u}{\partial y} \right). \tag{2.86}$$

This equation is derived in [White (2002)].

2.5.2 *Key parameters*

In order to identify the key asymptotic regimes, we follow the same procedure as in section 2.4.2. Much more extensive linear analysis is given in [Gill (1982)], and a linear analysis of the fully compressible equations in spherical geometry is given in [Thuburn et al. (2001)]. We linearise (2.83) about a state of rest given by

$$\begin{aligned} u = v = w &= 0, \\ \frac{g}{\theta_0}\frac{\partial \overline{\theta}}{\partial z} &= N^2, \\ \frac{\partial \overline{\varphi}}{\partial z} - g\frac{\overline{\theta}}{\theta_0} &= 0. \end{aligned} \tag{2.87}$$

where N^2 is a constant Brunt-Väisälä frequency. We seek a general solution $u = u', v = v', w = w', \theta' = \overline{\theta} + \theta", \varphi = \overline{\varphi} + \varphi'$. We temporarily assume periodic boundary conditions on $u', v', w', \theta", \varphi'$ in all three directions, and assume that f is constant. Assume that u' takes the form $\hat{u}\exp^{i(kx+ly+mz-\omega t)}$, with similar definitions for $\hat{v}, \hat{w}, \hat{\theta}$ and $\hat{\varphi}$. Then the condition for non-trivial solutions is that

$$\begin{aligned} \omega = & \quad 0, \\ = & \pm \tfrac{1}{m}\sqrt{N^2(k^2+l^2)+f^2m^2}. \end{aligned} \tag{2.88}$$

As in the shallow water case, section 2.4.2, the solution $\omega = 0$ corresponds to a Rossby wave. The other solutions correspond to inertia-gravity waves. The inertia-gravity wave frequency is

$$\varpi = \sqrt{N^2m^{-2}(k^2+l^2)+f^2}. \tag{2.89}$$

ϖ is made up of two terms, as in the shallow water case (2.36). The first describes pure gravity waves. This term can tend to zero if $(k^2+l^2)/m^2 \to 0$, which implies that the aspect ratio $H/L \to 0$. This is different from the shallow water case where the term can only tend to zero as $k^2 + l^2 \to 0$, implying infinitely large horizontal scale. This means that an asymptotic regime based on assuming that this contribution to ϖ will be uniformly large is not robust. The second term in ϖ is the same as in the shallow water case, implying that the inertia-gravity wave frequency is always greater than f. The two terms are equal if

$$1/\sqrt{(k^2+l^2)} = N/(mf) \equiv L_R \tag{2.90}$$

where L_R is the Rossby radius of deformation. The condition $L = L_R$ can also be written as that the aspect ratio $H/L = \sqrt{(k^2+l^2)}/m = N/f$. A typical value of this ratio is 0.01 in the troposphere, which is similar to the observed aspect ratio of weather systems. Flows with frequency less than ϖ and aspect ratios greater than f/N are stratification dominated, flows with frequency less than ϖ and aspect ratios less than f/N are rotation dominated.

2.5.3 *General equations for slow solutions*

As in section 2.4.3, we identify asymptotic regimes where the horizontal flow speed is smaller than the horizontal component of the inertia-gravity

wave speed. Using (2.89) we thus set

$$\varepsilon = U/\sqrt{N^2 m^{-2} + f^2(k^2+l^2)^{-1}}. \tag{2.91}$$

Equations (2.83) can be rewritten in terms of the vertical component of the vorticity, $\zeta = \partial v/\partial x - \partial u/\partial y$, and the horizontal divergence, $\Delta = \partial u/\partial x + \partial v/\partial y$, in the manner of (2.47). The horizontal momentum equations become

$$\begin{aligned} \frac{\partial \zeta}{\partial t} + u\frac{\partial(\zeta+f)}{\partial x} + v\frac{\partial(\zeta+f)}{\partial y} + (\zeta+f)\,\Delta + \\ \frac{\partial w}{\partial x}\frac{\partial v}{\partial z} - \frac{\partial w}{\partial y}\frac{\partial u}{\partial z} = 0, \\ \frac{\partial \Delta}{\partial t} + u\frac{\partial \Delta}{\partial x} + v\frac{\partial \Delta}{\partial y} + D^2 - 2J(u,v) + \\ \frac{\partial w}{\partial x}\frac{\partial u}{\partial z} + \frac{\partial w}{\partial y}\frac{\partial v}{\partial z} + \nabla_z^2\varphi - \nabla_z\cdot(fv,-fu) = 0, \end{aligned} \tag{2.92}$$

where $\nabla_z\cdot \equiv \partial/\partial x + \partial/\partial y$, $\nabla_z \equiv (\partial/\partial x, \partial/\partial y)$ and $\nabla_z^2 \equiv \nabla_z\cdot\nabla_z$. Write $(u,v,0) \equiv \mathbf{u}_z$. As before, we differentiate the second equation with respect to time and substitute from the first equation. This gives

$$\begin{aligned} \frac{\partial^2 \Delta}{\partial t^2} + f(\zeta+f)\Delta + \nabla_z^2\frac{\partial \varphi}{\partial t} = \\ g\Delta\nabla_z^2\varphi + 2g\nabla_z\Delta\nabla_z\varphi + \\ -f\mathbf{u}_z\cdot\nabla_z(\zeta+2f) + 2\frac{\partial}{\partial t}J(u,v) + \text{remainder}. \end{aligned} \tag{2.93}$$

Then differentiate with respect to z and substitute from the third, fourth and fifth equations of (2.83). This gives, after including additional terms in 'remainder',

$$\begin{aligned} -\frac{\partial^2}{\partial t^2}\frac{\partial^2 w}{\partial z^2} - f\frac{\partial}{\partial z}\left((\zeta+f)\frac{\partial w}{\partial z}\right) - \nabla_z^2\left(w\frac{g}{\theta_0}\frac{\partial \theta'}{\partial z}\right) = \\ \nabla_z^2\left(\frac{g}{\theta_0}\mathbf{u}_z\cdot\nabla_z\theta'\right) \\ +\frac{\partial}{\partial z}\left(-f\mathbf{u}_z\cdot\nabla_z(\zeta+2f) + 2\frac{\partial}{\partial t}J(u,v)\right) + \text{new remainder}. \end{aligned} \tag{2.94}$$

The linearisation of this equation is

$$\frac{\partial^2}{\partial t^2}\frac{\partial^2 w}{\partial z^2} + f^2\frac{\partial^2 w}{\partial z^2}, + N^2\nabla_z^2 w = 0 \tag{2.95}$$

where the Brunt-Väisälä frequency $N = \sqrt{\left(\frac{g}{\theta_0}\frac{\partial\theta'}{\partial z}\right)}$. This equation describes inertia-gravity waves with the frequency ϖ calculated in (2.89). Thus, as in section 2.4.3, equation (2.94) can be approximated in the regime $\varepsilon \ll 1$ by

$$f\frac{\partial}{\partial z}\left((\zeta+f)\frac{\partial w}{\partial z}\right) + \nabla_z^2(N^2 w) = \tag{2.96}$$
$$-\frac{g}{\theta_0}\nabla_z^2\left((u,v,0)\cdot\nabla_z\theta'\right) - \frac{\partial}{\partial z}\left(-f\mathbf{u}_z\cdot\nabla(\zeta+2f) + 2\frac{\partial}{\partial t}J(u,v)\right),$$

where once again it can be shown that it is consistent to have neglected the terms in 'new remainder'.

Introduce a stream-function ψ defined as in the text following (2.50). Then the approximation (2.96) to (2.94) can be shown to be consistent with approximating the second equation of (2.92) by

$$-2J\left(\frac{\partial\psi}{\partial x},\frac{\partial\psi}{\partial y}\right) + \nabla_z^2\varphi - \nabla_z\cdot(f\nabla_z\psi) = 0, \tag{2.97}$$

and the first equation by

$$\frac{\partial\zeta}{\partial t} + u\frac{\partial(\zeta+f)}{\partial x} + v\frac{\partial(\zeta+f)}{\partial y} + (\zeta+f)\,\Delta + \tag{2.98}$$
$$\frac{\partial w}{\partial x}\frac{\partial^2\psi}{\partial z\partial x} + \frac{\partial w}{\partial y}\frac{\partial^2\psi}{\partial z\partial y} = 0.$$

The third equation of (2.83) can be rewritten, using the fourth equation, as

$$\frac{\mathrm{D}}{\mathrm{D}t}\frac{\partial^2\varphi}{\partial z^2} + \Delta\frac{\partial^2\varphi}{\partial z^2} = -\frac{\partial u}{\partial z}\frac{\partial^2\varphi}{\partial z\partial x} - \frac{\partial v}{\partial z}\frac{\partial^2\varphi}{\partial z\partial y}. \tag{2.99}$$

The system of equations comprising the time derivative of equation (2.97) and equations (2.98), (2.97) and (2.99) are essentially the equations used in [McWilliams et al. (1999)], subject to changes in notation and the use of isentropic coordinates, (i.e. using potential temperature as a

coordinate), in that paper. They can be written

$$\begin{pmatrix} F & \partial^2/\partial z^2 & 0 \\ 0 & \nabla^2 & -M \\ G & 0 & \nabla^2 \end{pmatrix} \begin{pmatrix} \chi \\ \partial\varphi/\partial t \\ \partial\psi/\partial t \end{pmatrix} = \tag{2.100}$$
$$\begin{pmatrix} -J(\psi, \partial^2\varphi/\partial z^2) - J(\partial\psi/\partial z, \partial\varphi/\partial z) \\ 0 \\ -J(\psi, \zeta + f) \end{pmatrix},$$

where

$$\begin{aligned} \nabla_z^2 \chi &= \Delta, \\ F &= \nabla_z \cdot (\partial^2\varphi/\partial z^2 \nabla_z) + \nabla_z \cdot \partial\varphi/\partial z \partial/\partial z \nabla_z, \\ M &= \nabla_z \cdot (f\nabla_z) + 2\left(\frac{\partial^2\psi}{\partial x^2}\frac{\partial^2}{\partial y^2} + \frac{\partial^2\psi}{\partial y^2}\frac{\partial^2}{\partial x^2}\right) - 2\frac{\partial^2\psi}{\partial x \partial y}\frac{\partial^2}{\partial x \partial y}, \\ G &= \nabla_z \cdot ((\zeta + f)\nabla_z) + \nabla_z(\partial\psi/\partial z) \cdot \nabla_z \int_0^z \mathrm{d}z'. \end{aligned} \tag{2.101}$$

Write (2.100) symbolically as

$$\mathbf{Lu} = \mathbf{A}. \tag{2.102}$$

Solvability of this equation depends on the same conditions as those written out in section 2.4.3. Condition (i) is more restrictive in that it implies that $\partial\theta/\partial z$ does not change sign. It can be shown that the product of conditions (i) and (ii) requires that the potential vorticity does not change sign, so that spontaneous violations are only possible if both terms change sign simultaneously. Condition (iii) is again liable to spontaneous violations as it is not a constant of the motion. The same discussion as in section 2.4.3 applies to estimating the time for which condition (iii) will be satisfied, given assumptions on the initial data. We infer that it is not possible to define a slow manifold by a single set of equations for all cases where $\varepsilon \ll 1$. We therefore seek limit solutions in the cases $Fr < Ro$, $Fr = Ro$ and $Ro < Fr$ separately. These correspond to aspect ratios H/L greater than, equal to, or less than f/N respectively.

2.5.4 *Slow solutions on with large aspect ratio*

This case corresponds to $\varepsilon \ll 1$ with $Fr < Ro$. The limiting behaviour is extensively analysed in [Majda (2003)] and only a few key results are given here. In the shallow water case described in section 2.4.4, it was

shown that the limiting solution was given by the solution of the equations for two-dimensional incompressible flow. In the present case the solution is given by two-dimensional incompressible flow for each z. Laboratory experiments demonstrating this were shown by [Fincham et al. (1996)].

In a similar way to the shallow water case, the assumption that $Fr \ll 1$ but $Ro = O(1)$ requires that the horizontal gradients of $\partial\theta/\partial z$ are $\mathrm{O}(Fr^2)$ of the mean value. The third equation of (2.83) can then only be satisfied if $W \simeq Fr^2UH/L$ so that the fifth equation of (2.83) implies that $\Delta \simeq Fr^2U/L$. In the vorticity form of the momentum equation, (2.92), the assumption $Ro = O(1)$ means that the term $f\Delta$ is much smaller than $\mathbf{u}_z \cdot \nabla_z(\zeta + f)$. Therefore the general vorticity equation (2.98) for small ε can be further approximated by

$$\frac{\partial \zeta}{\partial t} - \frac{\partial \psi}{\partial y}\frac{\partial(\zeta + f)}{\partial x} + \frac{\partial \psi}{\partial x}\frac{\partial(\zeta + f)}{\partial y} = 0. \tag{2.103}$$

Equations (2.103) and (2.97) are exactly the equations for two-dimensional incompressible flow (2.57). Their analytic properties are thus as summarised in section 2.4.4. φ is determined diagnostically from (2.97). The third equation of (2.83) is no longer used, but is replaced by a calculation of θ' from φ using the fourth equation of (2.83). However, if the vertical scale becomes small, this calculation may give unrealistic values, noting that the third equation of (2.83) states that values of θ' have to be bounded by their initial values. The assumption of low Froude number means that the vertical scale is large compared with U/N. Thus, provided Fr remains small everywhere, the values of θ' should be realistic.

The conservation of the potential vorticity, (2.85), is replaced by the conservation of $(\zeta + f)N^2\theta_0/g$. The simplification of the thermodynamic contribution to the potential vorticity is expected because potential vorticity variations are similar to vorticity variations if the aspect ratio is large, exactly analogously to the shallow water case.

The weakness of this system is that there is no control over the vertical scale. Since each level can evolve independently, if there is any initial variation of $\mathbf{u}$ in z it will magnify in time. Such behaviour is illustrated by exact solutions in [Majda (2003)] and in the experiments of [Fincham et al. (1996)]. This means that the vertical scale of the flow will reduce in time. Thus the assumption $Fr < Ro$ which implies an aspect ratio $H/L > f/N$ will be violated as the solution develops, and equations (2.103) and (2.97) will no longer be an accurate approximation to the full governing equations.

As discussed by [Majda (2003)], the vertical scale can be controlled by

viscosity, in which case the small value of Fr can be maintained. It may also be controlled by rotation, in which case the reduction in aspect ratio is arrested when $H/L \simeq f/N$, and the quasi-geostrophic limit equations described in section 2.5.5 become appropriate.

2.5.5 *Quasi-geostrophic solutions*

In this section we assume $Ro = Fr \ll 1$. Thus $\varepsilon = Ro/\sqrt{2}$. As in the shallow water case, section 2.4.5, the lowest order solution contains no prognostic information and is self-contradictory if f is a function of position. We therefore define the geostrophic wind by

$$\begin{aligned} \frac{\partial \varphi}{\partial x} - f_0 v_g &= 0, \\ \frac{\partial \varphi}{\partial y} + f_0 u_g &= 0, \end{aligned} \tag{2.104}$$

where f_0 is a constant, representative, value of f. Then $\nabla_z \cdot \mathbf{u}_g = 0$ and so the vertical velocity w is entirely ageostrophic. The ageostrophic horizontal wind $(u, v, 0) - (u_g, v_g, 0)$ is assumed to be much less than $(u_g, v_g, 0)$. The vertical component of the vorticity ζ is thus approximated by its geostrophic value ζ_g. Equations (2.97) and (2.98) for the general case $\varepsilon \ll 1$ are further approximated by

$$\nabla_z^2 \varphi - f_0 \zeta_g = 0, \tag{2.105}$$

and

$$\frac{\partial \zeta_g}{\partial t} + u_g \frac{\partial (\zeta_g + f)}{\partial x} + v_g \frac{\partial (\zeta_g + f)}{\partial y} + f_0 \Delta = 0. \tag{2.106}$$

Equation (2.104), together with $Fr \ll 1$, means that $N^2 \nabla_z \simeq FrN^2/L$, so that the third equation of (2.83) can be approximated by

$$\frac{\partial \theta'}{\partial t} + u_g \frac{\partial \theta'}{\partial x} + v_g \frac{\partial \theta'}{\partial y} + wN^2 \frac{\theta_0}{g} = 0. \tag{2.107}$$

The system of equations is completed by the fourth and fifth equations of (2.83).

Once again the equations are to be solved in a closed region Γ. As in the shallow water case, in order to achieve energy conservation we require both $\mathbf{u_g} \cdot \mathbf{n} = 0$ and $\mathbf{u} \cdot \mathbf{n} = 0$ on the boundary of Γ. The former condition implies that φ is constant along the intersection of the boundary of Γ with

each constant z surface. The conserved energy integral is

$$E = \int_\Gamma \left(\frac{1}{2}(u_g^2 + v_g^2) - g\theta' z/\theta_0 \right) \mathrm{d}x\mathrm{d}y\mathrm{d}z. \tag{2.108}$$

The quasi-geostrophic potential vorticity,

$$\mathcal{Q}_g = (\zeta_g + f)\frac{\theta_0}{g}N^2 + f\frac{\partial \theta'}{\partial z} \tag{2.109}$$

satisfies the conservation law

$$\frac{\partial \mathcal{Q}_g}{\partial t} + \mathbf{u_g} \cdot \nabla \mathcal{Q}_g = 0. \tag{2.110}$$

Note that both the vorticity and the thermodynamic contributions to the potential vorticity (2.85) have been approximated. The solution of equations (2.105), (2.106) and (2.107) can therefore be obtained by transporting $\mathcal{Q}_g$ with velocity $\mathbf{u_g}$ and calculating the other fields from $\mathcal{Q}_g$. The potential vorticity inversion relation obtained from (2.109) is

$$\mathcal{Q}_g - \frac{f\theta_0 N^2}{g} = \frac{f_0^{-1}\theta_0}{g}\left(\nabla_z^2 \varphi + f_0^2 \frac{\partial^2 \varphi}{\partial z^2} \right). \tag{2.111}$$

This is a constant coefficient Poisson equation, so no solvability issues arise. It requires boundary conditions. In addition to those imposed by energy conservation requirements, it is normal to specify Neumann boundary conditions on constant z surfaces as in [Hoskins et al. (1985)]. This is equivalent to specifying θ'. While the solution of (2.111) for φ means that good regularity estimates can be obtained in the interior of Γ, it is an open question whether the regularity of θ' can be maintained along the boundary. Most results have therefore been proved with θ' required to be a constant on the parts of the boundary which are surfaces of constant z.

Results on the behaviour of these equations are given by [Babin et al. (1999)], [Babin et al. (2002)], [Bourgeois and Beale (1994)] and [Majda (2003)]. The results quoted are from [Bourgeois and Beale (1994)] as they are presented in a way consistent with the results we discuss later for the rotation dominated regime. As stated in that paper, the regularity assumptions are probably far from optimal.

In [Bourgeois and Beale (1994)] the system (2.105), (2.106), (2.107) and the last two equations of (2.83) are solved in a rectangular box with periodic boundary conditions with period L in x and y and rigid boundaries at $z = 0$ and $z = H$. Define the region of integration Γ as $B \times (0, H)$, where $B = \left((-\frac{1}{2}L, \frac{1}{2}L) \times (-\frac{1}{2}L, \frac{1}{2}L)\right)$. Write Γ_z for the horizontal cross-section

$B \times \{z\}$. Since the solution is unaltered by adding an arbitrary constant to the geopotential φ, set $\int_\Gamma \varphi(x,y,z)\mathrm{d}x\mathrm{d}y\mathrm{d}z = 0$. Assume that θ' is constant on $z = 0$ and $z = H$. Since $w = 0$ on $z = 0, H$, equation (2.107) ensures that θ' will remain constant there if it is constant initially. It is also assumed that f is given by the beta-plane approximation $f = f_0 + \beta y$. This gives the system QGS of [Bourgeois and Beale (1994)], p. 1030, subject to changes in notation.

In order to set out their results, we need to define some function spaces. Only brief definitions are given here. More detailed background can be found in the textbook of [Adams (1975)]. Here H^s denotes the Sobolev space of horizontally periodic functions on Γ with square integrable generalised derivatives up to order s. C denotes the space of continuous functions. The L^p norm of a function u on Γ is

$$\left(\int_\gamma u^p \mathrm{d}x\mathrm{d}y\mathrm{d}z\right)^{\frac{1}{p}}. \tag{2.112}$$

If $p = \infty$, the L^p norm is the maximum value of $|u|$. The notation $|u|_n$ indicates the sum of the L^2 norms of all partial derivatives of total orders up to n. If $u(t,\cdot)$ is a function of x, y, z and t, the notation $|u|_{n,T}$ represents $\sup_{0\le t\le T}|u(t,\cdot)|_n$

The first result is

Theorem 2.1 *(QGS short time existence). If the initial potential vorticity $\mathcal{Q}_g(0,x,y,z)$ is in $H^s(\Gamma)$ for some $s > 3$, with $|\mathcal{Q}_g(0,\cdot)| \le M$, then there exists a time $T^* > 0$ and a solution $\mathcal{Q}_g$ in $C([0,T^*)]; H^s(\Gamma))$ to QGS, where T^* depends only on M, Γ, N, f_0 and β. The potential vorticity satisfies the estimate $|\mathcal{Q}_g|_{s,T^*} \le 2M$.*

The next result is that

Theorem 2.2 *(QGS global existence). If $\mathcal{Q}_g(0,\cdot)$ is in $H^s(\Gamma)$ for some $s \ge 3$, then given any time $T > 0$ there exists a solution $\mathcal{Q}_g(t,\cdot) \in C([0,T]; H^s(\Gamma))$ to QGS.*

The latter result means that the quasi-geostrophic equations, with isentropic upper and lower boundary conditions, can be integrated for arbitrarily long times. They therefore from a slow manifold. We now wish to estimate the distance of the exact solution from the slow manifold. It would be natural to use equations (2.83) as the exact equations. However, the hydrostatic approximation included in these equations makes them impossible to solve. A solution is to relax the hydrostatic approximation to

give the 'non-hydrostatic Boussinesq' equations. The improved behaviour is demonstrated by [Lions et al. (1992)]. The fourth equation of (2.83) is replaced by

$$\frac{\mathrm{D}w}{\mathrm{D}t} + \frac{\partial \varphi}{\partial z} - g\frac{\theta'}{\theta_0} = 0. \tag{2.113}$$

The resulting equations are the same as the SPE equations of [Bourgeois and Beale (1994)] but in dimensional form. It is then proved that (Theorem 4.5 of [Bourgeois and Beale (1994)])

Theorem 2.3 *Assume we are given time $T > 0$ and initial QGS geostrophic wind $\mathbf{u}_g$ and potential temperature satisfying (2.104) and the fourth equation of (2.83) for some φ. φ has to be in $H^5(\Gamma)$ and satisfy the boundary conditions $\partial\varphi/\partial z = \partial^3\varphi/\partial z^3 = 0$ on Γ_0 and Γ_H. Let $\mathbf{U}_g$ in $C([0,T]); H^6(\Gamma))$ be the solution of QGS with this initial data. Consider initial SPE data $\mathbf{U}_\epsilon(0,\cdot) \equiv (u_\varepsilon(0,\cdot), v_\varepsilon(0,\cdot), w_\varepsilon(0,\cdot), \theta'_\varepsilon(0,\cdot))$ satisfying*

$$\begin{aligned} \partial u/\partial z = \partial^3 u/\partial z^3 = 0, \\ \partial v/\partial z = \partial^3 v/\partial z^3 = 0, \\ w = \partial^2 w/\partial z^2 = 0, \\ \theta = \partial^2\theta'/\partial z^2 = 0, \end{aligned} \tag{2.114}$$

on Γ_0 and Γ_z, and also satisfying the estimate

$$|\mathbf{U}_\varepsilon(0,\cdot) - \mathbf{U}_g(0,\cdot)|_4 = O(\varepsilon). \tag{2.115}$$

Then there exists $\varepsilon_0 > 0$ and solutions $\mathbf{U}_\epsilon(t,\cdot)$ in $C([0,T]); H^5(\Gamma))$ to SPE for all $\varepsilon \leq \varepsilon_0$ which converge to the QGS solution in $C([0,T]); H^5(\Gamma))$ with $O(\varepsilon)$ accuracy, i.e.

$$|\mathbf{U}_\varepsilon(t,\cdot) - \mathbf{U}_g(t,\cdot)|_{4,T} = O(\varepsilon). \tag{2.116}$$

Note that in [Bourgeois and Beale (1994)] the proof is only given for the case $\beta = 0$, but the result is stated as true for $\beta \geq 0$. The main limitation is that an arbitrary ε_0 cannot be specified,. It is very likely that ε_0 will decrease as the time T over which convergence is required increases. In particular, it is not clear whether T is large enough for physical relevance of the result.

It is also shown in [Bourgeois and Beale (1994)] that higher order estimates can be made if the quasi-geostrophic system is expanded to higher

order in ε. The method is first to solve QGS, and then to solve a similar equation for the next order correction. The result is

Theorem 2.4 *Given time $T > 0$, a solution $\mathbf{U}_g$ of QGS in $C([0,T]);H^{s+1}(\Gamma))$ and initial data $\mathbf{U}_1$ in $H^s(\Gamma)$, for some $s \geq 3$, there exists a unique solution $\mathbf{U}_1$ in $C([0,T]);H^s(\Gamma))$ for the first order correction to the geostrophic wind and potential temperature.*

The effect of this is that, after solving QGS, an auxiliary problem can be solved to correct the solution to higher accuracy. In [Muraki et al. (1999)] a similar procedure is followed, and shown by computations to agree much more closely with numerical solutions of (2.83). The result means that the QGS solutions have to be qualitatively correct over the entire time interval, so that they can be refined by a subsequent correction step. Thus the feedback of the correction term on the original QGS solution can be ignored, and does not prevent convergence of SPE to the corrected QGS at an $O(\varepsilon^2)$ rate over the entire time interval. The result is as follows:

Theorem 2.5 *Assume we are given time $T > 0$ and initial QGS geostrophic wind and potential temperature $\mathbf{U}_g(o,\cdot)$ in $H^6(\Gamma)$ satisfying the conditions stated in Theorem 2.3. Let $\mathbf{U}_g(t,\cdot)$ in $(C([0,T]);H^{s+1}(\Gamma))$ be the solution of QGS for this initial data. Define $\mathbf{U}_1(t,\cdot)$ in $H^5(\Gamma)$ by*

$$\begin{aligned} u_1(0,\cdot) &= -\left[\frac{\partial v_g}{\partial t} + \mathbf{u}_g \cdot \nabla v_g\right]_{t=0}, \\ v_1(0,\cdot) &= -\left[\frac{\partial u_g}{\partial t} + \mathbf{u}_g \cdot \nabla u_g\right]_{t=0}, \\ w_1(0,\cdot) &= -\left[\frac{\partial \theta}{\partial t} + \mathbf{u}_g \cdot \nabla \theta\right]_{t=0}, \\ \theta_1(0,\cdot) &= 0. \end{aligned} \tag{2.117}$$

Let $\mathbf{U}_1$ in $(C([0,T]);H^5(\Gamma))$ be the formal first order correction to QGS guaranteed by Theorem 2.4. Consider initial data for SPE satisfying (2.114) on Γ_0 and Γ_z and additionally satisfying

$$|\mathbf{U}_\varepsilon - (\mathbf{U}_g + \varepsilon \mathbf{U}_1)|_4 = O(\varepsilon^2). \tag{2.118}$$

Then if $\mathbf{U}_\varepsilon$ is the solution of SPE for this data for all $\varepsilon \leq \varepsilon_0$, whose existence is guaranteed by Theorem 2.3, the SPE solutions converge to $\mathbf{U}_g + \varepsilon \mathbf{U}_1$ with $O(\varepsilon^2)$ accuracy, i.e.

$$|\mathbf{U}_\varepsilon - (\mathbf{U}_g + \varepsilon \mathbf{U}_1)|_{3,T} = O(\varepsilon^2). \tag{2.119}$$

However, as with Theorem 2.3, the result is only true for $\varepsilon \leq \varepsilon_0$ for some ε_0 which may depend on T. We do not know if T is large enough for physical relevance. In particular, it may be that the value of ε_0 required for second order accuracy is much less than that required for first order accuracy. Subject to this limitation, the result implies very high predictability in this asymptotic regime, because solutions of QGS are well-behaved, as shown in Theorem 2.2.

The main limitation on the applicability of the quasi-geostrophic results is that the constant coefficient assumptions in equations (2.104) and (2.107) are not valid on large scales, thus explaining the failure of quasi-geostrophic models in operational weather forecasting trials in the 1950s. Another limitation is the choice of boundary conditions. However, the constant coefficient assumption and simple boundary conditions enable extensive studies of the analytic behaviour, as we have illustrated. They also enable analytic solutions which have been very important in understanding extra-tropical weather systems, see [Pedlosky (1987)] and [Gill (1982)].

2.5.6 *Slow solutions with small aspect ratio*

In this section we assume $Ro \ll 1$, $Ro < Fr$. This corresponds to assuming an aspect ratio less than f/N. The assumption $Ro \ll 1$ means that the first two equations of (2.83) can be approximated by the geostrophic relations

$$\begin{aligned} \frac{\partial \varphi}{\partial x} - fv &= 0, \\ \frac{\partial \varphi}{\partial y} + fu &= 0. \end{aligned} \tag{2.120}$$

Using the hydrostatic relation from (2.83), the second derivative with respect to z of (2.120) gives

$$\frac{g}{\theta_0}\frac{\partial^2 \theta'}{\partial z \partial x} = f\frac{\partial v}{\partial z}, \quad \frac{g}{\theta_0}\frac{\partial^2 \theta'}{\partial z \partial y} = -f\frac{\partial u}{\partial z}. \tag{2.121}$$

Thus, allowing for the possibility of a mean value of N^2 such that the left hand side of (2.121) is less than N^2/L, we have $N^2/L \geq fU/L$, so, as in section 2.4.6, $Fr^2 \leq Ro$. Thus the remaining equations in (2.83) cannot be approximated without incurring an error of order $\sqrt{(Ro)}$. The resulting equations are called the planetary geostrophic equations, or the Type 2 geostrophic equations of [Phillips (1963)]. Unlike the shallow water case analysed in section 2.4.6, the equations now have non-trivial solutions since

(2.120) does not imply that $\mathbf{u} \cdot \nabla\theta = 0$. The equations conserve the energy integral

$$\int_\Gamma -g\theta' z/\theta_0 \mathrm{d}x\mathrm{d}y\mathrm{d}z, \tag{2.122}$$

provided that $w = 0$ on those parts of the boundary which are not parallel to the z axis. In contrast to the case of large aspect ratio, the energy is entirely potential energy. However, equations (2.120) and the fifth equation of (2.83) may not be compatible with this condition unless f is constant, in which case $w = 0$ everywhere. The conserved potential vorticity is $f\partial\theta'/\partial z$, which retains the temperature dependence of the exact potential vorticity (2.85) but loses the velocity dependence.

The difficulty with the boundary conditions also makes the equations impossible to solve in a sufficiently general context to be useful. If the potential vorticity is known, $\partial^2\varphi/\partial z^2$ can be determined from the fourth equation of (2.83). It would then be possible to solve for φ if θ' was given on all parts of the boundary not parallel to the z axis. If Γ is rectangular, with boundaries including $z = 0, H$, then if f is constant and θ' is constant on $z = 0, H$ initially, it will remain so and the equations can be solved. However the assumption of large horizontal scale means that f should be regarded as a function of position, in which case no compatible boundary conditions are available.

As in the shallow water case, the semi-geostrophic approximation gives a more useful and mathematically well-posed system. The geostrophic wind is first defined by

$$\begin{aligned} \frac{\partial\varphi}{\partial x} &= fv_g, \\ \frac{\partial\varphi}{\partial y} &= -fu_g. \end{aligned} \tag{2.123}$$

The momentum is then replaced by its geostrophic value in (2.83), while the remaining equations are not approximated. The resulting system is

$$\begin{aligned}
\frac{\mathrm{D}u_g}{\mathrm{D}t} - fv + \frac{\partial \varphi}{\partial x} &= 0, \\
\frac{\mathrm{D}v_g}{\mathrm{D}t} + fu + \frac{\partial \varphi}{\partial y} &= 0, \\
\frac{\mathrm{D}\theta'}{\mathrm{D}t} &= 0, \\
\frac{\partial \varphi}{\partial z} - g\frac{\theta'}{\theta_0} &= 0, \\
\nabla \cdot \mathbf{u} &= 0.
\end{aligned} \tag{2.124}$$

These equations were introduced and analysed by [Hoskins (1975)]. Given the boundary conditions $\mathbf{u}\cdot\mathbf{n} = 0$ on the boundary of Γ, they conserve the energy integral

$$E_g = \int_\Gamma \left(\frac{1}{2}(u_g^2 + v_g^2) - g\theta' z/\theta_0 \right) \mathrm{d}x\mathrm{d}y\mathrm{d}z. \tag{2.125}$$

The kinetic energy has been approximated by its geostrophic value, but the potential energy is not approximated.

In the case when f is constant, the equations also conserve the potential vorticity

$$\mathcal{Q}_{sg} = \det \begin{pmatrix} f^2 + f\frac{\partial v_g}{\partial x} & f\frac{\partial v_g}{\partial y} & f\frac{\partial v_g}{\partial z} \\ -f\frac{\partial u_g}{\partial x} & f^2 - f\frac{\partial u_g}{\partial y} & -f\frac{\partial u_g}{\partial z} \\ \frac{g}{\theta_0}\frac{\partial \theta'}{\partial x} & \frac{g}{\theta_0}\frac{\partial \theta'}{\partial y} & \frac{g}{\theta_0}\frac{\partial \theta'}{\partial z} \end{pmatrix}. \tag{2.126}$$

The vorticity dependence of the true potential vorticity has been approximated. The temperature dependence is the same as that for the potential vorticity derived from the non-hydrostatic generalisation (2.113) of (2.83). However, if f is a function of position there is no invariant of this kind.

The geostrophic momentum approximation used to derive (2.124) is a Lagrangian approximation in the sense that the neglected term is $\mathrm{D}(\mathbf{u} - \mathbf{u}_g)/\mathrm{D}t$, but the $\mathrm{D}/\mathrm{D}t$ operator has not been approximated. As discussed in section 2.3, this is equivalent to requiring the rate of change of wind direction to be much less than f, but the rate of change of the magnitude of the wind is not restricted. Because the thermodynamic terms in the equations have not been approximated, the equations are also asymptotically correct in the limit $Fr \to 0$, even if there is no rotation. This is because the limiting solution of (2.83) as $Fr \to 0$ with $f = 0$ is a state of rest in hydrostatic balance where the fluid has been rearranged so that

θ' is monotonically increasing with z. This state is determined only by consistency with the last three equations of (2.83), none of which have been approximated. The semi-geostrophic equations, however, do not describe the flow accurately in this limit, the appropriate equations are those discussed in section 2.5.4. The correctness of this limit is important in applying semi-geostrophic theory globally, since it allows the correct limiting rest state to be obtained at the equator.

The assumption of small aspect ratio is appropriate for large-scale weather systems. The semi-geostrophic equations have a similar structure to the quasi-geostrophic equations discussed in section 2.5.5, but do not make the constant coefficient assumptions which prevented the quasi-geostrophic system being a useful tool for operational weather forecasting. In particular, the full Coriolis parameter is used wherever it appears, the static stability $\partial\theta'/\partial z$ is not replaced by a reference state value, and the natural boundary conditions of no normal flow are all that are required. The energy conservation property holds with this choice of boundary conditions. The remaining chapters of this book analyse this system, showing that it is well-posed and can thus define a slow manifold. They also demonstrate that the equations have solutions which contain much of the physics of observed large-scale flows.

Chapter 3

Solution of the semi-geostrophic equations in plane geometry

3.1 The solution as a sequence of minimum energy states

3.1.1 *The evolution equation for the geopotential*

In this chapter we show that, in the special case of constant Coriolis parameter f, the semi-geostrophic equations are well-posed, in the sense that they can be solved for arbitrarily large times given physically reasonable boundary conditions. The assumption of constant f is, of course, not compatible with the study of large-scale atmospheric flow. In sections 4.2 and 4.3 we show that the results can be extended to variable f. However, explicit solutions are much easier to construct with constant f, so this case is useful in understanding the physical nature of the solutions. For the same reasons, we use the three-dimensional Boussinesq formulation in pressure-related coordinates derived in section 2.5.1. These assumptions are withdrawn in section 4.1. In this section and section 3.2 we thus use equations (2.124) with f assumed constant. The resulting equations are of incompressible form and are solved with rigid wall boundary conditions.

The combination of incompressible equations with rigid wall boundary conditions in three dimensions is unrealistic as a description of the vertically averaged large-scale flow of the atmosphere. In section 3.3 we therefore study the shallow water semi-geostrophic equations derived in section 2.4.6. The free surface boundary condition allows a correct description of height-independent large-scale atmospheric flow.

Following [Schubert (1985)], equations (2.124) can be rewritten in a similar way to (2.77), which was derived from the shallow water semi-

geostrophic equations:

$$\mathbf{Q}\begin{pmatrix} u \\ v \\ w \end{pmatrix} + \frac{\partial}{\partial t}\nabla\varphi = \begin{pmatrix} f^2 u_g \\ f^2 v_g \\ 0 \end{pmatrix},$$

$$\mathbf{Q} = \begin{pmatrix} f^2 + f\frac{\partial v_g}{\partial x} & f\frac{\partial v_g}{\partial y} & f\frac{\partial v_g}{\partial z} \\ -f\frac{\partial u_g}{\partial x} & f^2 - f\frac{\partial u_g}{\partial y} & -f\frac{\partial u_g}{\partial z} \\ \frac{g}{\theta_0}\frac{\partial \theta'}{\partial x} & \frac{g}{\theta_0}\frac{\partial \theta'}{\partial y} & \frac{g}{\theta_0}\frac{\partial \theta'}{\partial z} \end{pmatrix}. \tag{3.1}$$

Use of the fifth equation of (2.124) then gives

$$\nabla \cdot \mathbf{Q}^{-1}\frac{\partial}{\partial t}\nabla\varphi = \nabla \cdot \mathbf{Q}^{-1}\begin{pmatrix} f^2 u_g \\ f^2 v_g \\ 0 \end{pmatrix}. \tag{3.2}$$

In principle, equation (3.2) can be solved for $\partial\varphi/\partial t$. This requires boundary conditions on $\partial\varphi/\partial t$. Apply the boundary conditions $\mathbf{u}\cdot\mathbf{n}$ to $\mathbf{Q}^{-1}$ times the first equation of (3.1). This gives the boundary condition for (3.2) as

$$\mathbf{Q}^{-1}\frac{\partial}{\partial t}\nabla\varphi\cdot\mathbf{n} = \mathbf{Q}^{-1}\begin{pmatrix} f^2 u_g \\ f^2 v_g \\ 0 \end{pmatrix}\cdot\mathbf{n} \tag{3.3}$$

on the boundary of Γ. If $\mathbf{Q}$ is positive definite and $(\mathbf{Qn})\cdot\mathbf{n} > 0$, then equation (3.2) with (3.3) becomes an elliptic equation to be solved for $\partial\varphi/\partial t$ with a Neumann type boundary condition, and we can expect to be able to solve it. It was stated in section 2.5.6 that det $\mathbf{Q}$ is a constant of the motion. Thus, if det $\mathbf{Q}> 0$ throughout Γ at $t = 0$ it will remain so for all t. However, det $\mathbf{Q}> 0$ is not a sufficient condition for $\mathbf{Q}$ to be positive definite, so there is some work to be done. We can also write $\mathbf{Q}$ as a function of φ as below.

$$\mathbf{Q} = \begin{pmatrix} f^2 + \frac{\partial^2\varphi}{\partial x^2} & \frac{\partial^2\varphi}{\partial x\partial y} & \frac{\partial^2\varphi}{\partial x\partial z} \\ \frac{\partial^2\varphi}{\partial y\partial x} & f^2 + \frac{\partial^2\varphi}{\partial y^2} & \frac{\partial^2\varphi}{\partial y\partial z} \\ \frac{\partial^2\varphi}{\partial z\partial x} & \frac{\partial^2\varphi}{\partial z\partial y} & \frac{\partial^2\varphi}{\partial z^2} \end{pmatrix}. \tag{3.4}$$

Equations (3.1) can be interpreted physically as stating that $\mathbf{u}$ is determined by the requirements of maintaining geostrophic and hydrostatic balance. In a sense, the equations describe a continuous geostrophic adjustment problem which is a nonlinear generalisation of the classical Rossby adjustment problem discussed in section 2.2, equation (2.38).

3.1.2 *Solutions as minimum energy energy states*

In this section we show that a geostrophic and hydrostatic state can be characterised as a stationary point of the energy with respect to Lagrangian parcel displacements, neglecting pressure perturbations resulting from the displacements. The physical significance of the class of variations used will be discussed below. More details of these arguments are given in [Shutts and Cullen (1987)], section 3.

Suppose we have a state of the fluid with an associated vector field $(\tilde{u}, \tilde{v})$ and scalar field $\tilde{\theta}'$. Associate with this state an energy given by the formula analogous to (2.125)

$$E = \int_\Gamma \left(\frac{1}{2}(\tilde{u}^2 + \tilde{v}^2) - g\tilde{\theta}' z/\theta_0 \right) \mathrm{d}x\mathrm{d}y\mathrm{d}z. \tag{3.5}$$

This is a functional of $\tilde{u}, \tilde{v}$ and $\tilde{\theta}'$, regarded as functions of position over Γ, which has the following property.

Theorem 3.1 *The conditions for the energy E to be stationary with respect to variations $\Xi = (\xi, \eta, \chi)$ of particle positions satisfying continuity $\delta(\mathrm{d}x\mathrm{d}y\mathrm{d}z) = 0$ via*

$$\nabla \cdot \Xi = 0 \tag{3.6}$$

in Γ and

$$\delta\tilde{u} = f\eta, \ \delta\tilde{v} = -f\xi, \ \delta\tilde{\theta}' = 0, \tag{3.7}$$

together with $\Xi \cdot \mathbf{n} = 0$ on the boundary of Γ, are that

$$(f\tilde{v}, -f\tilde{u}, g\tilde{\theta}'/\theta_0) = \nabla\tilde{\varphi} \tag{3.8}$$

for some scalar $\tilde{\varphi}$.

Proof We can write

$$\begin{aligned} \delta E &= \int_\Gamma \left(\tilde{u}\delta\tilde{u} + \tilde{v}\delta\tilde{v} - gz\delta\tilde{\theta}'/\theta_0 - g\tilde{\theta}'\chi/\theta_0 \right) \mathrm{d}x\mathrm{d}y\mathrm{d}z, \\ &= \int_\Gamma \left(f\tilde{u}\eta - f\tilde{v}\xi - g\tilde{\theta}'\chi/\theta_0 \right) \mathrm{d}x\mathrm{d}y\mathrm{d}z, \\ &= \int_\Gamma \left(-\Xi \cdot (f\tilde{v}, -f\tilde{u}, g\tilde{\theta}'/\theta_0 \right) \mathrm{d}x\mathrm{d}y\mathrm{d}z. \end{aligned} \tag{3.9}$$

For this to vanish for any Ξ satisfying (3.6) and the boundary conditions, (3.8) must be satisfied. □

Equation (3.8) means that $(\tilde{u}, \tilde{v}, \tilde{\theta}')$ represents a state in geostrophic and hydrostatic balance, with geopotential $\tilde{\varphi}$. We next show that if the stationary point is a minimum, the matrix $\mathbf{Q}$ calculated by replacing (u_g, v_g, θ') by $(\tilde{u}, \tilde{v}, \tilde{\theta}')$ in (3.1) is positive definite.

Theorem 3.2 *The condition for E to be minimised with respect to the class of variations defined in Theorem 3.1 is that the matrix*

$$\mathbf{Q} = \begin{pmatrix} f^2 + f\frac{\partial \tilde{v}}{\partial x} & f\frac{\partial \tilde{v}}{\partial y} & f\frac{\partial \tilde{v}}{\partial z} \\ -f\frac{\partial \tilde{u}}{\partial x} & f^2 - f\frac{\partial \tilde{u}}{\partial y} & -f\frac{\partial \tilde{u}}{\partial z} \\ \frac{g}{\theta_0}\frac{\partial \tilde{\theta}'}{\partial x} & \frac{g}{\theta_0}\frac{\partial \tilde{\theta}'}{\partial y} & \frac{g}{\theta_0}\frac{\partial \tilde{\theta}'}{\partial z} \end{pmatrix} \tag{3.10}$$

is positive definite.

Proof A minimum is also a stationary point, so we characterise the stationary point as satisfying $(\tilde{u}, \tilde{v}, \tilde{\theta}') = (u_g, v_g, \theta'_g)$ with

$$(fv_g, -fu_g, g\theta'_g/\theta_0) = \nabla\varphi_g. \tag{3.11}$$

Then we can write

$$\delta E = \int_\Gamma \left(\Xi \cdot (-f(\tilde{v} - v_g), f(\tilde{u} - u_g), -g(\tilde{\theta}' - \theta'_g)/\theta_0\right) \mathrm{d}x\mathrm{d}y\mathrm{d}z. \tag{3.12}$$

Then, taking a second variation

$$\delta^2 E = \int_\Gamma \left(\delta\left(f\Xi \cdot (-(\tilde{v} - v_g), (\tilde{u} - u_g), -g(\tilde{\theta}' - \theta'_g)/(f\theta_0)\right)\right) \mathrm{d}x\mathrm{d}y\mathrm{d}z, \tag{3.13}$$

and since $\tilde{\mathbf{u}} = \mathbf{u}_g$ when $\delta E = 0$, this reduces to

$$\int_\Gamma \left((f\xi, f\eta) \cdot (-\delta(\tilde{v} - v_g), \delta(\tilde{u} - u_g)) - g\chi\delta(\tilde{\theta}' - \theta'_g)/\theta_0\right) \mathrm{d}x\mathrm{d}y\mathrm{d}z. \tag{3.14}$$

Substituting for $\delta\tilde{\mathbf{u}}$ and $\delta\tilde{\theta}$ from (3.7) gives

$$\int_\Gamma \left((f\xi, f\eta) \cdot ((f\xi, f\eta) + \delta(v_g, -u_g)) + g\chi\delta\theta'_g/\theta_0\right) \mathrm{d}x\mathrm{d}y\mathrm{d}z. \tag{3.15}$$

We have $\delta(u_g, v_g) = \Xi \cdot \nabla(u_g, v_g)$ and $\delta(g\theta'_g/\theta_0) = \Xi \cdot \nabla(g\theta'_g/\theta_0)$, so (3.15) becomes

$$\int_\Gamma \Xi \cdot \left((f^2\xi, f^2\eta, 0) + (f\xi, f\eta, \chi) \cdot \nabla(v_g, -u_g, \theta'_g/\theta_0)\right) \mathrm{d}x\mathrm{d}y\mathrm{d}z. \tag{3.16}$$

After integration by parts, the last term integrates to zero because of (3.6) and the boundary conditions on Ξ. The result is

$$\delta^2 E = \int_\Gamma (\Xi \cdot \mathbf{Q} \cdot \Xi)\, \mathrm{d}x\mathrm{d}y\mathrm{d}z \tag{3.17}$$

where $\mathbf{Q}$ is as defined in (3.10). Thus positive definiteness of $\mathbf{Q}$ is equivalent to positive definiteness of $\delta^2 E$ which is the condition for E to be minimised. □

Note that the proofs of Theorems 3.1 and 3.2 have been written in a way that is equally valid when f is a function of position. This will be exploited in section 4.3. Since the main physical applicability of semi-geostrophic theory is to the case where f is a function of position, it is important that the energy minimisation property carries over to this case.

The requirement that $(v_g, -u_g, \theta_g')$ are the gradient of φ_g is necessary for $(v_g, -u_g, \theta_g')$ to be a solution of equations (2.124). However, this only means that the energy has to be stationary with respect to variations (3.6) and (3.7) while solvability of (3.2) requires that the energy is minimised. This is an additional constraint, which does not form part of equation (2.124).

3.1.3 *Physical meaning of the energy minimisation*

In this section we consider the physical meaning of the energy minimisation condition. For this we use the non-hydrostatic Boussinesq equations (2.83) with (2.113) from which the semi-geostrophic equations (2.124) were derived. Following [Shutts and Cullen (1987)], consider the conditions for a flow to be stable to perturbations consisting of small Lagrangian displacements. Such an analysis assumes that the time-scale over which the perturbations evolve is much shorter than the time-scale over which the basic state evolves. This is most straightforward if the displacements are applied to a steady state basic flow. Examples are straight or circular flows.

Consider a straight flow in the y direction. We give an impulsive velocity to a fluid parcel and study the ensuing motion under the condition that the perturbation pressure is zero ([Godson (1950)], [Van Meighem (1952)]). We refer to this as 'parcel stability analysis', [Emanuel (1983)]. We discuss this assumption below. The resulting motion is assumed to be independent of y and so we assume the parcel extends infinitely far in the y direction. The equations for the undisturbed straight flow $(\overline{v}, \overline{\theta}', \overline{\varphi})$ are derived from

equations (2.83) as

$$-f\overline{v} + \frac{\partial \overline{\varphi}}{\partial x} = 0, \qquad (3.18)$$
$$\frac{\partial \overline{\varphi}}{\partial z} - g\frac{\overline{\theta}'}{\theta_0} = 0.$$

Let the displacement be $\Xi = (\xi, 0, \chi)$, so that $u = \dot{\xi}, w = \dot{\chi}$. Then v and θ for the displaced parcel evolve according to (2.83) as

$$\frac{\mathrm{D}v}{\mathrm{D}t} + f\dot{\xi} = \frac{\mathrm{D}(v + f\xi)}{\mathrm{D}t} = 0, \qquad (3.19)$$
$$\frac{\mathrm{D}\theta'}{\mathrm{D}t} = 0,$$

and the fifth equation of (2.83) implies that, for small displacements

$$\frac{\partial \dot{\xi}}{\partial x} + \frac{\partial \dot{\chi}}{\partial z} = 0. \qquad (3.20)$$

The first equation of (3.19) means that the value of v following a parcel is equal to $\overline{v} - f\xi$ and we assume that φ is not changed by the displacement. Using these facts in (2.83), and using (2.113), gives the equations for the evolution of the displacement as

$$\ddot{\xi} + f^2\xi + \Xi \cdot \frac{\partial \overline{\varphi}}{\partial x} = 0, \qquad (3.21)$$
$$\ddot{\chi} + \Xi \cdot \frac{\partial \overline{\varphi}}{\partial z} = 0.$$

These equations can be rewritten as

$$\begin{pmatrix} \ddot{\xi} \\ \ddot{\chi} \end{pmatrix} + \mathbf{Q}\begin{pmatrix} \xi \\ \chi \end{pmatrix} = 0,$$
$$\mathbf{Q} = \begin{pmatrix} f^2 + \frac{\partial^2 \overline{\varphi}}{\partial x^2} & \frac{\partial^2 \overline{\varphi}}{\partial x \partial z} \\ \frac{\partial^2 \overline{\varphi}}{\partial z \partial x} & \frac{\partial^2 \overline{\varphi}}{\partial z^2} \end{pmatrix}. \qquad (3.22)$$

The matrix $\mathbf{Q}$ that appears in (3.22) is the two-dimensional version of the matrix $\mathbf{Q}$ appearing in (3.4). Thus for this case, the condition for parcel stability is that $\mathbf{Q}$ is positive definite, which is exactly the condition for (3.2) to be elliptic and therefore solvable.

It was shown by [Hoskins (1975)] that the three-dimensional semi-geostrophic equations (2.124) are exactly those for the straight flow case

but with the flow at an arbitrary direction to the coordinate axes. Thus the three-dimensional matrix $\mathbf{Q}$ given in (3.4) governs the parcel stability of a straight flow in an arbitrary direction to the coordinate axes.

The conditions under which the perturbation pressure can be neglected are discussed fully in [Shutts and Cullen (1987)]. We first assume that the response to the perturbation is hydrostatic. As discussed in section 2.2, this will be true in regimes where semi-geostrophic theory is relevant. The perturbation pressure $\delta\varphi$ is then generated by the perturbation $\delta\theta'$ to the potential temperature. If the parcel has a vertical scale H, then $\delta\varphi$ will be of order $gH\delta\theta'/\theta_0 = H^2N^2$, where N is the Brunt-Väisälä frequency. Thus the perturbation to the horizontal pressure gradient will be of order N^2H^2/L, where L is the horizontal scale of the parcel. The parcel stability analysis assumes that this is small compared to the change in fv given by (3.19) which is of order f^2L. Thus the condition is that the aspect ratio of the parcel is much less than f/N. This is the same condition as the flow itself has to satisfy for semi-geostrophic theory to be accurate, as discussed in section 2.5.6. Since parcels can be chosen to satisfy the condition for the analysis to be valid, the parcel stability condition is necessary for stability; but as other shapes of parcel could also be chosen, it is not sufficient.

It was shown in section 2.3 that semi-geostrophic theory was accurate if the Lagrangian Rossby number was small. This condition requires the assumption of two-dimensionality to be accurate, so that there is a separation between the time-scales of the perturbation and the time-scale on which the basic state evolves. The parcel stability condition for straight flow in the y direction is equivalent to the symmetric stability condition of [Bennetts and Hoskins (1979)]. For purely horizontal motion in the y direction, it reduces to the inertial stability condition given by the positivity of the corresponding diagonal element of $\mathbf{Q}$:

$$f^2 + \frac{\partial^2\varphi}{\partial x^2} \geq 0. \tag{3.23}$$

For purely vertical motion it reduces to the static stability condition $\partial^2\varphi/\partial z^2 \geq 0$, which is equivalent to $\partial\theta'/\partial z \geq 0$. A different form of the inertial stability condition applies to axisymmetric flows, as shown in section 4.4. For two-dimensional horizontal flows, the condition that $\mathbf{Q}$ is positive definite is a form of inertial stability condition, but is only physically relevant under the conditions discussed above. Other forms of the condition are discussed by [McWilliams et al. (1999)].

We finally state the *stability principle* under which we attempt to solve

the semi-geostrophic equations (2.124).

Definition 3.1 An admissible solution of the semi-geostrophic equations (2.124) on a region Γ is one that is characterised by a function $\varphi(t)$ whose evolution satisfies (3.2) in a suitable sense and where the matrix $\mathbf{Q}$ calculated from φ using (3.4) is positive definite.

In the rest of the chapter we show that existence of such solutions can be proved under appropriate assumptions. The results do not preclude the existence of additional solutions not satisfying the condition on $\mathbf{Q}$. However, such solutions are ignored as unphysical. This is analogous to the rejection of solutions of the equations of gas dynamics containing expansion shocks on the grounds that these are entropy reducing and so unphysical.

3.2 Solution as a mass transportation problem

3.2.1 *Solution by change of variables*

The analysis in section 3.1 suggests that robust solvability of equations (2.124) is plausible since it depends on the positive definiteness of $\mathbf{Q}$ and $\det\mathbf{Q}$ is a constant of the motion. In this and subsequent sections we develop a rigorous argument to this effect. The extra rigour is non-trivial, since it turns out that the solutions can be discontinuous in space, which invalidates the derivations leading to equation (3.2).

The first step is to use the change of variables introduced by [Hoskins (1975)]. Set

$$X = f^{-1}v_g + x,\ Y = -f^{-1}u_g + y,\ Z = g\theta'/(f^2\theta_0). \tag{3.24}$$

Defining P by

$$P = \frac{1}{2}(x^2 + y^2) + f^{-2}\varphi, \tag{3.25}$$

then

$$(X, Y, Z) = \nabla P. \tag{3.26}$$

Equations (2.124) can then be written as

$$\begin{aligned} \frac{\mathrm{D}X}{\mathrm{D}t} &= u_g, \\ \frac{\mathrm{D}Y}{\mathrm{D}t} &= v_g, \\ \frac{\mathrm{D}Z}{\mathrm{D}t} &= 0, \\ \nabla \cdot \mathbf{u} &= 0. \end{aligned} \tag{3.27}$$

Equations (3.26) and (3.27) are a system of seven equations for the unknowns (X, Y, Z, P, u, v, w). It was noted by Hoskins that this change of variables made the trajectory $\mathbf{u}$ implicit, while the geostrophic wind appears explicitly on the right hand side of (3.27). Rewriting the matrix $\mathbf{Q}$ defined in (3.4) in terms of P shows that $\mathbf{Q}$ is the Hessian matrix of P. Thus positive definiteness of $\mathbf{Q}$ is equivalent to convexity of P.

We now describe the energy minimisation property in these variables. We associate with each particle a vector field $(\tilde{X}, \tilde{Y}, \tilde{Z})$, and that given this field the energy of the system is defined by

$$E = \int_\Gamma f^2 \left(\frac{1}{2} \left((x - \tilde{X})^2 + (y - \tilde{Y})^2 \right) - z\tilde{Z} \right) \mathrm{d}x\mathrm{d}y\mathrm{d}z. \tag{3.28}$$

Theorems 3.1 and 3.2 can then be rewritten as follows:

Theorem 3.3 *The conditions for the energy E defined by (3.28) to be stationary with respect to variations Ξ of particle positions satisfying continuity $\delta(\mathrm{d}x\mathrm{d}y\mathrm{d}z) = 0$ via*

$$\nabla \cdot \Xi = 0 \tag{3.29}$$

in Γ and

$$\delta\tilde{X} = \delta\tilde{Y} = \delta\tilde{Z} = 0, \tag{3.30}$$

together with $\Xi \cdot \mathbf{n} = 0$ on the boundary of Γ, are that

$$(\tilde{X}, \tilde{Y}, \tilde{Z}) = \nabla\tilde{P} \tag{3.31}$$

for some scalar $\tilde{P}$. The condition for E to be minimised with respect to this class of variations is that $\tilde{P}$ is convex.

Proof The proof of the first statement is identical to the proof of Theorem 3.1 with the substitutions suggested by (3.24), namely $\tilde{X} = f^{-1}\tilde{v} + \tilde{x}$, $\tilde{Y} = -f^{-1}\tilde{u} + \tilde{y}$, $\tilde{Z} = g\tilde{\theta}'/(f^2\theta_0)$, where $\tilde{x}, \tilde{y}$ are the coordinates of the particle

positions. Theorem 3.2 and the substitution $\tilde{P} = \frac{1}{2}(x^2 + y^2) + f^{-2}\tilde{\varphi}$ show that the Hessian of $\tilde{P}$ is positive definite. Positive definiteness of the Hessian implies convexity. □

We now update Definition 3.1 to apply to this form of the equations.

Definition 3.2 An admissible solution of the semi-geostrophic equations (3.26), (3.27) on a region Γ is one that is characterised by a convex function $P(t)$ whose gradient $(X(t), Y(t), Z(t))$ satisfies (3.27) in a suitable sense.

We refer to this definition as the *convexity* principle.

The class of variations used in Theorem 3.3 can be described as *rearrangements* of $\tilde{X}$, $\tilde{Y}$ and $\tilde{Z}$ viewed as functions of (x, y, z). The theory of rearrangements is reviewed in this context by [Douglas (2002)]. Formal definitions will be given in section 3.5. If the energy minimisation problem of Theorem 3.3 can be solved uniquely, the solution of (3.26) and (3.27) can be viewed as constructing a sequence of energy minimising states, with X, Y and Z evolving in time according to (3.27). The velocity (u, v, w) defines a trajectory which performs the rearrangement required to maintain the energy minimisation property. If the velocity is smooth enough, the incompressibility condition in equations (3.27) means that the trajectory takes the form of a *measure-preserving mapping* from positions of fluid particles at a given time to the positions at a later time. This means that the volume of any subset of the fluid is conserved in time, though it may become highly distorted. We will see in sections 3.5.1 and 3.5.3 that solutions can indeed be defined in this way.

3.2.2 *The equations in dual variables*

In this section we interchange the definitions of dependent and independent variables, so that instead of $\mathbf{X} \equiv (X, Y, Z)$ being a function of (x, y, z), we say that $\mathbf{x} \equiv (x, y, z)$ is a function of (X, Y, Z). The right hand sides of the first three equations of (3.27) now define a 'velocity' in (X, Y, Z) space. This interpretation was noted by Hoskins. However, he did not transform the z coordinate. His *geostrophic* coordinates are (X, Y, z). The relation between his choice and ours is discussed by [Chynoweth and Sewell (1989)]. We rewrite equations (3.26) and (3.27) as a set of equations using (X, Y, Z) as independent variables. First note that equations (3.24) give $u_g = f(y - Y), v_g = f(X - x)$. Write the first three equations of (3.27) as

$$\frac{\mathrm{D}X}{\mathrm{D}t} = U, \quad \frac{\mathrm{D}Y}{\mathrm{D}t} = V, \quad \frac{\mathrm{D}Z}{\mathrm{D}t} = W, \tag{3.32}$$

where

$$(U,V,W) = (f(y-Y), f(X-x), 0). \tag{3.33}$$

If we consider $\mathbf{U} \equiv (U,V,W)$ to be a function of (X,Y,Z), then (3.32) means that $\mathbf{U}$ defines a velocity in (X,Y,Z) space. In order to calculate the velocity, we need to be able to calculate (x,y,z) as a function of (X,Y,Z). To do this, define

$$\begin{aligned} R(X,Y,Z) = x(X,Y,Z)X + y(X,Y,Z)Y + z(X,Y,Z)Z \\ -P(x(X,Y,Z), y(X,Y,Z), z(X,Y,Z)). \end{aligned} \tag{3.34}$$

Then

$$\frac{\partial R}{\partial X} = \frac{\partial x}{\partial X}X + x + \frac{\partial y}{\partial X}Y + \frac{\partial z}{\partial X}Z - \frac{\partial P}{\partial x}\frac{\partial x}{\partial X} - \frac{\partial P}{\partial y}\frac{\partial y}{\partial X} - \frac{\partial P}{\partial z}\frac{\partial z}{\partial X}. \tag{3.35}$$

Using (3.26) then gives

$$\frac{\partial R}{\partial X} = \frac{\partial x}{\partial X}X + x + \frac{\partial y}{\partial X}Y + \frac{\partial z}{\partial X}Z - X\frac{\partial x}{\partial X} - Y\frac{\partial y}{\partial X} - Z\frac{\partial z}{\partial X} = x. \tag{3.36}$$

Similar calculations for the Y and Z components give

$$\nabla R = (x,y,z). \tag{3.37}$$

This gives a characterisation of (x,y,z) as a function of (X,Y,Z), but to solve the equations we need to be able to calculate R.

The first step in doing this is to calculate $\nabla \cdot \mathbf{U}$. (3.33) gives

$$\begin{aligned} \nabla \cdot \mathbf{U} &= \tfrac{\partial f(y-Y)}{\partial X} + \tfrac{\partial f(X-x)}{\partial Y}, \\ &= f\tfrac{\partial^2 R}{\partial Y \partial X} - f\tfrac{\partial^2 R}{\partial X \partial Y} = 0. \end{aligned} \tag{3.38}$$

The next step is to note that, according to the convexity principle (Definition 3.2), we seek solutions with P convex. Equation (3.34) is exactly the statement that P and R are *Legendre transforms.* We will call (3.34) the *duality relation.* A full discussion of this transformation and its use in the theory of convex functions is given in [Rockafellar (1970)] and [Sewell (2002)]. In particular, the Legendre transform of a convex function is also convex, so that R is a convex function of (X,Y,Z). The effect of the convexity of P is that X is a monotone function of x, Y of y and Z of z, and similarly x is a monotone function of X, y of Y and z of Z. The coordinate transformation between (x,y,z) and (X,Y,Z) therefore makes sense.

We now define a *potential density* in (X,Y,Z) coordinates. This concept was introduced by W.H.Schubert, [Schubert and Magnusdottir (1994)].

Since we are considering an incompressible form of the equations in physical space, this is defined as the volume in physical space associated with a given volume in (X, Y, Z) space. Therefore the potential density σ is given by

$$\sigma \equiv \frac{\partial(x,y,z)}{\partial(X,Y,Z)} = \det \begin{pmatrix} \frac{\partial^2 R}{\partial X^2} & \frac{\partial^2 R}{\partial X \partial Y} & \frac{\partial^2 R}{\partial X \partial Z} \\ \frac{\partial^2 R}{\partial Y \partial X} & \frac{\partial^2 R}{\partial Y^2} & \frac{\partial^2 R}{\partial Y \partial Z} \\ \frac{\partial^2 R}{\partial Z \partial X} & \frac{\partial^2 R}{\partial Z \partial Y} & \frac{\partial^2 R}{\partial Z^2} \end{pmatrix}. \tag{3.39}$$

For a given $\sigma(X, Y, Z)$, equation (3.39) is a Monge-Ampère equation for R. The appropriate boundary condition to use is that $(x, y, z) = \nabla R \in \Gamma$. This expresses the fact that all the fluid has to stay within Γ. This form of boundary condition is standard in the theory of Monge-Ampère equations, and is called the 'second boundary value problem', [Pogorelov (1964)]. There are a number of proofs that the Monge-Ampère equation can be solved with this boundary condition. We will describe and use some of these results in sections 3.4 and 3.5. The definition of σ and the boundary condition means that the integral of σ over all (X, Y, Z) in $\mathbb{R}^3$ must be equal to the volume of Γ.

For any choice of velocity $\mathbf{U}(X, Y, Z)$, conservation of volume in physical space means that we can write

$$\frac{\partial \sigma}{\partial t} + \nabla \cdot (\sigma \mathbf{U}) = 0. \tag{3.40}$$

In the present case, equation (3.38) means that

$$\frac{\partial \sigma}{\partial t} + \mathbf{U} \cdot \nabla \sigma = 0. \tag{3.41}$$

We can then rewrite the full system (3.26) and (3.27) as a set of equations in *dual variables*:

$$\begin{aligned} \frac{\partial \sigma}{\partial t} + \mathbf{U} \cdot \nabla \sigma &= 0, \\ \det(\text{Hess } R) &= \sigma, \\ (x, y, z) &= \nabla R, \\ (U, V, W) &= (f(y - Y), f(X - x), 0). \end{aligned} \tag{3.42}$$

This is a set of eight equations for the unknowns $(U, V, W, x, y, z, R, \sigma)$. Given initial data for σ, R can be found from the second equation, (x, y, z) from the third, and (U, V, W) from the fourth. The first equation can then be used to advance σ in time. Solvability requires that the integral of σ at

$t = 0$ is equal to the volume of Γ. The only boundary conditions required are that $(x, y, z) = \nabla R \in \Gamma$. These are compatible with the condition $\mathbf{u} \cdot \mathbf{n} = 0$ stated with equation (2.124) and thus with the conservation of energy. No boundary conditions have to be imposed on the pressure or geostrophic wind. However, the problem is a free boundary problem in (X, Y, Z) space. If σ at $t = 0$ is only non-zero over a finite subset $\Sigma(0)$ of (X, Y, Z) space, the region $\Sigma(t)$ over which it is non-zero at later times will vary and can only be determined after the equations have been solved.

We need some concepts of formal analysis to discuss the solutions further. Brief definitions are given here. More detailed background can be found in the textbook by [Halmos (1950)]. We define the *support* of a function σ on $\mathbb{R}^3$ to be the set where it is non-zero. It is called *compact* if it is closed and bounded. The *measure* of a set is a positive function which measures the size of the set in some sense. We use the term measure to denote area, volume or mass as appropriate. In particular, we denote the standard Lebesgue measure (essentially area on $\mathbb{R}^2$, volume on $\mathbb{R}^3$) by $\mathcal{L}$.

We consider (X, Y, Z) space to be a subset of $\mathbb{R}^3$. We assume we are given a mapping $\mathbf{s}$ from $\mathbb{R}^3$ to Γ. The definition (3.39) of the potential density σ can be written as $\sigma \mathrm{d}X\mathrm{d}Y\mathrm{d}Z = \mathrm{d}x\mathrm{d}y\mathrm{d}z$. Thus it is natural to define the potential density associated with $\mathbf{s}$ in terms of the ratio of the measure of a set to its image under $\mathbf{s}$ as follows:

Definition 3.3 A mapping $\mathbf{s} : \mathbb{R}^m \to \mathbb{R}^n$ *pushes forward* a measure μ on $\mathbb{R}^m$ to another measure ν on $\mathbb{R}^n$ if, for any set B in $\mathbb{R}^n$ with measure $\nu(B)$, we calculate $\mathbf{s}^{-1}(\mathbf{x}) \in \mathbb{R}^m$ for every point $\mathbf{x}$ in B, then the total measure of these points in $\mathbb{R}^m$ is $\mu(B)$. We write $\mathbf{s}_{\#}\mu = \nu$.

This definition is closely associated with the ideas of rearrangements and measure-preserving mappings introduced in section 3.2.1. The potential density σ (3.39) associated with a mapping $\mathbf{s}$ from $\mathbb{R}^3$ to Γ satisfies

$$\mathbf{s}_{\#}\sigma = \mathcal{L}, \tag{3.43}$$

where $\mathcal{L}$ is the Lebesgue measure on Γ

We rewrite Theorem 3.3 in terms of these mappings. Let S be the set of all mappings $\mathbf{s}$ from $\mathbb{R}^3$ to Γ satisfying (3.43) with potential density σ. Given a mapping $\mathbf{s} \in S$, define the energy integral

$$E_s = \int_{\mathbb{R}^3} f^2 \left(\frac{1}{2} \left((\tilde{x} - X)^2 + (\tilde{y} - Y)^2 \right) - \tilde{z} Z \right) \sigma \mathrm{d}X\mathrm{d}Y\mathrm{d}Z, \tag{3.44}$$

where $(\tilde{x}, \tilde{y}, \tilde{z}) = \mathbf{s}(X, Y, Z)$. Theorem 3.3 then becomes

Theorem 3.4 *Given* $\sigma : \mathbb{R}^3 \to \mathbb{R}^+$, *with* $\int_{\mathbb{R}^3} \sigma \mathrm{d}X\mathrm{d}Y\mathrm{d}Z = \mathcal{L}(\Gamma)$, *the condition for the energy* E_s *to be minimised for maps* $\mathbf{s} \in S$ *is that*

$$\mathbf{s}(X, Y, Z) = \nabla \tilde{R}, \tag{3.45}$$

where $\tilde{R}$ *is convex. Such a minimising map, if it exists, is called an optimal map and written as* $\mathbf{t} : \mathbb{R}^3 \to \Gamma$.

Proof First note that the variations defined in the theorem are the same as the variations used in Theorem 3.3. Given a map $\mathbf{s} \in S$, identify fluid particles with fixed positions $\mathbf{X}$ in $\mathbb{R}^3$. Any variations in $\mathbf{s}$ generate variations Ξ of the position of the particles in Γ. (3.43) means that these variations will not be able to change the volume that the particles occupy within Γ, and all particles have to remain inside Γ. Therefore Ξ must satisfy (3.29) and (3.30). Conversely, variations satisfying (3.29) and (3.30) clearly generate a different map $\mathbf{s} \in S$. Theorem 3.3 then gives the condition for a stationary point to be $\mathbf{X}(x, y, z) = \nabla P(x, y, z)$ and for a minimiser that P is convex. Equations (3.34) and (3.37) are then used to define $\tilde{R}$ with $\tilde{R}$ convex. We can then define $\mathbf{s}(\mathbf{X})$ to be equal to $\nabla \tilde{R}$. □

A rigorous version of this theorem due to Brenier, which proves that there is a unique minimiser under appropriate assumptions, is given in section 3.5. The problem as stated in this theorem is an example of a *mass transportation problem.* Given a mapping between two spaces, the energy (3.44) is regarded as a 'cost'. This has to be minimised subject to the constraint that the mapping pushes forward a given measure μ to another measure ν. This type of problem was first stated by [Monge (1781)] in a military context, but has been found since in many other contexts, particularly probability and statistics. A review of applications and analysis of these problems is given in the book by [Villani (2003)].

We finally update Definition 3.2 to apply to the equations in dual variables. A rigorous version of this definition will be given in section 3.5.

Definition 3.4 An admissible solution of the semi-geostrophic equations (3.42) in dual variables is one that is characterised by a convex function $R(t)$, where $\det(\mathrm{Hess}(R))$ satisfies (3.40) in a suitable sense, with $\mathbf{U}$ given by (3.42).

3.2.3 *Consequences of the duality relation*

In this section we derive some important properties of semi-geostrophic solutions, exploiting the Legendre duality defined by equation (3.34). These

are discussed much more fully in [Purser and Cullen (1987)], and in more general contexts in [Sewell (2002)].

We first illustrate the meaning of the Legendre transform. It exploits the fact that a convex surface P can be regarded as the intersection of its tangent planes. Regard the surface as given by the equation

$$p = P(x, y, z) \tag{3.46}$$

in $\mathbb{R}^4$ with coordinates (x, y, z, p). The convention, following [Pogorelov (1964)], is that if P is a convex function of (x, y, z), then the surface defined by equation (3.46) is called convex in the direction $p < 0$. Since $(X, Y, Z) = \nabla P$, the equation of a typical tangent plane can be written as

$$p = -R + xX + yY + zZ \tag{3.47}$$

where R is a constant. This is consistent with the definition of R in equation (3.34), so we can interpret $-R(X, Y, Z)$ as the point where the tangent plane to p with gradient (X, Y, Z) intersects the hyperplane $(x, y, z) = 0$. This is illustrated for a one-dimensional case in Fig. 3.1.

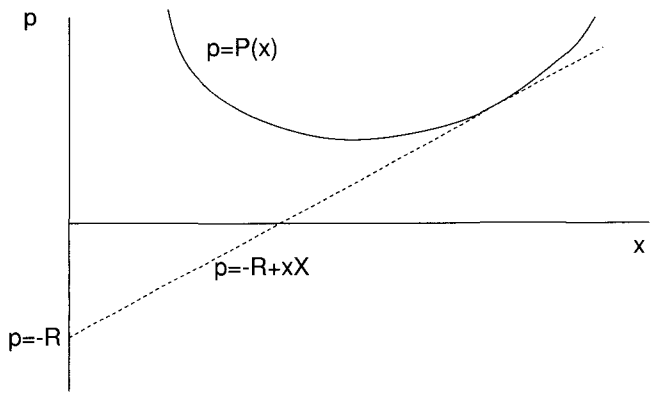

Fig. 3.1 The construction of the Legendre transform $R(X)$ of a convex surface $P(x)$.

We now write down the definition of a convex surface as the intersection of its tangent planes. This means that P takes the largest value of p at each (x, y, z) associated with any tangent plane, so that

$$P(x, y, z) = \sup_{X,Y,Z}(-R(X, Y, Z) + xX + yY + zZ). \tag{3.48}$$

This is illustrated in Fig. 3.2.

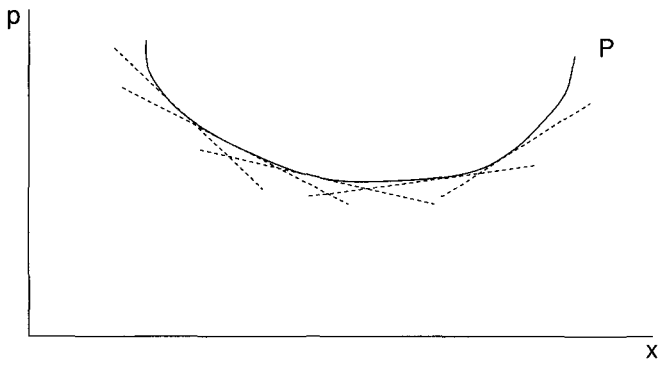

Fig. 3.2 The convex surface P as an intersection of its tangent planes.

Equation (3.48) implies that, for any (x, y, z) and (X, Y, Z),

$$P(x, y, z) + R(X, Y, Z) \geq xX + yY + zZ. \tag{3.49}$$

We can now use equation (3.25) to replace P by φ. Similarly, we can define $\Psi(X, Y, Z)$ by

$$\Psi = f^2 \left(\frac{1}{2}(X^2 + Y^2) - R \right). \tag{3.50}$$

Using equation (3.33), we see that

$$(U, V, W) = f^{-1} \left(-\frac{\partial \Psi}{\partial Y}, \frac{\partial \Psi}{\partial X}, 0 \right). \tag{3.51}$$

Thus Ψ is a stream-function for the flow in (X, Y, Z) coordinates in the same sense that φ is a stream-function for the geostrophic wind in (x, y, z)

space. Using (3.50) and (3.25) in (3.49) gives

$$-\varphi(x,y,z)+\Psi(X,Y,Z)\leq\frac{1}{2}f^2\left((x-X)^2+(y-Y)^2-zZ\right). \qquad (3.52)$$

The right hand side of this equation is now recognisable as the integrand of the energy (3.44).

We now exploit this identification by making some further definitions. Define a functional called the *cost function* depending on $\mathbf{x}$ and $\mathbf{X}$ equal to the integrand of (3.44). Assume, as in section 3.2.2, that $\mathbf{X}=\mathbf{s}^{-1}(\mathbf{x})$, and that the image of Γ under the map $\mathbf{s}^{-1}$ is Σ. Then the cost function can be written as

$$d(\mathbf{x},\mathbf{s}^{-1}(\mathbf{x}))=f^2\left(\frac{1}{2}(x-X)^2+(y-Y)^2)-zZ\right). \qquad (3.53)$$

Define the *d-transform* of a function Ψ on Σ as

$$\Psi^d(\mathbf{x})=\inf_{\mathbf{X}\in\Sigma}\{d(\mathbf{X},\mathbf{s}(\mathbf{X}))-\Psi(\mathbf{X})\}. \qquad (3.54)$$

Note that equation (3.52) takes exactly this form if we set $\Psi^d=-\varphi$. Apply the equivalent definition to a function on Γ. Then we call Ψ *involutive* if

$$(\Psi^d)^d=\Psi. \qquad (3.55)$$

It can be shown that this implies that $\mathbf{s}$ achieves the infimum in (3.54), so that $\mathbf{s}$ is an optimal map which we write as $\mathbf{t}$, and

$$\Psi^d(\mathbf{t}(\mathbf{X}))+\Psi(\mathbf{X})=d(\mathbf{X},\mathbf{t}(\mathbf{X})). \qquad (3.56)$$

Equation (3.56) is a duality relation.

Now suppose that P and R have been obtained as a result of solving the energy minimisation problem set out in Theorem 3.4. Then R satisfies (3.34). The optimal map $\mathbf{t}$ from (X,Y,Z) to (x,y,z) maps the gradient of all possible tangent planes onto the positions in Γ where the tangent plane meets P. Thus for $\mathbf{x}$ equal to $\mathbf{t}(\mathbf{X})$, we have (3.56). Making the identification $\Psi^d=-\varphi$, and using (3.25) and (3.46) we recover (3.34).

This argument shows that the duality relation (3.56) is another way of viewing Legendre duality. It is discussed in more detail in [Sewell (2002)], p.162. The fact that P and R are Legendre transforms is equivalent to the fact that Ψ is involutive. The importance of it is that we can use it in contexts where the idea of a convex function cannot be applied, such as on the sphere in section 4.3 and where the cost function d is more complicated,

as in the compressible case treated in section 4.1. This formulation is also critical in proving the rigorous theorems set out in section 3.5.

This derivation illustrates the symmetry between the equations defined with (x, y, z) as independent variables and those using (X, Y, Z) as independent variables. This was exploited by [Purser and Cullen (1987)] to derive solutions for two different physical problems from any one solution. One aspect of this is that the potential density conservation law (3.41) can be inverted to give a conservation law for the potential vorticity (2.126) which has to be satisfied by the physical space equations (3.26) and (3.27). This takes the form

$$\mathcal{Q}_{sg} \equiv \frac{\partial(X, Y, Z)}{\partial(x, y, z)}, \tag{3.57}$$

$$\frac{\partial \mathcal{Q}_{sg}}{\partial t} + \mathbf{u} \cdot \nabla q_{sg} = 0.$$

This conservation law was derived by [Hoskins (1975)] directly from (2.124).

The symmetry is, however, lost if the equations are solved in a closed region Γ. As noted in the previous section, if σ has compact support $\Sigma(t)$, the problem in (X, Y, Z) coordinates is a free boundary problem. The symmetry could be recovered if periodic boundary conditions were used in all three directions, but this does not correspond to a physically useful case.

An important property of the Legendre transform is that it maps the boundary of a convex set to the boundary of another convex set, as stated in the following theorem from [Cullen and Purser (1984)]:

Theorem 3.5 *Given a domain Σ in (X, Y, Z) and a convex domain Γ in (x, y, z), and a Legendre transform between them generated by a convex function $P(x, y, z)$, all points on the convex hull of Σ correspond to points on the boundary of Γ.*

Proof Let $A = (X_A, Y_A, Z_A)$ be a point on the convex hull of Σ whose image (x_A, y_A, z_a) is strictly inside Γ. Let (a, b, c) be the outward unit normal to the convex hull of Σ at A. Then convexity of the convex hull means that no point with coordinates of the form

$$(X_A, Y_A, Z_A) + (X', Y', Z'), \tag{3.58}$$
$$(X', Y', Z') \cdot (a, b, c) > 0,$$

is in Σ, and therefore no such point has an image in Γ. However, by convexity of P, $\nabla P\left((x_A, y_A, z_A) + \alpha(a, b, c)\right) \cdot (a, b, c)$ is an increasing function of α. Since for some α the point $(x_A, y_A, z_A) + \alpha(a, b, c)$ lies inside Γ, this

implies that it must have a gradient of the form given in equation (3.58), which is a contradiction. Thus any point on the boundary of Σ must map to a point on the boundary of Γ, as illustrated in Fig. 3.3. □

Rigorous results proving this and more general statements, due to Caffarelli, are described in section 3.5.

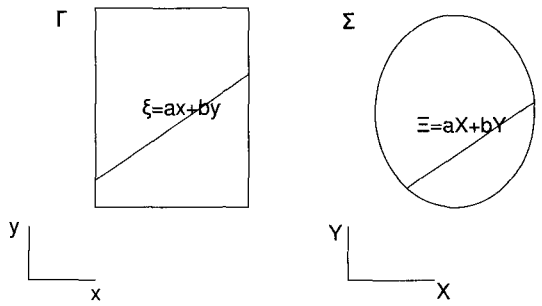

Fig. 3.3 The convex hull of Σ must map to the boundary of Γ.

If $\Sigma(t)$ is not convex, then points on the boundary of Σ can map to the interior of Γ. An example is shown in Figure 3.4. This creates a situation where two separate points, marked A and B, on the boundary of the convex hull of Σ can map onto adjacent points of the boundary of Γ. The intermediate point C, on the boundary of Σ, but not on the convex hull, maps to the interior of Γ. Now consider the integral of the potential vorticity Q defined in equation (3.57) over Γ. If the integral is taken round the boundary of Γ, it will include the portion of the convex hull of Σ within the dashed line connecting A and B in Fig. 3.4. Thus the integral will be greater than the ratio of the volume of Σ to the volume of Γ. As time evolves, equation (3.38) shows that the volume of Σ is conserved. However, the shape of Σ will vary in time, and the volume of extra parts of (X, Y, Z) space included in the integral of Q may vary. Thus the integrated potential vorticity is not conserved, even though the Lagrangian conservation law (3.57) is satisfied. In effect, potential vorticity from the boundary has been sucked into the fluid, an interpretation first made by F.P.Bretherton. The physical interpretation of this is discussed in section 3.4.2 in the context of frontogenesis. Examples are given in sections 3.4.2 and 6.2.

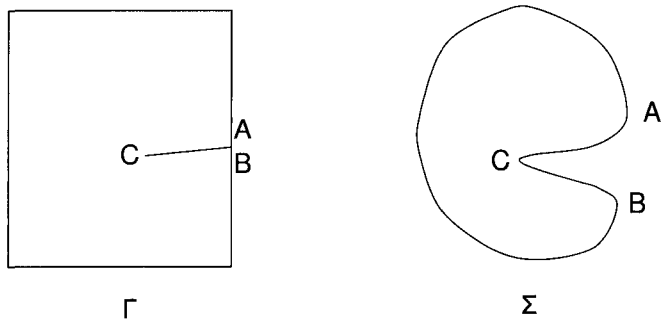

Fig. 3.4 Mapping a non-convex Σ to Γ. The points A, B and C indicate corresponding points in Γ and Σ.

3.3 The shallow water semi-geostrophic equations

3.3.1 *Solutions as minimum energy states*

In this section we analyse the solutions of the shallow water semi-geostrophic equations (2.74) and (2.75) under the assumption that f is constant. We follow the same steps as in sections 3.1 and 3.2, but only summarise the main results.

In section 2.4.6 the equations were rewritten, (2.78), as an evolution equation for h which was elliptic if the matrix $\mathbf{Q}$ defined in equation (2.77) was positive definite. The equations were shown to conserve the energy integral defined by (2.76).

We again characterise solutions with positive definite $\mathbf{Q}$ as minimum energy states. Suppose that associated with each particle is a vector field $(\tilde{u}, \tilde{v})$ and a scalar field $\tilde{h}$. Define the associated energy integral as

$$\int_{\Gamma} \left(\frac{1}{2} \tilde{h} \left(\tilde{u}^2 + \tilde{v}^2 \right) + \frac{1}{2} g \tilde{h}^2 \right) \mathrm{d}x\mathrm{d}y. \tag{3.59}$$

Then we prove

Theorem 3.6 *The conditions for the energy E (3.59) to be stationary with respect to variations $\Xi = (\xi, \eta)$ of particle positions satisfying continuity $\delta(\tilde{h}\mathrm{d}x\mathrm{d}y) = 0$ via*

$$\delta\tilde{h} = -\tilde{h}\nabla \cdot \Xi \tag{3.60}$$

in Γ *and*

$$\delta\tilde{u} = f\eta,\ \delta\tilde{v}_0 = -f\xi, \tag{3.61}$$

together with $\Xi \cdot \mathbf{n} = 0$ *on the boundary of* Γ, *are that*

$$(f\tilde{v}, -f\tilde{u}) = \nabla\tilde{h}. \tag{3.62}$$

The condition for the stationary point to be a minimum is that the matrix

$$\mathbf{Q} = \begin{pmatrix} f^2 + f\frac{\partial\tilde{v}}{\partial x} & f\frac{\partial\tilde{v}}{\partial y} \\ -f\frac{\partial\tilde{u}}{\partial x} & f^2 - f\frac{\partial\tilde{u}}{\partial y} \end{pmatrix}, \tag{3.63}$$

is positive definite.

Proof Write δ for a change following the particles, and ∂ for a change at a fixed position in space. The change to the energy resulting from the variation is then

$$\int_\Gamma \left(\tilde{h}\left(\tilde{u}\delta\tilde{u} + \tilde{v}\delta\tilde{v}\right) + g\tilde{h}\partial\tilde{h}\right) \mathrm{d}x\mathrm{d}y, \tag{3.64}$$

noting that (3.60) implies that $\delta(\tilde{h}\mathrm{d}x\mathrm{d}y) = 0$. (3.60) can be written as

$$\partial\tilde{h} + \nabla \cdot (\tilde{h}\Xi) = 0. \tag{3.65}$$

Using this, and integrating by parts, gives

$$\int_\Gamma \left(\tilde{u}\delta\tilde{u} + \tilde{v}\delta\tilde{v} + g\Xi \cdot \nabla\tilde{h}\right) \tilde{h}\mathrm{d}x\mathrm{d}y. \tag{3.66}$$

Using (3.61) then gives

$$\int_\Gamma \Xi \cdot \left(-f\tilde{v} + g\frac{\partial\tilde{h}}{\partial x}, f\tilde{u} + g\frac{\partial\tilde{h}}{\partial y}\right) \tilde{h}\mathrm{d}x\mathrm{d}y. \tag{3.67}$$

Therefore the condition for E to be stationary is (3.62) as required. At such a point, set $(\tilde{u}, \tilde{v}, \tilde{h}) = (u_g, v_g, h_g)$, with

$$(fv_g, -fu_g) = \nabla h_g. \tag{3.68}$$

Now take a second variation

$$\delta^2 E = \int_\Gamma \delta\left(f\Xi \cdot \left(-\tilde{v} + f^{-1}g\frac{\partial\tilde{h}}{\partial x}, \tilde{u} + f^{-1}g\frac{\partial\tilde{h}}{\partial y}\right)\right) \tilde{h}\mathrm{d}x\mathrm{d}y. \tag{3.69}$$

Since (3.62) holds at a stationary point, this reduces to

$$\int_\Gamma f\Xi \cdot \delta \left(-\tilde{v} + f^{-1}\frac{\partial \tilde{h}}{\partial x}, \tilde{u} + f^{-1}\frac{\partial \tilde{h}}{\partial y} \right) \tilde{h} \mathrm{d}x\mathrm{d}y. \tag{3.70}$$

Using (3.60) to substitute for $\delta\tilde{\mathbf{u}}$ gives

$$\int_\Gamma f\Xi \cdot \left((f\xi, f\eta) + \delta(f^{-1}g\nabla\tilde{h}) \right) \tilde{h} \mathrm{d}x\mathrm{d}y. \tag{3.71}$$

Writing $\delta(f^{-1}g\nabla\tilde{h}) = \partial(f^{-1}g\nabla\tilde{h}) + \Xi \cdot \nabla(f^{-1}g\nabla\tilde{h})$, using (3.65) for $\partial\tilde{h}$, and using (3.68) gives $\delta(f^{-1}g\nabla\tilde{h}) = -f^{-1}g\nabla\nabla \cdot (\tilde{h}\Xi) + \Xi \cdot \nabla(v_g, -u_g)$. Substituting this into equation (3.71) and integrating by parts then gives

$$\int_\Gamma f\Xi \cdot ((f\xi, f\eta) + \Xi \cdot (v_g, -u_g))\, \tilde{h} + g(\nabla \cdot (\tilde{h}\Xi))^2 \mathrm{d}x\mathrm{d}y. \tag{3.72}$$

The second term is positive definite. The energy will therefore be minimised if the first term is positive definite. It can be seen that it takes the form $\Xi \cdot \mathbf{Q} \cdot \Xi$ where $\mathbf{Q}$ is given by (2.77). Thus the energy will be minimised if $\mathbf{Q}$ is positive definite. □

Note that the variations used in Theorem 3.6 assume the perturbations to the depth $\tilde{h}$ do not affect $\delta\tilde{u}$ and $\delta\tilde{v}$. Recall the definition, (2.37), of the Rossby radius of deformation L_R. Our assumption is justified if the scale of the variations is greater than L_R, because the change to $g\nabla\tilde{h} \simeq g\nabla H\nabla \cdot \Xi$ will be of order $gH\Xi/L^2$ and the change to $f\tilde{u}$ is of order $f^2\eta$. The ratio of these is less than L_R/L. Thus, as in the three-dimensional case, the energy minimisation principle is valid under the same conditions as the semi-geostrophic approximation. The form of (3.72) suggests that positive definiteness of $\mathbf{Q}$ is not necessary for the stationary point to be a minimiser, only sufficient. We show in section 3.3.4 that this condition is actually necessary as well. We state the convexity principle under which we attempt to solve the semi-geostrophic equations (2.74) and (2.75).

Definition 3.5 An admissible solution of the semi-geostrophic shallow water equations (2.74) and (2.75) on a region Γ is one that is characterised by a depth $h(t)$ whose evolution satisfies (2.78) in a suitable sense and where the matrix $\mathbf{Q}$ calculated from h using (2.74) and (2.77) is positive definite.

Theorem 3.6 and Definition 3.5 both also hold if f is a function of position. This will be exploited in section 4.3.

3.3.2 *Solution by change of variables*

Introduce the same new variables as in the three-dimensional case (3.24). Then (2.75) can be rewritten as

$$\begin{aligned} \frac{\mathrm{D}X}{\mathrm{D}t} &= u_g, \\ \frac{\mathrm{D}Y}{\mathrm{D}t} &= v_g, \\ \frac{\partial h}{\partial t} + \nabla \cdot (h\mathbf{u}) &= 0. \end{aligned} \tag{3.73}$$

Equation (2.74) becomes

$$\begin{aligned} (X, Y) &= \nabla P, \\ P &= \frac{1}{2}(x^2 + y^2) + f^{-2} g h. \end{aligned} \tag{3.74}$$

We now describe the energy minimisation property in these variables. We suppose that associated with each particle is a vector field $(\tilde{X}, \tilde{Y})$ and a scalar field $\tilde{h}$, and that given these fields the energy of the system is defined by

$$E = \int_\Gamma \left(\frac{1}{2} h f^2 \left((x - \tilde{X})^2 + (y - \tilde{Y})^2 \right) + \frac{1}{2} g \tilde{h}^2 \right) \mathrm{d}x\mathrm{d}y. \tag{3.75}$$

Theorem 3.6 can then be rewritten as follows

Theorem 3.7 *The conditions for the energy E to be stationary with respect to variations Ξ of particle positions satisfying continuity $\delta(\tilde{h}\mathrm{d}x\mathrm{d}y) = 0$ via*

$$\delta \tilde{h} = -\tilde{h} \nabla \cdot \Xi \tag{3.76}$$

in Γ and

$$\delta \tilde{X} = \delta \tilde{Y} = 0, \tag{3.77}$$

together with $\Xi \cdot \mathbf{n} = 0$ on the boundary of Γ, are that

$$(\tilde{X}, \tilde{Y}) = \nabla \tilde{P}, \tag{3.78}$$

where $\tilde{P}$ is given by (3.74) with $h = \tilde{h}$. The condition for E to be minimised with respect to this class of variations is that $\tilde{P}$ is convex.

Proof The proof of the first statement is identical to the proof of the first part of Theorem 3.6 with the substitutions $\tilde{X} = f^{-1}\tilde{v} + \tilde{x}$, $\tilde{Y} = -f^{-1}\tilde{u} + \tilde{y}$, where $\tilde{x}$, $\tilde{y}$ are coordinates of particle positions. Use equation (3.68) to define values X_g, Y_g and h_g at the stationary point. The second statement then follows from the second part of Theorem 3.6, the definition (3.74) of $\tilde{P}$, and the fact that, in this case, the matrix $\mathbf{Q}$ defined in (2.77) can be rewritten in terms of h_g as

$$\mathbf{Q} = \begin{pmatrix} f + \frac{\partial^2 h_g}{\partial x^2} & \frac{\partial^2 h_g}{\partial x \partial y} \\ \frac{\partial^2 h_g}{\partial y \partial x} & f + \frac{\partial h_g}{\partial y^2} \end{pmatrix}. \square \tag{3.79}$$

Admissible solutions of the equations are still defined by Definition 3.5.

3.3.3 *The equations in dual variables*

In this section we exchange the definitions of dependent and independent variables, as in section 3.2.3. The same manipulations can be carried out as in the three-dimensional case. In particular, equation (3.34) becomes

$$R(X,Y) = x(X,Y)X + y(X,Y)Y - P(x(X,Y), y(X,Y)). \tag{3.80}$$

From this we can show that $\nabla R = (x, y)$. We now define the potential density in (X, Y) coordinates as the mass in physical space associated with a given region of (X, Y) space.

$$\sigma \equiv \frac{h\partial(x,y)}{\partial(X,Y)} = \det\left\{ h \begin{pmatrix} \frac{\partial^2 R}{\partial X^2} & \frac{\partial^2 R}{\partial X \partial Y} \\ \frac{\partial^2 R}{\partial Y \partial X} & \frac{\partial^2 R}{\partial Y^2} \end{pmatrix} \right\}. \tag{3.81}$$

We again can show that $\nabla \cdot \mathbf{U} = 0$ where $\mathbf{U} = (f(y - Y), f(X - x))$. We can then rewrite (3.73) and (3.74) as a set of equations in dual variables:

$$\begin{aligned} \frac{\partial \sigma}{\partial t} + \mathbf{U} \cdot \nabla \sigma &= 0, \\ (U, V) &= (f(y - Y), f(X - x)), \\ h\det(\text{Hess } R) &= \sigma, \\ (x, y) &= \nabla R, \\ \frac{1}{2}(x^2 + y^2) + f^{-2}gh + R &= xX + yY. \end{aligned} \tag{3.82}$$

We now rewrite Theorem 3.7 as a mass transportation problem as in Theorem 3.4. The definition of the potential density, (3.81), can be rewritten

as $\sigma \mathrm{d}X\mathrm{d}Y = h\mathrm{d}x\mathrm{d}y$. In terms of Definition 3.3, we write

$$\mathbf{s}_{\#}\sigma = h. \tag{3.83}$$

Let S be the set of all mappings $\mathbf{s}$ from $\mathbb{R}^2$ to Γ satisfying (3.83) with potential density σ . Any such mapping generates a depth $\tilde{h}$ satisfying (3.81). Associate with $\mathbf{s}$ and σ the energy E defined by

$$E = \int_{\mathbb{R}^2} \left(\frac{1}{2} f^2 |\mathbf{X} - \mathbf{s}(\mathbf{X})|^2 + \frac{1}{2} g\tilde{h} \right) \sigma \mathrm{d}X\mathrm{d}Y, \tag{3.84}$$

where $\mathbf{X} = (X, Y)$. Theorem 3.7 then becomes

Theorem 3.8 *Given $\sigma : \mathbb{R}^2 \to \mathbb{R}^+$, suppose that the energy E defined in (3.84) is minimised over maps $\mathbf{s} \in S$ by a map $\mathbf{t}$. Let h be the depth calculated by using $\mathbf{t}$ to evaluate (3.81). Then*

$$\mathbf{t}(\mathbf{X}) = \nabla R, \tag{3.85}$$

where R is convex and satisfies the last equation of (3.82). Such a minimising map, if it exists, is called an optimal map.

Proof As in the proof of Theorem 3.4, the result follows from identifying condition (3.83) with the variation $\delta(h\mathrm{d}x\mathrm{d}y) = 0$ used in Theorem 3.6. We then use Theorem 3.6 itself and, using the definition of R given in equation (3.80), the result follows. □

3.3.4 *Consequences of the duality relation*

We now identify the duality structure as in section 3.2.3. Let Σ be the image of Γ under the mapping $\mathbf{s}^{-1}$. Define the cost function associated with the mapping as

$$d(\mathbf{x}, \mathbf{s}^{-1}(\mathbf{x})) = f^2 \left(\frac{1}{2}(x - X)^2 + (y - Y)^2) \right), \tag{3.86}$$

where $(X, Y) = \mathbf{s}^{-1}(x, y)$. Unlike the cost function (3.53), the right hand side of equation (3.89) does not correspond to the whole of the integrand in the energy (3.84). As in (3.54), define the *d-transform* of a function Ψ on Σ as

$$\Psi^d(\mathbf{x}) = \inf_{\mathbf{X} \in \Sigma} \{ d(\mathbf{X}, \mathbf{s}(\mathbf{X}) - \Psi(\mathbf{X}) \}. \tag{3.87}$$

Suppose we are given a convex function $R(\mathbf{X})$ generated from an optimal map $\mathbf{t}$ as in Theorem 3.8. Then R will be the Legendre transform

of P defined by (3.80), and h will be related to P by (3.74). Define $\Psi = f^2\left(\frac{1}{2}(X^2+Y^2) - R\right)$. Then, for any pairs $\mathbf{x}$, $\mathbf{X}$, we will have

$$-gh(\mathbf{x}) + \Psi(\mathbf{X}) \leq \frac{1}{2}f^2\left((x-X)^2 + (y-Y)^2\right), \tag{3.88}$$

as discussed in section 3.2.3. If $\mathbf{x}$ is chosen as the tangent to R at $\mathbf{X}$, then

$$-gh(\mathbf{x}) + \Psi(\mathbf{X}) = \frac{1}{2}f^2\left((x-X)^2 + (y-Y)^2\right). \tag{3.89}$$

This choice corresponds to setting $\mathbf{x} + \mathbf{t}(\mathbf{X})$, where $\mathbf{t}$ is the optimal map. Comparing (3.87) and (3.88) implies that $\Psi^d = -gh$. As in section 3.2.3, the optimal map achieves the infimum in (3.87), so that the duality relation takes the form (3.89).

Though the cost function d defined in equation (3.86) does not correspond to the whole of the integrand in the energy (3.84), (3.89) is still important in analysing the shallow water case because it is possible to identify solutions of the shallow water energy minimisation problem with solutions of a two-dimensional version of the incompressible problem studied in section 3.2. This is important in proving the rigorous existence theorem of [Cullen and Gangbo (2001)], and demonstrates why positive definiteness of $\mathbf{Q}$ is actually a necessary condition for energy minimisation, despite the presence of an additional positive definite term in (3.72).

To state the identification, let ν be a potential density for the two-dimensional incompressible problem. Then we require $\int_{\mathbb{R}^2} \nu \mathrm{d}X\mathrm{d}Y = \mathcal{L}(\Gamma)$. Let S be the set of mappings $\mathbf{s} : \mathbb{R}^2 \to \Gamma$ such that $\mathbf{s}_{\#}\nu = \mathcal{L}$.

Theorem 3.9 *Let* $\mathbf{t}$ *be a solution of the two-dimensional version of the incompressible energy minimisation problem given in Theorem 3.4. Thus* $\mathbf{t} \in S$ *is a minimiser of*

$$\int_{\mathbb{R}^2} \left(\frac{1}{2}f^2|\mathbf{X} - \mathbf{s}(\mathbf{X})|^2\right) \nu \mathrm{d}X\mathrm{d}Y \tag{3.90}$$

for $\mathbf{s} \in S$. *Suppose the solution is characterised by a potential* $P(x,y)$. *Calculate a depth* $h = P - \frac{1}{2}(x^2+y^2)$. *If necessary, adjust* P *by an arbitrary constant to ensure* $h \geq 0$ *everywhere in* Γ. *Define* $\sigma = h(\mathbf{t}(X,Y)\nu$. *Then* h *and* $\mathbf{t}$ *define a solution of the shallow water energy minimisation problem, Theorem 3.8.*

Proof Consider a mapping $\mathbf{s} \in S$ which generates a depth ϱ using (3.81).

Then equation (3.88) and (3.89) mean that

$$\begin{aligned} -gh\left(\mathbf{s}(\mathbf{X})\right) + \Psi(\mathbf{X}) &\leq f^2\left(\mathbf{s}(\mathbf{X}) - \mathbf{X}\right)^2, \\ -gh\left(\mathbf{t}(\mathbf{X})\right) + \Psi(\mathbf{X}) &= f^2\left(\mathbf{t}(\mathbf{X}) - \mathbf{X}\right)^2. \end{aligned} \tag{3.91}$$

Now compare the shallow water energy (3.84) calculated using the two mappings. These are respectively

$$\begin{aligned} E_s &= \int_{\mathbb{R}^2} \left(\frac{1}{2} f^2 \left(\mathbf{s}(\mathbf{X}) - \mathbf{X}\right)^2 + \frac{1}{2} g\varrho\right) \sigma \mathrm{d}X\mathrm{d}Y, \\ E_t &= \int_{\mathbb{R}^2} \left(\frac{1}{2} f^2 \left(\mathbf{t}(\mathbf{X}) - \mathbf{X}\right)^2 + \frac{1}{2} gh\right) \sigma \mathrm{d}X\mathrm{d}Y. \end{aligned} \tag{3.92}$$

The first terms in each equation in (3.92) can be replaced using (3.91) to give

$$\begin{aligned} E_s &\geq \int_{\mathbb{R}^2} \left(-gh\left(\mathbf{s}(\mathbf{X})\right) + \Psi(\mathbf{X}) + \frac{1}{2} g\varrho\right) \sigma \mathrm{d}X\mathrm{d}Y, \\ E_t &= \int_{\mathbb{R}^2} \left(-gh\left(\mathbf{t}(\mathbf{X})\right) + \Psi(\mathbf{X}) + \frac{1}{2} gh\right) \sigma \mathrm{d}X\mathrm{d}Y. \end{aligned} \tag{3.93}$$

Let the common term $\int_{\mathbb{R}^2} \Psi(\mathbf{X}) \sigma \mathrm{d}X\mathrm{d}Y$ be E_h. Rewrite the remainder of the two expressions in (3.93) as integrals over Γ setting $\sigma \mathrm{d}X\mathrm{d}Y$ equal to $\varrho \mathrm{d}x\mathrm{d}y$ and $h\mathrm{d}x\mathrm{d}y$ respectively. After simplifying the two terms in each integral this gives

$$\begin{aligned} E_s - E_h &\geq \int_\Gamma \left(-gh + \frac{1}{2} g\varrho\right) \varrho \mathrm{d}x\mathrm{d}y, \\ E_t - E_h &= \int_\Gamma -\frac{1}{2} gh^2 \mathrm{d}x\mathrm{d}y. \end{aligned} \tag{3.94}$$

Subtracting the second from the first gives

$$E_s - E_t \geq \int_\Gamma \frac{1}{2} g(h - \varrho)^2 \mathrm{d}x\mathrm{d}y. \tag{3.95}$$

Thus $E_s \geq E_t$ as desired. □.

There is no reason why the fluid should occupy the whole of Γ. If the support Σ of σ is such that $x - X$ and $y - Y$ are large for $(x, y) \in \Gamma$, then the solution will have large $|\nabla h|$ for all $(x, y) \in \Gamma$. If the total available mass $\int_{\mathbb{R}^2} \sigma \mathrm{d}X\mathrm{d}Y$ is small, then this cannot be achieved if the fluid fills the whole of Γ, as illustrated in Fig. 3.5.

It is not possible to determine whether the fluid fills Γ until the whole problem is solved. It is possible in principle for the fluid to fill Γ at $t = 0$ and

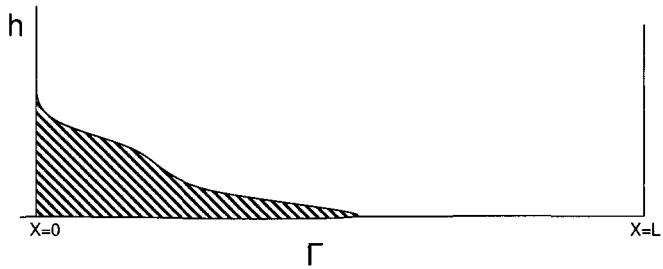

Fig. 3.5 A typical cross-section of the solution of the shallow water model showing that the water need not fill the whole of Γ.

then fail to fill it at a later time. The physical implications of this process, called 'outcropping', are discussed in section 3.4.3. In such a case, Theorem 3.9 can only be applied to an incompressible minimisation problem for that part of Γ where h is non-zero.

3.4 A discrete solution of the semi-geostrophic equations

3.4.1 *The discrete problem*

In this section we show that explicit solutions of the incompressible semi-geostrophic equations (3.26) and (3.27) can be constructed for the special case of piecewise constant data. This construction was developed independently by [Cullen and Purser (1984)]. It was subsequently discovered that this method is an example of a general method of constructing convex (hyper)surfaces with faces of given area or volume developed by Alexandrov and described by [Pogorelov (1964)]. This general method also applies to the shallow water case, equations (3.73) and (3.74).

We consider the case described in Theorem 3.3, so that we are given a vector field $(\tilde{X}, \tilde{Y}, \tilde{Z})$ for each (x, y, z). We assume this data is piecewise constant so that Γ is divided into n segments with volumes $\{\sigma_i\}$. On each of these segments we set $\tilde{X} = X_i, \tilde{Y} = Y_i, \tilde{Z} = Z_i$. The data is thus as illustrated for a two-dimensional example in Figure 3.6.

The problem is then to minimise the energy integral (3.28) by choosing an appropriate set of n segments with the volumes σ_i. According to Theorem 3.3, the minimiser will satisfy (3.26), so that $(\tilde{X}, \tilde{Y}, \tilde{Z})$ have to

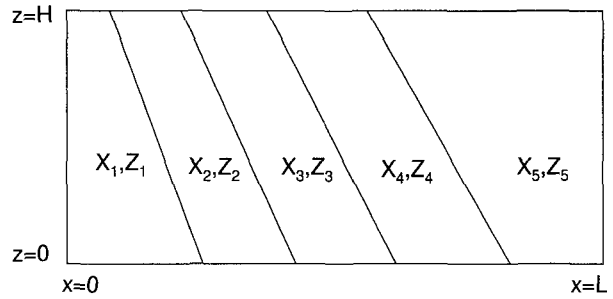

Fig. 3.6 Example data for (X_i, Z_i) as functions of (x, z) in Γ.

form the gradient of a convex function $\tilde{P}$. Since $(\tilde{X}, \tilde{Y}, \tilde{Z})$ take the discrete values (X_i, Y_i, Z_i), this means that P is a polyhedral hypersurface, with n hyperfaces with gradients (X_i, Y_i, Z_i) and each hyperface having a projection onto Γ with volume σ_i. The result of applying this construction to the data shown in Fig. 3.6 is shown in Fig. 3.7.

The desired solution can thus be constructed if we can prove that it is possible to construct a convex hypersurface on Γ with n hyperfaces of specified gradient and specified volume. The proof that this is possible is given in a theorem due to Alexandrov, independently rediscovered by R.J.Purser, [Cullen and Purser (1984)]. Under the Legendre transform, the hyperfaces become vertices and their volumes become the solid angles associated with those vertices, see [Sewell (2002)]. We therefore have to construct a hypersurface in (X, Y, Z, r) space given specified vertices (X_i, Y_i, Z_i), and solid angles associated with the vertices which project onto regions of Γ with specified volumes σ_i. The theorem and proof given here follow [Pogorelov (1964)], Chapter 2, Theorem 2, translated into our notation and written for the three-dimensional case.

First define the *limit angle* of the hypersurface. Given an infinite hypersurface R which is not a prism, draw from some point A above the hypersurface all rays which do not intersect the hypersurface. Their directions fill some solid angle which is called the limit angle of the hypersurface. It is defined to within a parallel displacement which depends on the choice of A.

Next, let s be a monotonic function defined on solid angles A_i with the

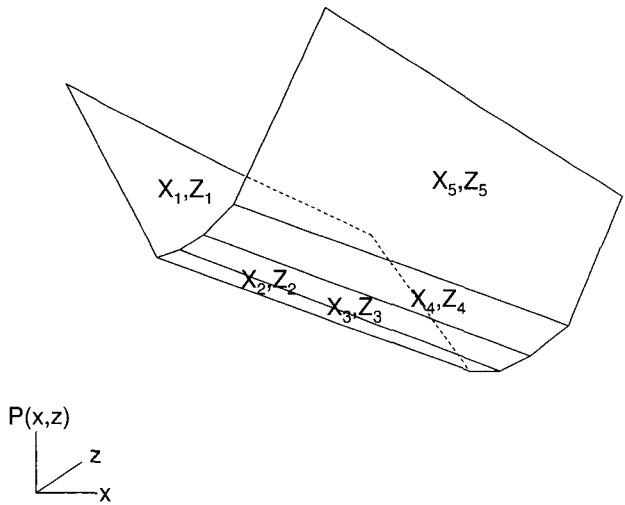

Fig. 3.7 The surface P constructed by rearranging the data shown in Fig. 3.6 to give a convex polyhedron with faces of specified areas.

following properties:

(i) s is continuous, non-negative and equal to zero only if A_i is zero.
(ii) If the angle A_2 is contained in the angle A_1, then $s(A_2) < s(A_1)$.
(iii) If A_2 is obtained from A_1 by a displacement in the direction $r < 0$, then $s(A_1) \leq s(A_2)$.

Theorem 3.10 *We work in $\mathbb{R}^4$ with coordinates (X, Y, Z, r). Let $\mathcal{G}$ be a solid angle with convexity directed towards $r < 0$ which projects onto a region Γ of (x, y, z) space. Let g_i be a set of lines parallel to the r-axis, intersecting the hyperplane $r = 0$ at the points (X_i, Y_i, Z_i). Let σ_i be a set of positive numbers, and let s be a monotonic function, satisfying the conditions above, defined on solid angles which have convexity in the direction $r < 0$ and with vertices on the lines g_i.*

Let $\mathcal{R}$ be the set of all infinite convex hypersurfaces, with limit angles equal to and parallel to those in $\mathcal{G}$ and with vertices A_i on the lines g_i.

Then there is a convex polyhedral hypersurface R in $\mathcal{R}$ for which the function s takes the given values σ_i on its solid angles. This hypersurface is

unique, except that an arbitrary displacement in the r direction is permitted unless s is strictly increasing under a displacement in the direction $r < 0$.

Proof Let $R_0 \in \mathcal{R}$ be a hypersurface with a single vertex A_1 with r coordinate r_1 with solid angle $\mathcal{G}$, so all the vertices $A_i : 2 \leq i \leq n$ are degenerate, with zero solid angles. Then, trivially,

$$s(A_i) \leq \sigma_i :, \; i \geq 2. \tag{3.96}$$

Let R_s be an arbitrary hypersurface in $\mathcal{R}$ for whose solid angles the condition (3.96) is satisfied and with the vertex A_1 having r coordinate r_1. The set $\mathcal{R}_s$ of such hypersurfaces is not empty, as the hypersurface R_0 belongs to it. It is closed because of the assumption that s is monotonic. Assume that the r coordinate of the ith vertex is r_{is}. Set $\varsigma(s) = \sum_{i=1}^{i=n} r_{is}$. Because of the fixing of r_1, the function ς is bounded on the set $\mathcal{R}_s$, and therefore attains its absolute minimum.

Let R_s^* be a hypersurface for which ς attains its minimum. Then we show that, for this hypersurface, $s(A_i) = \sigma_i$ for all i. Suppose not, and that for some j we have $s(A_j) < \sigma_j$. Displace this vertex a small distance δ in the direction $r < 0$ to give A_j'. Let $\mathcal{G}_s$ be the limit angle of the hypersurface R_S^*. Denote by R_s' the hypersurface with the maximum values of r for each (X, Y, Z) which contains the points $A_1, A_2..A_j', ...A_n$ and the angle $\mathcal{G}_s$. This hypersurface belongs to $\mathcal{R}$. If δ is sufficiently small, it also belongs to $\mathcal{R}_s$. The remaining solid angles can only become smaller, and their values of s will still satisfy (3.96). However, $\varsigma(s')$ is clearly less than $\varsigma(s^*)$, contradicting the assumption that S^* is a minimiser of ς. This establishes existence of the required hypersurface.

Now consider uniqueness. Suppose there are two hypersurfaces R_1 and R_2 whose vertices correspond by projection along the r axis and that s takes the same values on the corresponding vertices. If the hypersurfaces do not coincide, the r coordinates of their vertices r_{1i}, r_{2i} will differ for some i. Without loss of generality, let $\delta > 0$ be the maximum of $r_{1i} - r_{2i}$. Displace the hypersurface R_2 a distance δ in the direction $r > 0$. After this displacement we have

$$r_{1i} - r_{2i} \leq 0. \tag{3.97}$$

Let V_1 and V_2 be the set of vertices of R_1 and R_2 respectively which coincide after this displacement. We call two vertices *adjacent* if they belong to the same edge. We claim that a vertex of R_1 which is adjacent to a vertex in V_1 also belongs to V_1.

To show this, let A_1 be a vertex of R_1 which belongs to V_1. Suppose that there is a vertex of R_1 adjacent to A_1 which is not in V_1. Then the inequality (3.97) is strict, and the solid angle at A_2 is contained in the interior of a solid angle of R_1 at the vertex A_1. Since s takes the same value at A_1 and A_2, this contradicts the monotonicity of s.

Since all vertices which are adjacent to vertices in V_1 belong to V_1, all vertices of R_1 belong to V_1. Therefore R_1 and R_2 coincide after some displacement along the r-axis. If s strictly increases when the angle is displaced in the direction $r < 0$, then R_1 and R_2 have to coincide, since otherwise s would have to take on different values on the vertices situated on the same lines g_i but with different r coordinates. □

Theorem 3.10 can be translated into a theorem on the existence of a convex polyhedral hypersurface on Γ with n hyperfaces of specified gradient and specified volume.

Theorem 3.11 *We work in $\mathbb{R}^4$ with coordinates (x, y, z, p). Let $\mathcal{P}$ be the set of convex polyhedral hypersurfaces with convexity directed towards $p < 0$ defined on a region Γ of (x, y, z) space. Let (X_i, Y_i, Z_i) be a set of gradients of the hyperfaces of the hypersurfaces. Let σ_i be a set of positive numbers, and let s be a monotonic function defined on hyperfaces A_i with the following properties:*

(i) s is continuous, non-negative and equal to zero only if A_i has zero volume.

(ii) If the hyperface $A_2 \subset A_1$, then $s(A_2) < s(A_1)$.

(iii) If A_2 is obtained from A_1 by a displacement in the direction $p > 0$, then $s(A_1) \leq s(A_2)$.

Then there is a convex polyhedral hypersurface P in $\mathcal{P}$ for which the function s takes the given values σ_i on its hyperfaces. This hypersurface is unique, except that an arbitrary displacement in the p direction is permitted unless s is strictly increasing under a displacement in the direction $p > 0$.

Proof To start the construction, let $P_0 \in \mathbb{R}$ be a hypersurface with a single hyperface A_1 defined by the equation $p = xX_1 + yY_1 + zZ_1 + p_1$. Then, trivially, we have

$$s(A_i) \leq \sigma_i, \; i \geq 2. \tag{3.98}$$

The remainder of the proof is simply a rewrite of the proof of Theorem 3.10.□

Theorem 3.11 can be interpreted as the solution of a mass transportation problem, as discussed in section 3.2.2. This is done by defining the potential density σ to be a sum of Dirac masses

$$\sigma(X,Y,Z) = \sum_{i=1}^{i=n} \delta(X_i, Y_i, Z_i). \tag{3.99}$$

The theorem then asserts the existence of a unique map $\mathbf{t} : \mathbb{R}^3 \to \Gamma$ which pushes forward the measure defined in (3.99) to Lebesgue measure on Γ. Thus each of the points (X_i, Y_i, Z_i) is mapped to a hyperface A_i. The mapping is not defined at other points in $\mathbb{R}^3$, as the measure σ is zero at these points. The mapping generates a convex P, and therefore represents an energy minimiser in the sense of Theorem 3.4. The energy integral that is minimised is

$$E = \sum_{i=1}^{i=n} \int_{A_i} f^2 \left(\frac{1}{2} \left((x - X_i)^2 + (y - Y_i)^2 \right) - zZ_i \right) \mathrm{d}x\mathrm{d}y\mathrm{d}z. \tag{3.100}$$

The theorem proves the existence and uniqueness of an energy minimiser for this special choice of σ. It can also be interpreted in terms of an energy minimising rearrangement of a function which takes the values (X_i, Y_i, Z_i) on sets of volume σ_i, see [Douglas (2002)], section 5.

In applying this result equations to (3.26) and (3.27) we make the choice that the value of the function s is the volume of the hyperfaces projected onto the hyperplane $x = y = z = 0$. Since the ratio of the actual and projected volumes is fixed by the specified gradients, s satisfies the conditions of the theorem. It is then necessary to ensure that the total of the σ_i is equal to the volume of Γ. The actual construction is best started by choosing a P^* which has n hyperfaces with the required gradients and non-zero areas. This is achieved by choosing the 'Voronoi' solution. The simplest form of this is $P^* = \frac{1}{2}(x^2 + y^2 + z^2)$. The hyperplanes are then defined as

$$p = xX_i + yY_i + zZ_i - \frac{1}{2}(X_i^2 + Y_i^2 + Z_i^2). \tag{3.101}$$

The intersection of these hyperplanes will give a convex surface as shown in Fig. 3.2. The volumes of each hyperface can be calculated and compared with the required value σ_i. The solution can then be found by iteration on the coordinates p_i where the hyperplanes intersect $x = y = z = 0$. Convergence is guaranteed by Theorem 3.11. A more general form of (3.101)

and an efficient implementation of this algorithm, due to R.J.Purser, are described in section 5.3.2.

We discuss the application of Theorem 3.11 to the shallow water case in section 3.4.3.

3.4.2 *Example: frontogenesis*

In section 3.2.3 we showed, in Fig. 3.4, that it might be possible for two points in (X, Y, Z) space a finite distance apart to be mapped to adjacent points in (x, y, z) space. An example of this is provided by the simple frontogenesis problem introduced by [Hoskins and Bretherton (1972)]. This is set in a two-dimensional cross-section which is embedded in a three-dimensional deformation field. The cross-section thus shrinks in time. The equations are, using the formulation (3.25)-(3.27):

$$\begin{aligned} P(x,z) &= \frac{1}{2}x^2 + f^{-2}\varphi, \\ (X,Z) &= \nabla P, \\ \frac{\mathrm{D}X}{\mathrm{D}t} &= -\alpha X, \\ \frac{\mathrm{D}Z}{\mathrm{D}t} &= 0, \\ \frac{\partial u}{\partial x} + \frac{\partial w}{\partial z} &= -\alpha. \end{aligned} \tag{3.102}$$

The final equation of (3.102) implies that the area of a fluid cross-section shrinks at a rate α. The equations are to be solved in the time-dependent domain $\Gamma(t) = [-L\exp(-\alpha t), L\exp(-\alpha t)] \times [0, H]$.

Choose piecewise constant initial data, in the manner of Fig. 3.6. $\Gamma(0)$ is divided into elements with areas σ_i on each of which $(X, Z) = (X_i, Z_i)$. Then equations (3.102) give

$$\begin{aligned} X_i(t) &= X_i(0)\exp(-\alpha t), \\ Z_i(t) &= Z_i(0), \\ \sigma_i(t) &= \sigma_i(0)\exp(-\alpha t). \end{aligned}$$

The solution can now be constructed using Theorem 3.11.

An example is shown using the initial data given in Fig. 3.8, taken from [Cullen and Purser (1984)]. X is chosen so that $X = X(Z)$ is constant along lines of constant Z. This corresponds to the 'zero potential vorticity data' used by [Hoskins and Bretherton (1972)]. The relation $(X, Z) = \nabla P$

means that the slope of the contours has to be given by

$$\frac{\mathrm{d}z}{\mathrm{d}x} = \frac{\mathrm{d}X}{\mathrm{d}Z}. \tag{3.103}$$

Since this slope is constant along Z contours, these contours have to be straight lines.

The data used are shown in Fig. 3.8, plotted on a 200×20 grid. The change of slope at the upper and lower boundaries is because of the extrapolation of the data from the interior grid points. X is given implicitly by

$$\frac{x - X(x,z)}{z - \frac{1}{2}H} = \frac{-5}{1 + [5X(x,z)/L]^2}\frac{L}{H}, \tag{3.104}$$

and $Z = \left(1 + \tan^{-1}[5X(x,z)]\right) H$.

As time evolves, the third and fourth equations of (3.102) show that X becomes smaller as a function of Z. Then (3.103) shows that the slopes of the contours becomes shallower. The boundary conditions require the domain to shrink in the x-direction while staying the same size in the z-direction. The combination of the two effects means that contours collide. For the data defined in (3.104), this happens at time $\alpha t = 1.5$.

This can be most convincingly demonstrated by using piecewise constant data of the type illustrated in Fig. 3.6. X and Z are constant on each element, and X_i, Z_i and σ_i evolve in time according to (3.103). The solution as a function of (x,z) is then found by constructing the surface P as described in the previous section. The solution at time $\alpha t = 2.5$ is shown in Fig. 3.9. Contours of Z have been forced away from the boundary, because this is the only way the required slope can be maintained.

The physical meaning of this solution is that air initially in contact with the boundaries is forced away from it. This is what happens when an 'occluded front' forms in the atmosphere and warm air initially in contact with the ground is lifted away from it. In Fig. 1.3 the fronts marked with a combination of semi-circular and triangular symbols are occluded fronts. It also suggests that the strongest frontal discontinuities will be at the upper and lower boundaries. The rigid upper boundary used in these calculations is not physically realistic, so the conclusion only applies to the lower boundary. In the real atmosphere, it is certainly true that frontal discontinuities are strongest near the surface. However, their detailed structure is governed by other approximations to the Navier-Stokes equations which take into account, in particular, the effects of frictional drag. Fig. 1.4 is an

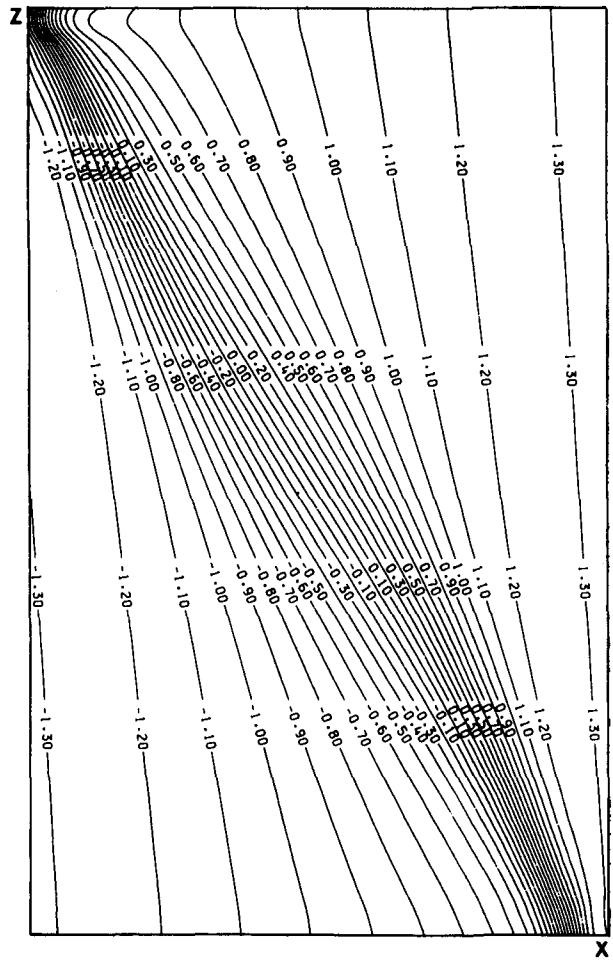

Fig. 3.8 Initial Z contours for the solution of equations (3.102) with $L = H = 1$. From [Cullen and Purser (1984)].

example of a gust front, governed by a different type of dynamics, which is triggered in the presence of an air-mass discontinuity created in the way we describe here.

These solutions have been derived purely from the Lagrangian form of equations (3.102), in which the last equation is written in the form

$$\frac{DV}{Dt} = -\alpha V \tag{3.105}$$

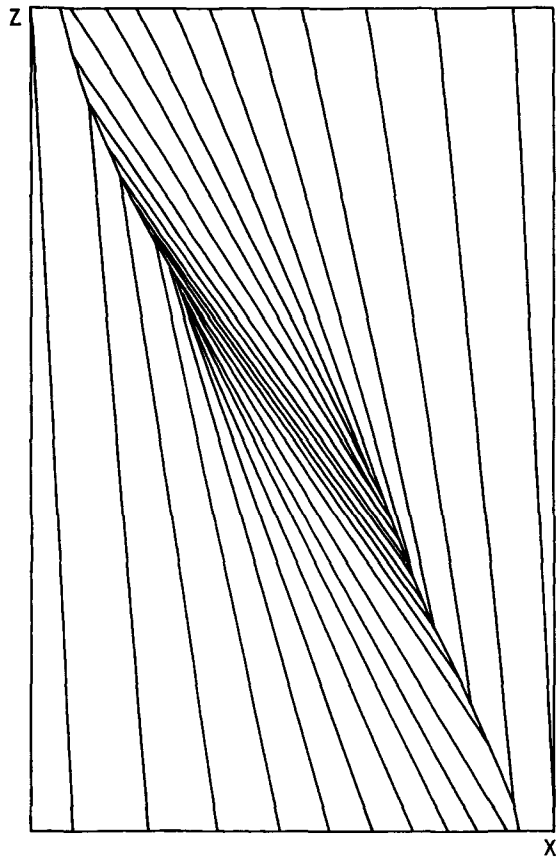

Fig. 3.9 Solution of (3.102) at time $\alpha t = 2.5$, using piecewise constant data of the type shown in Fig. 3.6. The x scale has been expanded so that the domain appears to be the same size as at $t = 0$. From [Cullen and Purser (1984)].

where V is the specific volume. While it is clear that the solution by construction of a convex polyhedron is consistent with the Lagrangian equations for piecewise constant data, which we extend to general data in section 3.5.3, it is not clear whether the solution makes sense as a solution of the Eulerian form of the equations. In particular, as noted in section 3.2.3, the integrated potential vorticity over Γ will not be conserved. Fig. 3.10 shows a solution of the Eulerian semi-geostrophic equations with the initial data shown in Fig. 3.8 at the same time as the solution shown in Fig.

3.9. Conventional finite difference methods are used. Suitable algorithms are discussed in section 5.3.3. Artificial viscosity has to be used to allow the discontinuity to be captured. Apart from local smoothing, the solutions agree quite well. This is gratifying, since finite difference methods are based on the existence of smooth solutions to the governing Eulerian equations, which is certainly not the case here.

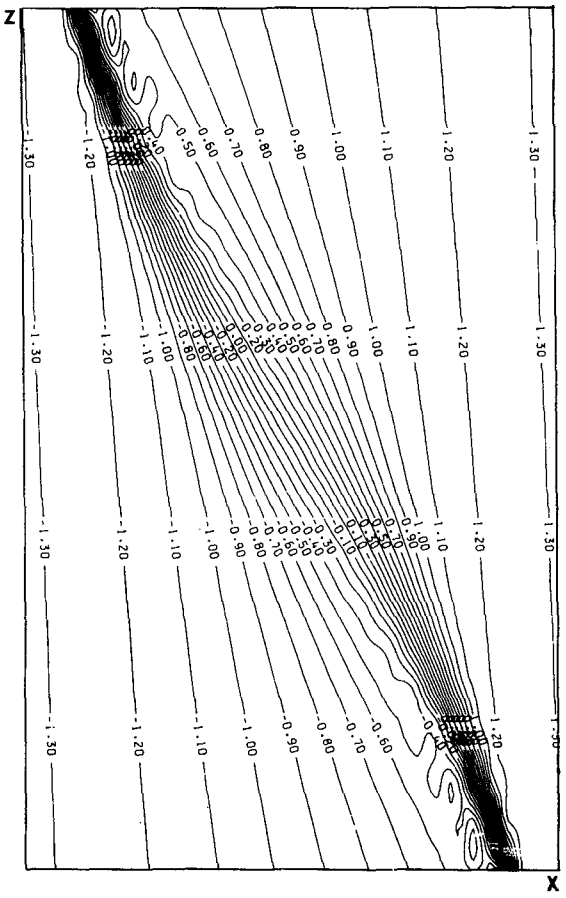

Fig. 3.10 A finite difference solution of equations (3.102) after a time $\alpha t = 2.5$. The x scale has been expanded so that the domain appears to be the same size as at $t = 0$. From [Cullen and Purser (1984)].

The important feature of the solutions as an approximation to a true solution of the Navier-Stokes equations is that there is no discontinuity in a Lagrangian sense. The evolution of X and Z following fluid parcels is continuous in time. The requirement that no fluid trajectory changes direction on a time-scale comparable to f^{-1} will certainly be met if the deformation rate $\alpha \ll f$. The main restriction on the validity of the solutions comes from the assumption of two-dimensionality. While a straight flow $v(x,z)$ in the y direction with a discontinuity in v in the (x,z) plane is an exact solution of the inviscid governing equations, it will be unstable to three-dimensional perturbations if the Richardson number,

$$Ri = \frac{g}{\theta_0}\frac{\partial\theta'}{\partial z}\Big/\left(\frac{\partial v}{\partial z}\right)^2, \tag{3.106}$$

is less than $1/4$. The slope of the discontinuity is given by (3.103) to be $f[v]\theta_0/g[\theta']$ where $[v]$ and $[\theta']$ are the jumps in v and θ' across the discontinuity. Then for a slope ς, the condition $Ri > 1/4$ implies that the jumps occur over a depth $\delta z > \varsigma f^{-1}[v]$. Allowing for the slope of the frontal zone, this implies a horizontal width $f^{-1}[v]$ which is about 1km for v=10ms^{-1}. Thus in general we can expect semi-geostrophic fronts to be realised as shear zones whose width is restricted by the local Richardson number. If the slope is large, so that $[v]/[\theta']$ is comparable to $g/f\theta_0$, then the depth of the zone implied by (3.106) has to be much greater, about 10km for $[v]$=1ms^{-1}. Since this is comparable to the depth of the troposphere, there will be no discontinuity at all unless created by some other type of dynamics. Such a situation is outside the validity of semi-geostrophic theory.

3.4.3 *Example: outcropping*

We now show how solutions of the semi-geostrophic shallow water equations (3.73) and (3.74) can be constructed using piecewise constant data. In applying Theorem 3.11 to this case, we use a two-dimensional form of the theorem. Construct a base solution $P_0 = \frac{1}{2}(x^2 + y^2)$. Choose the value of the function s to be the volume between the face A_i and P_0, as shown in Fig. 3.11. This satisfies the conditions of the theorem. We start the construction by choosing r_i so that the intersection of all the tangent planes with $\Gamma \times [0,\infty)$ lie below the surface P_0, giving $s_i = 0$ for all i, trivially less than σ_i. The rest of the proof follows that of Theorem 3.10.

We next illustrate solutions to the equations obtained using a conven-

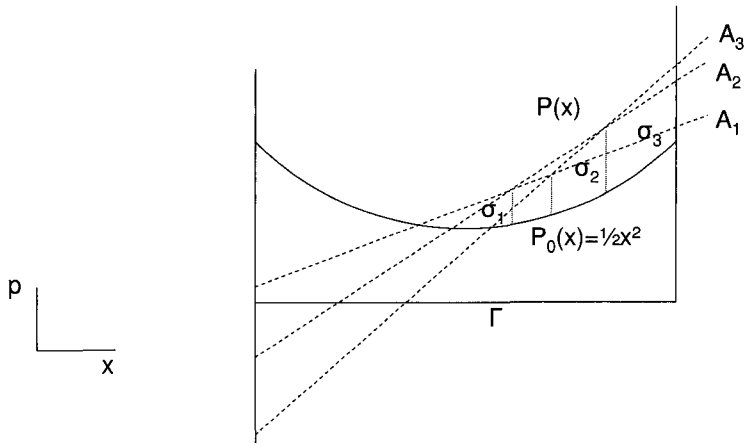

Fig. 3.11 Construction of the depth function for the solution of (3.73) and (3.74) in a one-dimensional cross-section, illustrating the notation used in the text.

tional Eulerian finite difference method by [Cloke and Cullen (1994)]. The model represents the evolution of a wind-driven ocean circulation. Equations (2.75) are rewritten as conservation laws for the momentum and mass. A wind stress (τ_x, τ_y) and frictional drag $-\epsilon(u_g, v_g)$ are applied to the momentum. This gives

$$\begin{aligned} h\frac{\partial u_g}{\partial t} + hu\frac{\partial u_g}{\partial x} + hv\frac{\partial u_g}{\partial y} + fh(v_g - v) &= \tau_x - \epsilon u_g, \\ h\frac{\partial v_g}{\partial t} + hu\frac{\partial v_g}{\partial x} + hv\frac{\partial v_g}{\partial y} - fh(u_g - u) &= \tau_y - \epsilon v_g, \\ \frac{\partial h}{\partial t} + \frac{\partial}{\partial x}(hu) + \frac{\partial}{\partial y}(hv) &= 0. \end{aligned} \tag{3.107}$$

The finite difference solution procedure is described in section 5.3.3. It solves for the mass fluxes (hu, hv) iteratively to enforce the conditions (2.74). The only boundary conditions used are that $\mathbf{u} \cdot \mathbf{n} = 0$ on the walls of the basin. Values of derivatives of u_g and v_g near the boundaries are calculated using one-sided differencing. If values of h become zero in the true solution during the integration period, the finite difference method may predict negative values of h. This is prevented by using a flux limiting procedure in the discretisation of the third equation of (3.107). The use of the mass fluxes rather than the velocities as implicit variables makes it easier to do this.

The problem is solved on a beta plane, so $f = f_0 + \beta y$. The initial data has constant h. The wind stress is chosen to act only in the x-direction.

$$\tau_x = \tau_0 \cos(\pi y/L), \tau_y = 0. \tag{3.108}$$

The model is integrated to a steady state, where the energy input through the wind stress is balanced by the frictional drag. We solve in a square domain with side 10000km. We choose $f_0 = 10^{-4}\text{s}^{-1}$, $\beta = 0.7 \times 10^{-11}\text{m}^{-1}\text{s}^{-1}$, $g = 10\text{ms}^{-2}$, $\epsilon = 3.3 \times 10^{-5}\text{ms}^{-1}$. In the first experiment, we set $\tau_0 = 1.15 \times 10^{-4}\text{m}^2\text{s}^{-1}$ and $h_0 = 16.4\text{m}$. These choices mean that the effect of the advection terms in the momentum equations is comparable to the Coriolis term on a scale of 175km, while frictional effects are important on scales less than 200km. Thus, on larger scales than this, the Type 2 geostrophic equations (2.71) should give similar results to the semi-geostrophic equations. The steady state semi-geostrophic solution is shown in Fig. 3.12, taken from [Cloke and Cullen (1994)] , compared with an analytic calculation of the solution due to [Parsons (1969)]. The solutions show a classic western boundary current. Because of the small mean depth, this can only be sustained if the fluid fails to fill the domain, giving an outcrop in the north-western corner. The solutions show qualitatively similar outcrop lines. The differences are due to the further simplifications made in the analytic model. [Cloke and Cullen (1994)] demonstrate that the semi-geostrophic solution is almost identical to a solution of (2.71) with the same forcing and drag obtained by [Bogue et al. (1986)].

In the second experiment we set $\tau_0 = 9.2 \times 10^{-4}\text{m}^2\text{s}^{-1}$ and $h_0 = 32.8\text{m}$, the other parameters are unaltered. The effect of the advection terms is now important on scales less than 350km, but the effect of the friction is only important on scales less than 100km. It can be shown that the solution of equations (2.71) and the analytic solution are unaltered from the previous experiment, but the solution of equations (3.107) is now different, as shown in Fig. 3.13. The western boundary current overshoots its previous position, due to the effect of the advection terms in the momentum equation.

The importance of this model is in the explanation of the separation of the Gulf Stream from the coast of the United States. It is believed that inertial effects as shown in Fig. 3.13 are important in this process. The outcropping process is also important in the modelling of layers of constant density in the ocean, which can reach the surface at some points. The depth of the layer then becomes zero as a function of horizontal position. A model which can treat this effect is very useful.

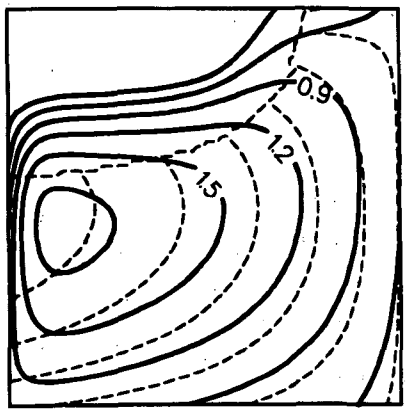

Fig. 3.12 Solid lines: Steady state solutions of equations (3.107) with parameters as given in the text. Dashed lines: Analytic solution. Reprinted from [Cloke and Cullen (1994)] with permission from Elsevier.

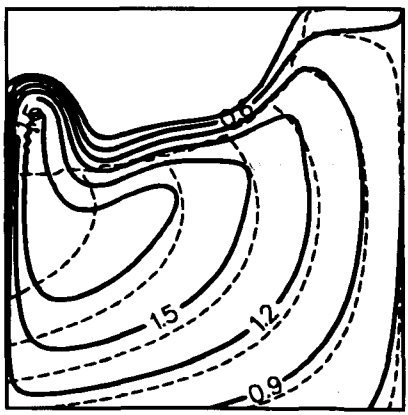

Fig. 3.13 Solid lines: Steady state solution of equations (3.107) using the second set of parameters defined in the text. Dashed lines: Analytic solution as in Fig. 3.12. Reprinted from [Cloke and Cullen (1994)] with permission from Elsevier.

3.5 Rigorous results on existence of solutions

3.5.1 *Solutions of the mass transport problem*

In this section we summarise the rigorous results that have now been obtained for more general cases. We translate the results into our notation

and discuss their physical significance. We do not give any proofs as these can be found in the original references. We start by seeking the existence of a unique energy minimiser in the sense of Theorem 3.3. Informally, we seek existence of a unique rearrangement of a vector-valued function $\mathbf{X} = (X, Y, Z)$ as the gradient of a convex function, where the term rearrangement implies enforcement of the incompressibility constraint (3.29).

A rigorous treatment requires a formal definition of a rearrangement. The following definitions is given in [Douglas (2002)].

Definition 3.6 Let Γ be a bounded set in $\mathbb{R}^3$ with measure μ, and let $F(\mathbf{x}), G(\mathbf{x}) : \Gamma \to \mathbb{R}^d$ be integrable functions. Then F and G are *rearrangements* if

$$\mu\left(\{\mathbf{x} : F(\mathbf{x}) \in B\}\right) = \mu\left(\{\mathbf{x} : G(\mathbf{x}) \in B\}\right), \tag{3.109}$$

for every Borel subset B of $\mathbb{R}^3$. A Borel subset is one for which this definition makes sense.

A simple one-dimensional example is shown in Fig. 3.14.

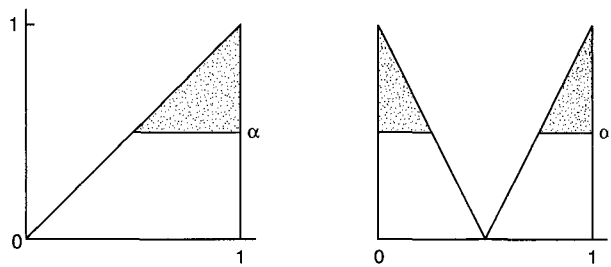

Fig. 3.14 Two scalar functions $F(x)$ and $G(x)$ on the unit interval which are rearrangements of each other. From [Cullen and Douglas (2003)]. ©Royal Meteorological Society, Reading, U.K.

There is a close link between this definition and Definition 3.3. The statement that F and G are rearrangements according to Definition 3.6 is equivalent to saying that, if $F_{\#}\mu = \nu$, then $G_{\#}\mu = \nu$, where ν is a measure on $\mathbb{R}^d$. Thus the set $S = \left\{\mathbf{s} : \mathbb{R}^3 \to \Gamma,\ \mathbf{s}_{\#}\sigma = \mathcal{L}\right\}$ used in Theorem 3.4 is equivalent to stating that $\mathbf{X}(\mathbf{s}(\mathbf{X})$ is a rearrangement of a given function $\mathbf{X}(\mathbf{x})$ which takes values in a given set $B \subset \mathbb{R}^3$ on a set of measure $\int_B \sigma \mathrm{d}X \mathrm{d}Y \mathrm{d}Z$ in Γ.

It is also necessary to formalise the definition of a measure-preserving mapping, which was introduced in section 3.2.1.

Definition 3.7 Given a measure μ on bounded subsets of $\mathbb{R}^3$, a measure-preserving mapping $\mathbf{s} : \mathbb{R}^3 \to \mathbb{R}^3$ satisfies

$$\mu\left(\{\mathbf{x} : \mathbf{s}(\mathbf{x}) \in B\}\right) = \mu(B) \tag{3.110}$$

for all measurable sets B.

The key result is the *polar factorisation* theorem proved by [Brenier (1991)]:

Theorem 3.12 *Given a map* $\mathbf{X} = (X, Y, Z)$ *from* Γ *to* $\mathbb{R}^3$, *that does not collapse sets of positive measure into sets of measure zero,* $\mathbf{X} = \nabla P \circ \mathbf{s}$, *where* $\mathbf{s} : \Gamma \to \Gamma$ *is measure-preserving and* P *is convex. The factorisation is unique up to treatment of sets of zero measure and continuously dependent on the data.*

Proof The main idea is, among all pairs of continuous functions $P(x, y, z)$, $R(X, Y, Z)$ that satisfy

$$P(x, y, z) + R(X, Y, Z) \geq xX + yY + zZ, \tag{3.111}$$

minimise

$$\int_{\Gamma} P \mathrm{d}x\mathrm{d}y\mathrm{d}z + \int_{\mathbb{R}^3} R\sigma \mathrm{d}X\mathrm{d}Y\mathrm{d}Z. \tag{3.112}$$

Condition (3.111) is exactly the duality relation (3.49). The dual problem is much easier to solve. □

This result states that there is a unique rearrangement of a vector-valued function (X, Y, Z) as the gradient of a convex function.This form of the result establishes the existence of a unique energy minimiser in the sense of Theorem 3.3. The restrictions on this result, called the 'non-degeneracy condition', exclude the finite dimensional case treated in section 3.4 where volumes in Γ are mapped onto single points in $\mathbb{R}^3$. Since (X, Y, Z) evolve continuously in time according to equations (3.27), we can expect that the function P whose existence is guaranteed by the polar factorisation will also evolve smoothly in time. The trajectory generated by the incompressible velocity (u, v, w) in physical space, concealed in the D/Dt operators in equations (3.27), is given by the measure-preserving mapping $\mathbf{s}$ as discussed in section 3.2.1.

The gradient of a convex function is the natural multi-dimensional generalisation of a monotonically increasing scalar-valued function, since, as discussed in section 3.2.3, each component of the gradient is an increasing function of the corresponding coordinate. It is possible to find a rearrangement of a general vector valued function which is the gradient of a convex function under much more general conditions. The following result is a special case of results due to [Brenier (1991)] and [McCann (1995)], (see [Douglas (2002)] p.320 for technical details):

Theorem 3.13 *Given $\Gamma \subset \mathbb{R}^3$ with the Lebesgue measure $\mathcal{L}$, with an integrable map $\mathbf{X} = (X, Y, Z)$ from Γ to $\mathbb{R}^3$. Then there is a rearrangement $\mathbf{X}^*$ of $\mathbf{X}$ such that $\mathbf{X}^* = \nabla P$ at the points where P is differentiable, with P convex. It is unique in the sense that if P_1 is another convex function such that ∇P_1 is a rearrangement of $\mathbf{X}$, then $\nabla P_1 = \mathbf{X}^*$ almost everywhere.*

If Γ is open and connected with a smooth boundary, then the mapping $\mathbf{X} \to \mathbf{X}^*$ is continuous in the space of integrable functions from Γ to $\mathbb{R}^3$.

In the physical problem, it is quite possible that the image under (X, Y, Z) of a volume of finite size in Γ has zero measure in $\mathbb{R}^3$. Using (3.24), this will be true, for instance, for a volume with uniform potential temperature θ. The non-degeneracy condition required by Theorem 3.12 will not then be satisfied. Integrability of (X, Y, Z) corresponds essentially to finite energy, so will be satisfied in the physical problem. Therefore Theorem 3.13 will apply under all physically relevant conditions. The difficulty is that there may not be a measure-preserving mapping, so that the trajectory in physical space required to maintain the energy minimisation property may not be achievable by a smooth velocity field. Even if a measure-preserving mapping exists, it may not be unique. We will see examples of this in sections 6.5 and 6.7.

Further progress beyond theorem 3.12 was made by [Burton and Douglas (1998)]. We call $\mathbf{X}$ *countably degenerate* if the non-degeneracy condition can be satisfied by removing countably many level sets. The piecewise constant data discussed in section 3.4 thus generates a map which is countably degenerate. Then [Burton and Douglas (1998)] prove

Theorem 3.14 *If $\mathbf{X}$ on Γ is countably degenerate, then it has a polar factorisation $\mathbf{X} = \mathbf{X}^* \circ \mathbf{s}$, where $\mathbf{s} : \Gamma \to \Gamma$ is measure preserving. Alternatively, if $\mathbf{X}^*$ is almost injective, then the polar factorisation exists and is unique.*

This extension allows the finite dimensional case of section 3.4 to be covered.

It does not, however, cover all cases of physical interest since any restriction on the existence of sets of constant potential temperature is unphysical.

Another important extension is to the periodic case. In section 3.4.2 we demonstrated the formation of discontinuities at the boundaries of Γ, but it was conjectured that no discontinuities could be generated in the interior. In order to find regularity estimates which do not see the effect of the boundaries, we choose $\Gamma = \mathbb{T}^3$, which represents a three-dimensional plane periodic domain with periodicity L in all directions. Though only the case where the horizontal coordinates are periodic is physically relevant, use of the three-dimensional periodic problem allows us to study the behaviour of the interior flow. The following theorem is given by [Loeper (2004)], based on earlier work by [Cordero-Erausquin (1999)].

Theorem 3.15 *Given a map $\mathbf{X} = (X, Y, Z)$ from $\mathbb{T}^3$ to $\mathbb{T}^3$, that does not collapse sets of positive measure into sets of measure zero, $\mathbf{X} = \nabla P \circ \mathbf{s}$, where $\mathbf{s} : \mathbb{T}^3 \to \mathbb{T}^3$ is measure-preserving, P is convex and $P - \frac{1}{2}(x^2+y^2+z^2)$ is periodic. The factorisation is unique up to treatment of sets of zero measure and continuously dependent on the data.*

If R is the Legendre transform of P, then the periodic boundary conditions mean that

$$|\nabla R(X, Y, Z) - (X, Y, Z)| \leq \frac{1}{2}\sqrt{3}L. \tag{3.113}$$

This shows that the velocity $\mathbf{U} = f(\frac{\partial R}{\partial Y} - Y, X - \frac{\partial R}{\partial X})$ is bounded uniformly in time. This is not true in the non-periodic case. It will be necessary to deduce bounds on the velocity in the non-periodic case in order to use Theorem 3.13. Such bounds are deduced from the evolution equations in section 3.5.2.

In section 3.2.2 we identified the energy minimisation problem derived from the semi-geostrophic equations as a mass transportation problem. In Theorem 3.4 we showed that the existence of energy minimisers was equivalent to the existence of an optimal map $\mathbf{t} : \mathbb{R}^3 \to \Gamma$, $\mathbf{t}_{\#}\sigma = \mathcal{L}$. In section 3.4.1 we proved the existence of an optimal map for the special case of piecewise constant data. Theorem 3.13 implies the following result.

Theorem 3.16 *Given probability measures σ, h with bounded supports $\Sigma \subset \mathbb{R}^n, \Gamma \subset \mathbb{R}^n$. Then there exist optimal maps $\mathbf{t} : \Sigma \to \Gamma$ and $\mathbf{t}^{-1} : \Gamma \to \Sigma$ which are inverses, satisfy $\mathbf{t}_{\#}\sigma = h$ and $\mathbf{t}^{-1}_{\#}h = \sigma$ respectively, and*

minimise the cost

$$\int_{\mathbb{R}^n} \left(\frac{1}{2} f^2 \left(\mathbf{t}(\mathbf{X}) - \mathbf{X} \right)^2 \right) \sigma \mathrm{d}X_1 \mathrm{d}X_2 \cdots \mathrm{d}X_n. \tag{3.114}$$

These maps are unique up to sets of measure zero.

Proof This result is a continuous version of an n-dimensional version of Theorem 3.11, with the scalar s in the theorem chosen as in the shallow water case discussed in section 3.4.3. The proof works by showing that there is a unique function Ψ satisfying (3.56). □.

The minimising value of (3.114) is called the *Wasserstein distance* between the measures σ and h, associated with the cost function defined by

$$d(\mathbf{x}, \mathbf{s}^{-1}(\mathbf{x})) = \frac{1}{2} f^2 |\mathbf{x} - \mathbf{X}|^2, \tag{3.115}$$

which forms the integrand of (3.114). Wasserstein distances can be defined for many choices of cost function, see [Villani (2003)]. Their analytic properties were exploited by [Cullen and Gangbo (2001)] to prove the existence of solutions to the semi-geostrophic shallow water equations as stated in section 3.5.2. A different form of Wasserstein distance is the key to the analysis of the compressible case in section 4.1 and in [Cullen and Maroofi (2003)].

The cost (3.114) with $n = 3$ is equivalent to the energy minimised in Theorem 3.4 provided that the integral $\int_{\mathbb{R}^3} \frac{1}{2} f^2 \left(z^2 + Z^2 \right) \sigma \mathrm{d}X \mathrm{d}Y \mathrm{d}Z$ is preserved for all maps $\mathbf{s}$:, $\mathbf{s}_{\#}\sigma = \mathcal{L}$, where we write $\mathbf{s}(X, Y, Z) = (x, y, z)$. This is certainly true for smooth maps $\mathbf{s}$, and is true for the optimal map $\mathbf{t}$ because of its monotonicity property. Further versions and generalisations of Theorem 3.16 are given in [Gangbo and McCann (1996)].

In Theorem 3.5 we showed that points on the boundary of Γ are mapped to points on the boundary of the convex hull of the support Σ of σ. This result suggests that there can be discontinuities in (X, Y, Z) as a function of (x, y, z) on the boundary of Γ as shown in Fig. 3.4. The example shown in section 3.4.2 shows that these can penetrate into the interior of Γ. It was suggested in [Cullen and Purser (1984)] that interior discontinuities were not possible if the potential vorticity Q given by (3.57) is non-zero and bounded. In the finite-dimensional example of section 3.4.1, the potential density σ consists of Dirac masses and Q is zero almost everywhere, so the solution is 'full' of discontinuities.

These questions are addressed by the regularity theory due to Caffarelli. We need some further definitions to explain the results.

Definition 3.8 A weak solution in the sense of Alexandrov to the Monge-Ampère equation (3.39) is a potential R such that for every Borel set B in $\mathbb{R}^3$ with measure ν, the volume of ∇R in $\mathbb{R}^3$ makes sense and is equal to $\sigma\nu(B)$.

Definition 3.9 The space $C^\alpha : 0 < \alpha < 1$ contains all continuous functions $F(\mathbf{X})$ on a set $B \subset \mathbb{R}^3$ such that there exists a constant c for which $|F(\mathbf{X}) - F(\mathbf{Y})| \leq c|\mathbf{X} - \mathbf{Y}|^\alpha$ for all $\mathbf{X}, \mathbf{Y}$ in B.

In addition, the space $W^{2,p}$ is the space of all functions whose second derivatives are integrable according to the usual L^p norm defined in equation (2.112).

The main results as applied to our case are as follows. In [Caffarelli (1992a)] it is proved that if Γ is convex and $\log(\sigma)$ is bounded, then the Monge-Ampère equation (3.39) for R is satisfied in the weak sense due to Alexandrov, and ∇R is a C^α map. Further, if σ is continuous, then R is $W^{2,p}$ for every $p < \infty$ and if σ is C^α, then R is $C^{2,\alpha}$ in the interior of Σ. The restriction $p < \infty$ means that the second derivatives can be locally infinite, so equation (3.39) does not have a solution in the classical sense.

In [Caffarelli (1992a)], it is proved that if both Σ and Γ are convex, then both ∇P and ∇R satisfy estimates of the type $|\nabla P(\mathbf{x}) - \nabla P(\mathbf{y})| \geq c|\mathbf{X} - \mathbf{Y}|^M$. Since ∇P and ∇R are inverses of each other, this means that both are continuous in this sense up to the boundary. This is consistent with Theorem 3.5.

The following theorem is proved in [Caffarelli (1996)].

Theorem 3.17 *If Γ and Σ are convex, and σ is strictly positive and bounded, then there exist a pair of strictly convex $C^{1,\alpha}$ functions P, R on Γ and Σ respectively such that*

(i) ∇P *maps* Γ *onto* Σ *and* ∇R *maps* Σ *onto* Γ.
(ii) ∇P *and* ∇R *are inverses of each other.*
(iii) $\det \mathrm{Hess} R = \sigma$ *in the Alexandrov sense.*
(iv) If σ is C^α, then P, R are strongly convex, i.e. their Hessians are strictly positive and $C^{2,\alpha}$.

This result shows that, if σ is bounded at $t = 0$ and strictly positive on a convex set $\Sigma(0) \subset \mathbb{R}^3$, then if σ is also C^α, both P and R will have second derivatives everywhere, and thus (X, Y, Z) will be continuously differentiable everywhere. This means that no discontinuities can be present. If the problem is posed with periodic boundary conditions, this suggests

that no discontinuities can form anywhere provided that σ remains C^α. If the problem is not given with periodic boundary conditions, then there is no reason why Σ, which evolves as a result of equations (3.42), should remain convex and discontinuities can form. In the atmosphere there are no lateral boundaries, but there is a rigid lower boundary. We can certainly expect discontinuities extending from the lower boundary, as illustrated in section 3.4.2.

It might have been expected that, if σ is bounded away from zero and infinity, there would be no purely interior discontinuities, because the second derivatives of P and R would be bounded. The necessity for the condition that σ is C^α was demonstrated by [Wang (1995)]. He constructed specific examples to show that, if σ is not continuous, then R is not $W^{2,p}$ for any p. He also included the example of the function

$$R(X,Y) = X^2/\log|\log(X^2+Y^2)| + Y^2\log|\log(X^2+Y^2)|. \qquad (3.116)$$

This function is strictly convex, and the potential density calculated from it is continuous and positive. However, it does not have bounded second derivatives at the origin.

It is also shown in [Wang (1995)] that, if the modulus of continuity of σ, defined by $\omega(r) = \sup(|\sigma(\mathbf{X}) - \sigma(\mathbf{Y})| : |\mathbf{X} - \mathbf{Y}| < r$, satisfies

$$\int_0^1 \frac{\omega(r)}{r} < \infty, \qquad (3.117)$$

then R is locally twice differentiable.

The only way to show that no interior discontinuities develop is to prove that σ remains C^α if it is C^α at $t = 0$, or to control $\omega(r)$. This requires use of the evolution equations, and so such result has yet been proved except for short times as will be discussed in the next section. If such interior discontinuities are formed, they do not appear to correspond to any known atmospheric behaviour and would probably represent artefacts introduced by the semi-geostrophic approximation.

3.5.2 *Existence of semi-geostrophic solutions in dual variables*

We now turn to the solution of the evolution equations. It is easiest to start with the equations in dual variables, (3.42). In principle, these can be solved by choosing initial data σ satisfying the conditions of Theorem 3.4, solving the Monge-Ampère equation for R, and then calculating $\mathbf{U}$. The

velocity $\mathbf{U}$ is used to solve the transport equation for σ. Since $\mathbf{U}$ is non-divergent, values of σ will be conserved along trajectories and the initial bounds on σ will be maintained uniformly in time, provided the velocity $\mathbf{U}$ is smooth enough for the transport equation to make sense. The difficulty is that boundedness of σ is not enough to make $\mathbf{U}$ differentiable, as discussed in the previous section. The main task in showing that (3.42) can be solved is to circumvent this difficulty.

It has been known for some time, [Diperna and Lions (1989)], that the transport equation could be solved if $\mathbf{U}$ was in the space L^1_{loc}, i.e. it has integrable first derivatives. However, the discussion above shows that this is only true in our case if σ is continuous, which cannot be guaranteed. This result was extended to vector fields $\mathbf{U}$ of bounded variation (BV) by [Ambrosio (2003)]. Since $\mathbf{U}$ is generated from the gradient of a convex function, and the gradient of a convex function cannot oscillate, it is BV.

Weak existence results for equations (3.42) were first obtained by [Benamou and Brenier (1998)] by smoothing $\mathbf{U}$ to give sufficient regularity. Subsequently, techniques introduced by [Cullen and Gangbo (2001)] together with the result of [Ambrosio (2003)] have allowed the result to be improved. The result below is given in [Cullen and Feldman (2004)]. We assume that σ is a non-negative function defined on $\mathbb{R}^3$ whose integral is the volume of Γ. Such a function is called a *probability measure* on Γ. We assume that the physical domain Γ is open, bounded and connected. We work in the space $C\left([0,T);L^p_w(\mathbb{R}^3)\right)$ of all σ on $\mathbb{R}^3 \times [0,T)$ such that $\sigma(t,\cdot) \in L^p(\mathbb{R}^3)$ for any $t \in [0,T)$, and for any $\{t_k\}_{k=1}^{\infty}, t^* \in [0,T)$ satisfying $\lim_{k\to\infty} t_k = t^*$, $\sigma(t,\cdot)$ converges weakly to $\sigma(t^*,\cdot)$ in $L^p(\mathbb{R}^3)$. Let $B(0,r) \subset \mathbb{R}^3$ be the open ball $|\mathbf{X}| \leq r$.

Theorem 3.18 *Let $p > 1$. For any $T > 0$ and $\sigma(0,\cdot) \in L^p(\mathbb{R}^3)$ with compact support $\Sigma(0)$ there exist functions*

$$\begin{aligned} \sigma &\in L^{\infty}\left([0,T);L^p(\mathbb{R}^3)\right) \cap C[0,T);L^p_w(\mathbb{R}^3), \\ P &\in L^{\infty}\left([0,T);W^{1,\infty}(\Gamma)\right) \cap C[0,T);W^{1,q}(\Gamma), \\ R &\in L^{\infty}\left([0,T);W^{1,\infty}(\mathbb{R}^3)\right) \cap C[0,T);W^{1,q}(B(0,r)), \end{aligned} \tag{3.118}$$

where q is any number in $[1,\infty)$, both P and R are convex functions of their spatial variables, satisfying (3.42) where the evolution equation for σ and the initial data $\sigma(0,\cdot)$ are understood in the weak sense: that is for any

$\varrho \in C_c^1([0,T) \times \mathbb{R}^3)$

$$\int_{\mathbb{R}^3 \times [0,T)} \left(\frac{\partial \varrho}{\partial t} + \mathbf{U} \cdot \nabla \varrho \right) \sigma \mathrm{d}X \mathrm{d}Y \mathrm{d}Z \mathrm{d}t + \int_{\mathbb{R}^3} \sigma(0,\cdot)\varrho(0,\cdot)\mathrm{d}X\mathrm{d}Y\mathrm{d}Z = 0. \tag{3.119}$$

The space C_c^1 contains all functions with a continuous first derivative which have compact support in $\mathbb{R}^3$. Moreover there exists $r > 0$ such that

$$\Sigma(t) \subset B(0,r) \text{ for all } t \in [0,T), \tag{3.120}$$

and we have $\nabla R(X,Y,Z) \in \Gamma$ for each $t \in [0,T)$ and almost every $(X,Y,Z) \in \mathbb{R}^3$.

This theorem shows that there are functions $P(\mathbf{x},t)$ and $R(\mathbf{X},t)$ which have the regularity associated with convex functions, but no more, and are continuous in time and solve equation (3.42) in an integrated sense. Therefore $P(\mathbf{x},t)$ and $R(\mathbf{X},t)$ can have discontinuous derivatives, but the derivatives cannot oscillate. Conditions (3.120) means that the support Σ of σ remains bounded. Thus ∇P is bounded, which ensures that $\mathbf{U} = (f(y-Y), f(X-x), 0)$ as defined in (3.42) remains bounded.

Weak existence of solutions to the shallow water semi-geostrophic equations using the dual variable formulation (3.82) was proved by [Cullen and Gangbo (2001)]. We assume that σ is a probability measure defined on $\mathbb{R}^2$ and h is a probability measure defined on the physical domain Γ, which is assumed to be open, bounded and connected. The characterisation of σ and h as probability measures enforces conservation of mass in both (X,Y) and (x,y) coordinates.

Theorem 3.19 *Let $1 < p < \infty$. Let $B(0,r)$ be a ball of radius r centred at the origin. Assume $\Gamma \subset B(0,r)$. Given $\sigma(0,\cdot) \in L^p(\mathbb{R}^3)$ with compact support $\Sigma(0) \subset B(r_0)$ for some r_0. Then, for any $T > 0$, there exist functions*

$$\begin{aligned} \sigma &\in L^\infty\left([0,T); L^p(\mathbb{R}^3)\right) \cap C[0,T); L_w^p(\mathbb{R}^3)), \\ h &\in L^\infty\left([0,T); W^{1,\infty}(\Gamma)\right) \cap C[0,T); W^{1,q}(\Gamma)), \\ R &\in L^\infty\left([0,T); W^{1,\infty}(\mathbb{R}^3)\right) \cap C[0,T); W^{1,q}(B(0,r)), \end{aligned} \tag{3.121}$$

where q is any number in $[1,\infty)$, both $P = f^{-2}gh + \frac{1}{2}(x^2+y^2)$ and R are convex in their spatial variables, satisfying (3.82) where the evolution

equation for σ and the initial data $\sigma(0,\cdot)$ are understood in the weak sense. The solution satisfies the estimate

$$\int_{\mathbb{R}^2\times\mathbb{R}^2} |\nabla R(t_1,\cdot)-\nabla R(t_2,\cdot)|\sigma \mathrm{d}X\mathrm{d}Y \leq fr(2+fT) \parallel \sigma(0,\cdot) \parallel_{L^1(\mathbb{R}^2)} |t_1-t_2|, \tag{3.122}$$

for all $t_1, t_2 \in [0,T]$. It also satisfies the estimate

$$\parallel \nabla R \parallel_{BV(\Sigma(t))} \leq cr(r_0 + frT)(1 + r_0 + frT), \tag{3.123}$$

where c is a constant independent of T.

The proof proceeds by first showing that, given $\sigma(t,.)$ satisfying the assumptions above, there is a unique probability measure h. The estimate (3.122) shows that, in an integrated sense, the position in Γ corresponding to any (X,Y) varies in a continuous way in time. This gives some information about the physical velocity $\mathbf{u}$. The estimate (3.123) of ∇R gives an estimate of $\mathbf{U}$ by using (3.42). In the three-dimensional case we had the generic estimate (3.120). It reflects the fact that $\Sigma(t)$ can only grow at a bounded rate. To illustrate this, plot the points (X,Y) in (x,y) space. Then $\mathbf{U}$ is at right angles to the line connecting (X,Y) to its image point with coordinates $\nabla R \in \Gamma$. We have assumed that Γ contains the origin. Suppose A with coordinates (X,Y) is the point of $\Sigma(t)$ furthest from Γ so that $\max_{\mathbf{x}\in\Gamma}|\mathbf{X}-\mathbf{x}|$ is largest. Let this maximum difference be between A and B. Then this maximum difference can increase with the component of $\mathbf{U}$ that is parallel to BA. This is illustrated in Fig. 3.15. It can be seen that the magnitude of this component is less than fr_0, so that, if $\Sigma(0)$ is initially within $B(r_0)$, after time t it is within $B(r_t)$ where $r_t \leq r_0 + frt$.

This theorem shows the existence of a time-continuous weak solution, characterised by a depth function $h(x,y)$ with $f^{-2}gh + \frac{1}{2}(x^2+y^2)$ convex. Thus h itself does not have to be convex, but its curvature is restricted. The depth h may vanish over part of the domain Γ as shown in Fig. 3.5. The theorem covers the resulting free boundary problem.

Both Theorems 3.18 and 3.19 are restricted to σ in L^1. As discussed in section 3.5.1, we need to treat cases where there is a region of physical space with uniform X,Y or Z, for instance regions of uniform potential temperature. This is expected to be more difficult because we cannot expect that there will be a trajectory in physical space which is generated by a measure-preserving mapping. We can, however, make progress in dual variables by extending the results to allow σ to be measure-valued. Such an extension is given by [Loeper (2004)]. We first define a solution of (3.42)

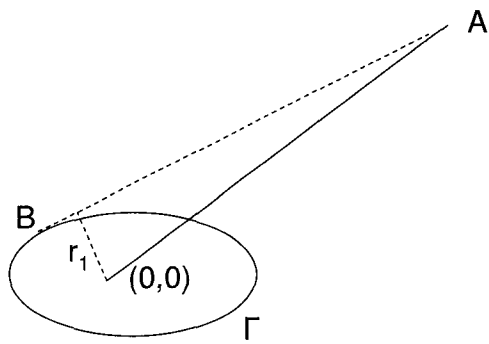

Fig. 3.15 Estimating the rate of growth of $\Sigma(t)$. The distance r_1 from the origin to the line BA is less than r_0, the radius of the ball containing Γ.

in a *weak measure* sense, which replaces (3.119) for $\varrho \in C_c^\infty([0,T) \times \mathbb{R}^3)$ by

$$\int_{[0,T)\times\mathbb{R}^3} \frac{\partial \varrho}{\partial t} \sigma \mathrm{d}X\mathrm{d}Y\mathrm{d}Z\mathrm{d}t + \int_{[0,T)\times\Gamma} f(-Y,X,0)\cdot\nabla\varrho(t,X,Y,Z)\mathrm{d}t\mathrm{d}x\mathrm{d}y\mathrm{d}z + \int_{\mathbb{R}^3} \sigma(0,\cdot)\varrho(0,\cdot)\mathrm{d}X\mathrm{d}Y\mathrm{d}Z = 0. \tag{3.124}$$

Replacing the second term in (3.119) by an integral over Γ avoids the problem that $\mathbf{U}$ is multi-valued at points (X,Y,Z) where σ is unbounded. The natural physical interpretation is that $\mathbf{U}$ is calculated at the centre of mass of the image of (X,Y,Z) in Γ. Loeper then proves

Theorem 3.20 *Let $\sigma(0,\cdot)$ be a probability measure with compact support Σ. Then there exists a weak measure solution of equations (3.42) with the properties that $\sigma \in C[0,T)$, there exists $r(t)$ such that for all $t \in [0,T]$, $\Sigma(t) \subset B(0,r(t))$, and (3.124) holds for all $\varrho \in C^\infty(\mathbb{R}^3 \times [0,T))$. In addition, for any $T > 0$, if $\{\sigma_n\}$ is a sequence of weak measure solutions with initial data $\sigma_n(0,\cdot)$ supported on $\Sigma_n(0) \subset B(0,r)$, for r independent of n, then the sequence is precompact and every converging subsequence of such solutions converges to a weak measure solution of (3.42).*

The second part of the theorem shows that it is possible to find solutions by taking the limit of sequences of approximations, even in this more

difficult case where $\mathbf{U}$ can be multi-valued. This property is necessary for physical usefulness of the equations. Theorems 3.18, 3.19 and 3.20 are all valid for arbitrarily large times, showing that the semi-geostrophic system defines a slow manifold. Physical usefulness of this, however, requires the extension to spherical geometry discussed in sections 4.2 and 4.3. The result would also be much more useful in defining limit solutions for the Navier-Stokes equations if uniqueness could be proved. Otherwise there is the possibility of convergence to different limit solutions in a stochastic manner, which would imply very low predictability.

We now move onto the case where the solutions are smooth. As discussed in section 3.5.1, it is only possible to prove that (X, Y, Z) are differentiable functions of (x, y, z) if Σ, the support of σ, is convex, and σ is continuous. We therefore study this problem in the three-dimensional periodic case used in Theorem 3.15. Equations (3.42) are to be solved with periodic boundary conditions on $R - \frac{1}{2}(X^2 + Y^2 + Z^2), \sigma, x, y$ and z. If smooth solutions can be maintained for large times in this geometry, we can expect that the interior flow will remain smooth in the three-dimensional case with a finite domain Γ, since then discontinuities will only emanate from the boundaries. A theorem of Loeper, using the condition (3.117) for R to be twice differentiable, is

Theorem 3.21 *Let $\sigma(\cdot, 0)$ be a probability measure on $\mathbb{T}^3$, such that σ is strictly positive and satisfies equation (3.117) everywhere. Then there exists $T > 0$ and c_1, c_2 depending on $\sigma(0, \cdot)$ such that on $[0, T]$ there exists a solution $\sigma(t, \cdot)$ of (3.42) that satisfies for all $t \in [0, T]$*

$$\int_0^1 \frac{\omega(t, r)}{r} \mathrm{d}r < \infty, \ \| R(t, \cdot) \|_{C^2(\mathbb{T}^3)} \leq c_2, \tag{3.125}$$

where $\omega(r)$ is as defined before equation (3.117).

None of the results quoted so far give uniqueness or continuous dependence on the data, even though the rearrangement problem solved in Theorem 3.13 has a unique solution which depends continuously on the data. This is because they rely on the construction of an approximating sequence of convex functions $R_n(t)$ which can be proved to have a limit which solves the equations, but may not have a unique limit. To prove uniqueness, we have to consider the case where two solutions R_1, R_2 of (3.42), with associated velocity fields $\mathbf{U}_1, \mathbf{U}_2$ and potential densities $\sigma_1(t, \cdot), \sigma_2(t, \cdot)$, evolve from the same initial data $\sigma_(0, \cdot)$. It is necessary to show that, if $|\sigma_1 - \sigma_2|$ is $\mathrm{O}(\delta t)$ then $|R_1 - R_2| = \mathrm{O}(\delta t)$. Alternatively, if we used the equations in

the real space form (3.27), we would have to show that if $\mathbf{X}_1 - \mathbf{X}_2 = O(\delta t)$ then $P_1 - P_2 = O(\delta t)$. Though Theorem 3.13 gives continuous dependence on the data, it does not give as strong an estimate of the differences as we require. If R and P are twice differentiable, however, the estimate can be obtained. In [Loeper (2004)], Theorem 3.21 is exploited to give a short time uniqueness result.

Theorem 3.22 *Let $\sigma(0,\cdot)$ be a probability measure which is C^α on $\mathbb{T}^3$. From Theorem 3.21, for some $T > 0$ there exists a solution to (3.42) such that $\sigma(\cdot,t)$ is C^α. Then every solution of (3.42) with this initial data that is C^β for $\beta > 0$ coincides with this solution.*

Note that the theorem does not prevent the existence of other solutions for which σ is not in C^β for any β.

3.5.3 *Solutions in physical variables*

The aim of the study of the semi-geostrophic equations is to approximate the Navier-Stokes equations in some asymptotic limit. It is therefore necessary to solve the equations written in a similar form to the Navier-Stokes equations, so that the differences can be estimated. Theorems 3.18 to 3.22 all apply to the equations in dual variables, (3.42) or (3.82). This has no natural counterpart in the Navier-Stokes equations, though we derive such a formulation in a formal way in section 5.1. In this section we extend the results to the Lagrangian equations in physical space, using the forms (3.27) or (3.73). Since the semi-geostrophic approximation is purely Lagrangian, it is appropriate that the governing equations take this form. It is unclear whether the Eulerian form of the semi-geostrophic equations makes sense. In section 3.2.3 we discussed the difficulties caused by the formation of discontinuities. In section 3.5.1 we noted that the measure-preserving mapping defined by the polar factorisation, which defines the physical trajectory, only exists under restrictive conditions which do not cover all physically important cases.

The necessary definitions and results were obtained by [Cullen and Feldman (2004)]. The first step is to define the Lagrangian flow.

Definition 3.10 Let $\Gamma \subset \mathbb{R}^3$ be an open set. Let $P(0,\cdot)$ be a bounded convex function in Γ. Then for any $T > 0$, a pair $(P(\cdot,t), F(\cdot,t))$, where

$$P \in L^\infty\left([0,T); W^{1,\infty}(\Gamma)\right) \cap C[0,T); W^{1,q}(\Gamma), \tag{3.126}$$

P is convex in Γ,

$$F : [0,T) \times \Gamma \to \Gamma,\ F \in C[0,T); L^q(\Gamma), \tag{3.127}$$

where q is any number in $[1,\infty)$, is called a weak Lagrangian solution of equations (3.27) if the following hold.

(i) $\mathbf{F}(0,x,y,z) = (x,y,z)$.

(ii) For any $t > 0$ the mapping $(x,y,z) \to \mathbf{F}(t,x,y,z)$ is measure-preserving in the sense that $\mathbf{F}(t,\cdot)_{\#}\mathcal{L} = \mathcal{L}$, where $\mathcal{L}$ is the Lebesgue measure on Γ.

(iii) For every $t \in (0,T)$ there exists a mapping $\mathbf{F}^*(t,\cdot)$ such that $\mathbf{F}^*(t,\cdot)_{\#}\mathcal{L} = \mathcal{L}$ and satisfies $\mathbf{F}^*(t,\cdot) \circ \mathbf{F}(t,x,y,z) = (x,y,z)$, $\mathbf{F}(t,\cdot) \circ \mathbf{F}^*(t,x,y,z) = (x,y,z)$ for almost every (x,y,z).

(iv) The function $\mathbf{X}(t,\cdot) = \nabla P(t,\cdot)$ satisfies the following. Define

$$\mathbf{Z}(t,\cdot) = \mathbf{X}(t,\mathbf{F}(t,\cdot)) \equiv \nabla P(t,\mathbf{F}(t,\cdot)). \tag{3.128}$$

Then $\mathbf{Z} \in L^\infty([0,t]\times\Gamma)$. Writing $\mathbf{Z} = (Z_1,Z_2,Z_3)$ and $\mathbf{F} = (F_1,F_2,F_3)$, $\mathbf{Z}$ is a weak solution of

$$\begin{aligned} \frac{\partial Z_1}{\partial t} &= f(F_2 - Z_2), \\ \frac{\partial Z_2}{\partial t} &= f(Z_1 - F_1), \\ \frac{\partial Z_3}{\partial t} &= 0, \end{aligned} \tag{3.129}$$

in $[0,T) \times \Gamma$ with $\mathbf{Z}(0,\cdot) = \nabla P(0,\cdot)$. The weak solution is in the sense that for any $\varrho \in C_c^1([0,T) \times \Gamma)$

$$\int_{[0,T)\times\Gamma} \left(Z_1 \frac{\partial \varrho}{\partial t} + f\varrho(F_2 - Z_2) \right) \mathrm{d}x\mathrm{d}y\mathrm{d}z\mathrm{d}t + \int_\Gamma \frac{\partial P(0,\cdot)}{\partial x} \varrho(0,\cdot)\mathrm{d}x\mathrm{d}y\mathrm{d}z, \tag{3.130}$$

with similar equations for the other two components of (3.129).

It can be shown that this type of solution is equivalent to a conventional solution if all the fields are smooth enough. Then [Cullen and Feldman (2004)] prove

Theorem 3.23 *Let Γ be open and bounded, and the closure of Γ be contained in $B = B(0,r)$. Let $P(\cdot,0)$ be a convex bounded function on B, and*

that its Legendre transform R satisfies

$$\det \operatorname{Hess} R \in L^p\left(\nabla P(0,\cdot)(\Gamma)\right) \tag{3.131}$$

for some $p > 1$. Then for any $T > 0$ there exists a weak Lagrangian solution $(P, \mathbf{F})$ of (3.27) in $[0,T)\times\Gamma$, where (3.126) and (3.127) are satisfied for any $q \in [1,\infty)$. Moreover, the function $\mathbf{Z}$ defined by (3.128) satisfies, possibly after modification on a negligible set, $\mathbf{Z} \in W^{1,\infty}([0,T);\mathbb{R}^3)$ for almost all $\mathbf{x} \in \Gamma$, and (3.129) is satisfied, in addition to the weak sense (3.130), for almost all (t,x,y,z) in $[0,T)\times\Gamma$.

This result shows that the three-dimensional incompressible Lagrangian semi-geostrophic equations in physical space can be solved for arbitrarily large times, subject to suitable initial data satisfying (3.131) which is a convexity condition on $P(0,\cdot)$. They therefore form a slow manifold. It is possible to prove an equivalent result for the shallow water semi-geostrophic equations (3.73). Since the definitions have to be modified to allow for the 'compressibility' of shallow water flow, we give them below. Note that, in this context, a measure-preserving mapping becomes a mass-preserving mapping to enforce the mass conservation property on the Lagrangian flow.

Definition 3.11 Let $\Gamma \subset \mathbb{R}^2$ be an open set. Let $P(0,\cdot)$ be a bounded convex function in Γ. Then for any $T > 0$, a pair $(P(t,\cdot), \mathbf{F}(t,\cdot))$, where P is convex in Γ and

$$\begin{aligned} P \in L^\infty\left([0,T); W^{1,\infty}(\Gamma\times[0,h(\cdot,x,y)])\right) \cap \\ C[0,T); W^{1,q}(\Gamma\times[0,h(\cdot,x,y)]], \\ \mathbf{F} : [0,T)\times\Gamma \to \Gamma,\ \mathbf{F} \in C[0,T); L^q(\Gamma\times[0,h(\cdot,x,y)]), \end{aligned} \tag{3.132}$$

where q is any number in $[1,\infty)$, is called a weak Lagrangian solution of equations (3.73) if the following hold.

(i) $\mathbf{F}(0,x,y) = (x,y)$.

(ii) For any $t > 0$ the mapping $(x,y) \to \mathbf{F}(t,x,y)$ satisfies $\mathbf{F}(t,\cdot)_\# h(0,\cdot) = h(t,\cdot)$.

(iii) For every $t \in (0,T)$ there exists a mapping $\mathbf{F}^*(t,\cdot)$ satisfying $\mathbf{F}^*(t,\cdot)_\# h(t,\cdot) = h(0,\cdot)$ and $\mathbf{F}^*(t,\cdot)\circ\mathbf{F}(t,x,y) = (x,y)$, $\mathbf{F}(t,\cdot)\circ\mathbf{F}^*(t,x,y) = (x,y)$ for almost every $\mathbf{x}$.

(iv) The function $\mathbf{X}(t,\cdot) = \nabla P(t,\cdot)$ satisfies the following. Define

$$\mathbf{Z}(t,\cdot) = \mathbf{X}(t,\mathbf{F}(t,\cdot)) \equiv \nabla P(t,\mathbf{F}(t,\cdot)) \tag{3.133}$$

Then $\mathbf{Z} \in L^\infty([0,t] \times \Gamma)$. Writing $\mathbf{Z} = (Z_1, Z_2)$ and $\mathbf{F} = (F_1, F_2)$, $\mathbf{Z}$ is a weak solution of

$$\begin{aligned} \frac{\partial Z_1}{\partial t} &= f(F_2 - Z_2), \\ \frac{\partial Z_2}{\partial t} &= f(Z_1 - F_1) \end{aligned} \tag{3.134}$$

in $[0,T) \times \Gamma$ with $\mathbf{Z}(0,\cdot) = \nabla P(0,\cdot)$. The weak solution is in the sense that for any $\varrho \in C_c^1([0,T) \times \Gamma)$

$$\int_{[0,T)\times\Gamma} \left(Z_1 \frac{\partial \varrho}{\partial t} + f\varrho(F_2 - Z_2) \right) h(0,\cdot) \mathrm{d}x\mathrm{d}y\mathrm{d}t + \int_\Gamma \frac{\partial P(0,\cdot)}{\partial x} \varrho(0,\cdot) h(0,\cdot) \mathrm{d}x\mathrm{d}y, \tag{3.135}$$

with a similar equation for the other component of (3.134).

Theorem 3.24 *Let Γ be open and bounded, and the closure of Γ be contained in $B = B(0,r)$. Let $h(0,\cdot) \geq 0$ be such that $P(0,\cdot) = f^{-2}gh(0,\cdot) + \frac{1}{2}(x^2+y^2)$ is a convex bounded function on B, and assume that*

$$\nabla P(0,\cdot)_\# h(0,\cdot) \in L^p(\nabla P(0,\cdot) \tag{3.136}$$

for some $p > 1$. Then for any $T > 0$ there exists a weak Lagrangian solution $(\mathbf{P},\mathbf{F})$ of (3.73) in $[0,T) \times \Gamma$, where (3.132) is satisfied for any $q \in [1,\infty)$. Moreover, the function $\mathbf{Z}$ defined by (3.128) satisfies, possibly after modification on a negligible set, $\mathbf{Z} \in W^{1,\infty}([0,T);\mathbb{R}^2)$ for almost all $\mathbf{x} \in \Gamma$, and (3.134) is satisfied, in addition to the weak sense (3.135), for almost all (t,x,y,t) in $[0,T) \times \Gamma$.

Theorem 3.20 on the existence of weak measure solutions has not yet been extended to a result in physical space. We may, however, conjecture that such an extension is possible by replacing the space C_c^1 by C_c^∞ in the definitions (3.130) and (3.135) of weak Lagrangian solutions. Assuming that this can be done, it would imply the existence of solutions where the physical velocity (u,v,w) can be measure-valued. The mapping of parcels with given (X,Y,Z) into physical space, and thus the trajectory, is still well-defined. Physically, this corresponds to a situation where mass is transported by a finite distance in zero time. Clearly this cannot happen as an exact solution of the Navier-Stokes equations. The effect of the semi-geostrophic approximation is to collapse time-scales faster then f^{-1} to zero; so that if the real system transports mass on faster time-scales, this will be

represented as instantaneous transport in the semi-geostrophic system. An example is the mass transport in convective clouds. In reality, this takes a time up to 1-2 hours. In a semi-geostrophic model it is instantaneous, as we will see in section 6.7. Another example occurs where the trajectory is constrained by mountain ranges, as shown in section 6.5.

This page is intentionally left blank

Chapter 4

Solution of the semi-geostrophic equations in more general cases

4.1 Solution of the semi-geostrophic equations for compressible flow

4.1.1 *The compressible equations in Cartesian geometry*

The basic semi-geostrophic equations derived in section 2.3 were derived by making the geostrophic momentum approximation in the hydrostatic shallow atmosphere approximation to the governing Navier-Stokes equations (2.1). The theory described in chapter 3 only covers the case of Cartesian geometry, with a uniform rotation rate and the axis of rotation parallel to the direction of the gravitational acceleration. The asymptotic analysis of sections 2.4.6 and 2.5.6 shows that the semi-geostrophic approximation is appropriate on large scales where the horizontal scale L is greater than NH/f. Thus for motions with the vertical scale of the troposphere, about 10km, L has to be greater than about 1000km. This means that spherical geometry and the variations of Coriolis parameter with latitude have to be considered. Moreover, on these scales the Boussinesq approximation and the use of rigid upper and lower boundary conditions on constant pressure surfaces are inappropriate.

In this section we take the first step towards relaxing these extra approximations by using the fully compressible equations, while retaining Cartesian geometry. The analysis follows [Shutts and Cullen (1987)]. While the rotation rate Ω remains uniform, it is no longer required to be about an axis parallel to the gravitational acceleration. We choose the z axis to be in the direction of the axis of rotation. We remove the viscous, diffusive and source terms from equations (2.1), and replace the gravitational term by the gradient of a geopotential which does not have to be in the z direction. We do not analyse the moisture equation. Then (2.1), using (2.3) and (2.4),

becomes

$$\begin{aligned} \frac{\mathrm{D}\mathbf{u}}{\mathrm{D}t} + (-fv, fu, 0) + C_p\theta\nabla\Pi + \nabla\Phi &= 0, \\ \frac{\partial\rho}{\partial t} + \nabla\cdot(\rho\mathbf{u}) &= 0, \\ \frac{\mathrm{D}\theta}{\mathrm{D}t} &= 0, \\ \theta = T(p/p_{ref})^{-R/C_p} &\equiv T/\Pi, \\ p &= \rho RT, \end{aligned} \tag{4.1}$$

where Φ is the geopotential and the Coriolis parameter f is equal to 2Ω. There are eight equations for the unknowns $(u, v, w, p, \Pi, \rho, \theta, T)$. At various stages in the argument it is easier to work with the pair (T, p) than (θ, Π), so we retain both options. The thermodynamic equation can be written in the alternative form

$$C_v\frac{\mathrm{D}T}{\mathrm{D}t} - \frac{p}{\rho^2}\frac{\mathrm{D}\rho}{\mathrm{D}t} = 0. \tag{4.2}$$

The domain Γ is assumed to take the form $\Gamma_z \times [0, \infty)$ and the boundary conditions are that $\mathbf{u}\cdot\mathbf{n} = 0$ on all finite parts of the boundary and that $p,\ \rho \to 0$ as $z \to \infty$.

Define the geostrophic wind by

$$\begin{aligned} -fv_g + C_p\theta\frac{\partial\Pi}{\partial x} + \frac{\partial\Phi}{\partial x} &= 0, \\ fu_g + C_p\theta\frac{\partial\Pi}{\partial y} + \frac{\partial\Phi}{\partial y} &= 0. \end{aligned} \tag{4.3}$$

The compressible semi-geostrophic equations are derived by making the hydrostatic and geostrophic momentum approximations in (4.1). The first two components of the first equation of (4.1) are replaced by

$$\begin{aligned} \frac{\mathrm{D}u_g}{\mathrm{D}t} - fv + C_p\theta\frac{\partial\Pi}{\partial x} + \frac{\partial\Phi}{\partial x} &= 0, \\ \frac{\mathrm{D}v_g}{\mathrm{D}t} + fu + C_p\theta\frac{\partial\Pi}{\partial y} + \frac{\partial\Phi}{\partial y} &= 0, \end{aligned} \tag{4.4}$$

and the third by

$$C_p\theta\frac{\partial\Pi}{\partial z} + \frac{\partial\Phi}{\partial z} = 0. \tag{4.5}$$

It is shown in [Shutts and Cullen (1987)] that these equations, with the boundary conditions above, conserve the energy integral

$$E = \int_\Gamma \rho \left(\frac{1}{2}(u_g^2 + v_g^2) + C_v T + \Phi \right) \mathrm{d}x\mathrm{d}y\mathrm{d}z. \tag{4.6}$$

The three terms represent respectively kinetic, internal and potential energy. The equations also conserve a form of potential vorticity, discussed in section 4.1.4.

The equations can be rewritten in the form

$$\mathbf{Q} \begin{pmatrix} u \\ v \\ w \end{pmatrix} + \frac{\partial}{\partial t} \begin{pmatrix} f v_g \\ -f u_g \\ \theta \end{pmatrix} = \begin{pmatrix} f^2 u_g \\ f^2 v_g \\ 0 \end{pmatrix},$$

$$\mathbf{Q} = \begin{pmatrix} f^2 + f\frac{\partial v_g}{\partial x} & f\frac{\partial v_g}{\partial y} & f\frac{\partial v_g}{\partial z} \\ -f\frac{\partial u_g}{\partial x} & f^2 - f\frac{\partial u_g}{\partial y} & -f\frac{\partial u_g}{\partial z} \\ \frac{\partial \theta}{\partial x} & \frac{\partial \theta}{\partial y} & \frac{\partial \theta}{\partial z} \end{pmatrix}. \tag{4.7}$$

Substitute for (u_g, v_g) in the time-derivative term using (4.3) and the third equation of (4.1). The time derivative of (4.5) gives

$$\frac{\partial \theta}{\partial t}\frac{\partial \Pi}{\partial z} + \theta \frac{\partial}{\partial t}\left(\frac{\partial \Pi}{\partial z}\right) = 0. \tag{4.8}$$

Using (4.5), we obtain

$$\frac{1}{\theta}\frac{\partial \Phi}{\partial z}\frac{\partial \theta}{\partial t} = C_p \theta \frac{\partial}{\partial t}\frac{\partial \Pi}{\partial z}. \tag{4.9}$$

Equation (4.7) can then be written

$$\mathbf{Q_1} \begin{pmatrix} u \\ v \\ w \end{pmatrix} + C_p \theta \frac{\partial}{\partial t} \nabla \Pi = \begin{pmatrix} f^2 u_g \\ f^2 v_g \\ 0 \end{pmatrix},$$

$$\mathbf{Q_1} = \begin{pmatrix} f^2 + f\theta\frac{\partial}{\partial x}\left(\frac{v_g}{\theta}\right) & f\theta\frac{\partial}{\partial y}\left(\frac{v_g}{\theta}\right) & f\theta\frac{\partial}{\partial z}\left(\frac{v_g}{\theta}\right) \\ -f\theta\frac{\partial}{\partial x}\left(\frac{u_g}{\theta}\right) & f^2 - f\theta\frac{\partial}{\partial y}\left(\frac{u_g}{\theta}\right) & -f\theta\frac{\partial}{\partial z}\left(\frac{u_g}{\theta}\right) \\ \frac{1}{\theta}\frac{\partial \Phi}{\partial z}\frac{\partial \theta}{\partial x} & \frac{1}{\theta}\frac{\partial \Phi}{\partial z}\frac{\partial \theta}{\partial y} & \frac{1}{\theta}\frac{\partial \Phi}{\partial z}\frac{\partial \theta}{\partial z} \end{pmatrix}. \tag{4.10}$$

Equation (4.10) can be written as

$$\mathbf{u} + \mathbf{Q_1}^{-1} C_p \theta \frac{\partial}{\partial t} \nabla \Pi = \mathbf{Q_1}^{-1} \begin{pmatrix} f^2 u_g \\ f^2 v_g \\ 0 \end{pmatrix}. \tag{4.11}$$

Now multiply by ρ and use the second equation of (4.1) to substitute for $\mathbf{u}$. To relate $\partial\rho/\partial t$ and $\partial\Pi/\partial t$, we differentiate the logarithm of the equation of state with respect to time, giving

$$\frac{1}{1-\gamma}\frac{\partial}{\partial t}\log\Pi + \frac{\partial}{\partial t}\log\rho + \frac{\partial}{\partial t}\log\theta = 0, \tag{4.12}$$

where $\gamma = C_p/C_v$. Now use (4.9) to give

$$\frac{1}{1-\gamma}\frac{\partial}{\partial t}\log\Pi + \frac{\partial}{\partial t}\log\rho + \frac{C_p\theta}{\frac{\partial\Phi}{\partial z}}\frac{\partial}{\partial t}\frac{\partial\Pi}{\partial z} = 0. \tag{4.13}$$

We thus obtain a single second order equation for $\frac{\partial\Pi}{\partial t}$:

$$\frac{1}{1-\gamma}\frac{\rho}{\Pi}\frac{\partial}{\partial t}\Pi + \frac{\rho C_p\theta}{\frac{\partial\Phi}{\partial z}}\frac{\partial}{\partial t}\frac{\partial\Pi}{\partial z} + \nabla\cdot\rho\mathbf{Q_1}^{-1}C_p\theta\frac{\partial}{\partial t}\nabla\Pi = \tag{4.14}$$

$$\nabla\cdot\rho\mathbf{Q_1}^{-1}\begin{pmatrix} f^2u_g \\ f^2v_g \\ 0 \end{pmatrix}.$$

We expect solvability of (4.14) to require that the coefficients of the highest order terms form a positive definite operator. This will be the case if $\mathbf{Q}_1$ is positive definite. To evaluate this condition, eliminate the θ derivatives from the first two rows of $\mathbf{Q_1}$ by subtracting multiples of the third row from the first two rows, and deduce

$$\det\mathbf{Q_1} = \frac{1}{\theta}\frac{\partial\Phi}{\partial z}\det\mathbf{Q}. \tag{4.15}$$

Thus solvability will be determined by the positive definiteness of $\mathbf{Q}$. This condition takes the same form as that obtained in section 3.1.

4.1.2 *The solution as a sequence of minimum energy states*

In this section we show that a geostrophic and hydrostatic state can again be characterised as a stationary point of the energy with respect to a certain class of variations. More details of these arguments are given in [Shutts and Cullen (1987)], section 4.

Suppose we have a state of the fluid with an associated vector field $(\tilde{u}, \tilde{v})$ and scalar fields $\tilde{\theta}, \tilde{\rho}$. We assume the equation of state is satisfied so that $\tilde{p}$ and $\tilde{T}$ can be derived from $\tilde{\theta}$ and $\tilde{\rho}$. Associate with this state an energy

integral given by the formula analogous to (4.6)

$$E = \int_\Gamma \left(\frac{1}{2}(\tilde{u}^2 + \tilde{v}^2) + C_v \tilde{T} + \Phi \right) \tilde{\rho} \mathrm{d}x\mathrm{d}y\mathrm{d}z. \tag{4.16}$$

This is a functional of $\tilde{u}$, $\tilde{v}$, $\tilde{\theta}$ and $\tilde{\rho}$, regarded as functions of position over Γ, which has the following property.

Theorem 4.1 *The conditions for the energy E to be stationary with respect to variations $\Xi = (\xi, \eta, \chi)$ of particle positions satisfying continuity $\delta(\tilde{\rho}\mathrm{d}x\mathrm{d}y\mathrm{d}z) = 0$ via*

$$\delta\tilde{\rho} = -\tilde{\rho}\nabla \cdot \Xi \tag{4.17}$$

in Γ, and

$$\delta\tilde{u} = f\eta, \ \delta\tilde{v} = -f\xi, \ \delta\tilde{\theta} = 0, \tag{4.18}$$

together with $\Xi \cdot \mathbf{n} = 0$ on the finite boundary of Γ and $p\Xi \to 0$ as $z \to \infty$, are that

$$(-f\tilde{v}, f\tilde{u}, 0) + \nabla\Phi + C_p\tilde{\theta}\nabla\tilde{\Pi} = 0. \tag{4.19}$$

Proof We can consider δE from a Lagrangian viewpoint, and so write

$$\delta E = \int_\Gamma \delta \left(\frac{1}{2}(\tilde{u}^2 + \tilde{v}^2) + C_v \tilde{T} + \Phi \right) \tilde{\rho} \mathrm{d}x\mathrm{d}y\mathrm{d}z. \tag{4.20}$$

Equation (4.2) implies that the condition $\delta\tilde{\theta} = 0$ is equivalent to $C_v\delta\tilde{T} - \frac{\tilde{p}}{\tilde{\rho}^2}\delta\tilde{\rho} = 0$. We then have

$$\begin{aligned} \delta E &= \textstyle\int_\Gamma \left((\tilde{u}\delta\tilde{u} + \tilde{v}\delta\tilde{v}) - \frac{\tilde{p}}{\tilde{\rho}}\nabla \cdot \Xi + \Xi \cdot \nabla\Phi \right) \tilde{\rho}\mathrm{d}x\mathrm{d}y\mathrm{d}z, \\ &= \textstyle\int_\Gamma \left((f\tilde{u}\eta - f\tilde{v}\xi) - \frac{\tilde{p}}{\tilde{\rho}}\nabla \cdot \Xi + \Xi \cdot \nabla\Phi \right) \tilde{\rho}\mathrm{d}x\mathrm{d}y\mathrm{d}z. \end{aligned} \tag{4.21}$$

Integrating by parts to eliminate $\nabla \cdot \Xi$, and using the boundary conditions, gives

$$\delta E = \int_\Gamma \Xi \cdot \left((-f\tilde{v}, f\tilde{u}, 0) + \frac{1}{\tilde{\rho}}\nabla\tilde{p} + \nabla\Phi \right) \tilde{\rho}\mathrm{d}x\mathrm{d}y\mathrm{d}z. \tag{4.22}$$

Use the equation of state and the definition of Π in equations (4.1) to replace $\frac{1}{\tilde{\rho}}\nabla\tilde{p}$ by $C_p\tilde{\theta}\nabla\tilde{\Pi}$. For this to vanish for any Ξ, (4.19) must be satisfied. □

We now consider the condition for the stationary point to be a minimum.

Theorem 4.2 *The condition for E to be minimised with respect to the class of variations defined in Theorem 4.1 is that the matrix $\mathbf{Q}$ defined by*

$$\mathbf{Q} = \begin{pmatrix} f^2 + f\frac{\partial \tilde{v}}{\partial x} & f\frac{\partial \tilde{v}}{\partial y} & f\frac{\partial \tilde{v}}{\partial z} \\ -f\frac{\partial \tilde{u}}{\partial x} & f^2 - f\frac{\partial \tilde{u}}{\partial y} & -f\frac{\partial \tilde{u}}{\partial z} \\ \frac{1}{\tilde{\theta}}\frac{\partial \Phi}{\partial z}\frac{\partial \tilde{\theta}}{\partial x} & \frac{1}{\tilde{\theta}}\frac{\partial \Phi}{\partial z}\frac{\partial \tilde{\theta}}{\partial y} & \frac{1}{\tilde{\theta}}\frac{\partial \Phi}{\partial z}\frac{\partial \tilde{\theta}}{\partial z} \end{pmatrix} \tag{4.23}$$

is positive definite.

Proof We carry out the proof on the assumption that f could be a function of position, as that will be needed in section 4.2. A minimum is also a stationary point, so we characterise the stationary point as satisfying

$$\begin{aligned} (\tilde{u}, \tilde{v}, \tilde{\theta}, \tilde{\rho}, \tilde{p}, \tilde{\Pi}) &= (u_g, v_g, \theta_g, \rho_g, p_g, \Pi_g), \\ (-fv_g, fu_g, 0) + \nabla\Phi + C_p\theta_g\nabla\Pi_g &= 0. \end{aligned} \tag{4.24}$$

Form a second variation starting from (4.22). Using (4.24) to substitute for the terms in the integrand not perturbed by the displacement, this gives

$$\begin{aligned} &\delta^2 E \\ &= \frac{1}{2}\int_\Gamma \Xi \cdot \delta\left\{ f\left((-\tilde{v}, \tilde{u}, 0) + \left(\frac{1}{f\tilde{\rho}}\nabla\tilde{p}\right) + \frac{1}{f}\nabla\Phi \right) \right\} \rho_g \mathrm{d}x\mathrm{d}y\mathrm{d}z, \end{aligned} \tag{4.25}$$

Since the term multiplying δf vanishes at the stationary point, this becomes, using (4.18),

$$\begin{aligned} &\delta^2 E \\ &= \frac{1}{2}\int_\Gamma \Xi \cdot f\left(f(\xi, \eta, 0) + \delta\left(\frac{1}{f\tilde{\rho}}\nabla\tilde{p}\right) + \delta\frac{1}{f}\nabla\Phi \right) \rho_g \mathrm{d}x\mathrm{d}y\mathrm{d}z. \end{aligned} \tag{4.26}$$

The condition $\delta\tilde{\theta} = 0$, together with the equation of state and the definition of $\tilde{\theta}$, imply that $\delta(\tilde{p}\tilde{\rho}^{-\gamma}) = 0$, so that, using (4.17)

$$\frac{\delta\tilde{\rho}}{\tilde{\rho}} = \gamma^{-1}\frac{\delta\tilde{p}}{\tilde{p}} = -\nabla \cdot \Xi. \tag{4.27}$$

As in the proof of Theorem 3.6, write ∂ for the change at a fixed position in space caused by a displacement. Then, also using (4.24), $\delta\tilde{p} = \partial\tilde{p} + \Xi \cdot \nabla\tilde{p} = \partial\tilde{p} + \Xi \cdot \nabla p_g$. Using (4.24) in the last part of (4.27) gives $\gamma^{-1}\delta\tilde{p} = -p_g\nabla \cdot \Xi$. Combining these gives

$$\partial\tilde{p} = -(\Xi \cdot \nabla p_g + p_g\gamma\nabla \cdot \Xi), \tag{4.28}$$

so that

$$\delta(\nabla\tilde{p}) = \partial(\nabla\tilde{p}) + \Xi\cdot\nabla(\nabla\tilde{p}) \tag{4.29}$$
$$= \Xi\cdot\nabla(\nabla p_g) - \nabla(\Xi\cdot\nabla p_g + p_g\gamma\nabla\cdot\Xi).$$

Using (4.27) and (4.29) and $\partial f = 0$, it can then be shown that

$$\rho_g\delta\left(\frac{1}{f\tilde{\rho}}\nabla\tilde{p}\right) =$$
$$\rho_g\Xi\cdot\nabla(\frac{1}{f\rho_g}\nabla p_g) + \frac{1}{f}\left(\nabla p_g\nabla\cdot\Xi - \nabla(\Xi\cdot\nabla p_g) + p_g\gamma\nabla\cdot\Xi\right) \tag{4.30}$$
$$= \rho_g\Xi\cdot\nabla(\frac{1}{f}C_p\theta_g\nabla\Pi_g) + \frac{1}{f}\left(\nabla p_g\nabla\cdot\Xi - \nabla(\Xi\cdot\nabla p_g) + p_g\gamma\nabla\cdot\Xi\right).$$

Since Φ and f are time-independent, we have $\delta\frac{1}{f}\nabla\Phi = \Xi\cdot\nabla(\frac{1}{f}\nabla\Phi)$ and, using (4.24), we obtain

$$\delta\frac{1}{f}\nabla\Phi = \Xi\cdot\nabla\left((v_g, -u_g, 0) - \frac{C_p\theta_g}{f}\nabla\Pi_g\right). \tag{4.31}$$

The first term on the right hand side of (4.30) and the last term of (4.31) cancel when they are substituted into equation (4.25). We then have

$$\delta^2E = \frac{1}{2}\int_\Gamma \left(\begin{array}{c}\Xi\cdot\mathbf{Q}_2\cdot\Xi + \\ \Xi\cdot(\Xi\cdot\nabla(\nabla p_g) + (\nabla p_g)\nabla\cdot\Xi - \nabla(\Xi\cdot\nabla p_g)) \\ +\Xi\cdot(p_g\gamma\nabla\cdot\Xi - C_p\theta\Xi\cdot\nabla(\nabla\Pi_g))\end{array}\right)\rho_g\mathrm{d}x\mathrm{d}y\mathrm{d}z, \tag{4.32}$$

where $\mathbf{Q}_2$ is defined by

$$\left(\begin{array}{ccc} f^2 + f\frac{\partial v_g}{\partial x} - C_p\frac{\partial\theta_g}{\partial x}\frac{\partial\Pi_g}{\partial x} & f\frac{\partial v_g}{\partial y} - C_p\frac{\partial\theta_g}{\partial y}\frac{\partial\Pi_g}{\partial x} & f\frac{\partial v_g}{\partial z} - C_p\frac{\partial\theta_g}{\partial z}\frac{\partial\Pi_g}{\partial x} \\ -f\frac{\partial u_g}{\partial x} - C_p\frac{\partial\theta_g}{\partial x}\frac{\partial\Pi_g}{\partial y} & f^2 - f\frac{\partial u_g}{\partial y} - C_p\frac{\partial\theta_g}{\partial y}\frac{\partial\Pi_g}{\partial y} & -f\frac{\partial u_g}{\partial z} - C_p\frac{\partial\theta_g}{\partial z}\frac{\partial\Pi_g}{\partial y} \\ -C_p\frac{\partial\theta_g}{\partial x}\frac{\partial\Pi_g}{\partial z} & -C_p\frac{\partial\theta_g}{\partial y}\frac{\partial\Pi_g}{\partial z} & -C_p\frac{\partial\theta_g}{\partial z}\frac{\partial\Pi_g}{\partial z}\end{array}\right). \tag{4.33}$$

It is then shown in [Shutts and Cullen (1987)] that, after integration by parts, (4.32) reduces to

$$\delta^2E = \frac{1}{2}\int_\Gamma\left(\Xi\cdot\mathbf{Q}_2\cdot\Xi + p_g\gamma\left(\nabla\cdot\Xi + \frac{1}{p_g\gamma}\Xi\cdot\nabla p_g\right)^2\right)\rho_g\mathrm{d}x\mathrm{d}y\mathrm{d}z. \tag{4.34}$$

Since the second term is positive definite, the condition for E to be minimised is that $\mathbf{Q}_2$ is positive definite. We can see that $\det\mathbf{Q}_2$ is equal to $\det\mathbf{Q}$, where $\mathbf{Q}$ is as defined in (4.7), by subtracting appropriate multiples of the third row from the first two rows and using (4.24) to replace the

factor $-C_p \frac{\partial \Pi_g}{\partial z}$ that multiplies the elements of the third row by the factor $\frac{1}{\theta_g} \frac{\partial \Phi_g}{\partial z}$ that appears in (4.7). Thus the condition for E to be minimised is the positive definiteness of $\mathbf{Q}$. □

We finally state the *stability principle* under which we attempt to solve the compressible semi-geostrophic equations.

Definition 4.1 An admissible solution of the compressible semi-geostrophic equations on a region Γ is one that is characterised by a function $\Pi(t)$ whose evolution satisfies (4.14) in a suitable sense and where the matrix $\mathbf{Q}$ calculated from Π using (4.7) and (4.3) is positive definite.

4.1.3 *Solution by change of variables*

We now seek to show that the compressible semi-geostrophic equations are solvable in the same manner as in section 3.3. The first step is to use the change of variables introduced by [Hoskins (1975)]. Set

$$X = f^{-1} v_g + x, \; Y = -f^{-1} u_g + y, \; Z = \theta. \tag{4.35}$$

The compressible semi-geostrophic equations assembled from equations (4.1), (4.3), (4.4) and (4.5) can then be written as

$$\begin{aligned}
\frac{\mathrm{D}X}{\mathrm{D}t} &= f(y - Y), \\
\frac{\mathrm{D}Y}{\mathrm{D}t} &= f(X - x), \\
\frac{\mathrm{D}Z}{\mathrm{D}t} &= 0, \\
\frac{\partial \rho}{\partial t} + \nabla \cdot (\rho \mathbf{u}) &= 0, \\
f^2(x - X, y - Y, 0) + C_p Z \nabla \Pi + \nabla \Phi &= 0, \\
Z = T(p/p_{ref})^{-R/C_p} &\equiv T/\Pi, \\
p &= \rho R T.
\end{aligned} \tag{4.36}$$

This is a system of ten equations for the unknowns $(X, Y, Z, T, p, \Pi, \rho, u, v, w)$. The options of different versions of the thermodynamic variables is retained for convenience below.

We now describe the energy minimisation property in these variables. We suppose that associated with each particle is a vector field $(\tilde{X}, \tilde{Y}, \tilde{Z})$ and a scalar field $\tilde{\Pi}$. We can calculate $\tilde{\rho}, \tilde{p}, \tilde{T}$ from $\tilde{\Pi}$ and $\tilde{Z}$ using the last

two equations of (4.36). Given these fields, define the energy integral

$$E = \int_\Gamma \left(\frac{1}{2} f^2 \left((x - \tilde{X})^2 + (y - \tilde{Y})^2 \right) + C_v \tilde{T} + \Phi \right) \tilde{\rho} \mathrm{d}x\mathrm{d}y\mathrm{d}z. \tag{4.37}$$

This is a functional of $(\tilde{X}, \tilde{Y}, \tilde{Z})$ and $\tilde{\Pi}$, regarded as functions of position over Γ, which has the following property.

Theorem 4.3 *The conditions for the energy E to be stationary with respect to variations Ξ of particle positions satisfying continuity $\delta(\tilde{\rho}\mathrm{d}x\mathrm{d}y\mathrm{d}z) = 0$ via*

$$\delta\tilde{\rho} = -\tilde{\rho}\nabla \cdot \Xi \tag{4.38}$$

in Γ and

$$\delta\tilde{X} = \delta\tilde{Y} = \delta\tilde{Z} = 0, \tag{4.39}$$

together with $\Xi \cdot \mathbf{n} = 0$ on the finite boundary of Γ and $\tilde{p}\Xi \to 0$ as $z \to \infty$, are that

$$f^2(\tilde{X} - x, \tilde{Y} - y, 0) + C_p \tilde{Z} \nabla\tilde{\Pi} + \nabla\Phi = 0. \tag{4.40}$$

The condition for E to be minimised is that the matrix $\mathbf{Q}$ defined by

$$\begin{pmatrix} f^2 \frac{\partial \tilde{X}}{\partial x} & f^2 \frac{\partial \tilde{X}}{\partial y} & f^2 \frac{\partial \tilde{X}}{\partial z} \\ f^2 \frac{\partial \tilde{Y}}{\partial x} & f^2 \frac{\partial \tilde{Y}}{\partial y} & f^2 \frac{\partial \tilde{Y}}{\partial z} \\ \frac{\partial \tilde{Z}}{\partial x} & \frac{\partial \tilde{Z}}{\partial y} & \frac{\partial \tilde{Z}}{\partial z} \end{pmatrix} \tag{4.41}$$

is positive definite.

The proof is a simple rewrite of that of Theorems 4.1 and 4.2. The definition of admissible solutions is a rewrite of Definition 4.1. However, we cannot simply state that it implies convexity of a scalar potential. It is necessary to use the formulation as a mass transportation problem introduced in section 3.2.2 to prove that the problem can be solved, and that the benefits of convexity in preventing oscillating solutions are retained in this case.

We therefore reinterpret Theorem 4.3 as a mass transportation problem, following [Cullen and Maroofi (2003)]. However, the notation of [Cullen and Maroofi (2003)] is changed to be consistent with the rest of the book. In particular their definitions of σ and ν have been interchanged. We first rewrite the energy integral (4.6), defined in (x, y, z) coordinates, in terms of

(X, Y, Z), and rewrite the internal energy term using the last two equations of (4.36). This gives

$$E = \int_\Gamma \left(\frac{1}{2} f^2((x-X)^2 + (y-Y)^2) + \Phi \right) \rho \mathrm{d}x\mathrm{d}y\mathrm{d}z + \int_\Gamma C_v \left(\frac{R}{p_{ref}} \right)^{\gamma - 1} (Z\rho)^\gamma \, \mathrm{d}x\mathrm{d}y\mathrm{d}z. \tag{4.42}$$

Write $\nu = Z\rho$. Then (4.42) becomes

$$E = \int_\Gamma \left(\frac{\frac{1}{2} f^2 \left((x-X)^2 + (y-Y)^2 \right) + \Phi}{Z} \right) \nu \mathrm{d}x\mathrm{d}y\mathrm{d}z + \int_\Gamma C_v \left(\frac{R}{p_{ref}} \right)^{\gamma - 1} \nu^\gamma \mathrm{d}x\mathrm{d}y\mathrm{d}z. \tag{4.43}$$

The third and fourth equations of (4.36) imply that

$$\frac{\partial \nu}{\partial t} + \nabla \cdot (\nu \mathbf{u}) = 0. \tag{4.44}$$

(4.50) states that, since Z is conserved on particles, the conservation of mass $\rho \mathrm{d}x\mathrm{d}y\mathrm{d}z$ by the compressible equations (4.36) implies conservation of $\nu \mathrm{d}x\mathrm{d}y\mathrm{d}z$. We can thus use $\nu \mathrm{d}x\mathrm{d}y\mathrm{d}z$ as a measure defined on Γ, which will play the role of the mass measure $h\mathrm{d}x\mathrm{d}y$ in the shallow water case.

We now suppose that the values of (X, Y, Z) as functions of (x, y, z) are given by a mapping $\mathbf{s}^{-1} : \Gamma \to \mathbb{R}^3$. According to Theorem 4.3, we seek such a mapping that minimises the energy integral (4.43). The constraints (4.38) and (4.39) on the energy minimisation imply that $\delta\nu = -\nu\nabla \cdot \Xi$. Using Definition 3.3, we define the potential density σ to be the push forward of the measure ν under the map $\mathbf{s}^{-1}$. Thus, given a set $B \subset \mathbb{R}^3$ and a map $\mathbf{s} : \mathbb{R}^3 \to \Gamma$, we have $\sigma(B) = \nu(\mathbf{s}(B))$ so that

$$\mathbf{s}^{-1}_{\#} \nu = \sigma. \tag{4.45}$$

We can now rewrite Theorem 4.3.

Theorem 4.4 *Let ν be a probability measure defined on Γ. Let S be the class of maps $\mathbf{s}^{-1} : \Gamma \to \mathbb{R}^3$ satisfying (4.45). For some $\mathbf{s}^{-1} \in S$ write*

$\mathbf{s}^{-1}(x,y,z) = (\tilde{X},\tilde{Y},\tilde{Z})$. *Define the associated energy integral by*

$$E = \int_\Gamma \left(\frac{\frac{1}{2}f^2((x-\tilde{X})^2 + (y-\tilde{Y})^2) + \Phi}{\tilde{Z}} \right) \nu \mathrm{d}x\mathrm{d}y\mathrm{d}z + \int_\Gamma C_v \left(\frac{R}{p_{ref}} \right)^{\gamma-1} \nu^\gamma \mathrm{d}x\mathrm{d}y\mathrm{d}z. \tag{4.46}$$

The conditions for the energy E to be minimised over maps $\mathbf{s}^{-1} \in S$ are that (4.40) is satisfied and that the matrix $\mathbf{Q}$ defined by (4.41) is positive definite. If such a map exists it is called an optimal map and written $\mathbf{t}^{-1}$: $\Gamma \to \mathbb{R}^3$.

Proof It is necessary to identify the definition of S with the class of variations used in Theorem 4.3. The constraints (4.38) and (4.39) used in Theorem 4.3 imply that $\nu \mathrm{d}x\mathrm{d}y$ is preserved under the displacements, so that the perturbed map $\mathbf{s}^{-1}$ stays in S. Conversely, equation (4.45) applied for a given $\tilde{Z}$ implies that (4.38) holds. □

4.1.4 *The equations in dual variables*

It is not practicable to solve the problem as stated in Theorem 4.4. As in the incompressible case, we need to restate the problem in dual variables. We therefore exchange the definitions of dependent and independent variables as in section 3.2.2, so that (x,y,z) are regarded as functions of the independent variables (X,Y,Z). The first three equations of (4.36) are now regarded as defining a velocity in (X,Y,Z) coordinates on $\mathbb{R}^3$ given by

$$\mathbf{U} = (U,V,W) = (f(y-Y), f(X-x), 0). \tag{4.47}$$

We now assume the converse of the conditions applied to Theorem 4.4, namely that we are given the potential density σ as a function of (X,Y,Z), and the converse of equation (4.45), namely

$$\mathbf{s}_\# \sigma = \nu, \tag{4.48}$$

or

$$\sigma \mathrm{d}X\mathrm{d}Y\mathrm{d}Z = \nu \mathrm{d}x\mathrm{d}y\mathrm{d}z. \tag{4.49}$$

Conservation of the measure ν in physical space becomes conservation of σ

in (X, Y, Z) coordinates, namely

$$\frac{\partial \sigma}{\partial t} + \nabla \cdot (\sigma \mathbf{U}) = 0. \tag{4.50}$$

We can therefore write the system of compressible semi-geostrophic equations in dual variables as

$$\begin{aligned} \frac{\partial \sigma}{\partial t} + \mathbf{U} \cdot \nabla \sigma &= 0, \\ (U, V, W) = (f(y - Y), (X - x), 0), & \\ \rho Z \frac{\partial(x, y, z)}{\partial(X, Y, Z)} &= \sigma, \\ f^2(X - x, Y - y, 0) = C_p Z \nabla \Pi + \nabla \Phi &= 0, \\ Z = T(p/p_{ref})^{-R/C_p} \equiv T/\Pi, & \\ p = \rho R T. & \end{aligned} \tag{4.51}$$

This is a system of eleven equations for the unknowns $(\sigma, x, y, z, U, V, W, \rho, \Pi, T, p)$. In order to solve it, we assume we are given σ at a particular time as a function of (X, Y, Z). We will seek to find (x, y, z) as a function of (X, Y, Z) by solving the energy minimisation problem for an optimal map $\mathbf{t}$. Assuming this can be done, (U, V, W) can be found from the second equation of (4.51) and the solution advanced in time.

We thus seek to solve the equations by constructing an optimal map $\mathbf{s} : \mathbb{R}^3 \to \Gamma$ satisfying (4.48). Let S be the set of such mappings. For $\mathbf{s} \in S$, write $\mathbf{s}(\mathbf{X}) = (\tilde{x}, \tilde{y}, \tilde{z})$. Then the energy integral (4.43) can be rewritten as

$$E = \int_\Gamma \left(\frac{\frac{1}{2} f^2((\tilde{x} - X)^2 + (\tilde{y} - Y)^2) + \Phi(\tilde{x}, \tilde{y}, \tilde{z})}{Z} \right) \sigma \mathrm{d}X \mathrm{d}Y \mathrm{d}Z + \int_\Gamma C_v \left(\frac{R}{p_{ref}} \right)^{\gamma - 1} \nu^\gamma \mathrm{d}x \mathrm{d}y \mathrm{d}z. \tag{4.52}$$

We can now rewrite Theorem 4.4 in these coordinates.

Theorem 4.5 *Let σ be a probability measure defined on Γ. Let S be the class of maps defined above. Then the conditions for the energy E defined by (4.52) to be minimised over maps $\mathbf{s} \in S$ are that (4.40) is satisfied and that the matrix $\mathbf{Q}$ defined by (4.41) is positive definite. If such a map exists it is called an optimal map.*

We now make the duality structure explicit, as in the identification of the dual potentials P and R in section 3.2.2. By analogy with (3.53), we

define a cost function equal to the first term of the energy integral (4.42). Thus

$$d(\mathbf{x}, \mathbf{s}^{-1}(\mathbf{x})) = \frac{\frac{1}{2}f^2(x-X)^2 + (y-Y)^2) + \Phi}{Z}. \tag{4.53}$$

The duality relation is given by equation (3.56) with d defined by (4.53). This new duality structure still falls within the general framework discussed by [Sewell (2002)], p.162. Suppose the map appearing in (4.53) is an optimal map. Then Ψ in (3.56) will be involutive. Given $\Psi(\mathbf{X})$, define Ψ^d as a function of $\mathbf{x}$ for a fixed $\mathbf{X}$ using (3.56). This gives

$$\Psi^d(x,y,z) + \Psi(X,Y,Z) = \frac{\frac{1}{2}f^2\left((x-X)^2 + (y-Y)^2\right) + \Phi(x,y,z)}{Z}. \tag{4.54}$$

Differentiate (4.54) with respect to $\mathbf{x}$ to give

$$Z\nabla\Psi^d = f^2(x-X, y-Y, 0) + \nabla\Phi. \tag{4.55}$$

If we identify Ψ^d as $-C_p\Pi$, we obtain exactly the geostrophic and hydrostatic relation (4.40). Now repeat, regarding Ψ as a function of $\mathbf{X}$ for fixed $\mathbf{x}$. This gives

$$Z\nabla\Psi = \left(f^2(X-x), f^2(Y-y), -d\right). \tag{4.56}$$

Substituting the definition of (U,V) from (4.47) gives

$$f(U,V) = \left(-Z\frac{\partial\Psi}{\partial Y}, Z\frac{\partial\Psi}{\partial X}\right). \tag{4.57}$$

This means that the velocity $\mathbf{U} = (U,V,0)$ is non-divergent in (X,Y,Z) coordinates, so that the conservation law (4.50) becomes the Lagrangian conservation law

$$\frac{\mathrm{D}\sigma}{\mathrm{D}t} = 0. \tag{4.58}$$

These results generalise the incompressible results obtained in section 3.2.2. The differentiations made to obtain (4.55) are equivalent to the calculus of variations used to prove the first part of Theorem 4.1. These relations were obtained in a slightly different context by [Shutts (1989)], p.556, using Hamilton's principle. Note that potentials of the form P and R do not appear. Instead, we work with functions Π and Ψ satisfying the duality relation (4.54) in the form $-C_p\Pi + \Psi = d$. In the incompressible case, we have functions φ and Ψ satisfying (3.56) in the form $-\varphi + \Psi = d$. In both cases it is a pressure-related function in physical space that appears.

In the compressible case we do not have convex potentials allowing us to exploit the geometrical properties of convex functions. Instead, we have to exploit (4.54) directly. In [Cullen and Gangbo (2001)] and [Cullen and Maroofi (2003)] it is shown how the regularity of convex functions extends to involutive functions as defined by (3.55) . This is sufficient for the analysis to proceed, since in particular, it can be proved that oscillatory behaviour of Π and Ψ is restricted.

4.1.5 *Rigorous weak existence results*

We first state a result of [Cullen and Maroofi (2003)], Theorem 3.3, that it is possible to find an optimal map, given two probability measures σ and ν, that minimises the cost obtained by integrating the cost function (4.53) over Σ. The theorem is stated in a somewhat different form from [Cullen and Maroofi (2003)] for consistency with the rest of the book. It generalises Theorem 3.16.

Theorem 4.6 *Given probability measures σ, ν with bounded supports $\Sigma \subset \mathbb{R}^3, \Gamma \subset \mathbb{R}^3$, where Σ takes the form $\Sigma_Z \times [\delta, \frac{1}{\delta}]$ for some $\delta > 0$ and Γ is convex. Assume that $\frac{\partial \Phi}{\partial z} \neq 0$, and that Φ is twice continuously differentiable. Then there exist optimal maps $\mathbf{t} : \Sigma \to \Gamma$ and $\mathbf{t}^{-1} : \Gamma \to \Sigma$ which are inverses, satisfy (4.48) and (4.45) respectively, and minimise the integral of (4.53). These maps are unique up to sets of measure zero. The minimum value of the cost is the Wasserstein distance between σ and ν associated with the cost function (4.53).*

Proof The proof works by showing that there is a unique function Ψ satisfying (4.54). □

In Theorem 3.9 we showed that the solution of the shallow water energy minimisation problem could be identified with the solution of an appropriately chosen incompressible problem. In a similar way, [Cullen and Maroofi (2003)] extend the solution of the problem solved by Theorem 4.6 to a solution of the energy minimisation problem Theorem 4.5. Their results are in Theorems 4.1 and 4.2 of [Cullen and Maroofi (2003)].

Theorem 4.7 *Given Γ, Σ, σ and Φ satisfying the conditions stated in Theorem 4.6. Then there is a unique probability measure ν and optimal map $\mathbf{t}$ with $\mathbf{t}(\mathbf{X}) = (x, y, z)$ which minimise the energy integral (4.52). The minimising map satisfies (4.55).*

Proof The first step is to prove the existence of a unique measure ν. This is given in Theorem 4.1 of [Cullen and Maroofi (2003)] and uses convexity arguments. Theorem 4.6 is then used to prove the existence of a pair of optimal maps. The calculations leading to (4.55) were given in section 4.1.4. The remaining argument is to show that involutive functions defined using d as in (4.53) have the same regularity properties as convex functions. □

In order to prove that weak solutions of the compressible semi-geostrophic equations exist for all finite times, it is necessary to show that $\mathbf{U}$ is bounded, and thus that the support Σ of σ remains bounded for all finite time. This is because Theorems 4.6 and 4.7 only apply to mappings between bounded domains. The same requirement had to be met to prove the results in section 3.5.2. In the present case, we also have to ensure that the energy integral (4.52) makes sense by making appropriate assumptions on Z. Let $B(0,r)$ be a ball of radius r centred at the origin. Assume $\Gamma \subset B(0,r)$. At $t = 0$, suppose that the support $\Sigma(0)$ of σ takes the form $\Sigma_Z \times [\delta, \frac{1}{\delta}]$ with $\Sigma_Z \subset \mathbb{R}^2$ for some $\delta > 0$. Then since the component W of $\mathbf{U}$ is zero, it will remain of this form for all t. If $B_z(0,r)$ is a ball in the plane z =constant, suppose that $\Sigma(t) \subset \cup_{z\in[\delta,1/\delta]} B_z(0,r(t))$. Then a similar argument to that giving (3.123) can be applied to show that $r(t)$ is bounded by $r(0) + frt$ for each t. For a given time $T \geq 0$, define $B_T = \cup_{z\in[\delta,1/\delta]} B_z(0, r(0) + frT)$.

Theorem 4.8 *Let $1 < p < \infty$ and $T > 0$. Assume that Γ and Φ satisfy the conditions of Theorem 4.6 and that we are given a probability measure $\sigma(0,\cdot)$ whose support $\Sigma(0) \subset B_0$ where B_0 is as defined above. Let B_T be the bounded subset of $\mathbb{R}^3$ defined above. Then the system (4.51) of semi-geostrophic equations in dual variables has an admissible weak solution $(\nu, \mathbf{t}^{-1})$ such that with $\sigma(t,\cdot) = \mathbf{t}^{-1}(t,\cdot)_{\#}\nu(t,\cdot)$ and $\mathbf{U}$ as defined in (4.51):*

$$\begin{aligned} \sigma \in L^p((0,T) \times B_T), \| \sigma(t,\cdot) \|_{L^p(B_T)} \leq \| \sigma(0,\cdot) \|_{L^p(B_T)}, \\ \nu \in W^{1,\infty}(\Gamma), \| \nu(t,\cdot) \|_{W^{1,\infty}}(\Gamma) \leq C(\Gamma, B_T, d(\cdot,\cdot)), \\ \mathbf{U} \in L^\infty, \| \mathbf{U} \|_{L^\infty} \leq C(\Gamma, B_T). \end{aligned} \tag{4.59}$$

where C are constants with the indicated dependencies, and $d(\cdot,\cdot)$ is as defined in (4.53).

This result shows that the assumptions of incompressible Boussinesq flow, which are unrealistic on large scales in the atmosphere, can be relaxed and that the resulting semi-geostrophic equations still define a slow

manifold. The proper boundary conditions as stated after equations (4.1) are applied, except that Γ is assumed finite with a rigid boundary all round. The generalisation to unbounded domains in z has been studied, but not yet achieved. The formulation of the equations and the results also relax the requirement that the axis of rotation and the gravitational acceleration are parallel. This is exploited in the next section, when spherical geometry is considered. In order to extend Theorem 4.8 to the spherical case, it would be necessary to replace the assumption on Φ with one of monotonicity in a radial coordinate. This has not yet been done.

4.2 Spherical semi-geostrophic theory

We now consider the appropriate form of the geostrophic momentum approximation to the deep atmosphere Navier-Stokes equations (2.1), and their shallow atmosphere counterpart (2.17), in spherical geometry. The shallow atmosphere approximation was discussed in section 2.2. Consider first the deep atmosphere equations (2.1)-(2.4) with viscous and forcing terms removed, and no moisture equation.

$$\begin{aligned} \frac{\mathrm{D}\mathbf{u}}{\mathrm{D}t} + 2\Omega \times \mathbf{u} + C_p\theta\nabla\Pi + g\hat{\mathbf{r}} &= 0, \\ \frac{\partial\rho}{\partial t} + \nabla\cdot(\rho\mathbf{u}) &= 0, \\ \frac{\mathrm{D}\theta}{\mathrm{D}t} &= 0, \\ \theta = T(p/p_{ref})^{-R/C_p} &\equiv T/\Pi, \\ p &= \rho RT. \end{aligned} \tag{4.60}$$

Equations (4.60) are exactly the same as equations (4.1) if the z axis is chosen in the direction of the axis of rotation, we set $\Phi = gr$, where r is the radial coordinate, and the domain Γ is a spherical semi-infinite annulus defined by $a \le r < \infty$. In practice, the equations have only been analysed using a fixed upper boundary, so that $\Gamma = \{r \in [a, a+H]\}$, see [White et al. (2005)] and [Wood and Staniforth (2003)].

The geostrophic momentum approximation to (4.60) can therefore be made in the same way as in (4.4). Write the equations in cylindrical polar coordinates $(\check{\lambda}, \check{r}, \check{z})$ with the $\check{z}$ axis in the direction of the axis of rotation. The associated velocity components are $(\check{u}, \check{v}, \check{w})$. The definition of the

geostrophic wind is

$$\begin{aligned} \frac{1}{\check{r}} C_p \theta \frac{\partial \Pi}{\partial \check{\lambda}} + 2\Omega \check{v}_g &= 0, \\ C_p \theta \frac{\partial \Pi}{\partial \check{r}} + \frac{g\check{r}}{\sqrt{\check{r}^2 + \check{z}^2}} - 2\Omega \check{u}_g &= 0. \end{aligned} \tag{4.61}$$

The momentum equations become

$$\begin{aligned} \frac{\mathrm{D}\check{u}_g}{\mathrm{D}t} + \frac{\check{u}\check{v}_g}{\check{r}} + \frac{1}{\check{r}} C_p \theta \frac{\partial \Pi}{\partial \check{\lambda}} + 2\Omega \check{v} &= 0, \\ \frac{\mathrm{D}\check{v}_g}{\mathrm{D}t} - \frac{\check{u}\check{u}_g}{\check{r}} + \frac{C_p \theta}{\check{r}} \frac{\partial \Pi}{\partial \check{r}} + \frac{g\check{r}}{\sqrt{\check{r}^2 + \check{z}^2}} - 2\Omega \check{u} &= 0, \\ C_p \theta \frac{\partial \Pi}{\partial \check{z}} + \frac{g\check{z}}{\sqrt{\check{r}^2 + \check{z}^2}} &= 0. \end{aligned} \tag{4.62}$$

The analysis in section 4.1 is applicable to these equations, since the only change is to the coordinate system. Following the method of section 4.1.3, define new variables $(\check{\Lambda},\ \check{\Upsilon},\ \check{Z})$ where $(\check{\Lambda}, \check{\Upsilon}) = (\check{\lambda}, \check{r})$ if $\check{u}_g = \check{v}_g = 0$. Then (4.35) gives

$$\begin{aligned} \check{\Upsilon} \cos \check{\Lambda} &= \frac{\check{u}_g}{2\Omega} + \check{r} \cos \check{\lambda} \\ \check{\Upsilon} \sin \check{\Lambda} &= \frac{\check{v}_g}{2\Omega} + \check{r} \sin \check{\lambda}, \\ \check{Z} &= \check{\theta}. \end{aligned} \tag{4.63}$$

The momentum equations from (4.36) are then

$$\begin{aligned} \frac{\mathrm{D}\check{\Upsilon}}{\mathrm{D}t} + \check{u}\check{\Lambda} - \check{v}_g &= 0, \\ \frac{\mathrm{D}\check{\Lambda}}{\mathrm{D}t} - \frac{\check{u}\Upsilon}{\check{r}^2} + \frac{\check{u}_g}{r} &= 0. \end{aligned} \tag{4.64}$$

The duality relation (4.54) becomes

$$\begin{aligned} -C_p \Pi(\check{\lambda}, \check{r}, \check{z}) + \Psi(\check{\Lambda}, \check{\Upsilon}, \check{Z}) = \\ \frac{2\Omega^2 \left((\check{r} \cos \check{\lambda} - \check{\Upsilon} \cos \check{\Lambda})^2 + (\check{r} \sin \check{\lambda} - \check{\Upsilon} \sin \check{\Lambda})^2 \right) + g\sqrt{\check{r}^2 + \check{z}^2}}{\check{Z}}. \end{aligned} \tag{4.65}$$

The potential density σ defined by (4.49) becomes

$$\sigma \check{\Upsilon} \mathrm{d}\check{\Lambda} \mathrm{d}\check{\Upsilon} \mathrm{d}\check{Z} = \rho \theta \check{r} \mathrm{d}\check{\lambda} \mathrm{d}\check{r} \mathrm{d}\check{z}. \tag{4.66}$$

The equations are to be solved in a region Γ corresponding to the atmosphere in spherical geometry given by

$$a \leq \sqrt{\check{r}^2 + \check{z}^2} \leq a + H. \tag{4.67}$$

The plane $\check{z} = 0$ is the equatorial plane. There will be conservation laws for energy in the form (4.6) and potential density in the form (4.58).

Note that the hydrostatic equation, which is the third equation of (4.62), is degenerate at $z = 0$, which corresponds to the equator where it reduces to $\partial\Pi/\partial\check{z} = 0$. This is the reason why the assumption $\partial\Phi/\partial z > 0$ is made in Theorems 4.6 to 4.8. It is not yet known if the results can be extended to this case. More seriously, the assumption that the kinetic energy is approximated by a geostrophic value in the equatorial plane, without regard to the local vertical, is not appropriate in shallow atmospheres, and does not correspond to observed behaviour, which shows that the wind is primarily horizontal on large scales, as discussed in section 2.2.

In [Shutts (1989)], this system was therefore further approximated by imposing the shallow atmosphere approximation as in section 2.2. [Shutts (1989)] achieved this by making the approximation within the framework of Hamilton's principle, thus ensuring that conservation laws for energy and potential density were retained. The method amounts to projecting the equations which would apply on the equatorial plane $\check{z} = 0$ onto a spherical annulus with radius a, and applying the hydrostatic approximation in the local vertical. We therefore use spherical polar coordinates (λ, ϕ, r) as in section 2.1, with the transformation from cylindrical coordinates given by

$$\lambda = \check{\lambda},\ r\cos\phi = \check{r},\ r = \sqrt{\check{r}^2 + \check{z}^2}. \tag{4.68}$$

Under the shallow atmosphere approximation, the metric factor r is replaced by a wherever it appears.

In the projection, vectors in the $\check{r}$ direction will be multiplied by a factor $\sin\phi$, recalling that ϕ is the latitude. The derivative $\partial/\partial\check{r}$ becomes $-\frac{1}{a\sin\phi}\frac{\partial}{\partial\phi}$ and velocities $\check{v}$ in the $\check{r}$ direction becomes velocities $-v\sin\phi$ in the ϕ direction. The definitions (4.61) become

$$\begin{aligned} \frac{1}{a\cos\phi} C_p\theta \frac{\partial\Pi}{\partial\lambda} - 2\Omega v_g \sin\phi = 0, \\ \frac{1}{a} C_p\theta \frac{\partial\Pi}{\partial\phi} + 2\Omega u_g \sin\phi = 0. \end{aligned} \tag{4.69}$$

The momentum equations become

$$\begin{aligned} \frac{\mathrm{D}u_g}{\mathrm{D}t} - \frac{uv_g \sin\phi}{a\cos\phi} + \frac{1}{a\cos\phi} C_p\theta \frac{\partial \Pi}{\partial \lambda} - 2\Omega v \sin\phi = 0, \\ \sin\phi \frac{\mathrm{D}v_g \sin\phi}{\mathrm{D}t} + \frac{uu_g \sin\phi}{a\cos\phi} + \frac{1}{a} C_p\theta \frac{\partial \Pi}{\partial \phi} + 2\Omega u \sin\phi = 0, \\ C_p\theta \frac{\partial \Pi}{\partial \check{r}} + g = 0. \end{aligned} \tag{4.70}$$

Solve these equations in the region $\Gamma : a \leq r \leq a+H$, with the boundary conditions $\mathbf{u} \cdot \mathbf{n} = 0$. The equations then conserve the energy integral

$$E = \int_\Gamma \rho \left(\frac{1}{2}(u_g^2 + (v_g \sin\phi)^2) + C_v T + gr \right) 4\pi a^2 \cos\phi \mathrm{d}\lambda \mathrm{d}\phi \mathrm{d}r. \tag{4.71}$$

Define new variables (Λ, Υ, Z), where (Λ, Υ) is equal to (λ, ϕ) if $u_g = v_g = 0$, by projecting the data back onto the equatorial plane. The Cartesian coordinates of the projection of the point (λ, ϕ, a) onto the equatorial plane are $(a\cos\phi\cos\lambda, a\cos\phi\sin\lambda)$. Using this, together with the other projection rules above, (4.63) becomes

$$\begin{aligned} \cos\Upsilon\cos\Lambda = \frac{u_g}{2a\Omega} + \cos\phi\cos\lambda, \\ \cos\Upsilon\sin\Lambda = \frac{v_g \sin\phi}{2a\Omega} + \cos\phi\sin\lambda, \\ Z = \theta. \end{aligned} \tag{4.72}$$

These definitions mean that the kinetic energy term in (4.71) is $2\Omega^2$ times the square of the Euclidean distance between the points (λ, ϕ, a) and (Λ, Υ, a) projected onto the equatorial plane. The momentum equations (4.70) become

$$\begin{aligned} a\frac{\mathrm{D}\Upsilon}{\mathrm{D}t} + u\Lambda - v_g = 0, \\ a\frac{\mathrm{D}\Lambda}{\mathrm{D}t} - u\Upsilon - u_g = 0. \end{aligned} \tag{4.73}$$

The duality relation (4.54) becomes

$$\begin{aligned} -C_p\Pi(\lambda, \phi, r) + \Psi(\Lambda, \Upsilon, Z) = \\ \frac{2\Omega^2 a^2 \left((\cos\phi\cos\lambda - \cos\Upsilon\cos\Lambda)^2 + (\cos\phi\sin\lambda - \cos\Upsilon\sin\Lambda)^2 \right) + gr}{Z}. \end{aligned} \tag{4.74}$$

The potential density σ defined by (4.49) becomes

$$\sigma \cos\Upsilon \mathrm{d}\Lambda \mathrm{d}\Upsilon \mathrm{d}Z = \nu \cos\phi \mathrm{d}\lambda \mathrm{d}\phi \mathrm{d}r. \tag{4.75}$$

Since the dependence of (4.74) on Λ and Υ takes the form of a squared Euclidean distance, as in equation (4.54), the arguments leading to the potential density conservation law (4.58) still hold.

These definitions are explored in a slightly different way by [Roulstone and Sewell (1996)]. In particular, it is demonstrated that no change of variables of the form (4.72) is possible in spherical geometry without the device of projecting to Cartesian geometry as used here. We show that the same properties of energy minimisation hold for equations (4.69) and (4.70) as for (4.3) and (4.4). Given a vector field $(\tilde{u}, \tilde{v})$ and scalar fields $\tilde{\theta}$ and $\tilde{\rho}$ as for Theorem 4.1, define the energy integral

$$E = \int_\Gamma \tilde{\rho} \left(\frac{1}{2}(\tilde{u}^2 + (\tilde{v}\sin\phi)^2) + C_v \tilde{T} + gr \right) 4\pi a^2 \cos\phi \mathrm{d}\lambda \mathrm{d}\phi \mathrm{d}r z. \tag{4.76}$$

Write particle positions as $(\tilde{\lambda}, \tilde{\phi}, \tilde{r})$ so that, given a displacement $\Xi = (\xi, \eta, \chi)$,

$$\xi = a\cos\tilde{\phi}\delta\tilde{\lambda}, \ \eta = a\delta\tilde{\phi}, \ \chi = \delta\tilde{r}. \tag{4.77}$$

Theorem 4.9 *The conditions for (4.76) to be minimised with respect to variations $\Xi = (\xi, \eta, \chi)$ of particle positions as specified above, which satisfy continuity in the shallow atmosphere sense, $\delta(\tilde{\rho}\cos\tilde{\phi}\mathrm{d}\lambda\mathrm{d}\phi\mathrm{d}r) = 0$, via*

$$\delta\tilde{\rho} = -\tilde{\rho}\nabla\cdot\Xi \tag{4.78}$$

in Γ, and

$$\begin{aligned} \delta\tilde{u} &= 2\Omega\sin\phi\eta + \frac{\tilde{v}\tan\phi}{a}\xi, \\ \sin\tilde{\phi}\delta(\tilde{v}\sin\tilde{\phi}) &= -2\Omega\sin\phi\xi - \frac{\tilde{u}\tan\phi}{a}\xi, \\ \delta\tilde{\theta} &= 0, \end{aligned} \tag{4.79}$$

together with $\Xi\cdot\mathbf{n} = 0$ on the boundary of Γ, are that

$$(-2\Omega\tilde{v}\sin\phi, 2\Omega\tilde{u}\sin\phi, 0) + (0,0,g) + C_p\tilde{\theta}\nabla\tilde{\Pi} = 0, \tag{4.80}$$

and that the matrix $\mathbf{Q}$ defined by

$$\mathbf{Q} = f\begin{pmatrix} f + \frac{1}{a\cos\tilde{\phi}}\frac{\partial\tilde{v}\sin\tilde{\phi}}{\partial\lambda} + \frac{\tilde{u}}{a\cos\tilde{\phi}} & \frac{1}{a}\frac{\partial\tilde{v}\sin\tilde{\phi}}{\partial\phi} & \frac{\partial\tilde{v}\sin\tilde{\phi}}{\partial r} \\ -\frac{1}{a\cos\tilde{\phi}}\frac{\partial\tilde{u}}{\partial\lambda} + \frac{\tilde{v}\tan\tilde{\phi}}{a} & f - \frac{1}{a}\frac{\partial\tilde{u}}{\partial\phi} & -\frac{\partial\tilde{u}}{\partial r} \\ \frac{1}{\tilde{\theta}}\frac{\partial\Phi}{\partial r}\frac{1}{a\cos\tilde{\phi}}\frac{\partial\tilde{\theta}}{\partial\lambda} & \frac{1}{\tilde{\theta}}\frac{\partial\Phi}{\partial r}\frac{1}{a}\frac{\partial\tilde{\theta}}{\partial\phi} & \frac{1}{\tilde{\theta}}\frac{\partial\Phi}{\partial r}\frac{\partial\tilde{\theta}}{\partial r} \end{pmatrix}, \tag{4.81}$$

where $f = 2\Omega\sin\tilde{\phi}$, is positive definite.

Proof Most of the proof follows that of Theorems 4.1 and 4.2. We only describe the differences. Set $f = 2\Omega \sin\phi$. The quantity $(\tilde{u}\delta\tilde{u} + \tilde{v}\delta\tilde{v})$ that appears in (4.21) is replaced by $(\tilde{u}\delta\tilde{u} + \tilde{v}\sin\tilde{\phi}\delta(\tilde{v}\sin\tilde{\phi})$. Using (4.79), this becomes $\eta 2\Omega \sin\phi\tilde{u} - \xi 2\Omega \sin\phi\tilde{v}$ which is $f(\eta\tilde{u} - \xi\tilde{v})$, which is identical to the expression in the proof of Theorem 4.1. The rest of the proof is the same.

In the second variation, the expression $\delta(-\tilde{v}, \tilde{u}, 0)$ has to be evaluated to pass from (4.25) to (4.26). The second component is straightforward, because using (4.79) gives $f\eta + \frac{\tilde{v}\tan\tilde{\phi}}{a}\xi$. This leads to the extra term in the second row of (4.81). To evaluate the first component, we take out a factor 2Ω rather than a factor f. Using (4.79) gives $\delta(\sin\tilde{\phi}\tilde{v}) = -2\Omega\xi - \frac{\tilde{u}}{a\cos\tilde{\phi}}\xi$. However, instead of $\left(\frac{1}{f}C_p\tilde{\theta}\nabla\tilde{\Pi}\right) + \frac{1}{f}\nabla\Phi$ in (4.30) and (4.31), which gives just v_g at the stationary point, we now have $\left(\frac{1}{2\Omega}C_p\tilde{\theta}\nabla\tilde{\Pi}\right) + \frac{1}{2\Omega}\nabla\Phi$ which is $v_g \sin\phi$. These changes lead to the changes in the first row of (4.81). □

Inspection of (4.81) shows that the conditions for inertial stability, given by the requirement that the diagonal elements of $\mathbf{Q}$ are positive, are respectively

$$2\Omega + \frac{1}{a\cos\tilde{\phi}}\frac{\partial\tilde{v}\sin\tilde{\phi}}{\partial\lambda} + \frac{\tilde{u}}{a\cos\tilde{\phi}} \geq 0, \qquad (4.82)$$

$$f - \frac{1}{a}\frac{\partial\tilde{u}}{\partial\phi} \geq 0.$$

After rewriting the second equation of (4.82) as $2\Omega + \frac{1}{a}\frac{\partial\tilde{u}}{\partial(\cos\phi)} \geq 0$, these can be seen to be exactly the inertial stability conditions for the flow projected onto the equatorial plane. This form of the condition is to be expected, since the equations were derived by projection onto the equatorial plane.

These equations have the disadvantage that the momentum and kinetic energy are approximated not by their geostrophic values, as in (4.4), but by the projection of their geostrophic values on the equatorial plane. If they are applicable on regions of the Earth's surface away from the poles small enough that $2\Omega \sin\phi$ does not change much across the region, they will be less accurate than the f-plane version of the equations used in chapter 3. An alternative procedure is to make the approximations in the reverse order. As in section 2.3, we make the shallow atmosphere and hydrostatic approximations first, and then make the geostrophic momentum approximation. The shallow atmosphere equations (2.17) in spherical polar coordinates, with the forcing and dissipation omitted as in equations (4.60), are

$$\frac{\mathrm{D}(u,v)}{\mathrm{D}t} + \frac{(-uv, u^2)\tan\phi}{a} + (-fv, fu) + C_p\theta\left(\frac{1}{a\cos\phi}\frac{\partial\Pi}{\partial\lambda}, \frac{1}{a}\frac{\partial\Pi}{\partial\phi}\right) = 0,$$

$$C_p\theta\frac{\partial\Pi}{\partial r} + g = 0,$$

$$f = 2\Omega\sin\phi,$$

$$\frac{\partial\rho}{\partial t} + \nabla\cdot(\rho\mathbf{u}) = 0, \quad (4.83)$$

$$\frac{\mathrm{D}\theta}{\mathrm{D}t} = 0,$$

$$\theta = T(p/p_{ref})^{-R/C_p} \equiv T/\Pi,$$

$$p = \rho RT.$$

Define the geostrophic wind by (2.18), with Π replacing Π':

$$\frac{1}{a\cos\phi}C_p\theta\frac{\partial\Pi}{\partial\lambda} - fv_g = 0, \quad (4.84)$$

$$\frac{C_p\theta}{a}\frac{\partial\Pi}{\partial\phi} + fu_g = 0.$$

Then make the geostrophic momentum approximation as in (2.19), giving

$$\frac{\mathrm{D}u_g}{\mathrm{D}t} - \frac{uv_g\tan\phi}{a} - fv + C_p\theta\frac{1}{a\cos\phi}\frac{\partial\Pi}{\partial\lambda} = 0, \quad (4.85)$$

$$\frac{\mathrm{D}v_g}{\mathrm{D}t} + \frac{uu_g\tan\phi}{a} + fu + C_p\theta\frac{1}{a}\frac{\partial\Pi}{\partial\phi} = 0.$$

Equations (4.83) with (4.85) on $\Gamma = \{r \in [a, a+H]\}$, with the boundary conditions $\mathbf{u}\cdot\mathbf{n} = 0$ on the boundary of Γ, conserve the energy integral

$$E = \int_\Gamma \rho\left(\frac{1}{2}(u_g^2 + v_g^2) + C_vT + gr\right)4\pi a^2\cos\phi\mathrm{d}\lambda\mathrm{d}\phi\mathrm{d}r. \quad (4.86)$$

The energy minimisation result of Theorems 4.1 and 4.2 also applies to this case. Given a vector field $(\tilde{u}, \tilde{v})$ and scalar fields $\tilde{\theta}$ and $\tilde{\rho}$ as for Theorem 4.1, define the energy integral

$$E = \int_\Gamma \tilde{\rho}\left(\frac{1}{2}(\tilde{u}^2 + \tilde{v}^2) + C_v\tilde{T} + gr\right)4\pi a^2\cos\phi\mathrm{d}\lambda\mathrm{d}\phi\mathrm{d}r. \quad (4.87)$$

We specify displacements as for Theorem 4.9, equation (4.77).

Theorem 4.10 *The conditions for (4.76) to be minimised with respect to variations $\Xi = (\xi, \eta, \chi)$ of particle positions, specified in spherical polar coordinates (λ, ϕ, r), which satisfy continuity in the shallow atmosphere sense, $\delta(\tilde{\rho}\cos\tilde{\phi}\mathrm{d}\lambda\mathrm{d}\phi\mathrm{d}r) = 0$, via*

$$\delta\tilde{\rho} = -\tilde{\rho}\nabla\cdot\Xi \tag{4.88}$$

in Γ and

$$\begin{aligned} \delta\tilde{u} &= f\eta + \frac{\tilde{v}\tan\phi}{a}\xi, \\ \delta\tilde{v} &= -f\xi - \frac{\tilde{u}\tan\phi}{a}\xi, \\ \delta\tilde{\theta} &= 0, \end{aligned} \tag{4.89}$$

together with $\Xi\cdot\mathbf{n} = 0$ on the boundary of Γ , are that

$$(-f\tilde{v}, f\tilde{u}, 0) + (0,0,g) + C_p\nabla\tilde{\Pi} = 0, \tag{4.90}$$

and that the matrix $\mathbf{Q}$ defined by

$$\mathbf{Q} = f\begin{pmatrix} f + \frac{1}{a\cos\tilde{\phi}}\frac{\partial\tilde{v}}{\partial\lambda} + \frac{\tilde{u}\tan\tilde{\phi}}{a} & \frac{1}{a}\frac{\partial\tilde{v}}{\partial\phi} & \frac{\partial\tilde{v}}{\partial r} \\ -\frac{1}{a\cos\tilde{\phi}}\frac{\partial\tilde{u}}{\partial\lambda} + \frac{\tilde{v}\tan\tilde{\phi}}{a} & f - \frac{1}{a}\frac{\partial\tilde{u}}{\partial\phi} & -\frac{\partial\tilde{u}}{\partial r} \\ \frac{g}{\tilde{\theta}}\frac{1}{a\cos\tilde{\phi}}\frac{\partial\tilde{\theta}}{\partial\lambda} & \frac{g}{\tilde{\theta}}\frac{1}{a}\frac{\partial\tilde{\theta}}{\partial\phi} & \frac{g}{\tilde{\theta}}\frac{\partial\tilde{\theta}}{\partial r} \end{pmatrix}, \tag{4.91}$$

is positive definite.

Proof We only describe the differences from the proofs of Theorems 4.1 and 4.2. Using (4.89), the quantity $(\tilde{u}\delta\tilde{u} + \tilde{v}\delta\tilde{v})$ that appears in (4.21) becomes $f(\eta\tilde{u} - \xi\tilde{v})$, which is identical to the expression in the proof of Theorem 4.1. The rest of the proof is the same.

In the second variation, the expression $\delta(-\tilde{v}, \tilde{u}, 0)$ has to be evaluated to pass from (4.25) to (4.26). This becomes $\left(f\xi + \frac{\tilde{u}\xi\tan\tilde{\phi}}{a}, f\eta + \frac{\tilde{v}\xi\tan\tilde{\phi}}{a}\right)$. The extra terms that then appear in (4.26) are the extra terms that appear in $\mathbf{Q}$ in (4.91). □

Equations (4.83)-(4.85) cannot be written straightforwardly in dual variables like the other systems treated in this book. The reasons will be made clear in the analysis in section 4.3. The structure can only be retained if the equations are further approximated in some way, for instance as by [Salmon (1985)] and [Magnusdottir and Schubert (1991)]. In [Salmon (1985)], the approximation is made within Hamilton's principle, thus ensuring that the

approximated system retains conservation laws for global angular momentum, energy and potential vorticity. The effect of the approximation is that the equations cannot be written down explicitly in physical space, and so it is difficult to estimate their accuracy as a limit of the Navier-Stokes equations. The approximation made by [Magnusdottir and Schubert (1991)] also retains conservation properties, though it is not made using Hamilton's principle. The physical space equations obtained are more implicit, so it is again difficult to assess their accuracy. In both cases the mapping from dual variables to physical space has to be found from a potential density σ of a form similar to (4.75), but it is not clear if it is always possible to do this.

Instead, we follow [Cullen et al. (2005)] and seek to prove that (4.83)-(4.85) can be solved, accepting some loss of structure. It should be noted that there is always a problem with the mathematical structure of the shallow atmosphere equations on the sphere, because the Coriolis term $(-fv, fu, 0)$ cannot be expressed as the curl of a vector. This leads to problems with the conservation of the globally integrated potential vorticity (P. Hydon, personal communication). The exact term $2\Omega \times \mathbf{u}$ can be so expressed.

In order to compare the physical usefulness of the alternative systems (4.60) with (4.69)-(4.70) and (4.83)-(4.85) we analyse the treatment of Rossby waves by both systems. The respective analyses are given by [Shutts (1989)] and [Mawson (1996)]. The equations for incompressible perturbations independent of r about a state of rest with $\theta = \theta_0$ derived from (4.69)-(4.70) are

$$\begin{aligned} \sin^2\phi \frac{\partial v_g'}{\partial t} + 2\Omega u' \sin\phi &= 2\Omega u_g' \sin\phi, \\ \frac{\partial u_g'}{\partial t} - 2\Omega v' \sin\phi &= -2\Omega v_g' \sin\phi, \\ \frac{\partial u'}{\partial \lambda} + \frac{\partial (v' \cos\phi)}{\partial \phi} &= 0, \end{aligned} \tag{4.92}$$

where

$$u_g' \sin\phi = -\frac{C_p\theta_0}{2\Omega a}\frac{\partial \Pi'}{\partial \phi}, \; v_g' \sin\phi = \frac{C_p\theta_0}{2\Omega a \cos\phi}\frac{\partial \Pi'}{\partial \lambda}. \tag{4.93}$$

[Shutts (1989)] makes the substitution

$$\Pi' = \mathrm{Re}[G_m(\varsigma) \exp i(m\lambda - \omega t)], \tag{4.94}$$

where $G_m(\varsigma)$ is the wave amplitude and $\varsigma = \sin\phi$. Then [Shutts (1989)] shows that $G_m(\varsigma)$ satisfies the equation

$$(1-\varsigma)^2 \frac{\mathrm{d}^2 G_m}{\mathrm{d}\varsigma^2} - \frac{2}{\varsigma}\frac{\mathrm{d}G_m}{\mathrm{d}\varsigma} + \left(\alpha_m - \frac{m^2}{1-\varsigma^2}\right) G_m = 0, \tag{4.95}$$

where $\alpha_m = m^2 - 2\Omega m/\omega$. Given the boundary conditions $G_m = 0$ at the poles $\varsigma = \pm 1$, equation (4.95) is an eigenvalue problem for α_m. [Shutts (1989)] shows that the frequencies of the permitted solutions α_{mk} are given by

$$\omega_k = \frac{-2\Omega m}{k(k+1) - m^2}. \tag{4.96}$$

The equivalent linearisation of equations (4.83)-(4.85) is

$$\begin{aligned} \frac{\partial v_g'}{\partial t} + 2\Omega u' \sin\phi &= 2\Omega u_g' \sin\phi, \\ \frac{\partial u_g'}{\partial t} - 2\Omega v' \sin\phi &= -2\Omega v_g' \sin\phi, \\ \frac{\partial u'}{\partial \lambda} + \frac{\partial (v' \cos\phi)}{\partial \phi} &= 0, \end{aligned} \tag{4.97}$$

together with (4.93). A similar analysis in [Mawson (1996)] shows that (4.96) is replaced by

$$\omega_k = \frac{-2\Omega m}{k(k+1)}. \tag{4.98}$$

Equation (4.98) is also the dispersion relation for the unapproximated equations for incompressible flow independent of r. Therefore it can be seen that the use of equations (4.83-(4.85) is advantageous in the treatment of Rossby waves, which are the basis of the motions producing weather systems. We therefore analyse this model, despite its lack of mathematical structure. Theorem 4.10 shows that the characterisation of the solutions as energy minimisers still holds. This is the basis of all the versions of semi-geostrophic theory analysed in this book and gives them a sound physical basis.

4.3 The shallow water spherical semi-geostrophic equations

4.3.1 *Solution procedure*

The analysis of equations (4.83)-(4.85) is difficult, because of the lack of a simple change of variables. In [Cullen et al. (2005)], it was shown how dual variables could be defined and used to solve the shallow water version of these equations. We summarise their analysis in this section. It is likely that the extension to the compressible equations (4.83)-(4.85) will be straightforward.

The shallow water equations in spherical polar coordinates can be derived from (2.74) and (2.75). The geostrophic wind is defined by

$$g\frac{1}{a\cos\phi}\frac{\partial h}{\partial\lambda} - fv_g = 0, \qquad g\frac{1}{a}\frac{\partial h}{\partial\phi} + fu_g = 0, \tag{4.99}$$

where $f = 2\Omega\sin\phi$, and the evolution equations are

$$\begin{aligned} \frac{\mathrm{D}u_g}{\mathrm{D}t} - \frac{uv_g\tan\phi}{a} + \frac{g}{a\cos\phi}\frac{\partial h}{\partial\lambda} - fv = 0, \\ \frac{\mathrm{D}v_g}{\mathrm{D}t} + \frac{uu_g\tan\phi}{a} + \frac{g}{a}\frac{\partial h}{\partial\phi} + fu = 0, \\ \frac{\partial h}{\partial t} + \frac{1}{a\cos\phi}\left(\frac{\partial}{\partial\lambda}(hu) + \frac{\partial}{\partial\phi}(hv\cos\phi)\right) = 0. \end{aligned} \tag{4.100}$$

The region of integration is the surface S^2 of the whole sphere, so no boundary conditions are required. The energy integral is given by (2.76). The following energy minimisation result holds. Given a vector field $(\tilde{u},\tilde{v})$ and a scalar field $\tilde{h}$, define the energy integral

$$\int_\Gamma \left(\frac{1}{2}\tilde{h}\left(\tilde{u}^2+\tilde{v}^2\right) + \frac{1}{2}g\tilde{h}^2\right) 4\pi a^2\cos\phi\mathrm{d}\lambda\mathrm{d}\phi. \tag{4.101}$$

Write particle positions as $(\tilde{\lambda},\tilde{\phi})$ so that, given a displacement $\Xi = (\xi,\eta)$,

$$\xi = a\cos\tilde{\phi}\delta\tilde{\lambda},\ \eta = a\delta\tilde{\phi}. \tag{4.102}$$

Theorem 4.11 *The conditions for (4.101) to be minimised with respect to the variations in particle positions specified in (4.102), which satisfy continuity* $\delta(\tilde{h}\cos\tilde{\phi}\mathrm{d}\lambda\mathrm{d}\phi) = 0$, *via*

$$\delta\tilde{h} = -\tilde{h}\nabla\cdot\Xi \tag{4.103}$$

in Γ, *and*

$$\delta\tilde{u} = f\eta + \frac{\tilde{v}\tan\phi}{a}\xi, \qquad (4.104)$$
$$\delta\tilde{v} = -f\xi - \frac{\tilde{u}\tan\phi}{a}\xi,$$

are that

$$(-f\tilde{v}, f\tilde{u}) + g\nabla\tilde{h} = 0, \qquad (4.105)$$

and that the matrix $\mathbf{Q}$ *defined by*

$$\mathbf{Q} = f\begin{pmatrix} f + \frac{1}{a\cos\tilde{\phi}}\frac{\partial\tilde{v}}{\partial\lambda} + \frac{\tilde{u}\tan\tilde{\phi}}{a} & \frac{1}{a}\frac{\partial\tilde{v}}{\partial\phi} \\ -\frac{1}{a\cos\tilde{\phi}}\frac{\partial\tilde{u}}{\partial\lambda} + \frac{\tilde{v}\tan\tilde{\phi}}{a} & f - \frac{1}{a}\frac{\partial\tilde{u}}{\partial\phi} \end{pmatrix} \qquad (4.106)$$

is positive definite.

Proof This is a restatement of Theorem 3.6 in spherical polar coordinates, noting that Theorem 3.6 was proved for the case where f is a function of position. The changes to deal with spherical coordinates were described in the proof of Theorem 4.10. □

The difficulty in finding dual variables was analysed by [Roulstone and Sewell (1996)] and [Roulstone and Sewell (1997)], eq. (7.20). It arises because the variations (4.104) are non-integrable. Integrability is essential if (4.104) is to be written in the form $\delta\tilde{X} = \delta\tilde{Y} = 0$, as in Theorem 3.7. For integrability, a finite displacement satisfying (4.104) has to give a well-defined change to $\tilde{\mathbf{u}}$. However, given $\tilde{u} = \tilde{v} = 0$ at $(0,0)$, displace a particle at that position to the point $(\pi/4, \pi/4)$, and calculate the change in $\tilde{\mathbf{u}}$ using (4.104). If the displacement proceeds via the point $(0, \pi/4)$, the result is $(\Omega a, -\Omega a(1+\pi/4))$. If it is via $(\pi/4, 0)$, the result is $(\Omega a\sqrt{2}, 0)$.

The method of [Cullen et al. (2005)] starts from the duality relation (3.89). The right hand side of this is $\frac{1}{2}f^2$ times the Euclidean distance between $\mathbf{x}$ and $\mathbf{X}$. We can interpret this as being the distance on the Euclidean plane with a metric proportional to f. We then assume that a similar identification will hold in the spherical case, and attempt to prove that an energy minimisation condition analogous to that used in Theorem 3.8 will correspond to (4.105) and (4.106).

We therefore first assume that each point $\mathbf{x} = (\lambda, \phi) \in S^2$ is associated with another point $\mathbf{X} = (\Lambda, \Upsilon) \in S^2$, such that we can identify the mass elements

$$h\cos\phi \mathrm{d}\lambda\mathrm{d}\phi = \sigma\cos\Upsilon\mathrm{d}\lambda\mathrm{d}\Upsilon. \qquad (4.107)$$

We work on a Riemannian manifold $\mathcal{M}_\epsilon$ which is the surface of the sphere, S^2, together with the metric

$$\hat{g}_{ij}^{S^2} = \mathcal{F}^2(\phi) g_{ij}^{S^2}, \; \hat{g}^{ijS^2} = \mathcal{F}^{-2}(\phi) g^{ijS^2}, \tag{4.108}$$

where $g_{ij}^{S^2}$ denotes the usual components of the metric on a sphere S^2 of radius a

$$g_{ij}^{S^2} = \begin{pmatrix} a^2 & 0 \\ 0 & a^2 \cos^2 \phi \end{pmatrix}. \tag{4.109}$$

$\mathcal{F}(\phi)$ is chosen to be a smooth modification of the function $2\Omega|\sin\phi|$ which is a twice differentiable function of ϕ, is equal to $2\Omega|\sin\phi|$ for $\phi > \phi_\epsilon > 0$ for some (small) ϕ_ϵ and has a minimum value $\epsilon > 0$. The resulting manifold $\mathcal{M}_\epsilon$ is topologically equivalent to the sphere. However, the limit as $\epsilon \to 0$ is not a smooth manifold. We identify points on S^2 and $\mathcal{M}_\epsilon$ with the same coordinates (λ, ϕ). Only the distance between points is different according to which manifold we work on.

We now propose a duality structure as in section 3.2.3. Consider a mapping $\mathbf{s}^{-1} : S^2 \to S^2$. By analogy with (3.86), define the cost function associated with the mapping as the square of the Riemannian distance between $\mathbf{x}$ and $\mathbf{s}^{-1}(\mathbf{x})$ calculated by projection onto $\mathcal{M}_\epsilon$. Write this as $d^2(\mathbf{x}, \mathbf{s}^{-1}(\mathbf{x}))$. We then seek to minimise the cost under mappings $\mathbf{s}^{-1} : S^2 \to S^2$, $\mathbf{s}_\#^{-1} h = \sigma$. Write S for the set of such mappings. The following theorems were proved by [McCann (2001)].

Theorem 4.12 *([McCann (2001)], Theorem 9). Given probability measures σ, h on a connected, compact Riemannian manifold $\mathcal{M}_\epsilon$ with C^3 regularity. Then there exists an involutive potential Ψ and optimal maps $\mathbf{t} = \exp_{\mathbf{X}}[-\nabla\Psi(\mathbf{X})]$ and its inverse $\mathbf{t}^{-1} : S^2 \to S^2$ which satisfy $\mathbf{t}_\# \sigma = h$ and $\mathbf{t}_\#^{-1} h = \sigma$ respectively, and minimise the cost*

$$\int_{\mathcal{M}_\epsilon} \left(\frac{1}{2} d^2(\mathbf{x}, \mathbf{s}^{-1}(\mathbf{x})) \right) \sigma 4\pi a^2 \cos\Upsilon \mathrm{d}\Lambda \mathrm{d}\Upsilon. \tag{4.110}$$

These maps are unique up to sets of measure zero.

The theorem shows that the association of points $\mathbf{x}$ and $\mathbf{X}$ assumed in writing equation (4.107) is possible. The definition of the regularised manifold $\mathcal{M}_\epsilon$ was chosen to satisfy the conditions of the theorem. Now interpret the identifications $\mathbf{t} = \exp_{\mathbf{X}}[-\nabla\Psi(\mathbf{X})]$ and $\mathbf{t}^{-1} = \exp_{\mathbf{x}}[\nabla(gh(\mathbf{x}))]$.

The definition of the exponential map is that

$$\exp_{\mathbf{x}}[\nabla g h(\mathbf{x})] = \mathbf{x} + g\nabla h + O(\nabla h)^2. \tag{4.111}$$

This means that $\mathbf{t}^{-1}(\mathbf{x})$ lies a distance $|g\nabla h|$ from $\mathbf{x}$ along a geodesic in the direction ∇h, where the geodesics are defined using the metric (4.108). The effect is illustrated on the sphere with the normal metric in Fig. 4.1. The conformal rescaling of the metric by the factor $\mathcal{F}^{-1}$ in (4.108) means that the geodesic bends towards the equator, where $\mathcal{F}$ is smaller, so distances 'cost less'. The distance $|d|$ calculated in the normal metric becomes $|\mathcal{F}^{-1} g\nabla h| = |\mathbf{u}_g|$. The cost function $\frac{1}{2}d^2$ is thus the kinetic energy density.

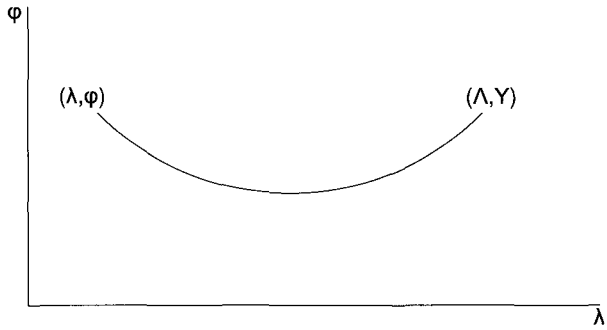

Fig. 4.1 A geodesic on part of a sphere with metric rescaled by the Coriolis parameter $2\Omega \sin\phi$.

Now write (3.89) in the form

$$-gh(\mathbf{t}(\mathbf{X})) + \Psi(\mathbf{X}) = \frac{1}{2}d^2(\mathbf{t}(\mathbf{X}), \mathbf{X}). \tag{4.112}$$

Differentiate this with respect to time, following particles. Use a dot to denote the time derivative. Then

$$-g\dot{h}(\mathbf{t}(\mathbf{X})) + \dot{\Psi}(\mathbf{X}) = d\dot{d}(\mathbf{t}(\mathbf{X}), \mathbf{X}). \tag{4.113}$$

The relation between h and Ψ is independent of time (the 'passive variable' property), so we set $\partial(gh)/\partial t + \partial\Psi/\partial t = 0$. Since d only depends on time through the change of positions of $\mathbf{X}$ and $\mathbf{t}(\mathbf{X})$, we have

$$-g\dot{\mathbf{x}} \cdot \nabla h + \dot{\mathbf{X}} \cdot \nabla\Psi = d\dot{d}(\mathbf{t}(\mathbf{X}), \mathbf{X}), \tag{4.114}$$

where $\dot{\mathbf{x}} = \mathrm{d}/\mathrm{d}t(\mathbf{t}(\mathbf{X}))$. Using $|d| = |\mathbf{u}_g|$ and using (4.105) in the form $\mathcal{F}\hat{\mathbf{r}} \times \mathbf{u}_g = g\nabla h$, where $\hat{\mathbf{r}}$ is a unit vector normal to the sphere, we have

$$-\mathcal{F}g\dot{\mathbf{x}} \cdot (\hat{\mathbf{r}} \times \mathbf{u}_g) + \dot{\mathbf{X}} \cdot \nabla\Psi = \dot{\mathbf{u}}_g \cdot \mathbf{u}_g. \tag{4.115}$$

We can write the evolution equations (4.100) as

$$\dot{\mathbf{u}}_g + \mathcal{F}\hat{\mathbf{r}} \times (\dot{\mathbf{x}} - \mathbf{u}_g) = 0. \tag{4.116}$$

Substituting this into (4.115) gives

$$\dot{\mathbf{X}} \cdot \nabla\Psi = 0. \tag{4.117}$$

Therefore the velocity $\mathbf{U}$ in dual variables is normal to $\nabla\Psi$. This is the same as in the Cartesian case, section 3.3.4. However, the magnitude of $\mathbf{U}$ is not determined.

We next identify the energy minimisers according to Theorem 4.11 with optimal maps defined by Theorem 4.12. This result is Theorem 6 of [Cullen et al. (2005)].

Theorem 4.13 *Given probability measures σ, h on $\mathcal{M}_\epsilon$, let $\mathbf{t}^{-1} : \mathbf{t}^{-1}_{\#} h = \sigma$ be the optimal map guaranteed by Theorem 4.12, so that $\mathbf{t}^{-1} = \exp_{\mathbf{x}}[\nabla(gh(\mathbf{x}))]$ for some h where $-gh$ is involutive. Then h defines a minimiser of the energy (4.101) with respect to the variations (4.102) satisfying (4.103) and (4.104). Conversely, suppose h defines a minimiser as in the previous sentence. Then h generates an optimal map for some σ in the sense of Theorem 4.12, and $-gh$ is involutive.*

The key point in the proof is that, if we modify the variations (4.104) to

$$\begin{aligned} \delta\tilde{u} &= \mathcal{F}\eta + \frac{\tilde{v}\tan\phi}{a}\xi + \varsigma\tilde{v}, \\ \delta\tilde{v} &= -\mathcal{F}\xi - \frac{\tilde{u}\tan\phi}{a}\xi - \varsigma\tilde{u}, \end{aligned} \tag{4.118}$$

for some ς, then the energy is not affected by the choice of ς. If the variations (4.104) were equivalent to the condition $\mathbf{t}^{-1}_{\#} h = \sigma$, then they would have to be integrable. The condition $\mathbf{t}^{-1}_{\#} h = \sigma$ is equivalent to (4.118), with ς chosen in such a way as to make the variations integrable. ς cannot be written down explicitly.

We can write the solution of equations (4.116) over a short time interval δt as

$$\delta\mathbf{u}_g + \mathcal{F}\hat{\mathbf{r}} \times (\delta\mathbf{x} - \mathbf{u}_g\delta t). \tag{4.119}$$

The variations (4.104) were chosen so that δx and $\delta \mathbf{u}_g$ could be determined, given $\mathbf{u}_g \delta t$. However, if we use the optimal map guaranteed by Theorem 4.12, we will obtain instead

$$\delta \mathbf{u}_g + \mathcal{F}\hat{\mathbf{r}} \times \delta \mathbf{x} - (\mathcal{F} - \varsigma)\mathbf{u}_g \delta t. \tag{4.120}$$

We can regard $\mathbf{U} = (\mathcal{F} - \varsigma)\mathbf{u}_g$ as defining a velocity in dual variables. The unknown ς corresponds to the fact that the magnitude of $\mathbf{U}$ is not determined by (4.117). Thus the equation in dual variables cannot be written down explicitly. This is the converse of the situation in [Salmon (1985)] where the equations in physical space could not be written down explicitly.

Since the problem cannot be solved directly in dual variables, it is necessary to find minimisers of the energy as defined in Theorem 4.11 directly. Once they have been found, Theorem 4.13 shows that they can be identified with optimal maps.

The following procedure for finding minimisers is set out by [Cullen et al. (2005)]. The non-integrability of the variations (4.104) is resolved by choosing a specific search direction, chosen to be a steepest descent path in energy. Assume we are given $\tilde{h}$ and $\tilde{\mathbf{u}}$ such that

$$\varrho = \left(\tilde{v} - \frac{g}{\mathcal{F} a \cos\phi} \frac{\partial \tilde{h}}{\partial \lambda}, -\tilde{u} - \frac{g}{\mathcal{F} a} \frac{\partial \tilde{h}}{\partial \phi} \right) \neq 0. \tag{4.121}$$

Minimise the energy integral (4.101) iteratively by calculating a displacement

$$\begin{aligned} \Xi &= \alpha \mathcal{F}^{-1} \varrho, \\ &= \alpha \left(\mathcal{F}^{-1}(\tilde{v} - \tilde{v}_g), -\mathcal{F}^{-1}(\tilde{u} - \tilde{u}_g) \right), \end{aligned} \tag{4.122}$$

where $\tilde{\mathbf{u}}_g$ is calculated from $\tilde{h}$ using (4.105), and using (4.103) and (4.104) to update $\tilde{h}, \tilde{u}, \tilde{v}$. The latter assumes that each iteration makes only a small displacement. α is an iteration parameter. Substituting the second equation of (4.122) into (4.104) gives that

$$\tilde{u}\delta\tilde{u} + \tilde{v}\delta\tilde{v} = -\alpha \left(\tilde{u}(\tilde{u} - \tilde{u}_g) + \tilde{v}(\tilde{v} - \tilde{v}_g) \right). \tag{4.123}$$

Then using (4.105) and (4.122); and following the same steps as in the proof

of Theorem 3.6, we obtain

$$\delta E = -\alpha \int_{S^2} \left((\tilde{u} - \tilde{u}_g)^2 + (\tilde{v} - \tilde{v}_g)^2\right) \tilde{h} 4\pi a^2 \cos\phi \mathrm{d}\lambda \mathrm{d}\phi, \qquad (4.124)$$

$$= -\alpha \int_{S^2} \varrho^2 \tilde{h} 4\pi a^2 \cos\phi \mathrm{d}\lambda \mathrm{d}\phi.$$

This is negative definite and vanishes when $\tilde{u} = \tilde{u}_g$. Since the energy is a positive definite quantity, the energy found by this iteration is bounded below, and convergence is thus guaranteed. According to Theorem 4.13, the resulting h will generate an optimal map as defined in Theorem 4.12 and $-gh$ will be involutive.

In order to use this in the solution procedure, we need to show that ϱ is reduced to zero by a displacement of order ϱ. (4.124) shows that the total reduction in energy will then be $O(\varrho^2)$, at least for sufficiently small ϱ. To show this, use (4.121) and (4.122) to write

$$\delta\varrho^2 = \int_{S^2} \varrho \cdot \delta\varrho \tilde{h} 4\pi a^2 \cos\phi \mathrm{d}\lambda \mathrm{d}\phi = \int_{S^2} \mathcal{F}\alpha^{-1}\Xi \cdot \delta\varrho \tilde{h} 4\pi a^2 \cos\phi \mathrm{d}\lambda \mathrm{d}\phi. \qquad (4.125)$$

Then use (4.104) to write

$$\delta\varrho = -\left(\mathcal{F}\xi + \frac{\tilde{u}_g}{a}\tan\phi\xi, \mathcal{F}\eta + \frac{\tilde{v}_g}{a}\tan\phi\xi\right) + \delta(\tilde{v}_g, -\tilde{u}_g). \qquad (4.126)$$

The same manipulations that lead from (3.70) to (3.72) then give

$$\delta\varrho^2 = \int_{S^2} \alpha^{-1}\left(\Xi \cdot \mathbf{Q} \cdot \Xi + g(\nabla \cdot (\tilde{h}\Xi))^2\right) \tilde{h} 4\pi a^2 \cos\phi \mathrm{d}\lambda \mathrm{d}\phi, \qquad (4.127)$$

$$= -\int_{S^2} \alpha\left(\mathcal{F}^{-2}\varrho \cdot \mathbf{Q} \cdot \varrho + g(\nabla \cdot (\tilde{h}\mathcal{F}^{-1}\varrho))^2\right) \tilde{h} 4\pi a^2 \cos\phi \mathrm{d}\lambda \mathrm{d}\phi,$$

where $\mathbf{Q}$ is the matrix defined in equation (4.106). This is negative definite. We require the stronger condition that the right hand side is $O(\varrho^2)$. A proof of this is not yet available. However, the only case where both terms of (4.127) vanish is where $\mathcal{F} + (\tilde{u}_g \tan\phi)/a = 0$, $\tilde{v}_g = 0$ and ϱ is parallel to $\tilde{\mathbf{u}}_g$. This case corresponds to an anticyclonic vortex with zero semi-geostrophic absolute vorticity centred at the pole. The associated σ defined by the dual variables calculated using (4.111) is a Dirac mass. In

the plane case studied in [Cullen and Gangbo (2001)], potential density conservation means that such a state cannot be generated unless it is present in the initial data. In the present case, it will be necessary to prove that such a case cannot be generated from an appropriate choice of initial data. Provided that the right hand side of (4.127) can be shown to be $O(\varrho^2)$, the reduction of energy during the iteration will also be $O(\varrho^2)$.

Assuming that this can be proved, we can solve a regularised form of (4.100). Solutions of (4.100) are invariant to a transformation which leaves h fixed, reverses the signs of f, $\partial/\partial\phi$, v and v_g, and leaves u, u_g and $\partial/\partial\lambda$ fixed. Thus we will solve (4.100) with the sign of f reversed in the southern hemisphere, and then with f replaced with the strictly positive function $\mathcal{F}$. After finding a solution h_ϵ of the regularised problem, we take the limit as $\epsilon \to 0$. If the limit solution satisfies necessary continuity conditions at the equator, it can be transformed back to a solution of (4.100).

(i) Start with an initial $h_\epsilon(0,\cdot)$ such that $-gh_\epsilon(0,\cdot)$ is involutive. Calculate $\mathbf{u}_g$ from it using (4.105).

(ii) Take a time-step δt. Make a first guess at the solution by setting $\tilde{\mathbf{u}}$ equal to $\mathbf{u}_g$ rotated by an angle $\mathcal{F}\delta t$ at each point.

(iii) Minimise the energy under variations (4.103) and (4.104) using the procedure described above. The initial ϱ for the iteration will thus be $O(\delta t)$, and the energy will be reduced by $O(\delta t^2)$. The result is written $h_\epsilon(\delta t,\cdot)$, where $-gh_\epsilon(\delta t,\cdot)$ is involutive.

(iv) We now use the methods of [Cullen and Gangbo (2001)]. For a given finite time interval, we discretise in time. For each choice of time-step δt we can generate a depth field $h_\epsilon(t,\cdot)$ such that $-gh_\epsilon$ is involutive at each time. As the time-step converges to zero, we generate a sequence of involutive functions. Given such a sequence, it is easy to see that they have a global Lipschitz bound. Now the Ascoli-Arzela theorem (on families of equicontinuous functions) yields the existence of a limit function. Moreover, standard arguments in the literature show that the limit function is involutive. The limit solution will conserve energy, as the total energy loss in the approximate solution over a fixed time interval will be $O(\delta t)$.

We next consider the limit as ϵ tends to zero, so that $\mathcal{F}$ tends to $|f|$. First consider the effect of the involutivity condition at the equator. Physically, this is a condition for inertial stability. Calculate the terms on the diagonal of $\mathbf{Q}$ as defined in (4.106) with $\tilde{u} = u_g$, $\tilde{v} = v_g$ as at the minimising point.

$$\begin{aligned} \frac{1}{a\cos\phi}\frac{\partial v_g}{\partial\lambda} &= \frac{g}{\mathcal{F}a^2\cos^2\phi}\frac{\partial^2 h}{\partial\lambda^2}, \\ \frac{u_g\tan\phi}{a} &\simeq 0, \\ -\frac{1}{a}\frac{\partial u_g}{\partial\phi} &= \frac{g}{\mathcal{F}a^2}\left(-\frac{\cos\phi}{\sin\phi}\frac{\partial h}{\partial\phi}+\frac{\partial^2 h}{\partial\phi^2}\right). \end{aligned} \tag{4.128}$$

Thus, as $\mathcal{F}\to 2\Omega\sin\phi$, the condition that $\mathcal{F}\left(\mathcal{F}-\frac{1}{a}\frac{\partial u_g}{\partial\phi}\right)>0$ requires that

$$\frac{g}{a}\frac{\partial h}{\partial\phi} \simeq \mathcal{F}U_0 + \mathcal{F}U_1(\lambda)\phi^2 + \mathrm{O}(\phi^4) \tag{4.129}$$

for some constant U_0 and function $U_1(\lambda)$. Thus $u_g \simeq U_0 + U_1\phi^2 + \mathrm{O}(\phi^3)$. The condition that $\mathcal{F}\left(\mathcal{F}+\frac{1}{a\cos\phi}\frac{\partial v_g}{\partial\lambda}\right)>0$ means that $\frac{\partial h}{\partial\lambda}=\mathrm{O}(\phi^2)$, which is less restrictive. These conditions on h are much more severe than those required for (u_g, v_g) to be finite at the equator. In particular, v_g must tend to zero at $\phi = 0$ as ϵ tends to zero. We can therefore reverse the transformation used to regularise the problem, noting that this requires reversing the signs of f, $\partial/\partial\phi$, v and v_g, without creating any discontinuity in h.

We finally state the definition of admissible solutions for semi-geostrophic theory on the sphere.

Definition 4.2 An admissible solution of the shallow water semi-geostrophic equations on a sphere is one that is characterised by a function $h(t)$ whose evolution satisfies (4.99) and (4.100) in a suitable sense and such that $-gh(t)$ is involutive in the sense of (3.55) using the metrics (4.108), (4.109).

4.3.2 *Demonstration of the solution procedure*

In this section, we use the iteration defined in (4.122) to calculate the optimal map (4.111) and its inverse for typical meteorological data. Since we are considering the shallow water case, the optimal map on the plane

is given by the transformation to geostrophic coordinates as introduced by [Hoskins (1975)]. Our construction gives a generalisation of these coordinates to the sphere. We use the model of [Mawson (1996)] described in section 5.3.3. Start with a given $\sigma(\Lambda, \Upsilon)$ defined by (4.107). Choose a first guess solution $\tilde{h}$ and $\tilde{\mathbf{u}}$

$$\tilde{h}(\lambda, \phi) = h_0 \sigma(\Lambda, \Upsilon), \tilde{u} = 0, \tilde{v} = 0. \tag{4.130}$$

Assuming the identity map, $\mathbf{x} = \mathbf{X}$, this satisfies (4.107). We now construct a displacement Ξ by iterating (4.122) so that the energy is minimised under (4.103, 4.104). According to Theorem 4.13, this displacement must have generated an optimal map in the sense of Theorem 4.12. If the displacement takes each point $\mathbf{X} = (\Lambda, \Upsilon)$ to a point $\mathbf{x} = (\lambda, \phi) = \mathbf{t}(\mathbf{X})$ and generates a depth $h(\lambda, \phi)$, then continuity as expressed by (4.103) implies that

$$\sigma = h \frac{\partial(\lambda, \phi)}{\partial(\Lambda, \Upsilon)} \frac{\cos\phi}{\cos\Upsilon}, \tag{4.131}$$

in agreement with (4.107), and $\mathbf{t}_{\#}\sigma = h$. We claim that, by making this special choice of initial data, we have constructed an optimal map in the sense of Theorem 4.12 for this σ. This will be true provided the displacement Ξ follows a geodesic according to the metric (4.108). It is known that the cost (4.110) reduces monotonically as $\mathbf{X}$ moves towards $\mathbf{x}$ along the geodesic. This is discussed in [Villani (2003)], chapter 5, and is related to time-continuous versions of the mass transportation problem, [Benamou and Brenier (1997)] and the displacement interpolation of [McCann (1997)]. The direction of displacement defined in (4.122) is the only direction guaranteed to reduce the energy, so it is likely that it can proved to be that of the geodesic. The distance covered by the displacement in this metric is equal to $|\mathbf{u}_g|$ because of (4.101), which agrees with the distance from $\mathbf{x}$ to $\mathbf{X}$ characterising the optimal map, (4.111).

The choice $\sigma/h_0 = 1$ represents a trivial state of balance with no flow. An example of a non-trivial choice is shown in the top panel of Fig. 4.2. This is designed to reproduce disturbances typical of a low-level atmospheric pressure field with geostrophic winds of about 15ms^{-1}.

The result of applying the construction to the first guess field shown in Fig. 4.2 is illustrated in Fig. 4.3. 100 iterations were used. The initialisation procedure described in [Mawson (1996)] (p.276: initialisation stage 2) is equivalent to using (4.122). The 'correction velocity' U_A defined on p.271 of that paper generates the displacement required by (4.122), and

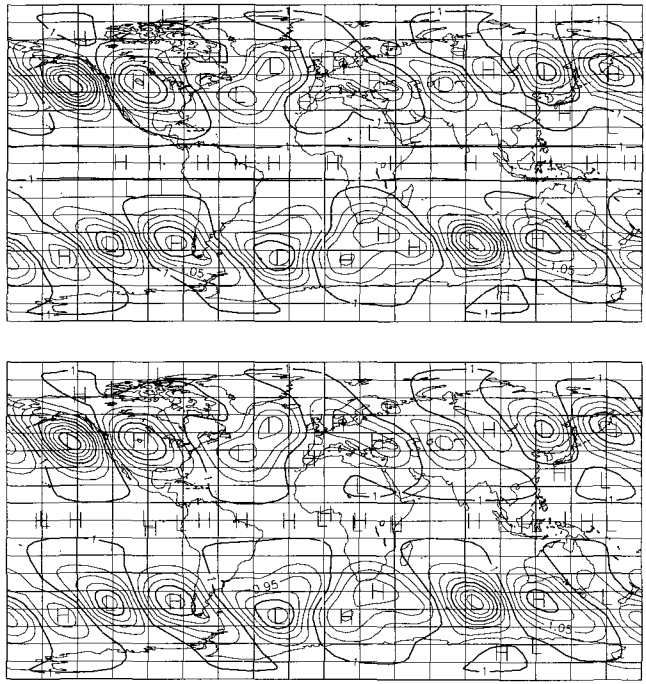

Fig. 4.2 Top: Initial distribution of the dimensionless quantity σ/h_0 for equation (4.130). Contour interval 0.025. Bottom: Final distribution of σ/h_0. Contour interval 0.025. From [Cullen et al. (2005)].

the updates using (4.103) and (4.104) are equivalent to equations (10) and (9) in that paper. Fig. 4.3 shows that positive anomalies in σ/h_0 become positive anomalies of h. The h field is smoother than the σ field. This is to be expected, since σ is related to the potential vorticity, which is expected to have smaller scales than the depth field.

The construction can also be reversed. Given initial data with depth $\tilde{h}$ and initial winds $\tilde{u} = u_g, \tilde{v} = v_g$ calculated from $\tilde{h}$ using (4.105), make an initial displacement Ξ parallel to ∇h, as required by (4.111). Then choose Ξ as minus the value given by (4.122), and iterate to a state where $u = v = 0$. Set σ equal to the final value of h. This procedure acts as a diagnosis of potential density from a given geostrophically balanced state, and thus plays

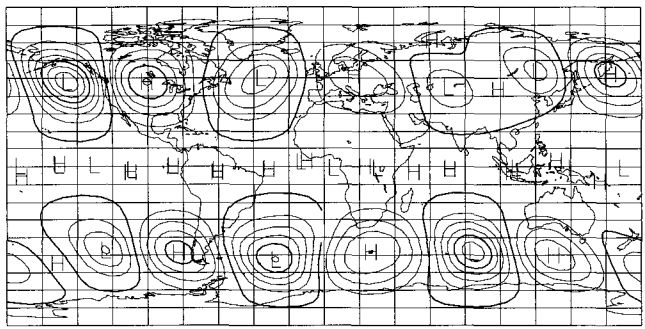

Fig. 4.3 Distribution of h derived from initial field shown in Figure 1. Contour interval $250m$. Bold contours at 10600, 10700, 10800 m. From [Cullen et al. (2005)].

the role of a potential vorticity inversion for semi-geostrophic solutions. The final values of h will be equal to the original σ, subject to numerical error. The bottom panel of Fig. 4.2 illustrates the final field. It is almost identical to the original field. Fig. 4.4 shows the values of (Λ, Φ) calculated from (λ, ϕ) by the construction. For the data chosen, the displacements are quite small, and the displacement of the latitude and longitude grid lines is only just visible. (Λ, Φ) can be regarded as the natural generalisation of geostrophic coordinates to the sphere.

In the f-plane theory, the velocity $\mathbf{U}$ in dual variables has been non-divergent in every case studied in this volume so far. This means that there is a Lagrangian conservation law for σ. In the present case, (4.120) shows that $\mathbf{U} = (1 - \varsigma/\mathcal{F})\mathbf{U}_g$, where ς is a scalar which may depend on position and time, and cannot be determined till the problem has been solved, and

$$\mathbf{U}_g = \frac{1}{2\Omega a}\left(-\frac{1}{\sin\Upsilon}\frac{\partial\Psi}{\partial\Upsilon}, \frac{1}{\sin\Upsilon\cos\Upsilon}\frac{\partial\Psi}{\partial\Lambda}\right). \tag{4.132}$$

The magnitude of ς reflects the curvature of the geodesic between $\mathbf{x}$ and $\mathbf{X}$ which arises from both the curvature of the original sphere, and the additional curvature of $\mathcal{M}_\epsilon$ induced by the conformal rescaling. ς is of order $(|\mathbf{u}_g|/\mathcal{F}a)^2$, since curvature effects will only be significant if $\mathbf{x}$ and $\mathbf{X}$ are separated by a distance comparable to the earth's radius. For geostrophic

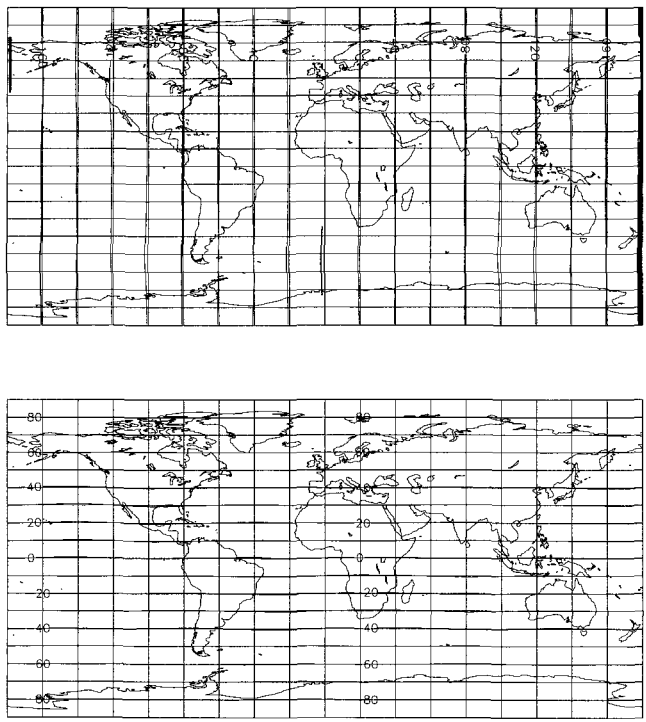

Fig. 4.4 Top: Λ plotted as a function of λ, ϕ, contours every 20°. Bottom: Υ plotted against λ, ϕ. Contours every 10°. From [Cullen et al. (2005)].

winds of order 15ms^{-1}, as used in our example solutions, $|\mathbf{u}_g|/\mathcal{F}a = 0.025$ in middle latitudes.

The divergence of $\mathbf{U}_g$ is given by

$$\frac{1}{2\Omega a^2 \cos\Upsilon}\left(\frac{\partial}{\partial\Lambda}\left(-\frac{1}{\sin\Upsilon}\frac{\partial\Psi}{\partial\Upsilon}\right)+\frac{\partial}{\partial\Upsilon}\left(\frac{1}{\sin\Upsilon}\frac{\partial\Psi}{\partial\Lambda}\right)\right). \tag{4.133}$$

It can be removed by making the additional rescaling

$$\mathrm{d}\hat{\Lambda} = \sin\Upsilon \mathrm{d}\Lambda,\ \mathrm{d}\hat{\Upsilon} = \mathrm{d}\Upsilon,\ \hat{U} = \sin\Upsilon U,\ \hat{V} = V. \tag{4.134}$$

This changes the factor $\cos\Upsilon$ in the metric of the sphere to $\sin 2\Upsilon$, and

transforms the sphere into two spheres, tangent at the equator. The use of this rescaling to create non-divergence was noted by [Salmon (1985)]. The effect is that the scaled potential density

$$\hat{\sigma} = \frac{h\partial(\lambda\cos\phi, \phi)}{2\Omega\cos\Upsilon\partial(\Lambda\cos\Upsilon, \Upsilon)} \tag{4.135}$$

is almost conserved in a Lagrangian sense (subject to the curvature effects estimated in the previous paragraph). The inverse of $\hat{\sigma}$ can readily seen to be an approximate form of the Ertel potential vorticity. There is, however, still divergence coming from the variations in ς discussed above which cannot be removed.

Since σ is a measure of mass in dual variables, standard kinematics yields the conservation law

$$\frac{\partial\sigma}{\partial t} + \nabla\cdot(\sigma\mathbf{U}) = 0. \tag{4.136}$$

Integrating (4.136) round a loop moving with the flow gives conservation of 'circulation' in dual variables, though it has nothing to do with the circulation in physical space. It is a semi-geostrophic analogue of the 'impermeability' result of [Haynes and McIntyre (1990)].

4.4 The theory of almost axisymmetric flows

4.4.1 *Minimum energy states for axisymmetric flows*

Semi-geostrophic theory takes advantage of the fact that straight flow in geostrophic balance is an exact steady-state solution of the inviscid Navier-Stokes equations. The condition that the Lagrangian Rossby number is small requires that variations in the flow direction are small. A straight flow is stable to parcel displacements if it satisfies the stability condition derived in section 3.1.3. The other case where a simple flow is an exact solution to the inviscid equations is the axisymmetric vortex. The stability of such vortices was studied by [Fjortoft (1946)] and [Eliassen and Kleinschmidt (1957)] by considering variations conserving angular momentum. A theory parallel to the semi-geostrophic theory of [Cullen and Purser (1984)] was developed by [Shutts, Booth and Norbury (1987)] and is described here. It is again based on the minimum energy principle.

We work with the hydrostatic Boussinesq equations (2.83), but write

$f = 2\Omega$ since we are only considering a local solution in a rotating coordinate system. Use cylindrical coordinates (λ, r, z) with associated velocity components (u, v, w). Steady axisymmetric solutions obey

$$\frac{u^2}{r} + 2\Omega u = \frac{\partial \varphi}{\partial r}, \qquad \frac{\partial \varphi}{\partial z} - g\frac{\theta'}{\theta_0} = 0. \tag{4.137}$$

The angular momentum associated with this state is $M = ur + \Omega r^2$. Then the first equation of (4.137) can be rewritten as

$$\frac{M^2}{r^3} = \frac{\partial}{\partial r}\left(\varphi + \frac{1}{2}\Omega^2 r^2\right). \tag{4.138}$$

Replace the coordinate r by

$$\varrho = \frac{1}{2}\left(\frac{1}{r_0^2} - \frac{1}{r^2}\right), \tag{4.139}$$

where r_0 is a constant. Then $r^{-3}\mathrm{d}r = \mathrm{d}\varrho$. Define

$$P = \varphi + \frac{1}{2}\Omega^2 r^2. \tag{4.140}$$

Then (4.138) and the second equation of (4.137) become

$$M^2 = \frac{\partial P}{\partial \varrho}, \; g\frac{\theta'}{\theta_0} = \frac{\partial P}{\partial z}. \tag{4.141}$$

Work in an annular region $\Gamma = (r_0 \leq r \leq r_1) \times [0, H]$. The region $r < r_0$ is excluded so that equation (4.139) makes sense. The energy integral associated with the state defined by (4.137) is

$$E = \int_\Gamma \left(\frac{1}{2}u^2 - g\theta' z/\theta_0\right) 2\pi r \mathrm{d}r\mathrm{d}z, \tag{4.142}$$

$$= \int_\Gamma \left(\frac{1}{2}\left(\frac{M}{r} - \Omega r\right)^2 - g\theta' z/\theta_0\right) 2\pi r \mathrm{d}r\mathrm{d}z.$$

Then the results of [Fjortoft (1946)] and [Eliassen and Kleinschmidt (1957)] can be stated as follows. Given a state $(\tilde{M}, \tilde{\theta}')$. Calculate the energy using the second equation of (4.142). Define axisymmetric variations $\Xi = (0, \eta, \chi)$ of particle positions $(\tilde{\lambda}, \tilde{r}, \tilde{z})$ satisfying

$$\eta = \delta\tilde{r}, \; \chi = \delta\tilde{z}. \tag{4.143}$$

Theorem 4.14 *The conditions for the energy E to be minimised with respect to the displacements Ξ defined in (4.143), satisfying continuity $\delta(\tilde{r}\mathrm{d}r\mathrm{d}z) = 0$ via*

$$\frac{1}{\tilde{r}}\frac{\partial(\tilde{r}\eta)}{\partial r} + \frac{\partial\chi}{\partial z} = 0 \tag{4.144}$$

in Γ, and conserving angular momentum and potential temperature via

$$\delta\tilde{M} = 0,\ \delta\tilde{\theta}' = 0, \tag{4.145}$$

together with $\Xi \cdot \mathbf{n} = 0$ on the boundary of Γ, are that

$$\begin{aligned} \tilde{M}^2 &= \frac{\partial\tilde{P}}{\partial\varrho}, \\ g\frac{\tilde{\theta}'}{\theta_0} &= \frac{\partial\tilde{P}}{\partial z}. \end{aligned} \tag{4.146}$$

for some $\tilde{P}$, and

$$\mathbf{Q} = \begin{pmatrix} \frac{\partial\tilde{M}^2}{\partial\varrho} & \frac{\partial\tilde{M}^2}{\partial z} \\ \frac{g}{\theta_0}\frac{\partial\tilde{\theta}'}{\partial\varrho} & \frac{g}{\theta_0}\frac{\partial\tilde{\theta}'}{\partial z} \end{pmatrix} \tag{4.147}$$

is positive definite.

Proof We have

$$\begin{aligned} \delta E &= \int_\Gamma \left((-\frac{\tilde{M}\eta}{\tilde{r}^2} - \Omega\eta)(\frac{\tilde{M}}{\tilde{r}} - \Omega\tilde{r}) - g\tilde{\theta}'\chi/\theta_0 \right) 2\pi\tilde{r}\mathrm{d}r\mathrm{d}z, \\ &= \int_\Gamma \left(-\eta\left(\frac{\tilde{M}^2}{\tilde{r}^3} - \Omega^2\tilde{r}\right) - \chi g\tilde{\theta}'/\theta_0 \right) 2\pi\tilde{r}\mathrm{d}r\mathrm{d}z. \end{aligned} \tag{4.148}$$

For this to be zero for any Ξ satisfying (4.144), we must have

$$\left(\left(\frac{\tilde{M}^2}{\tilde{r}^3} - \Omega^2\tilde{r}\right), g\tilde{\theta}'/\theta_0 \right) = \nabla\tilde{\varphi} \tag{4.149}$$

for some $\tilde{\varphi}$. This is exactly the condition given by (4.138) and the second equation of (4.137). Rewriting using the coordinate ϱ and defining $\tilde{P}$ from $\tilde{\varphi}$ using (4.140) gives (4.146).

As in the proof of Theorem 3.2, characterise the values at the stationary point as $(\tilde{M}, \tilde{\theta}') = (M_g, \theta_g')$ satisfying (4.146) with $\tilde{P} = P_g$. Then we can

write

$$\delta E = \int_\Gamma -\left(\frac{\eta}{r^3}, \chi\right) \cdot \left(\tilde{M}^2 - \frac{\partial P_g}{\partial \varrho}, g\tilde{\theta}'/\theta_0 - \frac{\partial P_g}{\partial z}\right) 2\pi\tilde{r}\mathrm{d}r\mathrm{d}z. \tag{4.150}$$

Now take a second variation, noting that $\eta/\tilde{r}^3 = \delta\tilde{\varrho}$. This gives, using the vanishing of the second term in the integrand at the stationary point,

$$\delta^2 E = \int_\Gamma -(\delta\tilde{\varrho}, \chi) \cdot \delta\left(\tilde{M}^2 - \frac{\partial P_g}{\partial \varrho}, g\tilde{\theta}'/\theta_0 - \frac{\partial P_g}{\partial z}\right) 2\pi\tilde{r}\mathrm{d}r\mathrm{d}z. \tag{4.151}$$

Since $\delta\tilde{M} = \delta\tilde{\theta}' = 0$, this reduces to

$$\delta^2 E == \int_\Gamma ((\delta\tilde{\varrho}, \chi) \cdot \mathbf{Q} \cdot (\delta\tilde{\varrho}, \chi))\, 2\pi\tilde{r}\mathrm{d}r\mathrm{d}z,$$

where $\mathbf{Q}$ is calculated from (4.147) with $\tilde{M} = M_g, \tilde{\theta}' = \theta_g'$. Thus the condition for a minimiser is that $\mathbf{Q}$ is positive definite. □

Using (4.146), the condition that $\mathbf{Q}$ is positive definite is equivalent to convexity of P as a function of (ϱ, z).

Define dual variables $\Upsilon = M^2, Z = g\theta'/\theta_0$. The energy integral (4.142) can then be rewritten as

$$E = \int_\Gamma \left(\frac{1}{2}\left(\frac{\sqrt{\Upsilon} - \Omega r^2}{r}\right)^2 - zZ\right) 2\pi r\mathrm{d}r\mathrm{d}z. \tag{4.152}$$

The continuity condition, (4.144), and the conditions (4.145) require that

$$\sigma' = \frac{\partial(M, \theta')}{r\partial(r, z)} \tag{4.153}$$

is conserved under the variations. We can rewrite this definition, removing constant factors, as

$$\sigma = \frac{\partial(\Upsilon, Z)}{r\sqrt{\Upsilon}\partial(r, z)}. \tag{4.154}$$

Theorem 4.14 can then be interpreted as a mass transportation problem, with the cost given by (4.152) and the constraint written as $\mathbf{s}_\# \sigma = \nu$, where $\mathbf{s}$ is a mapping from (Υ, Z) to (r, z) and the measure $\nu = \mathcal{L}\sqrt{M}$ with $\mathcal{L}$ being Lebesgue measure on Γ.

There is as yet no proof that this mass transportation problem can be solved. However, [Shutts, Booth and Norbury (1987)] proved that it can be solved for piecewise constant data. Their method can be interpreted as an application of Theorem 3.11. Suppose the data (Υ, Z) are given

as values (Υ_i, Z_i) on n sets A_i of $\mathbb{R}^3$ with specified volumes σ_i. Perform the construction in (ϱ, z) coordinates, but define the scalar function s that appears in Theorem 3.11 to be the physical volume multiplied by $\sqrt{\Upsilon_i}$. Then

$$s = \frac{\pi}{2}\sqrt{\Upsilon_i}\int_{A_i} \frac{\mathrm{d}\varrho\mathrm{d}z}{\left(\varrho - 1/(2r_0^2)\right)^2}. \tag{4.155}$$

Since this satisfies the conditions stated with Theorem 3.11, the problem has a unique solution. Examples of the solution are given in section 6.7.

A similar theory was developed by [Schubert and Hack (1983)] and exploited by [Schubert et al. (1991)] to model the axisymmetric response to tropical forcing in spherical geometry. They defined a potential radius coordinate as a dual variable. This is the value of r at which v is zero for a given angular momentum M, and so is equal to $\sqrt{M/\Omega}$.

The exclusion of the region $r < r_0$ is not significant in modelling tropical cyclones, as the central 'eye' region is typically inactive. However, it undermines the credibility of the axisymmetric assumption when modelling flows in spherical geometry, as there is clearly nothing special about atmospheric behaviour near the poles.

4.4.2 *Theories for non-axisymmetric flow*

Solutions for purely axisymmetric flow are of limited use, because they cannot describe departures from axial symmetry and can only evolve under the action of external forcing. However, there are a number of situations where the flow is nearly axisymmetric. The most obvious are tropical cyclones, but it is also believed that intense extra-tropical storms and polar lows often develop a central core with a near-axisymmetric flow regime as a result of convection, [Reed and Albright (1986)], [Rasmussen (1985)]. These will be discussed further in section 6.7. Approximately axisymmetric theory has also been applied to flows on a hemisphere which are approximately zonal, [Purser (2002)].

There are a number of theories for approximately axisymmetric flow formulated in a similar way to the semi-geostrophic formulations described in this book. However, as yet, none has been taken through a complete proof that the evolution problem can be solved. The simplest of these theories is due to [Craig (1991)]. It is derived by making the approximation within Hamilton's principle. The equations, written for shallow water flow on a hemisphere, are

$$
\begin{aligned}
g\frac{1}{a}\frac{\partial h}{\partial \phi} + \frac{u^2}{a} + fu &= 0, \\
\frac{\mathrm{D}u}{\mathrm{D}t} - \frac{uv\tan\phi}{a} + \frac{g}{a\cos\phi}\frac{\partial h}{\partial \lambda} - fv &= 0, \\
\frac{\partial h}{\partial t} + \frac{1}{a\cos\phi}\frac{\partial}{\partial \lambda}(hu) + \frac{\partial}{\partial \phi}(hv\cos\phi) &= 0.
\end{aligned}
\tag{4.156}
$$

where $f = 2\Omega\sin\phi$. These equations conserve the energy integral

$$
\int_\Gamma \left(\frac{1}{2}hu^2 + \frac{1}{2}gh^2\right) 4\pi a^2\cos\phi \mathrm{d}\lambda\mathrm{d}\phi. \tag{4.157}
$$

We can see that only the kinetic energy of the zonal velocity u is included. The equations can be solved by using the transformation to a potential latitude coordinate Υ defined by

$$
ua\cos\phi + \Omega a^2\cos^2\phi = \Omega a^2\cos^2\Upsilon. \tag{4.158}
$$

If the dual variables are (Λ, Υ), where $\Lambda = \lambda$, then (4.156) can be rewritten as

$$
2\Omega a\cos\Upsilon\frac{\mathrm{D}\Lambda}{\mathrm{D}t} = \frac{\partial\Psi}{\partial\Upsilon},\ 2\Omega\frac{\mathrm{D}\Upsilon}{\mathrm{D}t} = -\frac{1}{a\cos\Upsilon}\frac{\partial\Psi}{\partial\Lambda}, \tag{4.159}
$$

which imply conservation of the potential density

$$
\sigma = \frac{h\cos\phi\partial(\lambda,\phi)}{\cos\Upsilon\partial(\Lambda,\Upsilon)}. \tag{4.160}
$$

It is likely that this system can be analysed using the method described in section 4.4.1. However, it is clearly less accurate than the semi-geostrophic system (4.99)-(4.100) for flows with a large meridional component. It may be more relevant to other planetary atmospheres.

In [Purser (2002)], a set of dual variables is defined which allows both components of the kinetic energy to be included. We again illustrate these for the case of shallow water flow on a hemisphere, with coordinates (λ, ϕ) and dual variables (Λ, Υ). The problem is posed as a mass transportation problem, with cost as given by (4.110), where

$$
\begin{aligned}
d^2(\mathbf{x}, \mathbf{s}^{-1}(\mathbf{x})) = \frac{\Upsilon^4}{8}\left(\frac{1}{(a\cos\phi)^2} - 1\right)\cosh\left(\sqrt{8}(\Lambda - \lambda)\right) + \\
\frac{(a\cos\phi)^2}{8} - \frac{(a\cos\Upsilon)^2}{4} + \frac{(a\cos\Upsilon)^4}{8}.
\end{aligned}
\tag{4.161}
$$

This definition ensures that the transformation from (λ, ϕ) to (Λ, Υ) can be generated by a Legendre transform, so that if we define

$$(x, y) = a\cos\phi(\cosh\lambda, -\sinh\lambda), \qquad (4.162)$$
$$(X, Y) = a\cos\Upsilon(\cosh\Lambda, \sinh\Lambda),$$

then we have $(X, Y) = \nabla P, (x, y) = \nabla R, P + R = xX + YY$ as in section 3.2.2. This should allow a proof that the mass transportation problem defined by minimising (4.110) with d defined by (4.161) and σ defined by (4.160) can be solved. However, it is not clear what physical approximation to the kinetic energy (4.161) corresponds to. It is shown in [Purser (2002)] that it is geostrophic to leading order, and should thus be more accurate than the model of [Craig (1991)]. However, the method relies on the assumption of nearly axisymmetric flow, so will not be accurate near the poles.

This page is intentionally left blank

Chapter 5

Properties of semi-geostrophic solutions

5.1 The applicability of semi-geostrophic theory

5.1.1 *Error estimates*

In this section we derive the basic estimates of how close solutions of the semi-geostrophic equations are to those of the exact equations. We expect these estimates to be consistent with the assumption of small Lagrangian Rossby number used to derive the equations. For simplicity, we consider the exact equations to be the hydrostatic Boussinesq equations (2.83) with constant f. It is likely that error estimates made using these equations will extend to the fully compressible case treated in section 4.1 because, under the geostrophic momentum approximation, no approximations are made to the thermodynamic part of the equations. We restate these equations below.

$$\begin{aligned}
\frac{\mathrm{D}u}{\mathrm{D}t} - fv + \frac{\partial \varphi}{\partial x} &= 0, \\
\frac{\mathrm{D}v}{\mathrm{D}t} + fu + \frac{\partial \varphi}{\partial y} &= 0, \\
\frac{\partial \varphi}{\partial z} - g\frac{\theta'}{\theta_0} &= 0, \\
\frac{\mathrm{D}\theta'}{\mathrm{D}t} &= 0, \\
\nabla \cdot \mathbf{u} &= 0.
\end{aligned} \tag{5.1}$$

The semi-geostrophic approximation to these equations is given in (2.124). This is reproduced below with changes in notation so that quantities predicted from this system can be distinguished from equivalent quan-

tities predicted by solving (5.1).

$$\begin{aligned} \frac{\mathrm{D}u_g}{\mathrm{D}t} - f\dot{y} + \frac{\partial \varphi_g}{\partial x} &= 0, \\ \frac{\mathrm{D}v_g}{\mathrm{D}t} + f\dot{x} + \frac{\partial \varphi_g}{\partial y} &= 0, \\ \frac{\partial \varphi_g}{\partial z} - g\frac{\theta_g}{\theta_0} &= 0, \\ \frac{\mathrm{D}\theta_g}{\mathrm{D}t} &= 0, \\ \nabla \cdot \dot{\mathbf{x}} &= 0. \end{aligned} \tag{5.2}$$

Both sets of equations are solved in a closed region Γ. The boundary conditions are that, for (5.1) $\mathbf{u} \cdot \mathbf{n} = 0$, and for (5.2) $\dot{\mathbf{x}} \cdot \mathbf{n} = 0$, on the boundary of Γ. Equations (5.1) conserve an energy integral E

$$E = \int_\Gamma \left(\frac{1}{2}(u^2 + v^2) - g\theta' z/\theta_0 \right) \mathrm{d}x\mathrm{d}y\mathrm{d}z. \tag{5.3}$$

while (5.2) conserves the energy integral E_g given by (2.125).

We first note the first two equations of (5.1) imply that $|(u, v) - (u_g, v_g)|$ is of order $Ro_L|\mathbf{u}|$, where Ro_L is the Lagrangian Rossby number $f^{-1}\mathrm{D}/\mathrm{D}t$. The analysis of section 2.5 suggests that the error will also depend on whether the Rossby number Ro is smaller than the Froude number Fr. In equation (5.1), the choice of boundary conditions means that the vertically averaged flow is just two-dimensional incompressible flow which has a Froude number of zero. We therefore do not analyse the vertically averaged flow and thus assume the pressure is simply a function of θ' through the hydrostatic relation. The error in the pressure is thus of the same order as the error in the potential temperature. This reflects the fact that this choice of boundary conditions is not realistic for the large-scale flow of the atmosphere.

The error analysis follows [Cullen (2000)]. Make a change of variables for equations (5.1) suggested by (3.24):

$$X^* = f^{-1}v + x,\ Y^* = -f^{-1}u + y,\ Z^* = g\theta'/(f^2\theta_0). \tag{5.4}$$

Then we have

$$\frac{\mathrm{D}\mathbf{X}^*}{\mathrm{D}t} \equiv \mathbf{U}^* = \left(-\frac{\partial \varphi}{\partial y}, \frac{\partial \varphi}{\partial x}, 0 \right), \tag{5.5}$$

while applying (3.24) to (5.2) gives, in the notation of the latter:

$$\frac{\mathrm{D}\mathbf{X}}{\mathrm{D}t} \equiv \mathbf{U} = \left(-\frac{\partial \varphi_g}{\partial y}, \frac{\partial \varphi_g}{\partial x}, 0\right). \tag{5.6}$$

We calculate $\mathbf{X}^*(t,\cdot)$ from a solution of (5.1). Then define a possibly multi-valued mapping $\mathbf{s}^*(t)$ from $\mathbb{R}^3$ to Γ by inverting the mapping $\mathbf{X}^*(t,\cdot)$ and define $\sigma^*(t,\cdot)$ by setting

$$\mathbf{s}^*(t)_{\#}\sigma^*(t,\cdot) = \mathcal{L}. \tag{5.7}$$

This can be compared with the potential density σ calculated from the solution of (5.2). Differences between σ and σ^* are generated by differences between $\mathbf{U}$ as defined in (5.6) and $\mathbf{U}^*$ as defined in (5.5), and thus by differences between φ_g and φ. Using Theorem 3.4, we can construct the optimal map $\mathbf{t}^*(t) : \mathbb{R}^3 \to \Gamma$ satisfying $\mathbf{t}^*(t)_{\#}\sigma^*(t,\cdot) = \mathcal{L}$. The existence of a unique optimal map is guaranteed by Theorem 3.12. It will be associated with a geopotential field $\varphi^+(t,\cdot)$, flow variables u^+, v^+ and θ^+, and an energy $E^+(t)$. Since this energy is derived by an energy minimisation technique, and the solution of (5.1) conserves E, we have $E^+(t) \leq E$. Using (5.6) and mass continuity, as in deriving (3.40), we see that $\sigma^*(t,\cdot)$ obeys the evolution equation

$$\frac{\partial \sigma^*}{\partial t} + \nabla \cdot (\sigma^* \mathbf{U}^*) = 0. \tag{5.8}$$

We can therefore characterise a solution of (5.1) by a time-dependent potential density $\sigma^*(t,\cdot)$, together with an optimal map $\mathbf{t}^*(t)$ and the geopotential $\varphi^+(t,\cdot)$; and by the actual (multi-valued) map $\mathbf{s}^*(t)$ and geopotential $\varphi(t)$ derived directly from the solution. The solution of (5.2) is characterised by a potential density $\sigma(t,\cdot)$, obeying (3.40) with velocity $\mathbf{U}$ defined by (3.33), which generates an optimal map $\mathbf{t}(t)$ and geopotential $\varphi_g(t,\cdot)$ as described in section 3.2.2.

The difference between the solutions of (5.1) and (5.2) can be split into the difference $\sigma^*(t,\cdot) - \sigma(t,\cdot)$ and the difference $\mathbf{s}^*(t) - \mathbf{t}^*(t)$. The former represents the 'evolution error' in the potential density and the latter represents the 'imbalance', which represents the departure of solutions of (5.1) from geostrophic and hydrostatic balance..

We first assume that $\sigma^*(t,\cdot) = \sigma(t,\cdot)$, and estimate the differences resulting from the imbalance. We therefore assume that the solution of (5.1) is given by applying the mapping $\mathbf{s}^*(t)$ with the given σ^*. Calculate the optimal map $\mathbf{t}^*$ using an iteration procedure analogous to the procedure

(4.122) used in section 4.3 to construct semi-geostrophic shallow water solutions on the sphere. Thus we define a displacement $\Xi = (\xi, \eta, \chi)$ keeping $\mathbf{X}^*$ fixed on particles by setting

$$\begin{aligned} \nabla^2\vartheta &= \nabla \cdot \left(fv, -fu, g\tfrac{\theta'}{\theta_0}\right), \\ \frac{\partial\vartheta}{\partial n} &= \left(fv, -fu, g\tfrac{\theta'}{\theta_0}\right) \cdot \mathbf{n} \text{ on } \partial\Gamma, \\ \varrho &= f^{-1}\left\{\nabla\vartheta - \left(fv, -fu, g\tfrac{\theta'}{\theta_0}\right)\right\}, \\ \Xi &= -\alpha f^{-1}\varrho. \end{aligned} \tag{5.9}$$

α is an iteration parameter and $\partial\Gamma$ denotes the boundary of Γ. As noted above, $\varrho = \mathrm{O}(Ro_L|\mathbf{u}|)$.

Since $\mathbf{X}^*$ is fixed on particles, the resulting changes to u, v and θ' are given by

$$\xi + \delta(f^{-1}v) = \eta - \delta(f^{-1}u) = \delta\theta' = 0, \tag{5.10}$$

where δ denotes changes following the displacement. These equations imply that $\nabla \cdot \Xi = 0$ for small displacements and so are consistent with the condition $\mathbf{t}_{\#}\sigma = \mathcal{L}$. The change to the energy is

$$\delta E = \alpha \int_\Gamma \left\{ -u^2 - v^2 - \left(\frac{g\theta'}{f\theta_0}\right)^2 + f^{-2}\left(fv, -fu, g\frac{\theta'}{\theta_0}\right) \cdot \nabla\vartheta \right\} \mathrm{d}x\mathrm{d}y\mathrm{d}z. \tag{5.11}$$

Using the last equation of (5.9) and integrating by parts twice, this can be reduced to

$$\delta E = -\alpha \int_\Gamma \varrho^2 \mathrm{d}x\mathrm{d}y\mathrm{d}z. \tag{5.12}$$

Thus the iteration, with sufficiently small steps, will give a negative definite change to the energy and will converge when the optimal map is reached, so that integrating over all the steps we have $\int \Xi = \mathbf{t}(\mathbf{X}) - \mathbf{s}(\mathbf{X})$. As in section 4.3, we can show that the reduction in energy is $\mathrm{O}(f^2\Xi^2)$=$\mathrm{O}(\varrho^2)$ and that the total displacement required to achieve the optimal map is given by $(\int \Xi) \cdot \mathbf{Q} \cdot (\int \Xi) \simeq \varrho^2$, where $\mathbf{Q}$ is as defined in (3.1). This means that $\int \Xi = \mathrm{O}(f^{-1}\varrho)$, assuming that the eigenvalues of $\mathbf{Q}$ are of order f^2, f^2 and N^2 as they are for a state at rest, and noting that the effect of a vertical displacement χ on the third component of ϱ is of order $N^2 f^{-1}\chi$. Using (5.12), we deduce that $E - E^* = \mathrm{O}(f^2(\int \Xi)^2)$=$\mathrm{O}(\varrho^2)$.

The effect of the displacement is to find a state in geostrophic and hydrostatic balance with given σ. To study it, we perform a linear analysis of equations (5.1). Assuming that all variables are proportional to $\exp(i\omega t + ikx + ily + imz)$, with coefficients denoted by hats. The inertia-gravity wave frequency is given by (2.89) to be

$$\varpi = \sqrt{N^2 m^{-2}(k^2 + l^2) + f^2}. \tag{5.13}$$

Now calculate the balanced state $(\check{u}, \check{v}, \check{\theta})$, given data $(\hat{u},\ \hat{v},\ \hat{\theta})$ representing the imbalance. This is given by

$$\begin{aligned} \hat{Q} &= (ik\hat{v} - il\hat{u})N^2\theta_0/g - fim\hat{\theta}, \\ \begin{pmatrix} \check{u} \\ \check{v} \\ \check{\theta} \end{pmatrix} &= \frac{\hat{Q}}{\varpi^2 m^2} \begin{pmatrix} -gil/\theta_0 \\ gik/\theta_0 \\ fim \end{pmatrix}. \end{aligned} \tag{5.14}$$

The Rossby number Ro is now $f^{-1}\sqrt{(\hat{u}^2 + \hat{v}^2)}\sqrt{(k^2 + l^2)}$ and the Froude number Fr is $N^{-1}m\sqrt{(\hat{u}^2 + \hat{v}^2)}$. Then, if $\hat{u} = \hat{v} = 0$,

$$\begin{aligned} \check{\theta} &= \hat{\theta}\tfrac{f^2 m^2}{N^2(k^2+l^2)+f^2m^2}, \\ &= \mathrm{O}\left(\tfrac{Ro^{-2}}{Fr^{-2}+Ro^{-2}}\right)\hat{\theta}. \end{aligned} \tag{5.15}$$

while if $\hat{\theta} = 0$,

$$\begin{aligned} ik\check{v} - il\check{u} &= (ik\hat{v} - il\hat{u})\tfrac{N^2(k^2+l^2)}{N^2(k^2+l^2)+f^2m^2}, \\ &= \mathrm{O}\left(\tfrac{Fr^{-2}}{Fr^{-2}+Ro^{-2}}\right)(ik\hat{v} - il\hat{u}). \\ ik\check{u} + il\check{v} &= 0. \end{aligned} \tag{5.16}$$

This reflects the analysis in section 2.4 and 2.5. If $Ro < Fr$, the potential vorticity is determined largely by the potential temperature, and if $Fr < Ro$ it is determined largely by the vorticity.

Equations (5.15) and (5.16), the definition of ϱ, and the estimate $\varrho \simeq$

$Ro_L|\mathbf{u}|$ imply that

$$\begin{aligned}
\theta^+ - \theta' &\simeq \frac{f\theta_0}{g} Ro_L|\mathbf{u}| \left(\frac{Ro^{-2}}{Fr^{-2}+Ro^{-2}}\right), \\
u^+ - u &\simeq Ro_L|\mathbf{u}| \left(\frac{Fr^{-2}}{Fr^{-2}+Ro^{-2}}\right), \\
v^+ - v &\simeq Ro_L|\mathbf{u}| \left(\frac{Fr^{-2}}{Fr^{-2}+Ro^{-2}}\right).
\end{aligned} \tag{5.17}$$

As discussed after equation (5.7), the evolution error is determined by the difference between φ and φ_g. If we start with $\sigma^* = \sigma$ as above, then $\varphi^+ = \varphi_g$, and the evolution error will grow according to the difference $\varphi^+ - \varphi$, which is determined by $\theta^+ - \theta'$. Using (5.17), the condition for semi-geostrophic theory to be accurate can be stated as

$$\begin{aligned}
Ro_L(Ro/Fr)^2 \ll 1;\ Ro < 1 \text{ and } Ro \leq Fr, \\
Ro_L \ll 1 \text{ otherwise.}
\end{aligned} \tag{5.18}$$

The discussion in section 2.5.6 shows that $Fr^2 \leq Ro$, so that the difference becomes at best $O(RoRo_L)$. A 1% error would be achieved if $Ro = Ro_L = 0.1$ and $Fr = 0.316$. This estimate is closely related to the conditions for the parcel stability analysis of section 3.1.3 to be valid.

In the stratification dominated case studied in section 2.5.4, we have $Fr \ll 1$ with no assumption on Ro. (5.17) then shows that the error will be $O(Ro_L)$. The same applies if $Ro = Fr$, the case studied in section 2.5.5. In the non-rotating case, the only admissible solution has $u_g = v_g = 0$ and so $\nabla_z \varphi_g = \nabla_z \theta_g = 0$. This is trivially an exact solution of (5.1). This is important when the semi-geostrophic equations are used in spherical geometry as it shows that the correct rest state will be predicted, as discussed at the end of section 2.5.6.

Long time estimates are not yet practicable. One difficulty is that it is necessary to prove that, if $\sigma_1 - \sigma_2 = O(\epsilon)$, then $\mathbf{U}_1 - \mathbf{U}_2 = O(\epsilon)$. As noted in section 3.5.2, this is the result required to prove uniqueness of solutions to the semi-geostrophic equations, which is not yet possible.

In section 2.5.5 we described results proving that there are solutions of equations (2.83) with (2.113) close to those of the quasi-geostrophic equations.. A key element in obtaining long time results of this type is the ability to approximate the equations for the inertia-gravity waves by linear equations with constant coefficients. This cannot be done in the regime where semi-geostrophic theory is most relevant, so no long time results

have yet been obtained. A result has, however, been obtained for a semi-geostrophic approximation to the two-dimensional incompressible equations (2.57), which were derived in section 2.4.4 as the limit equation for the shallow water equations with $Fr \ll 1$ and $Fr < Ro$. The semi-geostrophic approximation to (2.57) takes the form (3.41). The difference is that the vorticity ζ is replaced by the potential density σ, and the physical space velocity $\mathbf{u}$ by the dual space velocity $\mathbf{U}$. Both velocities are non-divergent in their respective coordinates, and can thus be written in terms of stream-functions ψ and Ψ respectively. The difference is that in equation (2.57) we have

$$\begin{aligned} \nabla^2\psi &= \zeta, \\ \psi &= \text{constant on } \partial\Gamma, \end{aligned} \tag{5.19}$$

while for (3.41) we have

$$\begin{aligned} f^2R = \Psi + \frac{1}{2}f^2(X^2+Y^2), \\ \det Hess R = \sigma, \\ \nabla R \in \Gamma. \end{aligned} \tag{5.20}$$

Thus we are comparing a Monge-Ampère equation with a Poisson equation which is the linearisation of the Monge-Ampère equation, see [Roulstone and Norbury (1994)]. The expected difference is thus the relative size of the nonlinear term, $O(Ro)$, which would be consistent with the error estimate (5.18). The results, obtained with periodic boundary conditions, are due to [Loeper (2004)]. The function spaces and norms are as defined in section 2.5.5. The first result is an energy estimate.

Theorem 5.1 *Let (σ, Ψ) be a weak solution of (3.41) in $[0,T]\times\mathbb{T}^2$, and (ζ,ψ) be a smooth $C^3([0,T]\times\mathbb{T}^2)$ solution of (2.57). Choose initial data given by a stream-function $\psi(0,\cdot)$ for (2.57) and by a geopotential $\varphi(0,\cdot)$, such that $(fv_g, -fu_g) = \nabla\varphi$, for the semi-geostrophic equations. Then (3.52) implies that*

$$-\varphi(t,x,y) + \Psi(t,X,Y) = \frac{1}{2}f^2\left((x-X)^2+(y-Y)^2\right). \tag{5.21}$$

Use this to calculate $\Psi(0,\cdot)$ for (3.41). Define H_ϵ by

$$H_\epsilon(t) = \frac{1}{2}\int_{\mathbb{T}^2} |\nabla\psi - f^{-1}\nabla\varphi|^2 \mathrm{d}x\mathrm{d}y. \tag{5.22}$$

Then

$$H_\epsilon(t) \leq \Big(H_\epsilon(0) + C\epsilon^{2/3}(1+t)\Big)\exp(Ct), \tag{5.23}$$

where C depends on $|\psi|_{3,t}$ and $|\partial\psi/\partial t|_{2,t}|$, and $\epsilon = Ro$.

The second result is derived by assuming the solution of (3.41) is a perturbation to the solution of (2.57), suitably rescaled. Set $\epsilon = Ro$. Then we assume σ takes the form $\sigma_\epsilon = 1 + \epsilon\hat{\sigma}_\epsilon$ and $\Psi = \epsilon\hat{\Psi}$.

Theorem 5.2 *Let (ζ, ψ) be a solution of (2.57) such that $\zeta \in C^2(\mathbb{R}^+ \times \mathbb{T}^2)$. Let $\sigma_\epsilon(0,\cdot)$ be a sequence of initial data for (3.41) such that $(\hat{\sigma}_\epsilon(0,\cdot) - f^{-1}\zeta(0,\cdot))/\epsilon$ is bounded in $W^{1,\infty}(\mathbb{T}^2)$. Then there exists a sequence $(\sigma_\epsilon, \Psi_\epsilon)$ of solutions to (3.41) that satisfies: for all $T > 0$, there exists $\epsilon_T > 0$, such that the sequence*

$$\left(\frac{\hat{\sigma}_\epsilon - f^{-1}\zeta}{\epsilon}, \frac{\nabla\hat{\Psi} - \nabla\psi}{\epsilon}\right), \tag{5.24}$$

for $0 < \epsilon < \epsilon_T$, is uniformly bounded in $L^\infty([0,T], W^{1,\infty}(\mathbb{T}^2))$.

Proof This result exploits the facts that, for small geostrophic winds, (3.24) shows that $|\mathbf{x} - \mathbf{X}| = \mathrm{O}(\epsilon)$, that the potential vorticity (3.57) reduces to

$$\mathcal{Q}_{SG} = \frac{\partial(X,Y)}{\partial(x,y)} = 1 + f^{-1}\zeta_g + f^{-2}\mathrm{O}(|\zeta_g|^2), \tag{5.25}$$

and that $\sigma \simeq 2 - \mathcal{Q}_{SG}$ if $\mathcal{Q}_{SG} \simeq 1$. □

5.1.2 *Experimental verification of error estimates*

We now confirm the error predictions by computations with a shallow water model. We use this model rather than the three-dimensional Boussinesq model because accurate solutions of the latter cannot be obtained except in trivial cases. We use a shallow water version of the Met Office operational weather forecasting model, [Davies et al. (2005)], described in [Mawson (1996)], and the shallow water semi-geostrophic model of [Mawson (1996)]. We also use a shallow water nonlinear balanced model as described in [Cullen (2000)], which is based on the equations in section 2.4.3.

The initial data are chosen to give a wavenumber 2 pattern in each hemisphere, with no depth perturbation close to the equator. This satisfies the condition that the matrix $\mathbf{Q}$, (4.106), calculated from h using the geostrophic relations is positive definite. It is also sufficiently large-scale

that numerical errors in predicting its evolution will be small. The data are initialised for the semi-geostrophic model using the procedure given in (4.122), and then passed to the shallow water model. Both models are run for two days. The results from the shallow water model are then initialised using (4.122), and compared with the semi-geostrophic results. This gives the evolution error of the semi-geostrophic model. The imbalance $E - E^*$ in the shallow water model is estimated from the difference made by initialising the day 2 results. The procedure is shown diagrammatically in Fig. 5.1. The evolution error is $B - V$, and the imbalance of the shallow water solutions is $E(P) - E(V)$. The same procedure, with an initialisation appropriate for nonlinear balance, is used to evaluate integrations with the nonlinear balanced model.

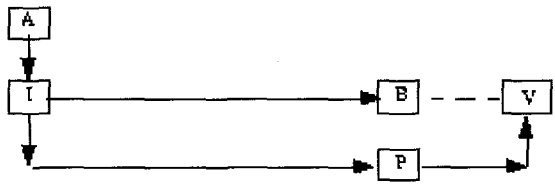

Fig. 5.1 Experimental set-up: A-analytic initial data, I-data initialised for balanced model, B-forecast using balanced model, P-forecast using full shallow water model, V-initialised end state from full shallow water model. From [Cullen (2000)]. ©Royal Meteorological Society, Reading, U.K.

The base resolution for the experiments was a latitude-longitude grid with 96 points around latitude circles and 65 points between the poles. The results were also generated using a higher resolution of 192x129 points. Though the general behaviour as the parameters were varied was the same for both resolutions, in the semi-geostrophic tests there were significant differences in individual results. The complete semi-geostrophic experiment was thus also run at the higher resolution, and a further check carried out using a 288x193 grid for one set of parameters. The nonlinear balance model is more compatible with the shallow water model. Sample runs with the 192x129 grid showed that it was unnecessary to repeat the whole experiment at higher resolution.

The experiments were designed to test the effect of varying Ro/Fr for fixed Ro. Since the Froude number for shallow water flow is $U/\sqrt{gH}$, this was achieved by using the same perturbation depth field for all runs, but varying the mean value h_0 from 5760m down to 182.5m. The amplitude of the superposed wave was $\pm 170m$, so that the lowest mean value used is just sufficient to avoid the depth becoming zero. The horizontal velocity had a maximum value of about $10ms^{-1}$. The gravity wave speed varied from $240ms^{-1}$ to $42ms^{-1}$. Table 1 lists the values used, together with typical Froude and Rossby numbers.

Table 5.1 Parameters used.

ϕ_0 m	$Ro = U/fL$	$Fr = U/\sqrt{(gh_0)}$
5760	0.04	0.04
2880	0.04	0.06
1440	0.04	0.08
720	0.04	0.11
360	0.04	0.16
180	0.04	0.22

The results for the height evolution errors are shown in Fig. 5.2. The imbalance calculated from the depth fields is shown in Fig. 5.3. Similar results for the wind fields are shown in [Cullen (2000)]. The partitioning of the error in the semi-geostrophic model could not be carried out at later times in high resolution runs because the shallow water model developed large depth gradients at the equator which could not be handled by the procedure (4.122). Results for individual cases run at higher resolution are also plotted to validate the results.

It is readily seen that the expected dependence of the evolution error of the semi-geostrophic model on $(Ro/Fr)^2$ is clearly demonstrated. The nonlinear balanced model also shows errors reducing with Ro/Fr for $Ro \ll Fr$. As discussed in section 6.1, this is because the solution is close to a steady state. The much lower errors for the balanced model for larger values of mean depth are consistent with the results of [Allen et al. (1990)]) and the analysis of section 2.4.3. Solvability issues did not arise because of the choice of very smooth initial data. The two models have comparable errors once the gravity wave speed is of the order of $50ms^{-1}$. The results quoted by ([Reiser (2000)], p.65) suggest a gravity wave speed of about 140ms^{-1} as giving the best match of shallow water flow to the barotropic part of

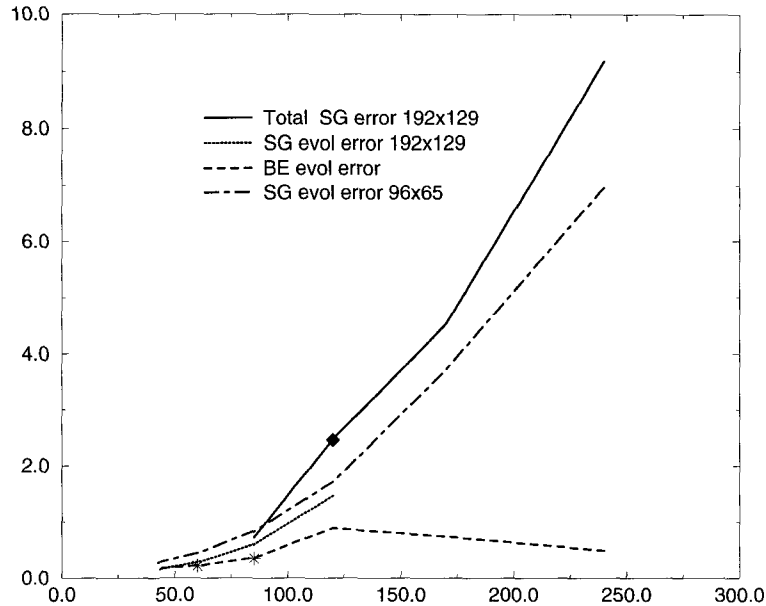

Fig. 5.2 Root-mean-square height-evolution errors (m) after 48 hours plotted against gravity-wave speed (ms^{-1}). Stars indicate balance-equation results on a 192×129 grid, the diamond a semi-geostrophic result on a 288×193 grid. From [Cullen (2000)]. ©Royal Meteorological Society, Reading, U.K.

atmospheric flow (i.e. that part whose direction is independent of height).

The measures of imbalance also show the expected behaviour. In the semi-geostrophic case, the $O((Ro/Fr)^2)$ dependence is clearly seen at high resolution, though the low resolution results are less reliable in this measure. In the balance equation results, the rate of generation of imbalance clearly reduces for small Ro/Fr. Neither model shows greater accuracy in predicting the potential vorticity than in predicting the total evolution. The rate of growth of imbalance from balanced initial data, and the errors in the potential vorticity evolution are of comparable size for all cases tested.

We finally illustrate an example of the differences between semi-

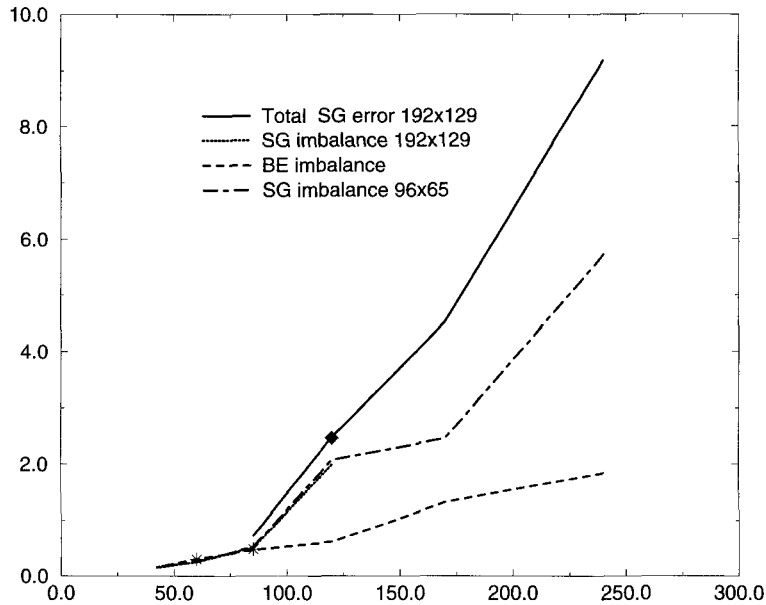

Fig. 5.3 Root-mean-square height imbalances (m) after 48 hours plotted against gravity-wave speed (ms^{-1}). Notation as Fig. 5.2. From [Cullen (2000)]. ©Royal Meteorological Society, Reading, U.K.

geostrophic and shallow water evolution for a real depth field given by [Mawson (1996)]. The data are taken from an analysis of 500hpa geopotential data for 1 February 1991. The mean depth h_0 is 5500m, giving a gravity wave speed of $235ms^{-1}$. As noted above, this is larger than the value giving the best match to the observed evolution. The initialised depth fields are shown in Fig. 5.4, showing that the use of (4.122) to generate admissible data for a semi-geostrophic model does not greatly affect real 500hpa data. Results after ten days of integration are shown in Fig. 5.5. Most features of the flow in the Northern hemisphere still match, though there are noticeable differences. In the Southern hemisphere, where the flow is less dependent on longitude, there is little correspondence. Results after three days shown by [Mawson (1996)] show that all features correspond well in the two integrations. The results shown in Figs. 5.2 and 5.3

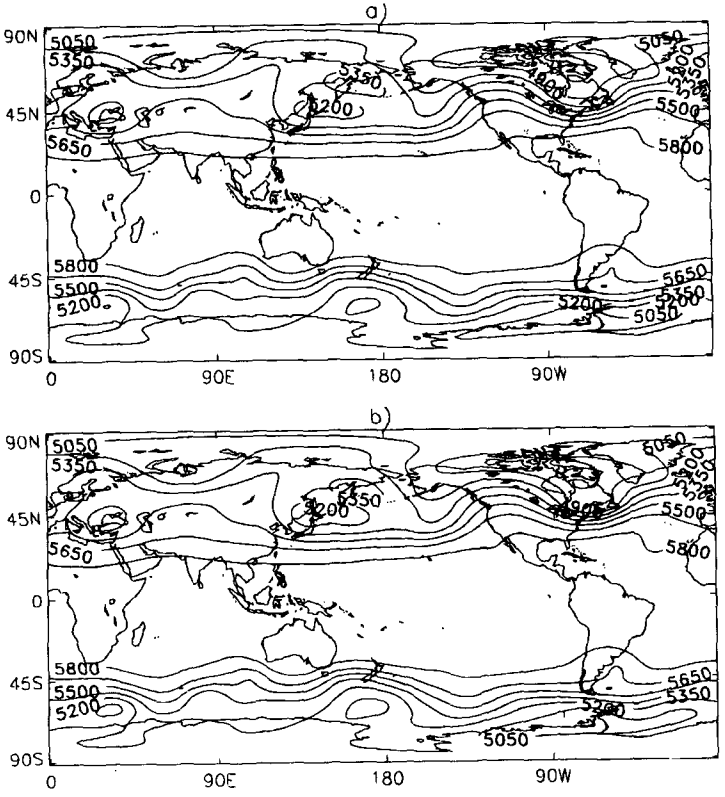

Fig. 5.4 500 hpa initialised height fields for 1 February 1991: (a) semi-geostrophic model, (b) shallow water model. Contour interval 150m. From [Mawson (1996)]. ©Royal Meteorological Society, Reading, U.K.

suggest that the differences would be smaller by a factor of about 3 if the more appropriate value $h_0 = 1400$m had been used for the mean depth.

5.2 Stability theorems for semi-geostrophic flow

5.2.1 *Extremising the energy by rearrangement of the potential density*

In this section we discuss the qualitative behaviour of large-scale atmospheric circulations using semi-geostrophic theory. This is appropriate if we assume that the effect of physical forcing is to create air masses with

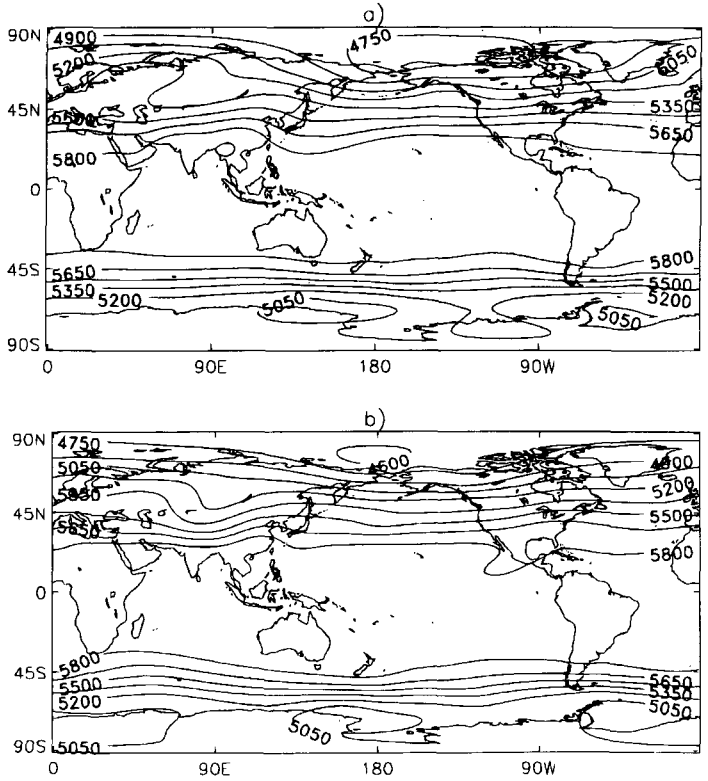

Fig. 5.5 10 day forecast using initial data from 1 February 1991: (a) semi-geostrophic model, (b) shallow water model. Contour interval 150m. From [Mawson (1996)]. ©Royal Meteorological Society, Reading, U.K.

different properties, but that the rate of change of air-mass properties is slow compared with the advective time-scale. We then regard the internal dynamics as semi-geostrophic, which is energy conserving, and conserves potential temperature and potential density following fluid particles. The minimum energy state that is consistent with potential temperature conservation is a 'rest' state, where the air masses are rearranged so that the potential temperature surfaces are horizontal. It is well known that the energy available to the internal dynamics is the difference between the actual energy and the energy of the rest state. In this paper we explore the additional restriction that the available energy is only the excess over that of a minimum energy state obtained by rearranging both potential density

and potential temperature. Such a minimum energy state will be nonlinearly stable using Kelvin's principles, [Thomson (1910)]: firstly that steady states are stationary points of the energy under rearrangements of the potential density and potential temperature, and secondly that stable steady states are extrema of the energy under these rearrangements. Application of these ideas to the atmosphere originated with [Fjortoft (1950)].

The problem, however, of minimising the energy with respect to simultaneous rearrangements of potential density and potential temperature is not generally well-posed. It is possible for there to be a sequence of rearrangements with successively smaller energies which do not converge to a limit. This corresponds to increasingly fine-scale filamentation of the potential density. The limiting state is actually a mixed state that is not a rearrangement. The widely used energy-Casimir method of analysing nonlinear stability, e.g. [Kusher and Shepherd (1995a)], [Kusher and Shepherd (1995b)], avoids this difficulty by replacing the rearrangement constraint by conservation of a particular function, the 'Casimir', of the potential density. An invariant is constructed using this function and the energy. The function is chosen so that if the basic state is perturbed, the change to the invariant is sign definite. This proves stability of the basic state to variations which conserve the invariant. The class of variations allowed is now larger than the rearrangements, so the stability results may be pessimistic. In the present paper, we adopt the alternative approach of considering the smallest (weakly) compact class of perturbations that includes the rearrangements. Compactness ensures that the minimisation problem will be well-posed. In particular, the class includes all states reached as the limit of a sequence of rearrangements. The energy-Casimir method cannot take account of these limit states, as they do not conserve the Casimirs.

This method has been used by [Burton and Nycander (1999)] to analyse the stability of a localised potential vorticity anomaly in a uniformly sheared environment using three-dimensional quasi-geostrophic theory. They have to allow for the possibility of mixing when posing the variational problem. However, the maximum energy states which they study are achieved by rearrangements and do not involve mixing. Similarly, it can be shown that the solution to the problem of minimising the energy with respect to rearrangements of potential temperature is a rearrangement with potential temperature monotonically increasing with height. Mixed solutions have a higher energy, see [Douglas (2002)].

The advantage of using rearrangement methods is that stability can be established with respect to all displacements, whether smooth or not.

It is also possible to derive results by geometrical arguments which may be difficult to establish by algebraic methods. For instance, [Ren (2000)] shows that it is very difficult to apply Arnold's stability methods to semi-geostrophic theory because of the nonlinear form of the potential density. However, the natural geometric interpretation of potential density can be readily used with rearrangement methods.

Here we summarise results obtained by [Cullen and Douglas (2003)] using rearrangement theory. More details of results from rearrangement theory are given in [Douglas (2002)]. We use the Boussinesq incompressible equations (2.124) as in section 5.1.1. We solve them in a domain Γ which is a channel of width $2D$ and height H, with periodicity $2L$ in the x-direction. Thus the boundary conditions are $v = 0$ on $y = \pm D$, $w = 0$ on $z = 0, H$, with all variables periodic in x.

Using the change of variables (3.24), the evolution equations are given by (3.27), repeated below:

$$\begin{aligned} \frac{\mathrm{D}X}{\mathrm{D}t} &= u_g, \\ \frac{\mathrm{D}Y}{\mathrm{D}t} &= v_g, \\ \frac{\mathrm{D}Z}{\mathrm{D}t} &= 0, \\ \nabla \cdot \mathbf{u} &= 0. \end{aligned} \tag{5.26}$$

The periodicity condition means that

$$\begin{aligned} \frac{\partial}{\partial t} \int_\Gamma Y \mathrm{d}x\mathrm{d}y\mathrm{d}z &= \int_\Gamma v_g \mathrm{d}x\mathrm{d}y\mathrm{d}z, \\ &= \int_\Gamma f^{-1} \frac{\partial \varphi}{\partial x} \mathrm{d}x\mathrm{d}y\mathrm{d}z = 0. \end{aligned} \tag{5.27}$$

This expresses the conservation of the momentum integral. The energy integral is given by (3.44)

$$E = \int_{\mathbb{R}^3} f^2 \left(\frac{1}{2} \left((x - X)^2 + (y - Y)^2 \right) - zZ \right) \sigma \mathrm{d}X\mathrm{d}Y\mathrm{d}Z. \tag{5.28}$$

The evolution can be written in dual variables in (X, Y, Z) coordinates on $\mathbb{T} \times \mathbb{R}^2$. Following (3.41), the evolution of potential density is given by

$$\begin{aligned} \frac{\partial \sigma}{\partial t} + \mathbf{U} \cdot \nabla \sigma &= 0, \\ \mathbf{U} &= (f(y - Y), f(X - x), 0). \end{aligned} \tag{5.29}$$

According to Theorem 3.18, extended to the periodic case, (5.29) can be solved for initial data $\sigma(0,\cdot)$ satisfying the compatibility condition

$$\sigma(X+L,Y) = \sigma(X-L,Y), \tag{5.30}$$
$$\int_{-L}^{L}\int_{-\infty}^{\infty}\int_{-\infty}^{\infty} \sigma \mathrm{d}X\mathrm{d}Y\mathrm{d}Z = \quad 4LDH.$$

Equation (5.29) shows that $\mathbf{U}$ is non-divergent and has no component in the Z direction. Thus the evolution can be considered as a rearrangement of σ on Z-surfaces in $\mathbb{T}\times\mathbb{R}^2$. The theorems discussed in section 3.5.2 show that the solutions are sufficiently regular for this statement to make sense.

Kelvin's principle applied to equation (5.29) says that steady states are stationary points of the energy with respect to rearrangements of σ along Z surfaces. Stable steady states correspond to maxima or minima of the energy under such rearrangements. It is likely that there will only be a small number of globally stable steady states corresponding to the maximum and the minimum energy that are obtainable over the whole class of rearrangements, including mixing, but there can also be a large class of locally stable states which are extrema of the energy subject to physically reasonable displacements.

5.2.2 *Properties of rearrangements*

We work with the definition of rearrangements given in Definition 3.6. Write the set of rearrangements of a given potential density as $\mathcal{R}(\sigma)$. Consider the problem of finding the maximum or minimum of the energy which can be obtained by rearranging a given potential density distribution on isentropic surfaces. A classical approach would be to choose a maximising (or minimising) sequence, and extract a subsequence converging to a maximiser (or a minimiser). However, this limit might not be a rearrangement, there is the possibility of 'mixing'. It is possible to construct an increasingly fine-grained sequence of rearrangements, which converge in a weak sense to a smoothed potential density distribution which is not a rearrangement. We give a simple one-dimensional example. Let the function ϱ_0 on $[0,1]$ be given by

$$\varrho_0(x) = \begin{cases} 0 \text{ if } x \in [0,1/2], \\ 1 \text{ if } x \in [1/2,1]. \end{cases} \tag{5.31}$$

Define, for n a positive integer,

$$\varrho_n(x) = \begin{cases} 0 \text{ if } x = 0, \\ 0 \text{ if } x \in (m/n, (2m+1)/2n], \\ 1 \text{ if } x \in ((2m+1)/2n, (m+1)/n], \end{cases}$$

where $m = 0, 1, ..., n-1$. The functions ϱ_3 and ϱ_8 are illustrated in Figure 5.6. For each integer n, ϱ_n is equal to zero on a set of length $1/2$, and equal to 1 on a set of length $1/2$. Therefore ϱ_n is a rearrangement of ϱ_0. However, given any $\vartheta \in L^2(0,1)$, it may be shown that $\int_0^1 \varrho_n \vartheta \mathrm{d}x \to 1/2 \int_0^1 \vartheta \mathrm{d}x$ as $n \to \infty$, that is ϱ_n converges weakly to the constant function with value $1/2$, which is not a rearrangement of ϱ_0.

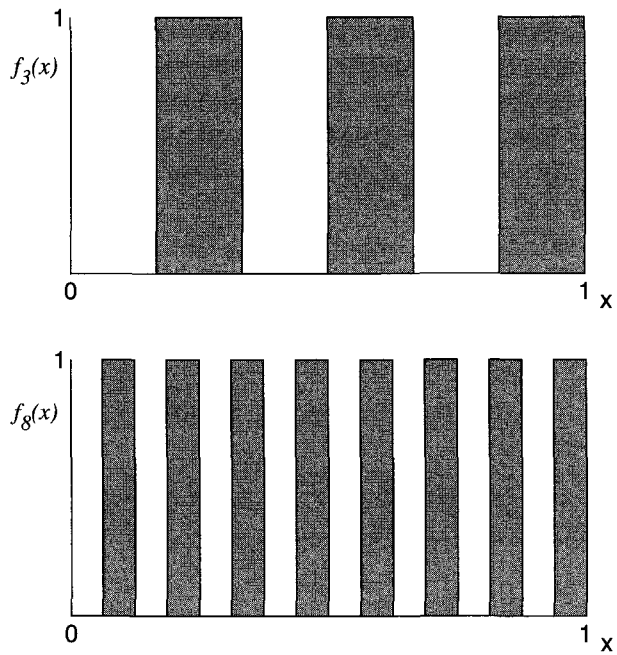

Fig. 5.6 Graphs of $\varrho_3(x)$ and $\varrho_8(x)$ as defined in (5.32). From [Cullen and Douglas (2003)]. ©Royal Meteorological Society, Reading, U.K.

This occurs in situations like the filamentation of potential vorticity at the stratospheric vortex edge. Physically, including these limit functions can be thought of as allowing for a small but finite viscosity or conductivity. The energy will be almost the same whether the fine-scale potential vorticity

filaments are present or are averaged out.

We attempt to solve the energy extremisation problem by extracting weakly convergent subsequences from an energy extremising sequence. In [Douglas (2002)], section 2.4, and [Burton and Nycander (1999)] it is shown that these limit solutions have to be included to ensure convergence. (In the problem solved by [Burton and Nycander (1999)], additional work showed that there is a solution which is a rearrangement.) A set is *weakly sequentially compact*, if for any sequence composed of elements of the set, we can find a subsequence which converges weakly to an element of the set. For a given σ, we seek the smallest such set which contains $\mathcal{R}(\sigma)$. It may be characterised, see for example [Ryff (1970)], as the closed convex hull of the set $\mathcal{R}(\sigma)$, which is the intersection of all the (strongly) closed convex sets that contain $\mathcal{R}(\sigma)$; we denote this set $\mathcal{C}(\sigma)$.

By choosing this set, we ensure that we make the most optimistic possible assessment of stability, since the energy extremisation is over the smallest possible set of perturbations which allow a solution. We now need to characterise this set. [Douglas (1994)] showed that $\varrho \in \mathcal{C}(\sigma)$ implies $\left(\int_\Gamma \varrho(\mathbf{x})^p d\mathbf{x}\right)^{1/p} \leq \left(\int_\Gamma \sigma(\mathbf{x})^p d\mathbf{x}\right)^{1/p}$ for every $p > 1$. This shows that the higher order moments of σ will, in general, be decreased when the limit solutions are included. This expresses the lack of robustness of the higher order moments of the potential density as constants of the motion, and that a state which extremises the energy may be obtained by selective decay of the higher order moments. These issues are discussed, for instance, by [Robert and Sommeria (1991)] and [Larichev and McWilliams (1991)].

We will make use of the following characterisation of $\mathcal{C}(\sigma)$ by Douglas (1994):

$$\mathcal{C}(\sigma) = \{\varsigma \geq 0 : \int_\Gamma (\varsigma(\mathbf{x}) - \alpha)_+ d\mathbf{x} \leq \int_\Gamma (\sigma(\mathbf{x}) - \alpha)_+ d\mathbf{x} \qquad (5.32)$$
$$\text{for each } \alpha > 0, \int_\Gamma \varsigma(\mathbf{x}) d\mathbf{x} = \int_\Gamma \sigma(\mathbf{x}) d\mathbf{x}.\},$$

where the $+$ subscript denotes the positive part of a function. If $\varsigma \in \mathcal{C}(\sigma)$ satisfies all the inequalities in (5.32) with equality, then $\varsigma \in \mathcal{R}(\sigma)$. In the following theorem, [Cullen and Douglas (2003)] prove that rearranging a function σ, followed by taking a local average, gives a member of $\mathcal{C}(\sigma)$.

Theorem 5.3 *Let non-negative $\sigma : \Gamma \to \mathbb{R}$ be square integrable, and suppose $\varsigma \in \mathcal{R}(\sigma)$. For a set $G \subset \Gamma$ of positive volume $\mu(G)$, define*

$$\varrho(x) = \begin{cases} \frac{1}{\mu(G)} \int_G \varsigma(\mathbf{x}) d\mathbf{x} \equiv \bar{\varsigma} & \text{if } \mathbf{x} \in G, \\ \varsigma(x) & \text{if } x \in \Gamma \backslash G. \end{cases}$$

Then $\varrho \in \mathcal{C}(\sigma)$.

In the one-dimensional example above, with ϱ_0 as in (5.31), it can be shown, by using the characterisation (5.32), that any integrable function ς on $[0,1]$ satisfying $0 \leq \varsigma(x) \leq 1$ for each $x \in [0,1]$, and $\int_0^1 \varsigma(x)dx = 1/2$, belongs to $\mathcal{C}(\varrho_0)$. This illustrates that $\mathcal{C}(\varrho_0)$ may be a large class of functions, in particular it includes the constant value $1/2$ as described earlier.

Another useful result, which follows from our characterisation of $\mathcal{C}(\sigma)$ as the closed convex hull of $\mathcal{R}(\sigma)$, is that $\mathcal{R}(\sigma)$ is weakly dense in $\mathcal{C}(\sigma)$ so that, for every $\varsigma \in \mathcal{C}(\sigma)$, we can find a sequence $(\varsigma_n) \subset \mathcal{R}(\sigma)$ which converges weakly to ς, see [Douglas (1994)].

In multi-dimensional problems, it is typical that the extremising states can be proved to be independent of one or more spatial coordinates. In the shear-flow problems described in this section, it can be proved that the extremising states are independent of X. It is then sufficient to analyse the properties of one-dimensional rearrangements. We therefore derive some one-dimensional results. Take σ to be a non-negative function on $[0,1]$ as illustrated in Fig. 3.14. It is stated in [Douglas (2002)] that there is an (essentially) unique rearrangement of σ which is an increasing function. Write it as $\tilde{\sigma}$. Similarly, σ has an (essentially) unique rearrangement which is decreasing; we denote it $\hat{\sigma}$. We will need to make use of the following result which follows from standard rearrangement inequalities:

Theorem 5.4 *Let non-negative* $\varrho, \sigma : [0,1] \to \mathbb{R}$ *be square integrable, and suppose* ϱ *is increasing. Then* $\int_0^1 \varrho(x)\varsigma(x)dx$ *is maximised for* $\varsigma \in \mathcal{C}(\sigma)$ *by the increasing rearrangement of* σ*, and is minimised by the decreasing rearrangement of* σ*. The reverse statements apply if* $\varrho(x)$ *is non-negative and decreasing.*

We also make use of a result on the stability of straight semi-geostrophic flows in the X-direction. For this case, y is a function of Y only, and the potential density σ is $\partial y/\partial Y$. The velocity U is $f(y-Y)$ and (5.28) shows that the kinetic energy density is $\frac{1}{2}f^2(y-Y)^2\sigma$. Take as an example, (Fig. 5.7), the case where the physical domain is $0 \leq y \leq \frac{1}{2}$ and $\sigma(Y)$ is a function of the same form as ϱ_0 defined in (5.31), so that $\sigma(Y) = 0 : 0 \leq Y \leq \frac{1}{2}; = 1 : \frac{1}{2} < Y \leq 1.$. The mean value of σ is $\frac{1}{2}$, so that the compatibility condition (5.30) is satisfied. The velocity U is derived by first calculating

$y(Y) = \int_0^Y \sigma(Y')\mathrm{d}Y'$, and then setting $U = f(y - Y)$. It is intuitively clear that the largest energy for $\varsigma \in \mathcal{R}(\sigma)$ will be obtained by choosing ς to be either the monotonically increasing or decreasing rearrangement of σ. Moreover, no larger value will be achieved by any other $\varsigma \in \mathcal{C}(\sigma)$. The energy will be minimised over $\varsigma \in \mathcal{R}(\sigma)$ by choosing ς to oscillate about $\frac{1}{2}$, the mean value of σ. If we define $\varsigma_n(Y) = \begin{cases} \varrho_n(Y + 1/(2n)) & \text{if } 0 \le Y \le 1, \\ 0 & \text{if } Y > 1, \end{cases}$ where ϱ_n is as defined in (5.32), then the energy is $\mathrm{O}\left(\frac{1}{n^2}\right)$. Note that a minimum energy state is not attained within $\mathcal{R}(\sigma)$, but that zero energy is achieved within $\mathcal{C}(\sigma)$.

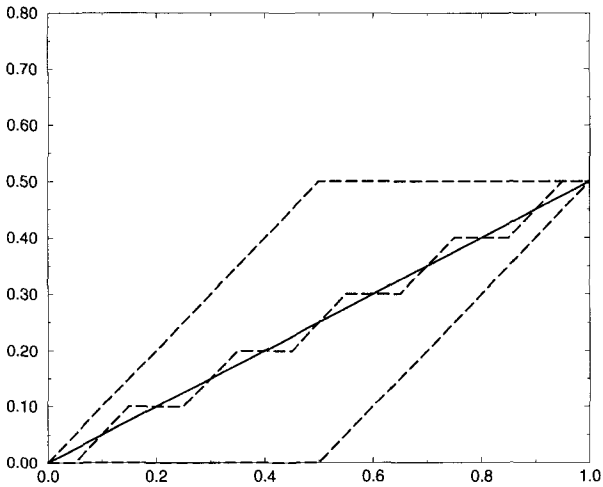

Fig. 5.7 Graphs of $y(Y) = Y/2$ (solid line) and various choices of $y(Y)$ obtained by setting $\varsigma(Y)$ to be a rearrangement of $\sigma(Y)$ of the form (5.31). These choices are the monotonically increasing and decreasing rearrangements, and the choice $\varsigma(x) = \varrho_5(Y + 0.1)$ as defined in (5.32). From [Cullen and Douglas (2003)]. ©Royal Meteorological Society, Reading, U.K.

This example shows that the minimiser will typically involve mixing while the maximiser will be a strict rearrangement. The physically important case for the global stability problem is usually an energy minimiser, because the global maximiser will often correspond to an unreachable or

unphysical state. However, the local stability problem may well be solved by an energy maximiser, as in the study of [Burton and Nycander (1999)].

Now consider general $\sigma(Y)$ with the same physical domain $0 \le y \le \frac{1}{2}$. The compatibility condition (5.30) requires that $\int_{-\infty}^{\infty} \sigma(Y)dY = \frac{1}{2}$. Let $y(Y) = \int_0^Y \sigma(Y')\mathrm{d}Y'$. Theorem 5.3 shows that $\mathcal{C}(\sigma)$ contains all local averages. Thus in particular, given any Y_1, Y_2, if $y(Y)$ is replaced by its linear interpolant between Y_1 and Y_2, then the associated $\varsigma = \partial y/\partial Y$ will be in $\mathcal{C}(\sigma)$ because $\sigma(Y)$ has been replaced by its average value over the range (Y_1, Y_2). In the example shown in Fig. 5.7, the linear interpolant between 0 and 1 gives the function $y(Y) = Y/2$. Thus $\frac{1}{2} \in \mathcal{C}(\sigma)$ and the sequence $\varsigma_n(x)$ in $\mathcal{R}(\sigma)$ has the weak limit $\varsigma(x) = \frac{1}{2}$, giving zero energy.

In order to obtain useful nonlinear stability results, it is necessary to require the potential density to have compact support . The same condition was required to prove the results in section 3.5. We showed there that, given initial data with compact support, it remains compact for all finite times. In the following theorem, we assume without loss of generality that the finite region is $[0, 1]$.

Theorem 5.5 *Let $\sigma : [0,1] \to \mathbb{R}$ be square integrable. Given $\varsigma \in \mathcal{C}(\sigma)$, set $y_\varsigma(Y) = \int_0^Y \varsigma(Y')\mathrm{d}Y'$. Then, for each $Y \in [0,1]$, we have $y_{\hat{\sigma}}(Y) \ge y_\varsigma(Y)$ for every $\varsigma \in \mathcal{C}(\sigma)$, where $\hat{\sigma}$ denotes the decreasing rearrangement of σ. Consequently $\int_0^1 y_{\hat{\sigma}}(Y)dY \ge \int_0^1 y_\varsigma(Y)dY$.*

5.2.3 *Analysis of semi-geostrophic shear flows*

We now use these results to analyse the stability of semi-geostrophic shear flows. In order to apply Kelvin's principle we seek a class of perturbations which is dynamically consistent with (5.29). It is shown by [Cullen and Douglas (2003)] that if the support of σ at $t = 0$ is within an interval $[-S, S]$, the support at time T will be contained within $[-(S + fLT), S + fLT]$. We therefore assume that the perturbations are within the class $\mathcal{C}_h(\sigma)$, defined by

$$\varsigma \in \mathcal{C}_h(\sigma) \text{ if } \begin{cases} \varsigma(.,Z) \in \mathcal{C}(\sigma(.,Z)) \text{ for almost all } Z \\ \int Y\varsigma \mathrm{d}X\mathrm{d}Y\mathrm{d}Z = \int Y\sigma \mathrm{d}X\mathrm{d}Y\mathrm{d}Z \\ \text{supp } \varsigma \subset \Sigma = [-(S + fLT), S + fLT] \end{cases} \tag{5.33}$$

The first condition restricts the rearrangements of σ to the (X, Y) variables

only, and includes the weak limits. This is similar to the space of 'stratified' rearrangements used by [Burton and Nycander (1999)]. The additional condition is that the mean Y over the particles cannot be changed. This corresponds to the conservation of the momentum integral (5.27). We write $\mathcal{R}_h(\sigma)$ for functions ρ satisfying (5.33) with $\mathcal{R}$ replacing $\mathcal{C}$.

The problem of extremising the energy with respect to perturbations in $\mathcal{C}_h(\sigma)$ only makes physical sense if weak convergence of a sequence of potential density distributions to a limit implies convergence of the energy associated with the distributions. It is shown in [Cullen and Douglas (2003)] that, given a sequence $\varsigma_n \in \mathcal{R}_h(\sigma)$ with energies E_n converging weakly to a member ς of $\mathcal{C}_h(\sigma)$ with energy E, E_n converges to E. Then if we take a maximising or minimising sequence for the energy we can extract a weakly convergent subsequence converging to some $\varsigma \in \mathcal{C}_h(\sigma)$, by weak sequential compactness of $\mathcal{C}_h(\sigma)$.

We next characterise the steady states of (5.29) as stationary points of the energy with respect to appropriate variations. Given compactly supported $\sigma = \sigma(X, Y, Z)$ satisfying (5.30), we seek necessary conditions for $\delta E = 0$ for perturbations satisfying $\sigma + \delta\sigma \in \mathcal{R}_h(\sigma)$. We generate such variations by keeping σ fixed on particles in $\mathbf{X}$ space and perturbing X and Y with an incompressible displacement field $\Xi = (\xi, \eta)$. As the displacement is infinitesimal, it must be non-divergent, so we can write $(\xi, \eta) = (-\partial\vartheta/\partial Y, \partial\vartheta/\partial X, 0)$ for some arbitrary function $\vartheta(X, Y)$, and must satisfy the periodicity condition $\vartheta(X - L, Y) = \vartheta(X + L, Y)$ The restriction that the mean Y cannot be changed is then automatically enforced.

In both original and perturbed solutions (x, y, z) is defined as a function of (X, Y, Z) by an optimal map, respectively $\mathbf{t}(\mathbf{X})$ and $\mathbf{t}'(\mathbf{X})$. We write the changes to $\mathbf{x}$ following a particle as $(\delta x, \delta y, \delta z)$. Since the value of σ is not changed following particles, their volume in physical space is preserved, and so $\nabla \cdot (\delta x, \delta y, \delta z) = 0$. We then have, integrating over particles:

$$\delta E = f^2 \int_{-L}^{L}\int_{-\infty}^{\infty}\int_{-\infty}^{\infty}((X-x)\xi + (Y-y)\eta - X\delta x - Y\delta y - Z\delta z)\sigma \mathrm{d}X\mathrm{d}Y\mathrm{d}Z. \tag{5.34}$$

The condition that the original $\mathbf{x}$ is given as a function of $\mathbf{X}$ by an optimal map means that

$$f^2 \int_{-L}^{L}\int_{-\infty}^{\infty}\int_{-\infty}^{\infty}(-X\delta x - Y\delta y - Z\delta z)\sigma \mathrm{d}X\mathrm{d}Y\mathrm{d}Z = 0. \tag{5.35}$$

By substituting (5.35) into (5.34), using the definition (5.29) of $\mathbf{U}$, and after some further manipulations, [Cullen and Douglas (2003)] show that the condition for a stationary point is

$$U\frac{\partial\sigma}{\partial X}+V\frac{\partial\sigma}{\partial Y}=0, \tag{5.36}$$

which is the condition for the flow to be steady.

We next consider the stability of barotropic shear flows where σ is a function of (X,Y) only, and the energy is

$$E=\frac{1}{2}f^2\int_{-L}^{L}\int_{-\infty}^{\infty}(x-X)^2+(y-Y)^2\sigma\mathrm{d}X\mathrm{d}Y. \tag{5.37}$$

The maximum energy attainable for $\varsigma\in\mathcal{C}_h(\sigma)$ is a function of the assumed maximum value of $|Y|$ in the support Σ of σ. Using (5.33), this can be calculated as $2f^4L^3TD$. It is therefore only physically meaningful to seek minimum energy states. In the stability problem for two-dimensional incompressible flow, however, the maximum energy state is physically meaningful. This is because the evolution equation is written in physical space and so the displacements have to be within the physical domain. This problem was treated by [Burton and McLeod (1991)].

Given σ, we therefore seek to minimise E for $\sigma+\delta\sigma\in\mathcal{C}_h(\sigma)$. (5.28) shows that the minimum energy is attained by making the map $\mathbf{t}$ from (X,Y) to (x,y) as close as possible to the identity. Therefore we expect that the minimum energy will be achieved by mixing the values of σ to give a potential density σ_0 defined by

$$\sigma_0=1:|Y-Y_0|\le D,X\le|L|\text{ and }\sigma_0=0\text{ elsewhere}, \tag{5.38}$$

with Y_0 chosen to satisfy the second equation of (5.33). Then (5.29) shows that $\mathbf{U}=(-fY_0,0)$ for all (X,Y). This will give the lowest energy consistent with the requirement that the mean velocity and hence the momentum integral is specified. This distribution is not always achievable by mixing the given σ, as [Cullen and Douglas (2003)] show in the following theorem:

Theorem 5.6 *If Σ has area greater than $4DL$, then σ_0 as defined by (5.38) is not in $\mathcal{C}_h(\sigma)$.*

It follows from Theorem 5.6 that, if the mean value $\overline{\sigma}$ of σ is less than 1 over Σ, then $\sigma_0 \notin \mathcal{C}_h(\sigma)$. Fig. 5.8 shows three possibilities for $\overline{\sigma}$, assuming $Y_0 = 0$. Recalling that σ is the inverse of the potential vorticity, the anticyclonic case corresponds to $\overline{\sigma} > 1$. The distribution shown can be mixed to give σ_0. The cyclonic case has $\overline{\sigma} < 1$, Theorem 5.6 applies, and σ cannot be mixed to give σ_0. In that case, the minimum energy will be obtained by getting as close to σ_0 as possible. The following stability result for shear flows independent of Z is then proved by [Cullen and Douglas (2003)]:

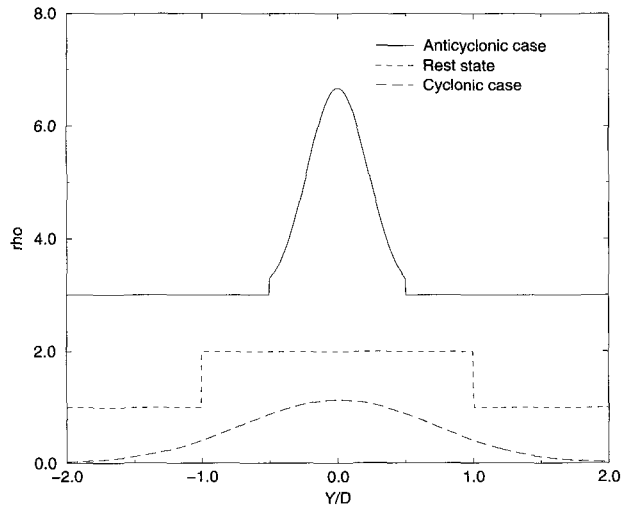

Fig. 5.8 Graphs of $\sigma(Y)$ against Y for the cyclonic and anticyclonic cases defined in the text and the rest state $\sigma_0(Y) = 1, |Y| \leq D$. The base values are shifted for clarity. From [Cullen and Douglas (2003)]. ©Royal Meteorological Society, Reading, U.K.

Theorem 5.7 *Given $\sigma(X,Y)$ satisfying (5.30) with compact support $\Sigma \subset \mathbb{R}^2$ with area μ. If $\mu > 4DL$, the minimiser of E over $\mathcal{C}_h(\sigma)$ takes the form*

$$\varsigma(X,Y) = \begin{cases} 1 & \text{if } |Y - Y_0| \leq Y_1, \\ \tilde{\sigma} & \text{if } Y_1 < |Y - Y_0| \leq \mu/4L, \\ 0 & \text{otherwise,} \end{cases} \tag{5.39}$$

where $\tilde{\sigma}$ is a monotonically decreasing function of $|Y - Y_0|$ and $0 \leq Y_1 < \mu/4L$. Y_0 is chosen to satisfy the momentum integral constraint. If $\mu \leq 4DL$ the minimiser is defined by (5.38).

Theorem 5.7 shows that the only minimum energy states are distributions independent of X with $\sigma \leq 1$ everywhere. Thus there can be no stable states with $\sigma > 1$ at any point. Since σ is an inverse potential vorticity, this condition excludes values of potential vorticity less than 1, which correspond to anticyclonic relative vorticity. This agrees with the result of [Kusher and Shepherd (1995a)], [Kusher and Shepherd (1995b)], that there were no stable shear flows with anticyclonic shear. This argument also shows that no steady states with anticyclonic relative vorticity can be stable in any limited domain with rigid boundary conditions under semi-geostrophic dynamics. They could be stable in doubly periodic flows, because there is then no region with $\sigma = 0$ in the (X, Y) plane to mix with the non-zero values. [Ren (2000)] discusses the physical relevance of this stability condition, suggesting that it may be most relevant in the baroclinic case discussed next.

Now consider the baroclinic case where σ depends on Z. Write, for a given Z, $\mu(Z) = \frac{1}{2}\max(S(Z), 2D)$, where $2LS(Z)$ is the area of $\Sigma \cap \{Z\}$. Set $M = \max_Z(\mu(Z))$, for all Z. Since σ can only be rearranged on Z surfaces, we expect the energy minimiser ς to be obtained by first assuming a zero momentum integral on each Z surface, and then minimising the energy on each Z surface separately using Theorem 5.7. It may then be advantageous to remove the Z dependence by mixing σ uniformly over the whole region $|Y| \leq M$. The momentum constraint, which is vertically integrated, is then used to displace the entire solution by some distance Y_0 in Y. For each Z, the area of the support of ς cannot be less than the area of the support of σ. However, zero values can be mixed in to increase the size of the set to $4DL$ for each Z. If $M \leq D$, σ can be mixed to give ς as a function of Z only whose energy will be the minimum rest state potential energy. However, if $M > D$, this state is not in $\mathcal{C}_h(\sigma)$. There then has to be kinetic energy in the minimum energy state. These situations are illustrated schematically in Fig. 5.9.

We formalise these procedures in:

Theorem 5.8

(i) If $M \leq D$, $\varsigma = \{\text{constant}, |Y| \leq D, = 0, |Y| > D\}$ is in $\mathcal{C}_h(\sigma)$ and minimises E over $\mathcal{C}_h(\sigma)$. The geostrophic wind then takes a uniform

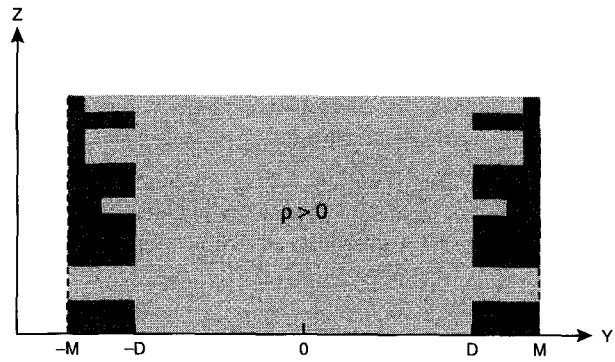

Fig. 5.9 Schematic illustration of the region of the (Y, Z) plane for which ς is non-zero in the energy minimising state for the two extreme cases; total shaded area: $fl/NH \gg 1$, light shaded area: $fl/NH \ll 1$. From [Cullen and Douglas (2003)]. ©Royal Meteorological Society, Reading, U.K.

value on Γ. *This value is equal to the minimum rest state potential energy if the specified momentum integral is also zero.*

ii) If $M > D$, *and the specified momentum integral is zero, the minimum possible kinetic energy achievable for* $\varsigma \in \mathcal{C}_h(\sigma)$ *is* $4L \int_D^{\mu(Z)} \int_{-\infty}^{\infty} (D - \hat{Y})^2 \hat{\sigma}(Y, Z) dY dZ$, *where* $\hat{\sigma}(Y, Z)$ *takes the form (5.39) for each* Z *and* $\hat{Y}(y)$ *is defined by* $dY^*/dy = (\hat{\sigma})^{-1}$.

(iii) The potential energy is minimised for $\varsigma \in \mathcal{C}_h(\sigma)$ *by choosing* ς *to take a uniform value for* $|Y - Y_0| \leq M$ *for each* Z.

If $M > D$, then the solution will contain kinetic energy even if the specified momentum integral is zero. The solution will be scale-dependent, according to whether potential or kinetic energy perturbations contribute more to the total energy. As discussed in section 2.5, this depends on whether the horizontal length scale l is smaller than the Rossby radius of deformation L_R. If $l < L_R$, it is most important to minimise the kinetic energy. The distribution of Theorem 6(ii) requires there to be less kinetic energy than that of Theorem 6(iii), since there only has to be kinetic energy associated with values of Z for which $\mu(Z) > D$. The minimum energy state will thus be Z dependent. If $l > L_R$, it is more important to minimise the potential energy. This is achieved by the distribution of Theorem 6(iii).

A real example of a highly unstable state is shown in Figure 5.10. The geopotential contours at 500hpa are illustrated. These correspond to a narrow strip of large geostrophic winds, which imply a strip of cyclonic

vorticity to the north of a strip of anticyclonic vorticity. This is close to a locally maximum energy state, and is thus very unstable. It preceded the development of two violent storms which did a lot of damage in Northern France.

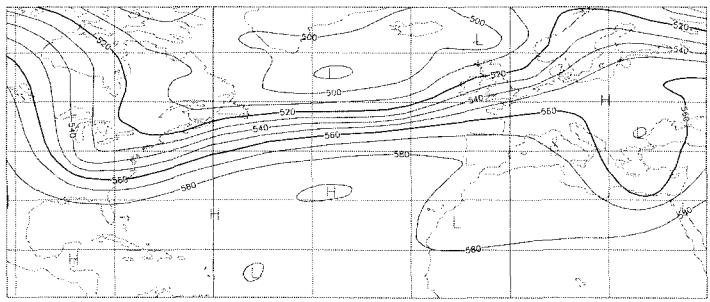

Fig. 5.10 500hpa height over part of the Northern hemisphere at 1200UTC on 24 December 1999. Source: ECMWF.

In general, we have shown that there are minimum energy states with more energy than the rest state potential energy. This gives more control over the possible dynamic evolution of the system, since only the excess energy above this minimum value is available for transient motion. It will be interesting to see if these results can be extended to spherical geometry.

5.3 Numerical methods for solving the semi-geostrophic equations

5.3.1 *Solutions using the geostrophic coordinate transformation*

Most numerical solutions of the three-dimensional semi-geostrophic equations have been produced by the geostrophic coordinate transformation introduced by [Hoskins (1975)]. An early example of such solutions was the simulation of a growing baroclinic wave by [Hoskins and West (1979)]. The description of the method here follows [Snyder, Skamarock and Rotunno (1991)]. Consider the f-plane, Boussinesq form of the equations (2.124). Solve them in a region $\Gamma = \mathbb{T}^2 \times [0, H]$, so that there are horizontal boundaries at $z = 0, H$ where $w = 0$. The potential vorticity equation is given by (3.57). Transform the equations to the geostrophic coordinates (X, Y, Z_g),

where X and Y are defined by (3.24) and $Z_g = z$. Then (3.57) becomes

$$\frac{f^2}{Q_{SG}}\frac{\partial^2\Psi}{\partial Z_g^2} + \frac{\partial^2\Psi}{\partial X^2} + \frac{\partial^2\Psi}{\partial Y^2} - \frac{1}{f^2}J_{XY}\left(\frac{\partial\Psi}{\partial X}, \frac{\partial\Psi}{\partial Y}\right) = f^2,$$

$$J_{cd}(a,b) \equiv \frac{\partial a}{\partial c}\frac{\partial b}{\partial d} - \frac{\partial a}{\partial d}\frac{\partial b}{\partial c}, \tag{5.40}$$

$$\Psi = \frac{f^2}{2}\left((x-X)^2 + (y-Y)^2\right).$$

The definition of Ψ is similar to that given by assuming equality in (3.52). The difference arises because the vertical coordinate has not been transformed. The hydrostatic relation transforms to

$$\frac{\partial\Psi}{\partial Z_g} = g\frac{\theta'}{\theta_0}. \tag{5.41}$$

In the cases studied by [Hoskins and West (1979)] and [Snyder, Skamarock and Rotunno (1991)], Q_{SG} was assumed uniform initially, and so it is assumed it will remain uniform. Therefore equation (3.57) does not have to be solved. It is shown in section 3.2.3 that this property will in general be lost if there is frontogenesis. It is not clear how much this would alter the conclusions of these papers. Given this assumption, a solution can be obtained by predicting θ' on the horizontal boundaries. Since $w = 0$ at $z = Z_g = 0, H$ and using (5.41), this requires solving

$$\frac{\partial}{\partial t}\frac{\partial\Psi}{\partial Z_g} = \frac{1}{f}\left(\frac{\partial\Psi}{\partial Y}\frac{\partial}{\partial X} - \frac{\partial\Psi}{\partial X}\frac{\partial}{\partial Y}\right)\frac{\partial\Psi}{\partial Z_g}, \tag{5.42}$$

at $Z_g = 0, H$.

The solutions in [Hoskins and West (1979)] were obtained by neglecting the nonlinear term in the first equation of (5.40). This equation is then a linear constant coefficient elliptic equation for Ψ, which was solved by using a second order spatial finite difference representation, fast Fourier transforms in the horizontal, and a tri-diagonal inversion in the vertical. Equation (5.42) was integrated forward in time using a positive-definite advection scheme. The equations were solved in (X, Y, Z_g) coordinates and only transformed back to physical coordinates for plotting purposes. If the nonlinear terms in (5.40) are included, the solution has to be iterated, using the previous iterate to calculate the nonlinear terms. It was found by [Snyder, Skamarock and Rotunno (1991)] that neglecting the nonlinear terms increased the difference between semi-geostrophic solutions and solutions of (2.83).

While this method appears much simpler than the solution procedure described in section 3.2.2 using the Monge-Ampère equation, it relies on the transformation back to physical space being single-valued. It is shown in [Hoskins and West (1979)] that this is not the case in general. However, the consequences were assumed small in these studies. The resulting error is not known.

The geostrophic coordinate transformation has also been used when using semi-geostrophic theory to derive a 'balanced' part of the solutions of (5.1). It is thus equivalent to the procedure described in section 5.1.1, equation (5.9). It was shown by [Hoskins and Draghici (1977)] that, under this transformation, the semi-geostrophic omega equation takes the same form as the quasi-geostrophic omega equation in physical coordinates. In [Pedder and Thorpe (1999)], this was exploited to diagnose the ageostrophic circulation predicted by semi-geostrophic theory from fields predicted by a solution of (5.1). We summarise the method below.

The omega equation for the three-dimensional quasi-geostrophic equations (2.106) and (2.107) is

$$N^2\nabla_z^2 w + f^2\frac{\partial^2 w}{\partial z^2} = 2\nabla_z\cdot\mathbb{Q}, \tag{5.43}$$

$$\mathbb{Q} = \left\{-\frac{g}{\theta_0}\left(\frac{\partial u_g}{\partial x}\frac{\partial\theta'}{\partial x}+\frac{\partial v_g}{\partial x}\frac{\partial\theta'}{\partial y}\right), -\frac{g}{\theta_0}\left(\frac{\partial u_g}{\partial y}\frac{\partial\theta'}{\partial x}+\frac{\partial v_g}{\partial y}\frac{\partial\theta'}{\partial y}\right)\right\}.$$

If the nonlinear term in equation (5.40) is neglected, then the semi-geostrophic omega equation can be written in (X, Y, Z_g) coordinates as

$$\left(\frac{g}{f\theta_0}\nabla_{Z_g}^2\mathcal{Q}_{SG} + f^2\frac{\partial^2}{\partial Z_g^2}\right)\left(w\frac{\partial(x,y)}{\partial(X,Y)}\right) = 2\nabla_{Z_g}\cdot\left(\mathbb{Q}\frac{\partial(x,y)}{\partial(X,Y)}\right), \tag{5.44}$$

where $\mathcal{Q}_{SG}$ is defined by (3.57) and $\mathbb{Q}$ is defined in (5.43).

In [Pedder and Thorpe (1999)], equation (5.44) is solved with $\mathbf{u}_g, \mathbb{Q}$ and $\frac{\partial(x,y)}{\partial(X,Y)}$ calculated from real data on a regular grid in (x, y, z) coordinates. Values X_j and Y_j are also calculated on this grid. A regular grid (X_i, Y_i, Z_{gi}) is then chosen in (X, Y, Z_g) coordinates, and the corresponding values of (x, y, z) determined by iteration. Assuming the values of z and Z_g correspond, we only consider interpolation in (x, y). The first guess is obtained by interpolating $\mathbf{u}_g$ from (X_j, Y_j) to (X_i, Y_i), and then calculating

$$x_i = X_i - f^{-1}v_{gi}, y_i = Y_i + f^{-1}u_{gi}. \tag{5.45}$$

We can then interpolate $\mathbf{u}_g$ from the original grid to the points (x_i, y_i) and use these values in (5.45) to update the values of (x_i, y_i). We then

interpolate the values of $\mathbb{Q}$ and $\frac{\partial(x,y)}{\partial(X,Y)}$ to the points (x_i, y_i) and solve (5.44).

The method of [Pedder and Thorpe (1999)] works if $f\mathcal{Q}_{SG} > 0$ and $\frac{\partial(x,y)}{\partial(X,Y)} > 0$. These are implied by the convexity condition in Definition 3.1. When (5.44) is used diagnostically with the right hand side calculated from real data, it is unlikely that this condition will be satisfied. In [Pedder and Thorpe (1999)], a case of this is demonstrated, and resolved by local modifications to φ. These are calculated by solving the inverse problem $\frac{\partial(X,Y)}{\partial(x,y)} = \max(\mathcal{Q}, \mathcal{Q}_0)$ for φ at each z, where $\mathcal{Q}$ is the original value of $\frac{\partial(X,Y)}{\partial(x,y)}$ and $\mathcal{Q}_0$ a small positive value. Any changes made to φ are applied equally to all values of z. The procedure is iterated over the levels till no further changes result.

An application of this method due to [Thorpe and Pedder (1999)] is shown in section 6.3.

5.3.2 *The geometric method*

The geometric algorithm used in sections 3.4.2 and 6.2 is based on the explicit construction procedure of Theorem 3.11. It has so far only been implemented in two space dimensions. The original implementation was by [Chynoweth (1987)]. In principle, the solution can be obtained by iteration on the intersection p_i of the face A_i defined by the equation $p = xX_i + yY_i + p_i$ with $x = y = 0$. Convergence is guaranteed by Theorem 3.11. The cost of the original algorithm was $O(N^3)$ operations, where N is the number of faces.

An efficient implementation was developed by R. J. Purser (private communication). This has a cost of $O(N \log N)$ operations . Given data $(X_i, Y_i) : i = 1, N$, the efficiency of the algorithm depends on the sorting procedure which uses the convex hull algorithm developed by [Preparata and Hong (1977)].

The first step is to choose values p_i such that all faces of the polyhedron

$$p(x, y) = \sup_i(xX_i + yY_i + p_i), \tag{5.46}$$

have a non-zero area. This is achieved by the Voronoi solution, a simple form was shown in (3.101). More generally, suppose $\Gamma = [a, b] \times [c, d]$ and

that $(X_i, Y_i) \in [A, B] \times [C, D]$. Then set

$$p_i = -\frac{1}{2}\left(\frac{b-a}{B-A}X_i^2 + \frac{d-c}{D-C}Y_i^2\right) + \left(a - A\frac{b-a}{B-A}\right)X_i + \left(c - C\frac{d-c}{D-C}\right)Y_i. \quad (5.47)$$

We then use the divide and conquer algorithm of [Preparata and Hong (1977)] to calculate the geometry of the intersections between the planes $p(x, y) = xX_i + yY_i + p_i$. Sort (X_i, Y_i) values into groups of up to four elements by successive binary subdivision using alternately the X_i and Y_i values. Construct the geometry of a four-element patch. If the faces of the polyhedron associated with two pairs (X_i, Y_i) and (X_j, Y_j) have a common edge, we draw a link between the pairs as shown in Figure 5.11. Figure 5.11 shows the two possibilities within a four element patch.

We next knit two disjoint patches together using the algorithm of [Preparata and Hong (1977)]. If we suppose that elements 3 and 2* have a common edge, we join the two patches by an arc from 3 to 2*. Now test that the new link is consistent with convexity of the combined patch. The links have thus to reflect the monotonic change of X and Y as we move across the polyhedron. In the example shown a link from 3 to 2* clearly will be consistent with this, while joining 2 and 3* will not. We then complete the connections between the patches, to form a joint convex hull, and repeat up through the binary tree, building up the whole solution.

At some points, this successive build-up may lead to incorrect linkages, so that the surface defined by assuming corresponding intersections between planes is not convex. The panel-beater algorithm is used to resolve these. Typically it will involve exchanging links between the two formats shown in Fig. 5.11. The metrical properties of the polyhedron are now calculated. In particular we need the area of each face in (x, y) space, and its rate of change with respect to its value of p_i. Increasing a value of p_i will increase the area of the corresponding face at the expense of its neighbours. The iteration to the correct area thus has the same structure as the discrete solution of an elliptic partial differential equation, and so can be handled by conjugate gradient or multigrid methods.

5.3.3 *Finite difference methods*

We first describe the method of [Mawson (1996)] for the shallow water semi-geostrophic equations (2.74), (2.75), demonstrated in sections 4.3, 5.1.2

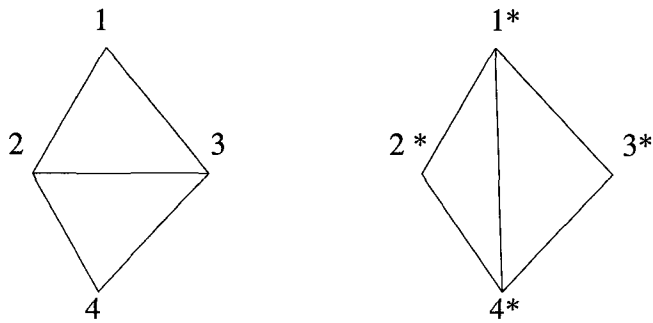

Fig. 5.11 Two patches of four elements, showing the possible linkages between vertices, and defining the notation for the discussion in the text.

and 6.4. The same method, with some refinements, was used by [Cloke and Cullen (1994)] as described in section 3.4.3. Finite difference methods for the equations expressed as a mass transportation problem have been developed by [Benamou and Brenier (1997)] and [Angenent et al. (2003)].

The data (h, u, v, u_g, v_g) are represented on a grid as shown in Fig. 5.12. Thus u_g is held at a different point from u and v_g at a different point from v. This choice is natural for the definition of the geostrophic wind, (2.74), and for the continuity equation in (2.75). In the spherical case described by [Mawson (1996)], depth values are stored on the equator. This is because semi-geostrophic solutions admissible according to Definition 4.2 do not allow h to vary along the equator. The constraint is easier to enforce with this choice of grid.

Given initial data for (h, u, v, u_g, v_g), h, u_g and v_g can be advanced in time for a step δt by a standard numerical scheme. This gives $h = h^*, u_g = u_g^*, v_g = v_g^*$. The result will not in general satisfy (2.74). This guess is therefore corrected by using a discrete form of (2.77) and the third

i	$i+\frac{1}{2}$	$i+1$	
h	u,v_g	h	j
v,u_g		v,u_g	$j+\frac{1}{2}$
h	u,v_g	h	$j+1$

Fig. 5.12 Grid staggering for the solution of the semi-geostrophic shallow water equations. From [Mawson (1996)]. ©Royal Meteorological Society, Reading, U.K.

equation of (2.75).

$$\begin{aligned} \mathbf{Q}\delta t \begin{pmatrix} \delta u \\ \delta v \end{pmatrix} + g\nabla \left(h^{t+\delta t} - h^*\right) &= 0, \\ h^{t+\delta t} - h^* + \delta t \nabla \cdot (h^* \delta \mathbf{u}) &= 0, \\ \mathbf{Q} = \begin{pmatrix} f^2 + f\frac{\partial v_g}{\partial x} & f\frac{\partial v_g}{\partial y} \\ -f\frac{\partial u_g}{\partial x} & f^2 - f\frac{\partial u_g}{\partial y} \end{pmatrix}. \end{aligned} \tag{5.48}$$

As in the derivation of (2.78), these equations can be converted into a single equation for $h^{t+\delta t}$ by eliminating δu and δv:

$$(h^{t+\delta t} - h^*) - \nabla \cdot h^* \mathbf{Q}^{-1} g \nabla (h^{t+\delta t} - h^*) = 0. \tag{5.49}$$

If $\mathbf{Q}$ is positive definite, (5.49) is elliptic and can be solved for $h^{t+\delta t}$. Then the first equation of (5.48) can be solved for δu, δv.

If the matrix $\mathbf{Q}$ is derived in discrete form from the discretisation of (2.75), with the variables arranged on the grid as shown in Fig. 5.12, then the various terms in $\mathbf{Q}$ are naturally calculated at different points, and $\mathbf{Q}$ cannot be inverted. In [Mawson (1996)], an iterative method was therefore

used where the kth iterate $h^{(k)}$ to $h^{t+\delta t}$ is defined by solving

$$(h^{(k)} - h^*) - \nabla \cdot h^* \mathbf{Q}_1^{-1} g \nabla (h^{(k)} - h^*) = \nabla \cdot h^* (\mathbf{Q}^{-1} - \mathbf{Q}_1^{-1}) g \nabla (h^{(k-1)} - h^*). \tag{5.50}$$

The matrix $\mathbf{Q}_1$ is the diagonal part of $\mathbf{Q}$, so that the positive definiteness of $\mathbf{Q}$ implies the positive definiteness of $\mathbf{Q}_1$. The term $f^2 + f\frac{\partial v_g}{\partial x}$ is computed at v_g points and the term $f^2 - f\frac{\partial u_g}{\partial y}$ is computed at u_g points. The corresponding entries in the inverse matrix $\mathbf{Q}_1^{-1}$ are therefore also held at v_g and u_g points respectively. The use of an iterative method allows the flux-limiting required in the outcropping problem of [Cloke and Cullen (1994)] to be incorporated, ensuring that h cannot become negative.

Though the analysis of section 4.3.1 shows that the positive definiteness of $\mathbf{Q}$ is maintained in the analytic solution, it may not be maintained by the discrete solution because of numerical errors, particularly close to the equator. This was resolved in [Mawson (1996)] by adding a selective smoothing terms to the right hand side of (2.75), chosen to be large wherever $\det\mathbf{Q}$ is small.

The discretisation as given will not work at the equator where $f = 0$ and $\mathbf{Q}$ cannot be inverted. We require h to be a constant h_e along the equator. We therefore first calculate the zonal mean solution $\overline{h}^{t+\delta t}$ from the integral of (5.49) round lines of latitude. In particular, this gives $h_e = h^{t+\delta t}$ at the equator. We then solve (5.49) for $h^{t+\delta t}$ separately in each hemisphere, with the boundary condition $h^{t+\delta t} = h_e$ at the equator. The first equation of (5.48) is then solved for δu and δv.

Now consider a discrete solution of the semi-geostrophic equations in a vertical slice. In [Cullen (1989b)], solutions were obtained to the frontogenesis problem described in section 3.4.2 and the flow over a mountain ridge described in section 6.5. In both cases, the solution contains discontinuities, and it is not clear whether an Eulerian finite difference method should be

able to find the correct solution. The equations derived from 2.124) are

$$\begin{aligned} -fv_g + \frac{\partial \varphi}{\partial x} &= 0, \\ \frac{\mathrm{D}v_g}{\mathrm{D}t} + fu + \frac{\partial \varphi_0}{\partial y} &= 0, \\ \frac{\mathrm{D}\theta'}{\mathrm{D}t} + v_g \frac{\partial \vartheta}{\partial y} &= 0, \\ \frac{\partial \varphi}{\partial z} - g\frac{\theta'}{\theta_0} &= 0, \\ \frac{\partial \varphi_0}{\partial z} - g\frac{\vartheta}{\theta_0} &= 0, \\ \nabla \cdot \mathbf{u} &= 0. \end{aligned} \tag{5.51}$$

Here $\varphi_0(y,z)$ and $\vartheta(y,z)$ are given functions satisfying the fifth equation of (5.51). $\mathbf{u} = (u,w)$ and $\mathbf{u}, v_g, \theta'$ and φ are functions of (x,z) only. (5.51) is to be solved in a closed region Γ with $\mathbf{u}\cdot\mathbf{n} = 0$ on the boundary.

Equations (5.51) can be discretised using the arrangement of variables on the grid shown in Fig. 5.13. As in the shallow water case, given u, w, v_g, θ' and φ at time t, we can make explicit estimates v_g^* and θ^* of the values $v_g^{t+\delta t}$ and $\theta^{t+\delta t}$ using standard methods. These values will not satisfy the geostrophic and hydrostatic relations. We calculate $\delta u, \delta w$ to enforce these relations by solving

$$f\frac{\partial}{\partial z}(\mathbf{u}\cdot\nabla v_g + fu) - \frac{g}{\theta_0}\frac{\partial}{\partial x}(\mathbf{u}\cdot\nabla\theta') = f\frac{\partial v_g^*}{\partial z} - \frac{g}{\theta_0}\frac{\partial \theta^*}{\partial x}. \tag{5.52}$$

The left hand side of (5.52) can be written as $\mathbf{Q}\begin{pmatrix} u \\ w \end{pmatrix}$, where $\mathbf{Q}$ is the two-dimensional version of the matrix defined in (3.1). To solve (5.52), we impose the constraint $\frac{\partial \delta u}{\partial x} + \frac{\partial \delta w}{\delta z} = 0$ by setting $\delta u = -\frac{\partial \delta \psi}{\partial \delta z}, \delta w = \frac{\partial \delta \psi}{\partial \delta x}$. The boundary condition for (5.51) implies that $\delta\psi$ is constant on the boundary of Γ. Equation (5.52) then becomes a second order equation for $\delta\psi$, which is elliptic if $\mathbf{Q}$ is positive definite and can be solved.

In [Cullen (1989b)] this procedure was found satisfactory for continuous solutions, but when discontinuities occurred, the positive definiteness of $\mathbf{Q}$ was violated in the discrete solution. The remedy was to solve (5.52) iteratively be a similar method to (5.50), only retaining the diagonal terms of $\mathbf{Q}$ on the left hand side. A small amount of smoothing had to be added to the right hand side of (5.52) to control numerical errors, as in the shallow water case. indexartificial viscosity

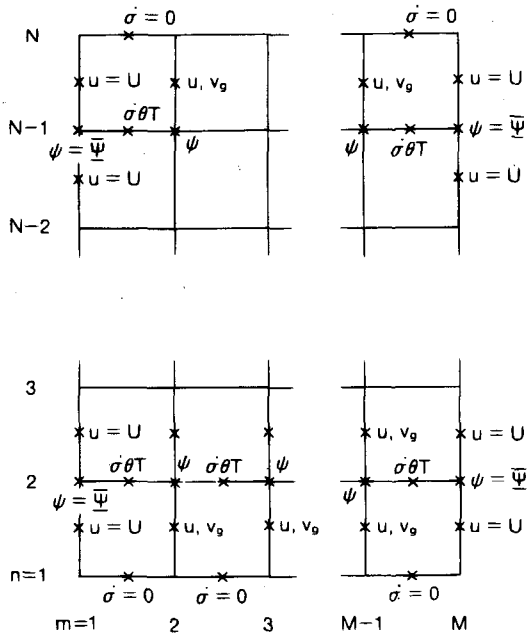

Fig. 5.13 Arrangement of variables on grid in (x, z) plane for the solution of (4.49). Reprinted from [Cullen (1989b)] with permission from Elsevier.

When the method is used to solve flow over a ridge, terrain-following coordinates are used as shown in Fig. 5.14. Such coordinates are standard in weather forecasting models. The procedure above is followed, with the refinement that the derivative $\partial\delta\psi/\partial x$, that appears when (5.52) is written as an equation for $\delta\psi$, is calculated at constant z, rather than on the sloping coordinate surfaces. The equation for $\delta\psi$ therefore involves 7 points, as shown in Fig. 5.14, rather than the 5 that would be required when the coordinate surfaces were orthogonal.

There have been relatively few three-dimensional solutions using finite difference techniques in physical coordinates. The solutions of [Cullen and Mawson (1992)] shown in section 6.6 were obtained by applying the procedure for the vertical slice in an alternating direction formulation, where the problem was successively solved in the (x, z) and (y, z) planes. An alternative is to solve (2.124) for $\varphi^{t+\delta t}$ directly using a formulation based on (3.1).

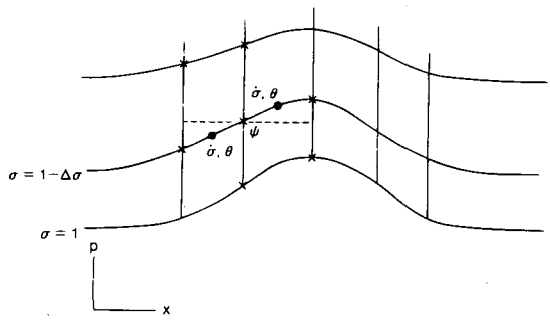

Fig. 5.14 Construction of approximation to (5.52) over variable terrain height. Reprinted from [Cullen (1989b)] with permission from Elsevier.

This was used by [Wakefield and Cullen (2005)]. The iterative strategy of inverting only the diagonal elements of $\mathbf{Q}$, and the addition of smoothing to the right hand side of the equation for $\varphi^{t+\delta t}$ to eliminate numerical errors, are required.

Chapter 6

Application of semi-geostrophic theory to the predictability of atmospheric flows

6.1 Application to shallow water flow on various scales

In section 2.4.4 we showed that the shallow water equations are well approximated by the equations for two-dimensional incompressible flow, (2.57), if the Froude number $U/\sqrt{gh_0}$ was small. It is well-known that these equations support a cascade of enstrophy, ζ^2, to small scales and an inverse cascade of energy to large scales, e.g. [Leith and Kraichnan (1972)]. We can see this mechanism by writing the equation for the evolution of the vorticity gradients:

$$\frac{\mathrm{D}}{\mathrm{D}t}\nabla\zeta + \begin{pmatrix} \frac{\partial u}{\partial x} & \frac{\partial v}{\partial x} \\ \frac{\partial u}{\partial y} & \frac{\partial v}{\partial y} \end{pmatrix} \nabla\zeta = 0. \tag{6.1}$$

This can be written in terms of the stream-function ψ as

$$\frac{\mathrm{D}}{\mathrm{D}t}\nabla\zeta + \begin{pmatrix} -\frac{\partial^2\psi}{\partial x\partial y} & \frac{\partial^2\psi}{\partial x^2} \\ -\frac{\partial^2\psi}{\partial y^2} & \frac{\partial^2\psi}{\partial y\partial x} \end{pmatrix} \nabla\zeta = 0. \tag{6.2}$$

These equations can be used to estimate the rate of increase of vorticity gradients, using a bound on the velocity gradients in terms of the vorticity and its gradients ([Gérard (1992)], p 424):

$$\| \nabla\mathbf{u}(t,\cdot) \| \leq C\log(2+ \| \nabla\zeta(t,\cdot) \|) \tag{6.3}$$

Exact definitions of the norms used are given by [Gérard (1992)]. However, they are essentially maximum norms. The bound is derived by solving the

Poisson equation (5.19) for ψ in terms of ζ and then calculating $\mathbf{u}$, giving

$$u(x,y) = \int_\Gamma \frac{(y-y', x'-x)}{|x-x'|^2} q\zeta(x',y')\mathrm{d}x'\mathrm{d}y'. \tag{6.4}$$

Because of the dependence of the bound in (6.3) on the vorticity gradients, the estimate of vorticity gradients obtained from (6.1) allows exponential growth in time. A discussed in section 2.4.2, this does not prevent regularity being proved for all time, but allows the accumulation of enstrophy at small scales. This can be expressed as a statement that

$$\| \nabla \mathbf{u}^2 \| \leq C \| \mathbf{u}^2 \| \tag{6.5}$$

where C grows exponentially in time. If the L^2 norm is used instead of the maximum norm, then an estimate of the form (6.5) holds with C independent of time, but dependent on the domain size. Thus the mean scale of the flow is bounded, but local regions where small scales are generated are permitted. This agrees with widespread computational experience. In particular, equation (6.4) shows that a line of large vorticity gradients will generate a line of large velocity gradients. Equation (6.2) can also be used to analyse the regions of the flow where rapid stretching occurs, e.g. [Ehlmaidi et al. (1993)].

As discussed in section 5.1.1, the semi-geostrophic approximation to (2.57) generates an equation of identical form to (6.2), with σ, Ψ, X, Y replacing ζ, ψ, x, y, for the rate of change of the gradient of potential density σ. The change will thus be governed by the eigenvalues of the matrix

$$\begin{pmatrix} -\frac{\partial^2 \Psi}{\partial X \partial Y} & \frac{\partial^2 \Psi}{\partial X^2} \\ -\frac{\partial^2 \Psi}{\partial Y^2} & \frac{\partial^2 \Psi}{\partial Y \partial X} \end{pmatrix}. \tag{6.6}$$

Using (3.50), this can be written as

$$\begin{pmatrix} -0 & f^2 \\ -f^2 & 0 \end{pmatrix} - f^2 \begin{pmatrix} -\frac{\partial^2 R}{\partial X \partial Y} & \frac{\partial^2 R}{\partial X^2} \\ -\frac{\partial^2 R}{\partial Y^2} & \frac{\partial^2 R}{\partial Y \partial X} \end{pmatrix}. \tag{6.7}$$

This is a combination of a matrix representing a solid body rotation, which cannot change the potential density gradients, and a matrix with eigenvalues

$$\pm \sqrt{\left(\frac{\partial^2 R}{\partial X \partial Y}\right)^2 \frac{\partial^2 R}{\partial X^2} \frac{\partial^2 R}{\partial Y^2}}, \tag{6.8}$$

which have to be pure imaginary and equal to $\pm i\sqrt{\sigma}$ according to the admissibility condition, Definition 3.4, which requires R to be convex. If the matrix (6.6) were constant following fluid particles, this would prevent any growth in the potential density gradients. Since, in general, the matrix is time-dependent, growth will be possible but restricted, see [Cullen (2002)].

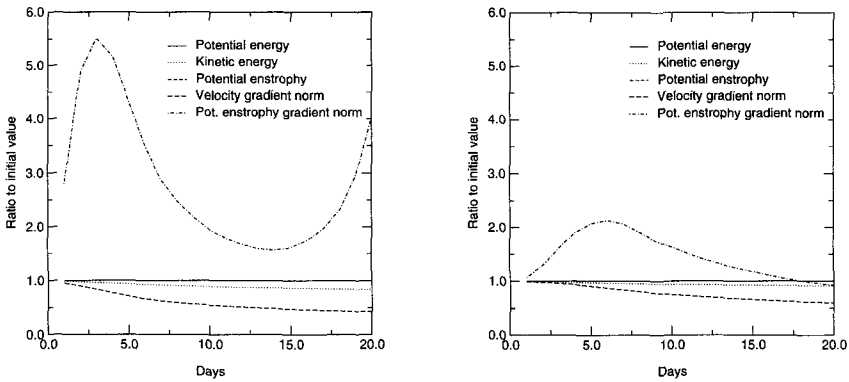

Fig. 6.1 Graphs of diagnostics from integration of (left) shallow water model and (right) semi-geostrophic model against time. $gh_0 = 10^5$. From [Cullen (2002)]. ©Royal Meteorological Society, Reading, U.K.

The effect is illustrated in Fig. 6.1, taken from [Cullen (2002)]. The data used are as shown in Fig. 2.2, so that the length scale of the depth field is less than the Rossby radius of deformation L_R and (2.57) is a good approximation to the shallow water equations. The equations were solved in spherical geometry to avoid boundary issues, but with a constant Coriolis parameter. Similar numerical methods were used to integrate the shallow water equations and their semi-geostrophic approximation (2.75). We plot the potential and kinetic energy , the potential enstrophy $\int_\Gamma h\zeta^2 \mathrm{d}x\mathrm{d}y$, the velocity gradient norm

$$\int_\Gamma \left\{ \left(\frac{\partial u}{\partial x}\right)^2 + \left(\frac{\partial u}{\partial y}\right)^2 + \left(\frac{\partial v}{\partial x}\right)^2 + \left(\frac{\partial v}{\partial y}\right)^2 \right\} \mathrm{d}x\mathrm{d}y, \tag{6.9}$$

and the potential enstrophy gradient norm

$$\int_\Gamma \left\{ \left(\frac{\partial \zeta}{\partial x} \right)^2 + \left(\frac{\partial \zeta}{\partial y} \right)^2 \right\} \mathrm{d}x\mathrm{d}y. \tag{6.10}$$

In the semi-geostrophic case, $\mathcal{Q}_{SG}$ as defined by (5.25) replaces ζ in (6.10).

The results show much more rapid growth in the vorticity gradients in the shallow water model than in the potential vorticity gradients in the semi-geostrophic model. After two days the growth saturates but, as discussed in [Cullen (2002)], this probably reflects the limited resolution of the calculations. The large difference is consistent with the analysis above, and demonstrates the unsuitability of the semi-geostrophic model for describing this regime.

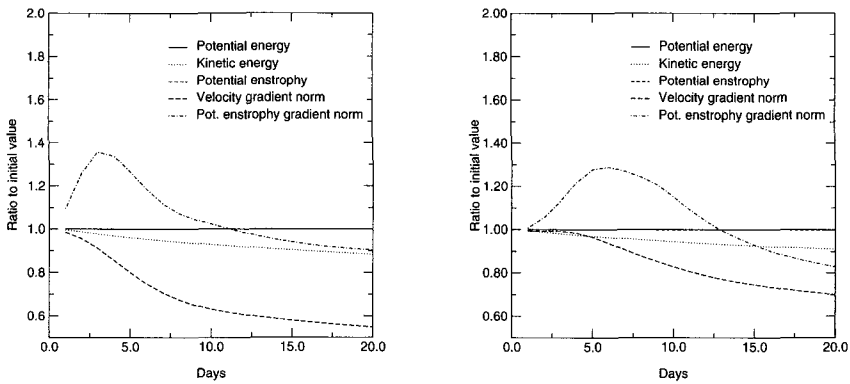

Fig. 6.2 Graphs of diagnostics from integration of (left) shallow water model and (right) semi-geostrophic model against time. $gh_0 = 5000$. From [Cullen (2002)]. ©Royal Meteorological Society, Reading, U.K.

Now consider the large-scale case where $L > L_R$. As discussed in section 2.4.6, the potential vorticity is dominated by variations in the depth field. This means that if f is constant, and the flow geostrophic, the depth field will never change, since $\nabla \cdot (h\mathbf{u}) = 0$. Thus any state will be stable in practice, even though the stability analysis of section 5.2 suggests that only a few states can be stable. This is illustrated in Fig. 6.2. The data used for the integrations are as shown in Fig. 2.3, so that most of the variations in depth are on a scale larger than L_R. The growth rates are much lower

than those shown in Fig. 6.1, and the semi-geostrophic solution is much more accurate, as expected from the error estimate (5.18).

The important practical application of this case is where f is a function of position. In this case the divergence of the geostrophic wind will be non-zero and we will not have steady states. The results shown in Fig. 5.5 illustrate that the amplitude of perturbations to the zonal flow is larger in the semi-geostrophic integration, which is consistent with the suppression of the cascade of energy to large scales. Another distinction is illustrated by calculating the Rossby wave speed by linearising the quasi-geostrophic potential vorticity equation (2.68) about a state of rest. We make the beta plane approximation $f = f_0 + \beta y$. We use (2.69) and (2.63) to give v_g in terms of $\mathcal{Q}_g$. Assuming all variables are proportional to $\exp i\,(kx + ly - \omega t)$ as in section 2.4.2, we obtain

$$\omega = \frac{-\beta g H k}{(gH(k^2 + l^2) + f_0^2)}. \tag{6.11}$$

This is the dispersion relation for Rossby waves. It can be rewritten as

$$\frac{\omega}{\beta} = \frac{-L_R^2 k}{(L_R^2(k^2 + l^2) + 1)}. \tag{6.12}$$

The phase speed is westwards because of the negative sign. For scales larger than L_R the first term of the denominator is small compared with the second and the phase speed, $\omega/k \simeq -\beta L_R^2$. This is independent of wavelength, showing that the waves are non-dispersive and that structures of arbitrary shape can propagate without change of form. This is consistent with the existence of large-scale long-lived disturbances of the tropospheric circulation which are responsible for persistent spells of weather. For scales less than L_R, the phase speed is approximately $-\beta k/(k^2 + l^2)$. This does depend on wavelength, so small-scale Rossby waves are dispersive and thus less likely to persist.

This behaviour is consistent with results on the stability of Rossby-Haurwitz waves, e.g. [Thuburn and Li (2000)], which show that wavenumbers greater than three are unstable if H is chosen to be 8km, giving a Rossby radius of deformation of one-half the distance round the Earth at 45°N. Though the analysis of section 5.2 has not yet been extended to the spherical case, the symmetry of the problem makes it very unlikely that any states which vary with longitude will be extremisers of the energy. The non-turbulent behaviour of the large-scale flow discussed in Chapter 1 is more likely to reflect the natural barotropic dynamics on scales larger than

L_R. It suggests high predictability on the weekly time-scale, because the barotropic dynamics only evolves on this time-scale. It is not encouraging for seasonal predictability, because it suggests that there are no dynamically preferred solutions, and thus any state can occur. This is in agreement with experience.

6.2 The Eady wave

We now consider the Eady model, [Gill (1982)], p. 556. This describes baroclinic instability, which is responsible for the development of weather systems in the extra-tropics. It also includes frontogenesis, as described in section 3.4.2. The equations are solved on a domain $\Gamma : [-L, L] \times [0, H]$ in the (x, z) plane with periodic boundary conditions in x and rigid wall conditions $w = 0$ on $z = 0, H$. The semi-geostrophic equations are derived from (5.51) by choosing $\partial\theta/\partial y = -C$.

$$\begin{aligned} -fv_g + \frac{\partial\varphi}{\partial x} &= 0, \\ \frac{\mathrm{D}v_g}{\mathrm{D}t} + fu - \frac{Cg}{\theta_0}(z - H/2) &= 0, \\ \frac{\mathrm{D}\theta'}{\mathrm{D}t} - Cv_g &= 0, \\ \frac{\partial\varphi}{\partial z} - g\frac{\theta'}{\theta_0} &= 0, \\ \nabla \cdot \mathbf{u} &= 0. \end{aligned} \tag{6.13}$$

All variables are considered as functions of (x, z) only.

Energy conservation is deduced by defining the energy density $\tilde{E}$ as

$$\tilde{E} = \frac{1}{2}(v_g)^2 - g\theta'(z - H/2)/\theta_0 \tag{6.14}$$

and calculating from (6.13)

$$\begin{aligned} \frac{\mathrm{D}\tilde{E}}{\mathrm{D}t} &= \frac{Cg}{\theta_0}(z - H/2)v_g - fuv_g - \frac{g}{\theta_0}(Cv_g(z - H/2) + \theta' w), \\ &= -u\frac{\partial\varphi}{\partial x} - w\frac{\partial\varphi}{\partial z}. \end{aligned} \tag{6.15}$$

The last expression integrates to zero because of the condition $\nabla \cdot \mathbf{u} = 0$ and the boundary conditions.

Equations (6.13) can be rewritten using (3.24) as

$$\begin{aligned} \frac{\mathrm{D}X}{\mathrm{D}t} - \frac{Cg}{f\theta_0}(z - H/2) &= 0, \\ \frac{\mathrm{D}Z}{\mathrm{D}t} - \frac{Cg}{f\theta_0}(X - x) &= 0, \\ P = \frac{1}{2}x^2 + f^{-2}\varphi, & \\ \nabla P = (X, Z), & \\ \nabla \cdot \mathbf{u} = 0. & \end{aligned} \tag{6.16}$$

We can then set $\mathbf{U} \equiv (U, W) = \frac{Cg}{f\theta_0}(z - H/2, X - x)$. Using (3.37) we find that $\nabla \cdot \mathbf{U} = 0$, so (3.40) shows that the potential density $\sigma = \partial(x, z)/\partial(X, Z)$ is conserved in a Lagrangian sense, and then (3.57) shows that the potential vorticity is also conserved in a Lagrangian sense.

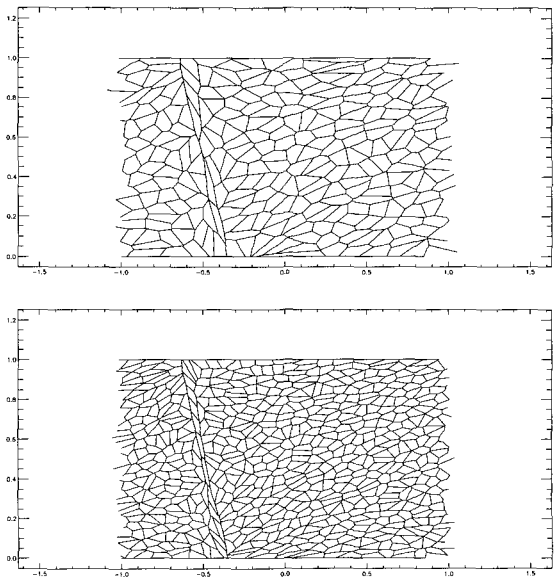

Fig. 6.3 Distribution of elements after 8 days integration of (6.13). Top: 21×13 elements, Bottom: 40×16 elements.

Solutions of (6.13) for initial data of the form

$$\theta' = N_0^2 \theta_0 z/g + B \sin\left(\pi(x/L + z/H)\right), \tag{6.17}$$

where N_0^2 and B are positive constants, are illustrated. The data used are taken from [Nakamura (1994)], so that $L = 1000\text{km}$, $H = 10\text{km}$, $N_0^2 = 2.5 \times 10^{-5}\text{s}^{-2}$, $f = 10^{-4}\text{s}^{-1}$, $g = 10\text{ms}^{-1}$, $\theta_0 = 300\text{K}$, $C = 3 \times 10^{-6}\text{m}^{-1}\text{K}$. This data corresponds to an unstable mode of the linearised equations (6.13). As discussed in [Gill (1982)], p. 556, if the isentropes have negative slope $\mathrm{d}x/\mathrm{d}z$, then v_g will increase with z, and the evolution equation for θ' will increase the vertical gradient of θ, giving a positive feedback. It represents conversion of potential energy from the infinite reservoir implied by the imposed basic state $\partial\theta/\partial y$ into kinetic energy.

The integrations are done using the efficient geometric algorithm described in section 5.3.2, modified to work with periodic boundary conditions. These update the original solution given in [Cullen and Roulstone (1993)], which used the version of the geometric algorithm developed by [Chynoweth (1987)]. The initial data are chosen as piecewise constant in X and Z. Two resolutions are used, as illustrated in Fig. 6.3 after 8 days integration.

At this point there is strong frontogenesis, as illustrated by the potential temperature plot in Fig. 6.4.

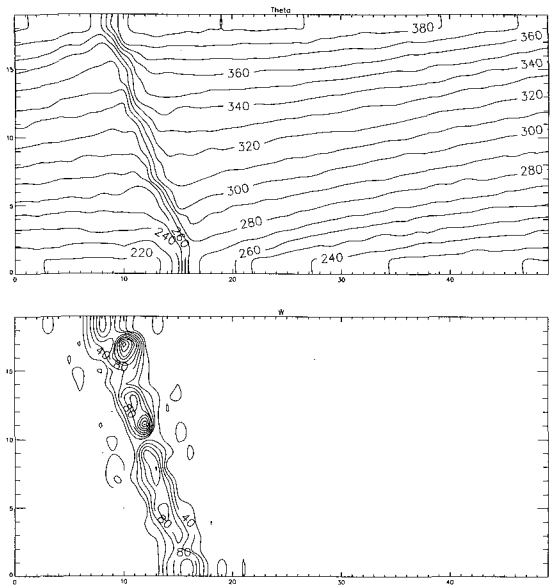

Fig. 6.4 Plots of potential temperature (degrees K, contour interval 10K), and potential vorticity scaled by N_0^2 (contour interval 20), in the region Γ after 8 days.

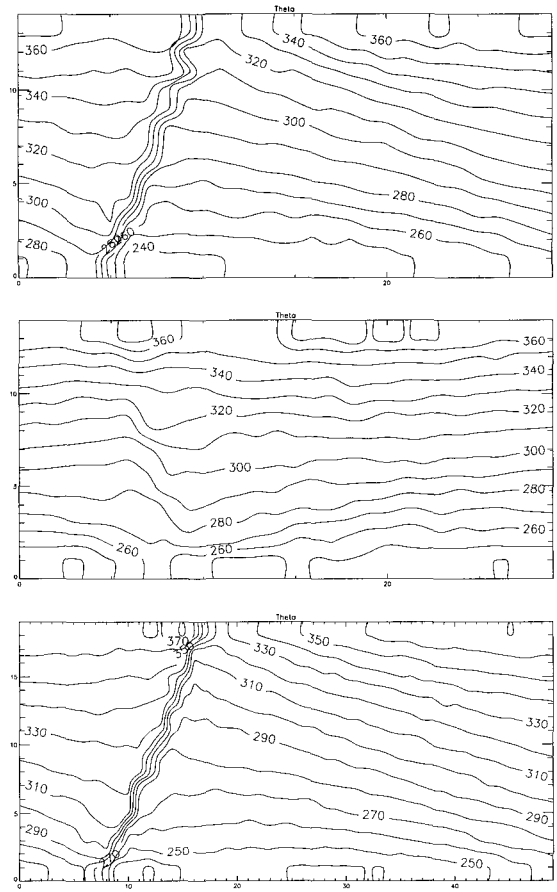

Fig. 6.5 Graphs of potential temperature after 10, 15 and 19 days.

The potential vorticity $\mathcal{Q}_{SG}$, as defined in (5.25), is initially equal to the uniform value N_0^2. At the front it becomes very large. As discussed in section 3.2.3 and 3.4.2, there is actually a Dirac mass in the potential vorticity, which is represented as large values by the plotting software. The irregularities are due to the use of piecewise constant data and thus the irregularity of the boundaries between elements. The small negative values are artefacts of the plotting. The formation of the fronts at the upper and lower boundaries destroys the normal mode property of the initial data, and the vertical shear in the basic state reverses the slope of the isentropes

by day 10, as shown in Fig. 6.5. The front is then destroyed. By day 15, it is very weak, but starting to build up again as can be seen by the negative slope of the isentropes. By day 19 it has again saturated, the tilt has been reversed, and the front weakens again.

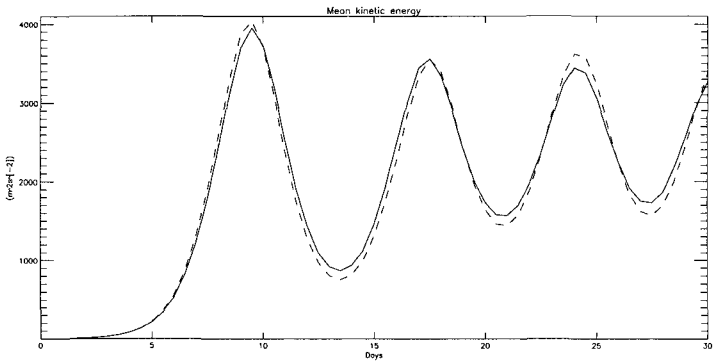

Fig. 6.6 Graph of domain averaged kinetic energy m^2s^{-2} against time for the solution of (6.13) by the geometric method. Solid line: 40×16 elements, dashed line: 21×13 elements.

A graph of the kinetic energy against time is shown in Fig. 6.6. This shows that after 8 days the maximum kinetic energy is reached. It then illustrates the next cycle, as shown in Fig. 6.5. The periodic oscillations continue to day 30. The graphs for the two resolutions are almost identical, showing that the solution is highly predictable, despite the formation of fronts. The system (6.13) has a natural period equal to $2Lf\theta_0/(CgH)$, the length of time between when features at the upper and lower boundaries come back into phase under the action of the basic state wind. With the data chosen, the difference in the basic state wind between the boundaries is $10ms^{-1}$ for the data chosen, giving a period of about 2.3 days, much shorter than the period observed. This reflects the fact that the vertical shear is impeded during the growth phase. It also shows that the prediction of the same period by two different discretisations is a non-trivial achievement.

Some of the results obtained by [Nakamura (1994)] for the same data are shown in Fig. 6.7. In the integration shown, horizontal diffusion was used to prevent the formation of discontinuities. The method used was a finite difference discretisation of the equation for potential vorticity in physical space, not the method described in section 5.3.3. The results show the

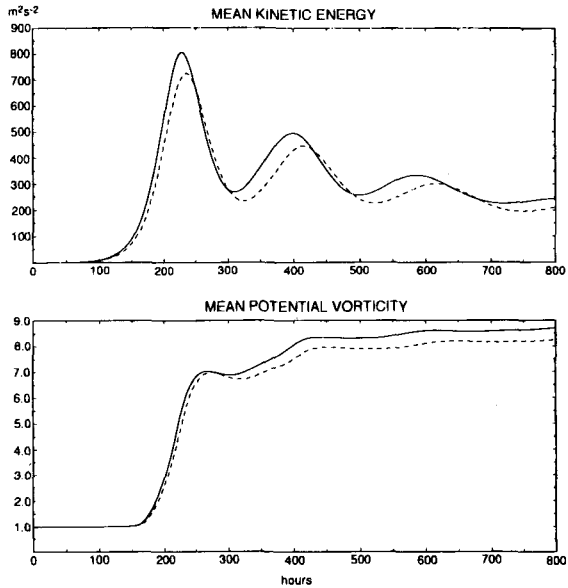

Fig. 6.7 Evolution of domain-averaged kinetic energy (top) and potential vorticity (bottom) for solutions with horizontal diffusion. Solid curves: solutions of (6.13) with diffusion. Dashed curves: solutions of (2.83) with diffusion. From [Nakamura (1994)].

same periodicity as Fig. 6.6, but there is strong damping. The peak value of the kinetic energy is one quarter of that shown in Fig. 6.6. The second maximum is predicted, but the third is very weak. Comparison with a solution of a two-dimensional version of (2.83) shows quite close agreement. The large potential vorticity source shown in Fig. 6.4 is evident in Fig. 6.7. However, there is an important difference. In the finite difference model, once the potential vorticity has been generated, by the horizontal diffusion, it remains in the solution. In the geometric model, it disappears again as the front weakens, and then returns on the next cycle. It is never actually part of the flow, which, as noted after equation (6.16), maintains conservation of potential vorticity in a Lagrangian sense throughout. Thus the Eulerian solution illustrated in Fig. 6.7 and the Lagrangian solution illustrated in Fig. 6.6 are fundamentally different. This is consistent with the doubts over the existence of Eulerian solutions discussed in section 3.5.3. It is not known whether finite difference solutions using the methods of section 5.3.3, which do not use potential vorticity as a variable, would be able to

remove the potential vorticity when the fronts weaken.

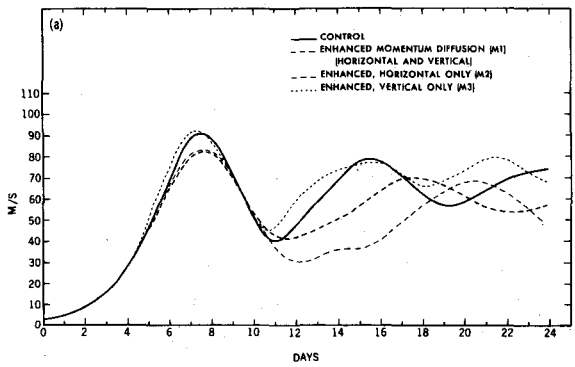

Fig. 6.8 Evolution of maximum value of v_g ms^{-1} from solutions of two-dimensional version of (2.83) with different combinations of horizontal and vertical momentum diffusion. Solid curve: control. Dashed curve: both the horizontal and vertical diffusion four times the control value. Thin dashed curve: only the horizontal diffusion is four times greater. Dotted curve: only the vertical diffusion is increased. From [Nakamura and Held (1989)].

In an earlier study, [Nakamura and Held (1989)] investigated the effect of different choices of diffusion on solutions of the problem with (2.83). Some of the results are shown in Fig. 6.8. The control integration includes both horizontal and vertical diffusion of momentum, so differs from the experiment shown in Fig. 6.7. The other integrations have increased values of one or both coefficients. After the first maximum value is attained, the second cycle is strongly affected and the period changed when the horizontal diffusion is increased. Overall, the experiment suggests that integrations of (2.83) do not maintain the predictability demonstrated for Lagrangian semi-geostrophic solutions in Fig. 6.6. It is not known whether Eulerian semi-geostrophic solutions can be computed which do maintain the predictability.

6.3 Simulations of baroclinic waves

We first illustrate the extra accuracy given by semi-geostrophic theory over quasi-geostrophic theory by summarising the results of [Thorpe and Pedder (1999)]. They integrated (2.83) with (2.113) to provide a simulation of a growing baroclinic wave. They then diagnosed the vertical motion using the quasi-geostrophic omega equation (5.43) and compared the result with the vertical motion predicted directly from (2.83) and (2.113) . The procedure was then repeated using the semi-geostrophic omega equation (5.44), which they solved using the methods outlined in section 5.3.1. The data used for the comparisons shown here is shown in Fig. 6.9. It is an idealised baroclinic wave at the stage of maximum development. There has been marked frontogenesis at the surface.

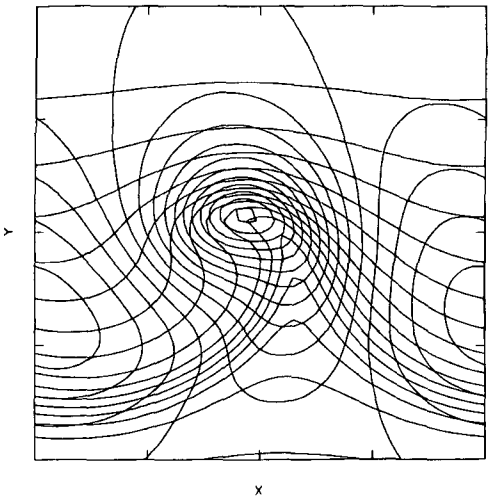

Fig. 6.9 Horizontal section at the surface showing contours of pressure (full lines; contour interval 3hpa) and temperature (dashed lines; contour interval 3K) at day 7. From [Thorpe and Pedder (1999)]. ©Royal Meteorological Society, Reading, U.K.

The comparison between the estimates of vertical motion made by the omega equation is shown in Fig. 6.10. The agreement between the semi-geostrophic omega equation estimate of vertical motion and the direct model prediction is closer than the agreement between the quasi-geostrophic version and the direct prediction. The difference is most marked at upper

levels. The detailed examination of the results in [Thorpe and Pedder (1999)] shows that the horizontal variations of potential vorticity and the variations in static stability included in the left hand side of (5.44) are important. There are also important effects from the calculation of the forcing on the right hand side, because the geostrophic coordinate transformation has a significant effect. The main disagreements between the semi-geostrophic diagnosis and the model prediction are in regions of ascent. Further examination in [Thorpe and Pedder (1999)] shows that these are mostly at low levels, and the semi-geostrophic potential vorticity calculated from the model data is negative in this region. The discussion following equation (5.12) shows that the displacement required to maintain geostrophic balance becomes large if the potential vorticity matrix $\mathbf{Q}$ has a small eigenvalue, implying large ageostrophic velocities. The overestimate by the semi-geostrophic diagnosis is thus not surprising. The model predictions in this region are strongly influenced by the artificial viscosity needed to maintain stability. The effect of artificial viscosity on frontogenesis was illustrated in section 6.2, and the model predictions may not be reliable here.

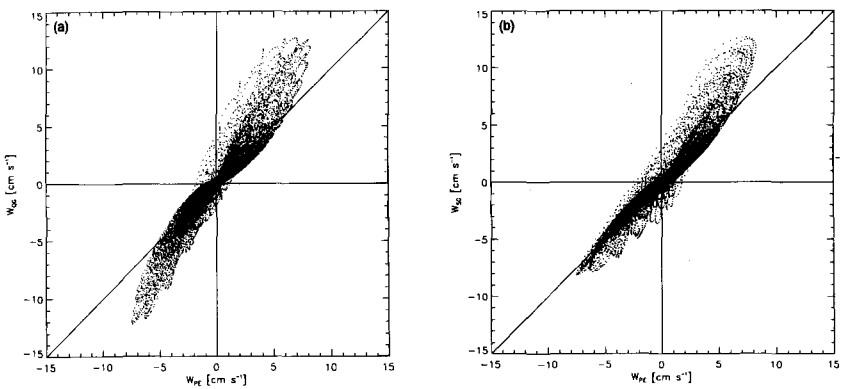

Fig. 6.10 (a) Scatter plot of the quasi-geostrophic vertical motion against the model vertical motion for day 7 ; (b) as (a) but for semi-geostrophic vertical motion versus the model. From [Thorpe and Pedder (1999)]. ©Royal Meteorological Society, Reading, U.K.

We next show results from [Malardel et al. (1997)] on the stability of frontal zones in geostrophic balance. The fronts are characterised by a potential vorticity anomaly as shown in Figure 6.4. Two cases are studied.

Front 1 has a width of 330km. The aspect ratio of the anomaly is less than f/N, so that the effect of the anomaly is therefore mainly seen in the potential temperature. Front 2 has a narrower anomaly, about 150km, with the same vertical extent. The aspect ratio is now greater than f/N and so the effect of the anomaly is mainly seen in the vorticity field.

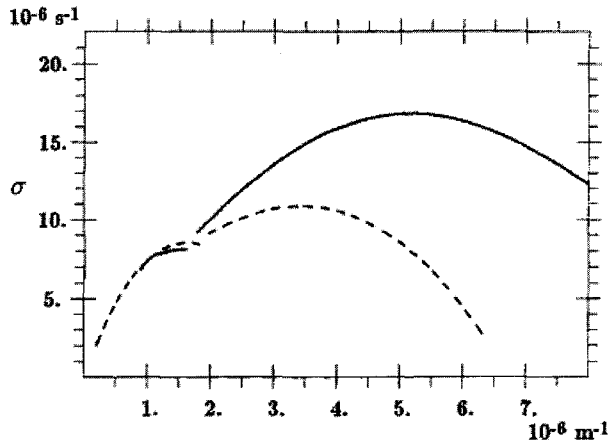

Fig. 6.11 Growth rates ($10^{-6}s^{-1}$) as a function of the along-front wave-number ($10^{-6}m^{-1}$) for Front 1. Dashed curve, semi-geostrophic results; solid curve-results for exact equations. From [Malardel et al. (1997)].

In the Eady model considered in section 6.2, the initial potential vorticity is independent of x, so the only instability is baroclinic. However, Theorem 5.7 shows that a state with the potential vorticity depending on x, which arises in the Eady model after a discontinuity has formed, is unstable to horizontal perturbations according to semi-geostrophic theory. It is also unstable according to the Charney-Stern theorem for two-dimensional incompressible flow. The detailed analysis in [Malardel et al. (1997)] shows that both types of instability occur, but in different ranges of horizontal wavelength. Baroclinic instability requires a wavelength greater than about 2000km. Barotropic instability predominates on smaller scales. Observations of instabilities on fronts, such as the weather systems illustrated in Fig. 1.2, suggest that instabilities which grow to a significant amplitude are baroclinic. Barotropic instability is likely to be important in the stratification dominated regime discussed in section 2.5.4. As noted there, this regime is not often robust, and so barotropic instability is less significant

in practice.

In applying the error estimate (5.18) for semi-geostrophic solutions, we assume the Lagrangian Rossby number depends on the horizontal wavelength of the instability. The additional accuracy obtained if $Ro < Fr$ will apply if the cross-frontal structure has an aspect ratio smaller than f/N, so we expect the errors for Front 1 to be up to 5 times smaller than for Front 2.

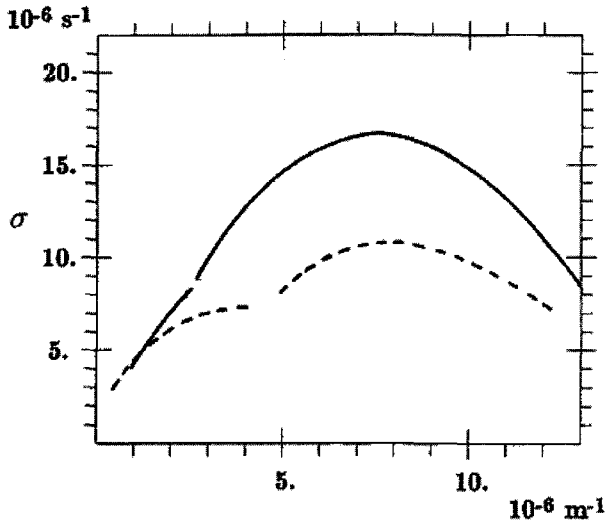

Fig. 6.12 As Fig. 6.11 for Front 2. From [Malardel et al. (1997)].

The results show the growth rates computed from an 'exact' model similar to (2.83) and a semi-geostrophic model similar to (2.124). In Fig. 6.11 we show the results for Front 1. There is fairly good agreement for wavelengths greater than 3000km, but a large under-estimation of the growth of smaller-scale perturbations. It is shown in [Malardel et al. (1997)] that this mainly reflects an inaccurate treatment of the barotropic instability which is governed by vortex dynamics. The result is thus consistent with the behaviour shown in section 6.1 and with the error estimate (5.18). Though such a flow is unstable according to semi-geostrophic theory, the restrictions on the growth rates of vorticity gradients demonstrated in section 6.1 lead to a severe underestimate of the growth rate. However, baroclinic instability is more accurately represented because the Lagrangian Rossby

number Ro_L computed from the wave-number of the disturbance is smaller. In Fig. 6.12 we show the result for Front 2. The difference in the solutions is now large for wavelengths less than 2000km, and increases more rapidly as a function of wave-number. This is consistent with (5.18). As discussed above, significant instabilities on fronts are usually baroclinic, so the poor treatment of barotropic instability by semi-geostrophic theory may not be so significant.

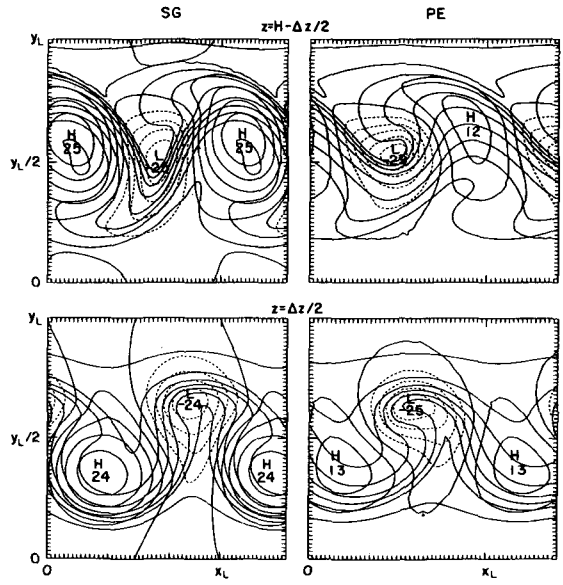

Fig. 6.13 Semi-geostrophic solutions (left) and solutions of (2.83) with (2.113) (right) at day 6.3. Solid lines, potential temperature θ', contour interval 5K. Dashed lines, geopotential φ, contour interval $500\text{m}^2\text{s}^2$. Solutions are shown as a function of (x, y) for $z = 0.225$ km (bottom) and 8.775 km (top). From [Snyder, Skamarock and Rotunno (1991)].

We next illustrate the difference between semi-geostrophic simulations of a baroclinic wave and those made by (2.83) with (2.113). A comparison by [Snyder, Skamarock and Rotunno (1991)], after 6 days of integration from initial data similar to that used by [Thorpe and Pedder (1999)], is shown in Fig. 6.13. The integrations were carried out in a domain Γ : $(0, x_L) \times (0, y_L) \times (0, H)$ with periodic boundary conditions in (x, y), and rigid boundaries at $z = 0, H$. The numerical method used is described in

section 5.3.1. The results shown had $x_L = 4090$km, $y_L = 5623$km and $H = 9$km.

As discussed by [Gill (1982)], p. 556, baroclinic instability has to occur with aspect ratio comparable to f/N, so the accuracy of semi-geostrophic theory as given by (5.18) will be $O(Ro_L)$. There are significant differences in the structure of the wave by 6.3 days, the time illustrated. There is more distortion of the potential temperature contours in the 'exact' solution. This difference is consistent with the reduced growth of vorticity gradients illustrated in section 6.1. As discussed in section 5.3.1, the results shown neglected the nonlinear term in the geostrophic coordinate transformation. They also ignore the effect of frontogenesis in computing the transformation. Both were estimated as being smaller than the differences shown in Fig. 6.13.

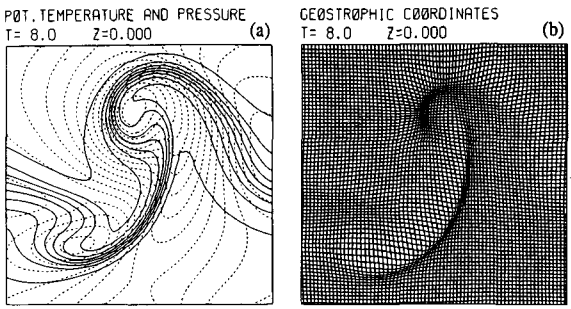

Fig. 6.14 Left: surface potential temperature (solid lines) contour interval 2.1K, and surface pressure (dashed lines), contour interval 3.2hpa, after 4 days. The domain size is 14640×7000 km. Right: Geostrophic space as viewed from physical space. From [Schar and Wernli (1993)]. ©Royal Meteorological Society, Reading, U.K.

Another study, by [Schar and Wernli (1993)], showed that the structure of semi-geostrophic baroclinic waves was strongly influenced by the initial data. Their study showed that all the main features of observed waves could be reproduced qualitatively, including simultaneous warm and cold fronts, well marked cold and warm 'conveyor belts' associated with the fronts, and concentrated ascent within the warm front. In Fig. 6.14 we show results after 4 days for one of their experiments. The potential temperature is now highly distorted, as in the 'exact' solution of [Snyder, Skamarock and Rotunno (1991)].

These results suggest that semi-geostrophic theory is sufficiently accu-

rate to describe the qualitative features of observed extra-tropical weather systems. It is not clear how significant the quantitative errors are in relation to other effects not included in these studies, particularly latent heat release and frictional drag.

6.4 Semi-geostrophic flows on the sphere

In this section we consider the behaviour of weather systems in the tropics, as described by semi-geostrophic theory. Obviously, any theory based on geostrophic balance will be very restrictive near the equator, as the vertical component of the rotation vector tends to zero.

In section 4.3.1 we derived the condition (4.129) that h has to satisfy to be an admissible solution of the semi-geostrophic shallow water equations on the sphere. Since the north-south component v_g of the geostrophic wind is given by $v_g = \frac{g}{2\Omega a \sin\phi\cos\phi}\frac{\partial h}{\partial\lambda}$, we have

$$\begin{aligned} \frac{gh}{a} &\simeq 2\Omega U_0\phi^2 + 2\Omega U_1(\lambda)\phi^4 + \mathrm{O}(\phi^5), \\ u_g &\simeq 2U_0 + 4U_1(\lambda)\phi^2 + \mathrm{O}(\phi^3), \\ v_g &\simeq \frac{1}{\cos\phi}\frac{\mathrm{d}U_1}{\mathrm{d}\lambda}\phi^3 + \mathrm{O}(\phi^4). \end{aligned} \tag{6.18}$$

Consider the condition for inertial stability stated before (4.129). This requires

$$2\Omega\sin\phi > \frac{1}{a}\frac{\partial u_g}{\partial\phi}, \tag{6.19}$$

which gives $4U_1 < \Omega a$, and the amplitude of the $\mathrm{O}(\phi^4)$ term in h as less than $\frac{1}{2g}\Omega^2 a^2$. At latitude 6°, this means the variation in h is restricted to about 1m. A verification of (6.19) against observations was carried out by [Veitch and Mawson (1993)]. Aircraft data was used from flights in the region 30°N to 30°S. In cases of parallel flow, where (6.19) can be tested by direct calculation from the data, only 5 cases out of 121 showed any violations of (6.19) using wind data 80km apart. Thus the semi-geostrophic model is likely to be useful at least down to this scale most of the time. It is probable that the condition would be less relevant for more closely-spaced data.

In section 4.2 we showed that the non-divergent semi-geostrophic equations on the sphere had the same Rossby wave speeds as the equations for

two-dimensional incompressible flow. However, [Mawson (1996)] shows that Rossby normal modes in spherical geometry can have pressure gradients along the equator, which are inadmissible in semi-geostrophic solutions. It is possible to modify (4.94) to allow analysis of the consequences. Recalling that, in (4.94), $\varsigma = \sin\phi$, set

$$gh' = \varsigma^4 \mathrm{Re}[G_m(\varsigma) \exp i(m\lambda - \omega t)], \tag{6.20}$$

where the factor ς^4 has been inserted to satisfy (6.18). It is now possible to analyse the eigenvalue problem. The modified normal mode with wave-number 4 has a phase speed reduced to two-thirds of the equivalent normal mode for two-dimensional incompressible flow.

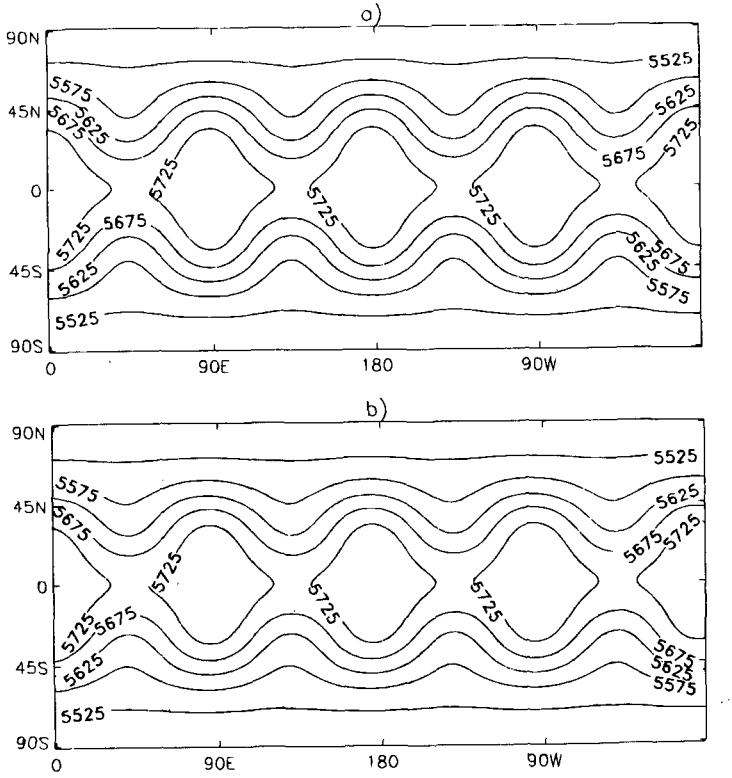

Fig. 6.15 Rossby-Haurwitz wave test case: (a) shallow water model initialised depth field, (b) shallow water model depth field after five days. Contour interval 50m. From [Mawson (1996)]. ©Royal Meteorological Society, Reading, U.K.

These normal modes were used to define initial data for the shallow water model with a mean depth of 5.5km, giving a Rossby radius of deformation equivalent to wave-number 3. Thus wave-number 4 corresponds to $L < L_R$ and the non-divergent approximation is reasonable. Fig. 6.15 shows the structure of the normal mode which is used to initialise the shallow water model. After five days the wave has propagated westwards by almost exactly the 93° predicted by the linear analysis.

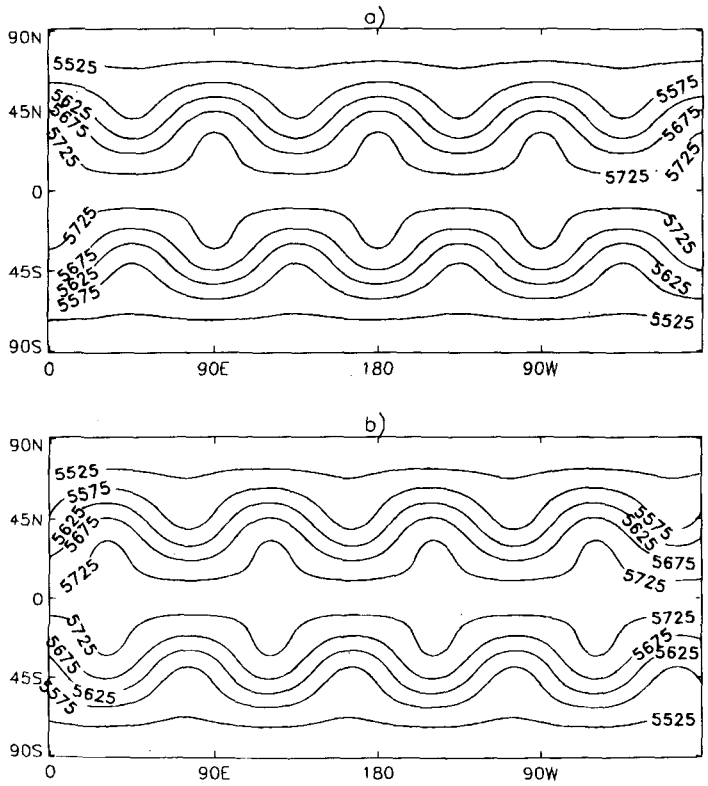

Fig. 6.16 Rossby-Haurwitz wave test case: (a) semi-geostrophic model initialised depth field, (b) semi-geostrophic model depth field after five days. Contour interval 50m. From [Mawson (1996)]. ©Royal Meteorological Society, Reading, U.K.

The same data was inserted into the semi-geostrophic model, and initialised using the procedure set out after (4.122). The result is shown in Fig. 6.16. The depth gradients at the equator have been eliminated, and reduced in the tropics generally to conform with (6.18). The wave propagates

about 60° in five days without change of form. This agrees with solutions of the eigenvalue problem derived from (6.20) by [Mawson (1996)].

An important consequence of (6.18) is the inability to generate tropical cyclones close to the equator. Once formed, these systems are governed by the axisymmetric theories discussed in section 4.4. However, they need a significant rotating disturbance to initiate them. If no horizontal pressure gradients can be supported, as illustrated in Fig. 6.16, then no such disturbance can exist. Fig. 6.17, from [Gordon et al. (1998)], shows that there are very few cases of cyclone formation within 5 degrees of the equator. The occasional exception occurs where rotation can be created by other means.

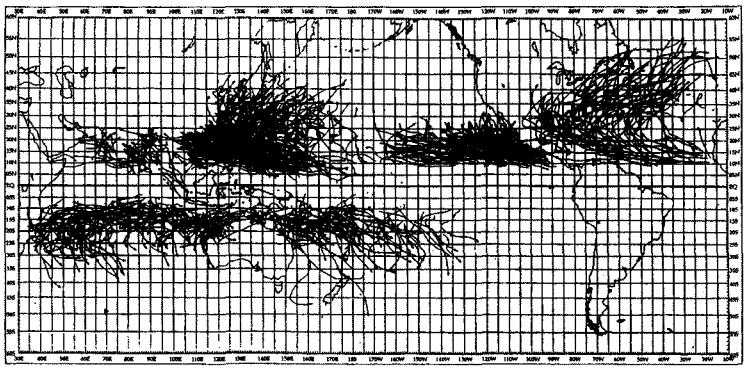

Fig. 6.17 Tracks of tropical cyclones (maximum winds > 17 ms^{-1}) for the period 1979-88 (from [Neumann (1993)], [Gordon et al. (1998)]).

Since semi-geostrophic theory can only describe flows where the pressure and potential temperature have little horizontal variation in the tropics, the only forecasting that can be carried out is the computation of the response of the circulation to heat sources. Such a study is described in section 6.7. This sort of response is important for seasonal forecasting, and can explain the success of seasonal prediction in the tropics based on predicting anomalies of ocean surface temperature. However, the important sub-seasonal variability requires tropical waves, [Gill (1982)] p.434, which are excluded by semi-geostrophic theory. So far, forecasts of this type of variability have been less successful.

6.5 Orographic flows

We first describe solutions of the semi-geostrophic equations in a vertical slice, as in the Eady model (6.13) of section 6.2. However, we assume the flow is driven by a pressure gradient in the y-direction which is independent of z. The equations are then

$$\begin{aligned} -fv_g + \frac{\partial \varphi}{\partial x} &= 0, \\ \frac{\mathrm{D}v_g}{\mathrm{D}t} + fu - fU &= 0, \\ \frac{\mathrm{D}\theta'}{\mathrm{D}t} &= 0, \\ \frac{\partial \varphi}{\partial z} - g\frac{\theta'}{\theta_0} &= 0, \\ \nabla \cdot \mathbf{u} &= 0. \end{aligned} \tag{6.21}$$

Once again, we assume all variables are functions of (x, z) only. In order to model the effect of flow over a mountain ridge, we solve on a region $\Gamma = [-L, L] \times [h(x), H]$ with periodic boundary conditions in x and $\mathbf{u} \cdot \mathbf{n} = 0$ on the upper and lower boundaries. The orography is defined by the function $z = h(x)$. This problem was first solved by [Cullen, Chynoweth and Purser (1987)], and then by [Shutts (1987a)] and [Shutts (1998)].

The main characteristics of the solution to the ridge problem are shown in the top part of Fig. 6.18 which shows the flow in an (x, z) cross-section. A particular feature is the blocking of cold air near the surface on the upstream side of the ridge and the associated barrier jet. This occurs because the admissibility for semi-geostrophic solutions, Definition 3.2, requires in this context that $\varphi + \frac{1}{2}f^2x^2$ is a convex function, so that

$$\left(f^2 + \frac{\partial^2 \varphi}{\partial x^2}\right)\frac{\partial^2 \varphi}{\partial z^2} \geq \left(\frac{\partial^2 \varphi}{\partial x \partial z}\right)^2. \tag{6.22}$$

For a state at rest, with Brunt-Väisälä frequency given by $\frac{g}{\theta_0}\frac{\partial \theta'}{\partial z} = N^2$, this means that

$$\left|\frac{\partial \theta'}{\partial x}\right| \leq \sqrt{(\theta_0/g)}fN. \tag{6.23}$$

Thus if the ridge $z = h(x)$ is an isentrope, we must have

$$\left|\frac{\mathrm{d}h}{\mathrm{d}x}\right| \leq f/N. \tag{6.24}$$

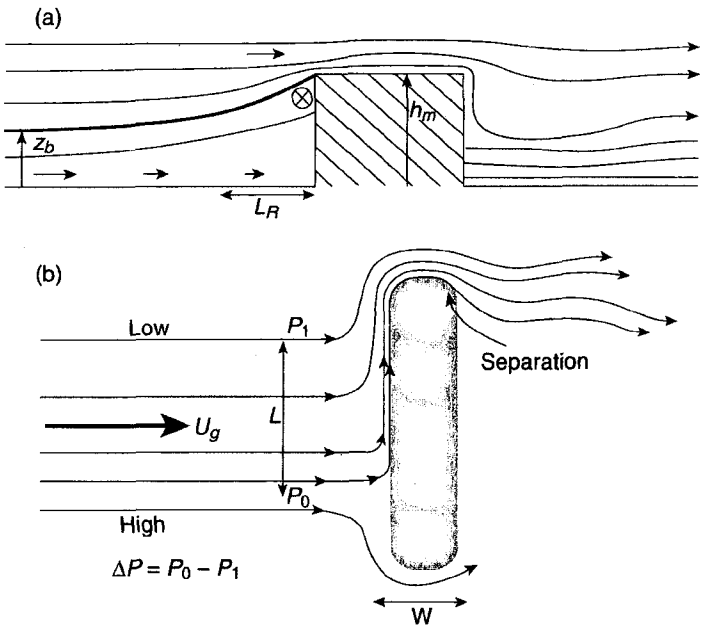

Fig. 6.18 Schematic view of the flow around a mesoscale mountain ridge. (a) Elevation view showing contours of potential temperature in relation to a rectangular block mountain. Arrows indicate the strength of the cross-mountain flow component, and the circle containing a cross marks the location of a barrier jet into the picture. (b) Plan view of the flow streamlines splitting around the mesoscale mountain ridge. The oncoming geostrophic flow is diverted to the left in the Northern hemisphere, forming a barrier jet. This mesoscale jet-stream eventually separates from the northern tip of the ridge. From [Shutts (1998)].

If the ridge is steeper than this, it cannot be an isentrope. However, isentropes can extend from the top of the ridge with slope f/N. We can consider this as defining a broader ridge, over which the flow is smooth, with blocking occurring within the region $x = x_0 \pm Nh(x_0)/f$, where x_0 is the position of the ridge top. This states that the influence of the ridge occurs for a horizontal distance equal to the Rossby radius of deformation based on the ridge height. Further discussion is given in [Purser and Cullen (1987)].

Consider the solution procedure as set out in section 3.1.2. This defines solutions as minimum energy states in the sense of Theorems 3.1 and 3.2. If we replace the rectangular block in Fig. 6.18 by a vertical barrier with

zero width, the solution does not need to change significantly from that shown in Fig. 6.18. However, it is clearly not a global energy minimiser, because if the barrier were removed, the solution would have a discontinuity in φ and would not be admissible in the sense of Definition 3.1. The solution with the barrier is admissible because φ does satisfy the conditions of Definition 3.1 within the domain which excludes the barrier. It is thus an energy minimiser in the sense of Theorem 3.2, but not a global energy minimiser in the sense of the theorems in section 3.5.1 which show that there is an (essentially) unique energy minimiser for this problem. It is therefore necessary to seek local rather than global energy minimisers. The results of section 3.5.2 do not address this issue, and it will be necessary to generalise the theory significantly.

We therefore describe the solution in a formal way. We assume that the flow is always in a locally energy minimising state, and can be constructed by a solution procedure similar to that described in section 5.3.3. Given admissible initial data, we step the solution forward in time for a time δt to give a first guess to the solution which is not in geostrophic and hydrostatic balance. We then find the solution by minimising the energy using the iteration (5.9). This requires the energy to decrease through the iteration, and would prevent the fluid temporarily increasing its energy by rising to the top of the ridge before achieving a lower energy on the downstream side.

Apply this procedure to solve (6.21) with initial data $\theta'(0,\cdot) = \theta_1(z)$, $v_g(0,\cdot) = 0$. This is clearly admissible. The first guess solution will have $\theta^*(\delta t,\cdot) = \theta_1(z)$, $v_g^*(\delta t,\cdot) = fU\delta t$. In the absence of orography, the energy minimising solution would be given by choosing $u = U$, so that $v(\delta t,\cdot) = 0$. However, with orography, this requires transport through the ridge and is not possible. We therefore obtain a solution like that shown in the top panel of Figure 6.18 with $v_g > 0$, the barrier jet on the upstream side. Observational support for this picture is provided by [Schwerdtfeger (1975)]. Since $\partial v_g/\partial z < 0$ in this region, we must have $\partial\theta'/\partial x < 0$, so the air next to the ridge is colder than the upstream air at a given height. On the downstream side, the solution $u = U$ is allowed. However, it would leave a vacuum on the downstream side of the ridge. The actual solution has to look like that shown in Fig. 6.18.

The solution has a pressure force acting on the ridge, which is a model of orographic drag. This can easily be estimated for a vertical barrier by integrating the hydrostatic equation down from the top of the barrier and noting the difference in potential temperature at given heights across

the barrier. The model as formulated in (6.21) conserves energy. This is because the pressure gradient fU in the y direction is imposed. In a real case, the drag would act to reduce this gradient and the associated geostrophic wind. Air trapped on the upstream side of the ridge will have v_g increasing with time, as u is constrained to be zero. Therefore the slopes of the isentropes, which are related to $\partial v_g/\partial z$, will increase with time and trapped air will reach the top of the ridge. At this point, the minimum energy position of such a parcel will be near $x = x + f^{-1}v_g$, so the parcel will 'jump' downstream. This will correspond to a measure-valued velocity, though it will still fall within the scope of Definition 3.10. In reality, there would be a rapid down-slope wind not described by semi-geostrophic theory. Such winds often occur downstream of mountain ranges. The rate of loss of energy in these jumps has to equal the rate of working by the ridge on the fluid.

In the three-dimensional case, the flow will be like the lower part of Fig. 6.18. Since the trapped air has $v_g > 0$, the air can reach the end of the ridge before it reaches the top. At this point there will again be a jump in the parcel position to near $x = x + f^{-1}v_g$. The preferred deflection of the upstream flow to the left in the Northern hemisphere is regularly seen in observations. We now estimate when this happens. Since the upstream influence of the ridge extends for a distance Nh/f, the maximum displacement due to the ridge of a parcel with given $X = x + f^{-1}v_g$ will be of order Nh/f, and so the maximum barrier jet velocity will be of order Nh. Since (6.21) implies that $\mathrm{D}X/\mathrm{D}t = fU$, the y coordinate of a trapped parcel obeys the equation

$$\frac{\mathrm{d}^2 y}{\mathrm{d}t^2} = fU. \tag{6.25}$$

Thus the parcel will reach the end of a ridge of length D in a time $\sqrt{(2D/fU)}$ with a velocity $\sqrt{(2fUD)}$. This is less than the maximum barrier jet velocity if

$$D < N^2h^2/(2fU). \tag{6.26}$$

If this condition is satisfied, the parcel will flow round the end of the ridge. This problem is discussed more fully in [Shutts (1998)]. The condition (6.26) implies that $Fr^2 < \frac{1}{2}Ro$, where Ro is calculated using the length of the ridge.

We now compare the solution to the two-dimensional ridge problem with that given by the full equations (2.83) with (2.113). The Lagrangian Rossby

number Ro_L for the ridge problem is U/fl, where U is the velocity across the ridge and l the width of the ridge. This is because all the fluid has to cross the ridge. In the three-dimensional case, if (6.26) is satisfied, the fluid does not have to cross the ridge and Ro_L will be $\sqrt{(2fUD)}/fD$, where D is the length of the ridge. (5.18) gives the error in the semi-geostrophic solution as $O(Ro_L(Ro/Fr)^2)$. We show a test where the cross-ridge velocity U is varied, with F, N and the definition of the ridge $z = h(x)$ fixed. The error should then be proportional to U.

The results illustrated are obtained by solving the full compressible Navier-Stokes equations (4.1) in a vertical cross-section, using the integration scheme from the Met Office Unified Model, [Davies et al. (2005)]. These are compared with a solution of a fully compressible semi-geostrophic model, (4.4), calculated using methods similar to those described in section 5.3.3. The solutions of the semi-geostrophic model will include measure-valued velocities as noted above. Therefore the success of finite difference methods is not guaranteed, though an iteration based on (5.9) should give the correct solution.

The results shown are for a ridge 300km wide and 2km high, with $f = 10^{-4}\text{s}^{-1}$ and Brunt-Väisälä frequency $N = 10^{-2}\text{s}^{-1}$. This gives $Ro/Fr = 0.67$. The solutions are obtained by integrating for 60 hours with various wind speeds, and treated as estimates of the steady-state solution. The drag across the ridge is compared. The steady-state drag from the semi-geostrophic solution is independent of the wind speed, since the solution after a time-step is determined by $U\delta t$. If U is increased, then the same solution will be obtained but after a shorter time. The steady-state solution must therefore be the same. The Navier-Stokes solutions depend strongly on U. The values chosen range from 0.625ms^{-1} to 10ms^{-1}. This gives Froude numbers ranging from 0.03 to 0.5.

Fig. 6.19 shows the results. The estimates of the drag from the Navier-Stokes solutions are made by calculating the drag at 15 hour intervals for each wind speed. There is a clear linear convergence to a non-zero drag of about 4.5 units at $U = 0$. The drag that would be given hydrostatically by a potential temperature difference of $hN^2\theta_0/g$, where h is the ridge height, is about 7.5 units. The semi-geostrophic computations give a value of about 4 units. The under-estimate probably reflects the difficulties of obtaining an accurate finite difference solution in this case. The drag calculated from the Navier-Stokes integrations is double the semi-geostrophic value for $U = 2.5\text{ms}^{-1}$, which gives $Ro_L = 0.08$.

If, instead, the limit is taken as $Ro/Fr \to 0$, then the effect is that

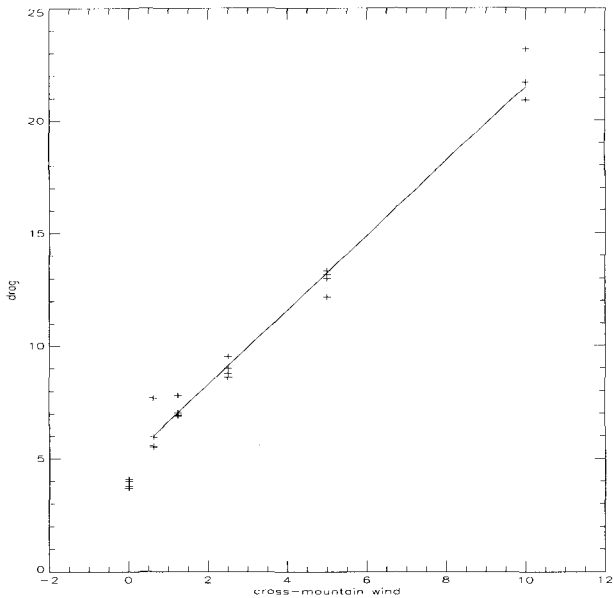

Fig. 6.19 Drag across the ridge (arbitrary units) plotted against cross-ridge wind speed (ms^{-1}). Values plotted for $U \neq 0$ are from the Navier-Stokes solutions, with the best linear fit shown. Values plotted for U=0 are from the semi-geostrophic model.

the height of the ridge is reduced, condition (6.24) is satisfied, and it is possible to obtain smooth semi-geostrophic solutions, which, as expected from (5.18), agree much more closely with the Navier-Stokes solutions.

6.6 Inclusion of friction

The main deficiency in representing large-scale atmospheric dynamics by a semi-geostrophic model is the neglect of frictional drag. Though this neglect makes it much easier to study the problem, actual predictions made without including frictional drag give completely unrealistic results. In the atmospheric boundary layer, frictional drag is of similar magnitude to the pressure gradient and the Coriolis acceleration. In the tropics, frictional drag can balance the pressure gradient. It is therefore important to de-

velop a method for incorporating it in the boundary layer in a way that is consistent with the semi-geostrophic approximation above the boundary layer. This problem has been studied by [Cullen (1989a)] and [Ostdiek and Blumen (1997)].

Since, as discussed in section 2.2, the semigeostrophic approximation is only appropriate for flows with small aspect ratio, we can approximate the viscous terms like $\nu\nabla^2 u$ in (2.17) by $\nu\partial^2 u/\partial z^2$. Since frictional drag is small above the boundary layer, it is desirable for the coefficient ν to depend on z, and in that case the drag should be written in conservation form. We therefore define the 'geotriptic' wind (u_e, v_e) by setting

$$\begin{aligned} \frac{\partial \varphi}{\partial x} &= f v_e + \frac{\partial}{\partial z}\left(\nu(z)\frac{\partial u_e}{\partial z}\right), \\ \frac{\partial \varphi}{\partial y} &= -f u_e + \frac{\partial}{\partial z}\left(\nu(z)\frac{\partial v_e}{\partial z}\right). \end{aligned} \tag{6.27}$$

The three-dimensional semi-geostrophic equations (2.124) are then generalised to

$$\begin{aligned} \frac{\mathrm{D}u_g}{\mathrm{D}t} - fv + \frac{\partial \varphi}{\partial x} &= \frac{\partial}{\partial z}\left(\nu(z)\frac{\partial}{\partial z}(2u_e - u)\right), \\ \frac{\mathrm{D}v_g}{\mathrm{D}t} + fu + \frac{\partial \varphi}{\partial y} &= \frac{\partial}{\partial z}\left(\nu(z)\frac{\partial}{\partial z}(2v_e - u)\right), \\ \frac{\mathrm{D}\theta'}{\mathrm{D}t} &= 0, \\ \frac{\partial \varphi}{\partial z} - g\frac{\theta'}{\theta_0} &= 0, \\ \nabla \cdot \mathbf{u} &= 0. \end{aligned} \tag{6.28}$$

The equations are solved in an atmospheric context in a domain $\Gamma = \mathbb{T}^2 \times [0, H]$, with $\mathbf{u} = \mathbf{u}_e = 0$ at $z = 0$ and $w = 0$ at $z = H$. This avoids difficulties with boundary layers at lateral boundaries, which would be important in the ocean. It is assumed that $\nu = 0$ above some value $z = z_{bl} < H$. The energy E_e is defined similarly to (2.125):

$$E_e = \int_\Gamma \left(\frac{1}{2}(u_e^2 + v_e^2) - g\theta' z/\theta_0\right) \mathrm{d}x\mathrm{d}y\mathrm{d}z. \tag{6.29}$$

Using the boundary conditions, and the vanishing of ν for large z, the

evolution equation for the energy can be shown to be

$$\frac{\mathrm{d}E_e}{\mathrm{d}t} = -\int_\Gamma \nu \left(\left(\frac{\partial u_e}{\partial z} \right)^2 + \left(\frac{\partial v_e}{\partial z} \right)^2 \right) \mathrm{d}x\mathrm{d}y\mathrm{d}z, \tag{6.30}$$

so that the energy decreases with time.

We now show that Theorem 3.1 can be extended to the case with frictional drag, so that geotriptic balance can be regarded as a stationary energy state with respect to displacements in a frozen pressure field. Suppose we have a state of the fluid with an associated vector field $(\tilde{u}, \tilde{v})$ and scalar field $\tilde{\theta}'$. Associate with this state an energy E given by a formula analogous to (6.29). This energy is a functional of $\tilde{u}, \tilde{v}$ and $\tilde{\theta}'$, regarded as functions of position over Γ, which has the following property.

Theorem 6.1 *The conditions for the energy E to be stationary with respect to variations $\Xi = (\xi, \eta, \chi)$ of particle positions satisfying continuity $\delta(\mathrm{d}x\mathrm{d}y\mathrm{d}z) = 0$ via*

$$\nabla \cdot \Xi = 0 \tag{6.31}$$

in Γ and

$$\delta\tilde{u} = f\eta - \frac{\partial}{\partial z}\left(\nu(z) \frac{\partial \xi}{\partial z} \right), \ \delta\tilde{v} = -f\xi - \frac{\partial}{\partial z}\left(\nu(z) \frac{\partial \xi}{\partial z} \right), \ \delta\tilde{\theta}' = 0, \tag{6.32}$$

together with $\Xi \cdot \mathbf{n} = 0$ on the boundary of Γ, are that

$$\left(f\tilde{v} - \frac{\partial}{\partial z}\left(\nu(z) \frac{\partial \tilde{u}}{\partial z} \right), -f\tilde{u} - \frac{\partial}{\partial z}\left(\nu(z) \frac{\partial \tilde{v}}{\partial z} \right), g\tilde{\theta}'/\theta_0 \right) = \nabla\tilde{\varphi} \tag{6.33}$$

for some scalar $\tilde{\varphi}$.

Proof We can write

$$\begin{aligned} \delta E = & \int_\Gamma \left(\tilde{u}\delta\tilde{u} + \tilde{v}\delta\tilde{v} - gz\delta\tilde{\theta}'/\theta_0 - g\tilde{\theta}'\chi/\theta_0 \right) \mathrm{d}x\mathrm{d}y\mathrm{d}z, \qquad (6.34) \\ = & \int_\Gamma \left(f\tilde{u}\eta - \tilde{u}\tfrac{\partial}{\partial z}\left(\nu(z)\tfrac{\partial \xi}{\partial z} \right) - f\tilde{v}\xi - \tilde{v}\tfrac{\partial}{\partial z}\left(\nu(z)\tfrac{\partial \eta}{\partial z} \right) - g\tilde{\theta}'\chi/\theta_0 \right) \mathrm{d}x\mathrm{d}y\mathrm{d}z. \end{aligned}$$

Integrating by parts twice, and using the boundary conditions and the vanishing of ν for large z, this becomes

$$\int_\Gamma \left(-\Xi \cdot \left(f\tilde{v} - \frac{\partial}{\partial z}\left(\nu(z)\frac{\partial \tilde{u}}{\partial z} \right), -f\tilde{u} - \frac{\partial}{\partial z}\left(\nu(z)\frac{\partial \tilde{v}}{\partial z} \right), g\tilde{\theta}'/\theta_0 \right) \right. \mathrm{d}x\mathrm{d}y\mathrm{d}z. \tag{6.35}$$

For this to vanish for any Ξ satisfying (6.31) and the boundary conditions, (6.33) must be satisfied. □

Equation (6.33) means that $(\tilde{u}, \tilde{v}, \tilde{\theta}')$ represents a state in geotriptic and hydrostatic balance, with geopotential $\tilde{\varphi}$. We conjecture that it should also be possible to extend Theorem 3.2 to derive conditions for the energy to be minimised, and relate them to the solvability of (6.21). For the present, we demonstrate the conditions for a linearised version of (6.28) to be solvable. Write a linearisation of (6.28) about a state of rest with $\frac{g}{\theta_0}\frac{\partial \theta'}{\partial z} = N^2$ in a form similar to (3.1).

$$\mathbf{Q}\begin{pmatrix} u \\ v \\ w \end{pmatrix} + \frac{\partial}{\partial t}\begin{pmatrix} v_e \\ -u_e \\ g\theta'/(N\theta_0) \end{pmatrix} = \mathbf{H},$$

$$\mathbf{H} = \begin{pmatrix} fu_e + \frac{\partial}{\partial z}\left(\nu \frac{\partial v_e}{\partial z}\right) \\ fv_e - \frac{\partial}{\partial z}\left(\nu \frac{\partial u_e}{\partial z}\right) \\ 0 \end{pmatrix}, \tag{6.36}$$

$$\mathbf{Q} = \begin{pmatrix} f & \frac{\partial}{\partial z}\left(\nu \frac{\partial}{\partial z}\right) & 0 \\ -\frac{\partial}{\partial z}\left(\nu \frac{\partial}{\partial z}\right) & f & 0 \\ 0 & 0 & N \end{pmatrix}.$$

We can also write (6.27) as

$$\nabla \varphi = \mathbf{Q}\begin{pmatrix} v_e \\ -u_e \\ \frac{g}{\theta_0}\frac{\theta'}{N} \end{pmatrix}. \tag{6.37}$$

We can then rewrite (6.36) as

$$\mathbf{Q}^2\begin{pmatrix} u \\ v \\ w \end{pmatrix} + \frac{\partial}{\partial t}\nabla \varphi = \mathbf{Q}\mathbf{H}. \tag{6.38}$$

Solvability of (6.38) depends on $\mathbf{Q}^2$ being positive definite. While this would always be true in the linear case if $f \neq 0$, the inclusion of the frictional drag increases $\det\mathbf{Q}$. Therefore the solvability condition is likely to be easier to satisfy in the nonlinear case. Thus we can expect the validity of the semi-geotriptic equations (6.28) to extend beyond cases where semi-geostrophic theory is valid.

We confirm this by illustrating that these equations are much more useful for explaining many observed phenomena than the equations without friction. We show solutions in a two-dimensional cross-section, as in sections 6.2 and 6.5. The equations are obtained by omitting the term $\partial\varphi/\partial y$ from (6.28). The problem is forced by assuming the lower boundary is land for

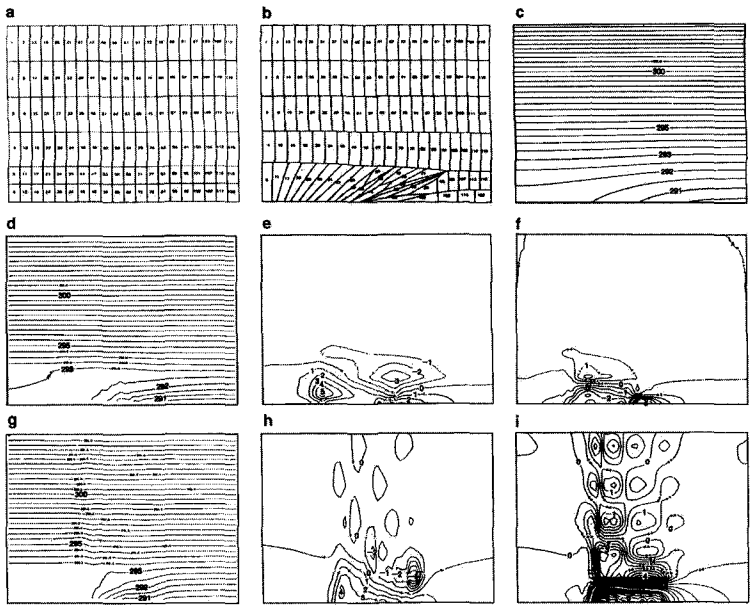

Fig. 6.20 Solutions after 12 hours with no basic state wind and a surface heating coefficient of 2.5Kh^{-1}.over the land (the left half of the domian shown). Plots are of θ', units K, contour interval 0.5K; u and v, units ms^{-1}, contour interval 1ms^{-1}. GEOM: geometric algorithm, S.G.: finite difference solutions of (6.28), P.E.: finite difference solutions of (2.83) with friction. From [Cullen (1989a)]. ©Royal Meteorological Society, Reading, U.K.

$L < 0$ and sea for $L > 0$. The land is heated, and a heat conduction of the form $\kappa_h \nabla^2 T$ as in (2.1), where T is the temperature, is used to transfer the heat into the atmosphere.

Numerical solutions are obtained using a finite difference method similar to that described in section 5.3.3. They are compared with the solutions of the geometric model described in section 5.3.2. However, the formulation of the geometric algorithm cannot deal with geotriptic balance, so the equations can only be solved if the x-component of the frictional terms in (6.27) and (6.28) is omitted, so only the y-component of friction is included. The solutions are compared with those of (2.83) with the same form of the frictional drag and the same thermal conductivity.

The solutions in Fig. 6.20 show that, as heat is input through the lower boundary, air moves inland to preserve geostrophic balance, In the geometric model solutions, where there is no friction in the x-direction,

there is a smooth gradient of potential temperature at $z = 0$. However, when friction is included, a discontinuity forms corresponding to a sea-breeze front. The solution from (2.83) is similar at the surface, suggesting that the formation of the front is strongly controlled by frictional drag. The solution also contains inertia-gravity waves which are not well resolved in this simulation, but certainly occur in reality in association with sea-breeze fronts.

In Fig. 6.21 we show results with a basic state wind across the coastline. This is modelled by imposing a basic state pressure gradient independent of z in (6.27) and (6.28). Observations discussed in [Cullen (1989a)] show that sea-breezes are stronger when the basic state wind is from the north-west across an east-west coastline with the sea to the south. This effect is seen in Fig 6.21. This shows that large-scale dependencies of the sea-breeze circulation can be modelled by the semi-geotriptic equations, though small-scale details will not be.

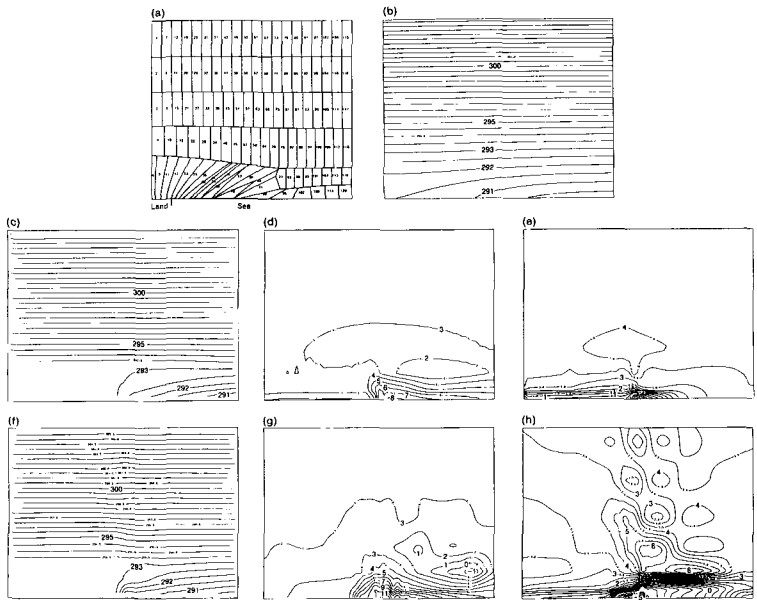

Fig. 6.21 Solutions after 12 hours as in Fig. 6.20 but with basic state wind of 5ms^{-1} in direction 225°. The positive x axis is towards 90°. From [Cullen (1989a)]. ©Royal Meteorological Society, Reading, U.K.

6.7 Inclusion of moisture

The effects of moisture on semi-geostrophic dynamics can be modelled by including the additional terms in the thermodynamic equations shown in equations (2.17). We thus modify (2.124) by setting

$$\begin{aligned} \frac{\mathrm{D}\theta'}{\mathrm{D}t} &= S : q < q_{sat}(\theta', z), \\ &= S - L\frac{\mathrm{D}q_{sat}}{\mathrm{D}t} : q = q_{sat}, \\ \frac{\mathrm{D}q}{\mathrm{D}t} &= 0 : q < q_{sat}(\theta', z), \\ q &= q_{sat} \text{ otherwise.} \end{aligned} \tag{6.39}$$

q now represents the moisture content, L the coefficient of latent heating and S a source term used to ensure the possibility of non-trivial steady state solutions. In the atmosphere it represents radiative cooling which compensates the convective heating. The physics behind (6.39), described in [Haltiner and Williams (1980)], is that q_{sat} is the maximum moisture content which an air parcel can have. It is a strongly monotonically increasing function of temperature. As an air parcel rises, while conserving its potential temperature, its temperature decreases and so q_{sat} decreases while q is conserved. Thus it is common for the condition $q = q_{sat}$ to be met, leading to condensation and release of latent heat. Equations (6.39) represent the simplest model which contains this physics.

It is clear that there will not be a unique global energy minimiser in the sense of Theorem 3.2 when these effects are included. If $q < q_{sat}$ everywhere, then the theorems of section 3.5.1 still hold. If $q = q_{sat}$ everywhere, and we assume that $\frac{\mathrm{d}q_{sat}}{\mathrm{d}z}$ is a (negative) constant, then the conserved thermodynamic quantity becomes

$$\theta' + L\frac{\mathrm{d}q_{sat}}{\mathrm{d}z}z. \tag{6.40}$$

Since $L\frac{\mathrm{d}q_{sat}}{\mathrm{d}z}z$ is independent of x and y, Theorem 3.2 can be extended to this case by using the new thermodynamic variable defined by (6.40). The vertical component of the condition for the matrix $\mathbf{Q}$ of section 3.1 to be positive definite, which was $\partial\theta'/\partial z \geq 0$ is replaced by

$$\frac{\partial\theta'}{\partial z} \geq -L\frac{\mathrm{d}q_{sat}}{\mathrm{d}z}. \tag{6.41}$$

Since the right hand side of (6.41) is positive, this is a more severe condition.

Thus, while the global energy minimisation methods will apply to cases where q is either less than q_{sat} everywhere or equal to q_{sat} everywhere, all realistic cases have a mixture of the two. The effect of moisture on the dynamics is then highly non-trivial, giving rise to the complex phenomena observed in reality. No rigorous mathematics has been done in such cases.

As in the case of flow over a mountain ridge, it is necessary to seek local energy minimisers. Iterative methods of doing this have been developed by [Holt (1990)] using the geometric algorithm, [Shutts (1995)] and [Wakefield and Cullen (2005)]. These all use variations on the following method.

(i) Given initial data defining a geostrophic and hydrostatic state, step equations (2.124) with (6.39) forward for a time-step δt, assuming that $q < q_{sat}$ everywhere. This gives values $\tilde{u}, \tilde{v}, \tilde{\theta}', \tilde{q}$.

(ii) Evaluate $q_{sat}(\delta t, \cdot)$. Set

$$\check{\theta}' = \tilde{\theta}' + L(\tilde{q} - q_{sat}) : \tilde{q} > q_{sat}, = \tilde{\theta}' : \tilde{q} \leq q_{sat}, \qquad (6.42)$$
$$\check{q} = q_{sat} : \tilde{q} > q_{sat}, = \tilde{q} : \tilde{q} \leq q_{sat}.$$

The resulting state may have $\partial\check{\theta}/\partial z < 0$.

(iii) Construct a monotonically increasing rearrangement of $\check{\theta}$ for each (x, y), allowing for further changes to $\check{\theta}$ according to (6.40) as the parcels are rearranged. Note that there is no proof available that this is possible. However, it has been found to be achievable in discrete models under quite general conditions, so we conjecture that a proof is possible. This yields values $\hat{\theta}', \hat{q}$.

(iv) Using these values of $\hat{\theta}'$ together with $\tilde{u}, \tilde{v}$, find the unique energy minimising state given by u^*, v^*, θ^* guaranteed by Theorem 3.12. Calculate the trajectory from (3.1) and use it to transport $\check{q}$, giving a value q^*.

(v) If this state has $q^* \geq q_{sat}$, the procedure has to be iterated starting from step (ii). It is found that step (iii) is a very effective preconditioner for this iteration.

(vi) The result is then $(u(\delta t, \cdot), v_g(\delta t, \cdot), \theta'(\delta t, \cdot), q(\delta t, \cdot))$, and we proceed to the next time-step.

We now illustrate the results. In Fig. 6.22 we show a solution of the frontogenesis problem (3.102), with moisture included according to (6.39), obtained by [Holt (1990)] using the geometric algorithm. Only the hatched elements contain moisture. The effect of the frontogenesis is that the air is forced up at the front, as shown in section 3.4.2. Some of the air becomes saturated, and therefore θ' is increased, leading to further upward motion.

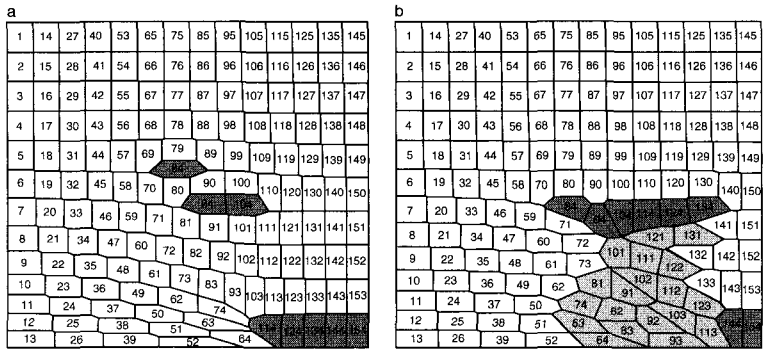

Fig. 6.22 Fluid element pictures showing a vertical cross-section of a frontal zone with moisture. Left: the hatched elements are moist. Right: the striped elements have been cooled by precipitation falling from the convecting hatched elements. From [Cullen and Salmond (2003)]. ©Royal Meteorological Society, Reading, U.K.

This gives a positive feedback which strengthens the frontogenesis. This is the reason why weather systems are intensified by latent heat release. Fig. 6.22 shows a further effect, not included in (6.39). If the excess moisture falls out as rain, some of it will re-evaporate into the air below, thus cooling it. This effect occurs in the striped elements in the right-hand panel of Fig. 6.22, and gives a further positive feedback as the convergence into the front is increased. The position of the rainfall relative to the front is critical for whether the feedback is positive or negative.

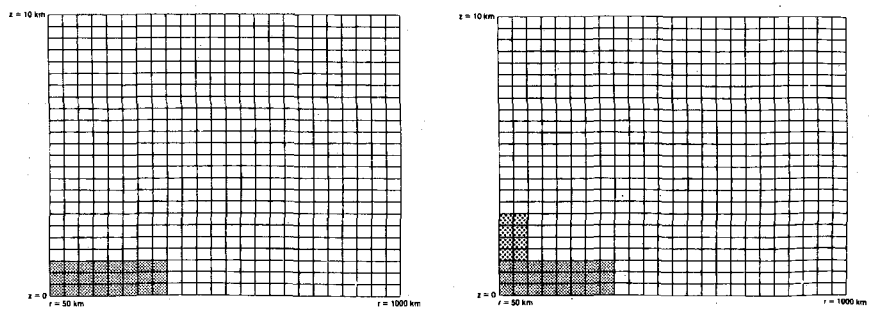

Fig. 6.23 Initial element geometries for the convective mass transfer experiments. The shaded elements are moist. In the right panel, the stippled region is to be cooled. From [Shutts, Booth and Norbury (1987)].

A similar effect occurs in tropical cyclones. Fig. (6.23) shows the initial

data for an integration of (4.137) with the geometric algorithm carried out by [Shutts, Booth and Norbury (1987)]. These equations only describe steady states. Fig. 6.23 shows the initial element configuration, which is regular in (r, z) coordinates. The annular domain extends from an inner radius of 50km to an outer radius of 1000km. The depth was 10km and the Brunt-Väisälä frequency was $1.3\times10^{-2}\mathrm{s}^{-1}$. The rotation rate Ω was $3\times10^{-5}\mathrm{s}^{-1}$.

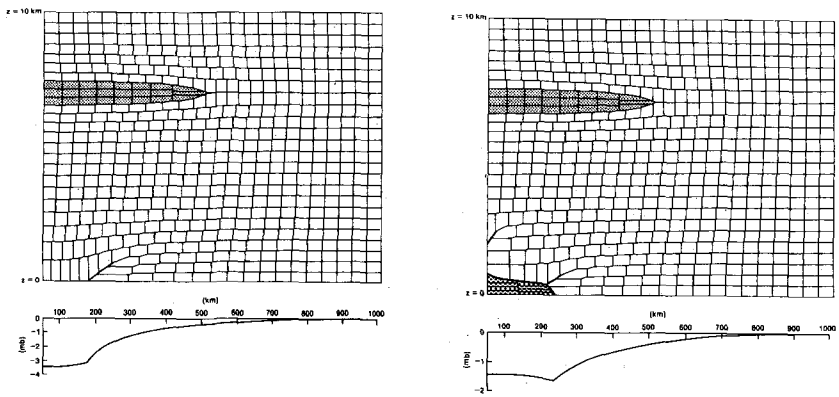

Fig. 6.24 The final states after the corresponding shaded elements in Fig. 6.23 have convected. The pressure perturbation is shown below. Bold lines correspond to frontal surfaces. From [Shutts, Booth and Norbury (1987)].

The end-state obtained as a result of heating the shaded elements, thus imitating the effect of solving (6.39), is shown in Fig. 6.24. The heating was such that the elements convected up to about 7km, forming a 'lens'. This is more obvious than in Fig. 6.22 because the heating is a uniform value. An eye-wall discontinuity is formed at a radius of 175km. Within the eye, the surface pressure perturbation is about -3.5hpa, and the temperature perturbation about $+6°$K. The warm core arises from the subsiding of warmer air from above to replace the air that has been heated and convected away. In the second experiment, shown in the lower panels of Fig. 6.23 and Fig. 6.24, some elements indicated by stippling are cooled. This represents the effect of the evaporation of rainfall, which will be large in the region of the eye-wall. This creates a surface cold dome, which displaces the eye-wall outwards. These effects are qualitatively like those that occur in real tropical cyclones, though the latter are much more intense. The experiments

are discussed in more detail in [Shutts, Booth and Norbury (1987)].

The effect of solving the moist equation (6.39) can also be studied using the dual formulation (3.42). This becomes

$$\begin{aligned} &\frac{\partial \sigma}{\partial t} + \mathbf{U} \cdot \nabla \sigma = 0, \\ &\mathbf{U} = (U, V, W), \\ &\quad = \left(f(y - Y), f(X - x), S : q < q_{sat}; S - L\frac{\mathrm{D}q_{sat}}{\mathrm{D}t} : q = q_{sat} \right). \end{aligned} \tag{6.43}$$

Thus the latent heat release term creates a positive W if there is upward vertical motion. If the stability condition (6.41) is violated, parcels will jump in the vertical to new stable positions, as shown in Figs. 6.22 and 6.24. As in the mountain ridge case, section 6.5, the jumps will result in energy loss. In that case W becomes measure-valued as does the physical space velocity w. The potential density σ represents a mass density in (X, Y, Z) coordinates. The effect of the jump is to create a mass source at large Z and a corresponding sink at small Z. Since the potential vorticity is the inverse of the potential density, the effect can be seen in the potential vorticity calculated from the solutions in physical space as an source at low levels and a sink at high levels.

An example is shown in Fig. 6.25, from [Shutts and Gray (1994)]. The solutions were obtained using a model similar to (2.83) with (2.113). Moist effects were included but with a more accurate representation than the simple one used in (6.39). The initial potential vorticity was independent of x and y, and increasing with z, as shown away from the convecting region in Fig. 6.25. The domain size was 20km square in (x, y) and 12km deep. The Brunt-Väisälä frequency was $1.2 \times 10^{-2}\mathrm{s}^{-1}$. Two values of rotation rate were used, $1 \times 10^{-3}\mathrm{s}^{-1}$ giving $f/N = 0.08$ and $2 \times 10^{-5}\mathrm{s}^{-1}$ giving $f/N = 0.16$. Convection was initiated by creating a warm bubble at the surface, which convects to about 7km. For the parameters chosen, the horizontal spreading of the effect of this convection on the semi-geostrophic solution would be about 80km and 40km respectively. The actual spreading is much less, as explained using an analytic solution in [Shutts and Gray (1994)]. The potential vorticity source at low levels and sink at high levels, leading to weakly negative values, are easily seen. Other diagnostics calculated by [Shutts and Gray (1994)] show that 40% of the total production of energy by latent heat release is retained in the balanced flow, the rest being dissipated. In a semi-geostrophic solution, this dissipation is represented by the energy lost in the convective jumps.

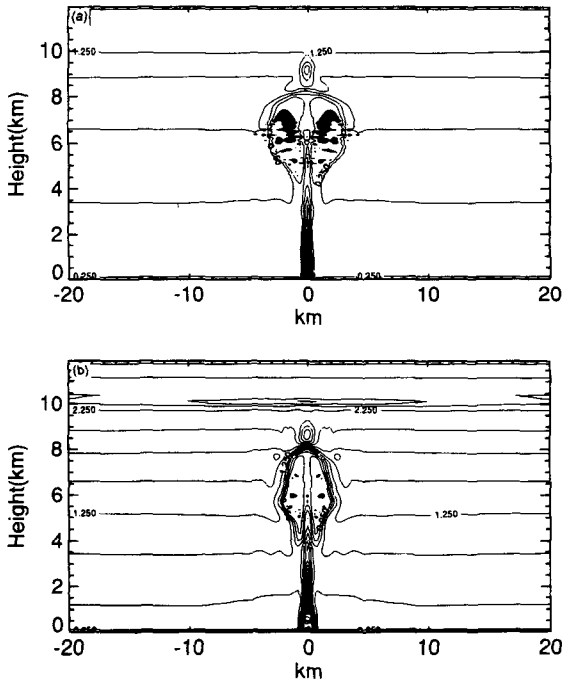

Fig. 6.25 The potential vorticity field for experiments with (a) $f = 1 \times 10^{-3}\mathrm{s}^{-1}$ and (b) $f = 2 \times 10^{-3}\mathrm{s}^{-1}$. Contour interval $0.25 \times 10^{-5}\mathrm{m}^2\mathrm{s}^{-1}\mathrm{Kkg}^{-1}$. Regions of negative potential vorticity are shaded. From [Shutts and Gray (1994)]. ©Royal Meteorological Society, Reading, U.K.

We can expect semi-geostrophic theory to give useful predictions of convection if the instability is created by large-scale effects which lead to violations of (6.41). In Fig. 6.26 we show a case where a storm developed over eastern England on the north side of a vortex in the upper troposphere. In Fig. 6.27 the vertical motion diagnosed by the omega equation (5.43) is shown by the + and − signs. It indicates upward motion associated with the vortex. Fig. 6.27 also shows the warming and moistening of the low level troposphere by the large-scale flow. The effect is to create instability according to (6.41), because the upward motion creates saturation and brings the more stringent condition into effect.

The final example is shown in Fig. 6.28. This is a study of the large-scale response to a heat source placed over the Tibetan plateau computed by a semi-geotriptic model, with frictional drag included as described in

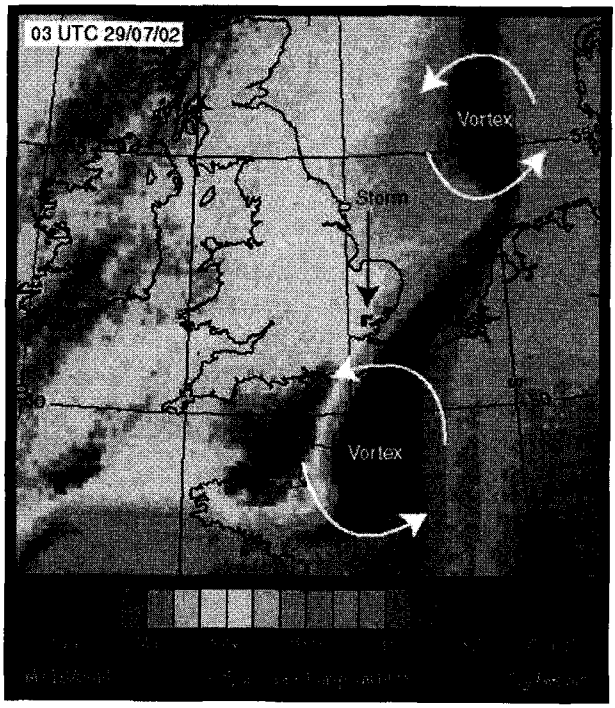

Fig. 6.26 Case study for 29 July 2002 over the U.K. The shading indicates cloud-top heights, the darker shading is high cloud. The position of an upper level vortex is marked, together with the position of a severe convective storm. Source: N. Roberts, JCMM, Met Office. ©Crown copyright 2005 Published by the Met Office.

section 6.6. The results are compared with a model similar to (2.83) with the same frictional drag. The heat source generates low pressure at the surface with an associated cyclonic circulation. The rising motion over Tibet has to be fed by low-level convergence. Since the Coriolis parameter is small near the equator, the region of influence of the heating is greater, and the convergence has to cross the equator. This is clearly seen in Fig. 6.28. The extra ingredient is the inclusion of the mountain ridge in East Africa. This forces the converging flow to form a jet-stream at low levels across the equator. This is routinely observed. The simulations by the two models are very similar, showing that the semi-geotriptic model is accurate for flows on this scale, which are typical of the tropical response to heat sources. The inclusion of frictional drag allows pressure gradients to be non-zero at the equator, which considerably improves the realism of the

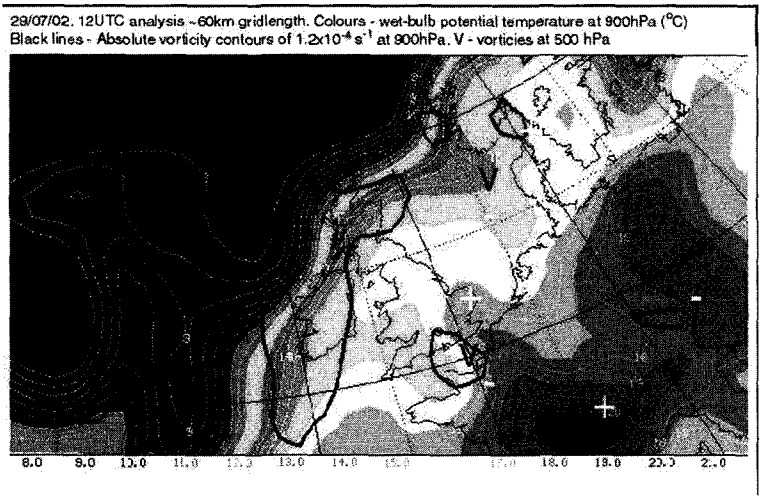

Fig. 6.27 The same case as in Fig. 6.26. Shading indicates wet-bulb potential temperature at 900hpa. High values indicate almost saturated air. The plus and minus signs indicate upward and downward motion diagnosed using (5.43). Source: N. Roberts, JCMM, Met Office. ©Crown copyright 2005 Published by the Met Office.

results.

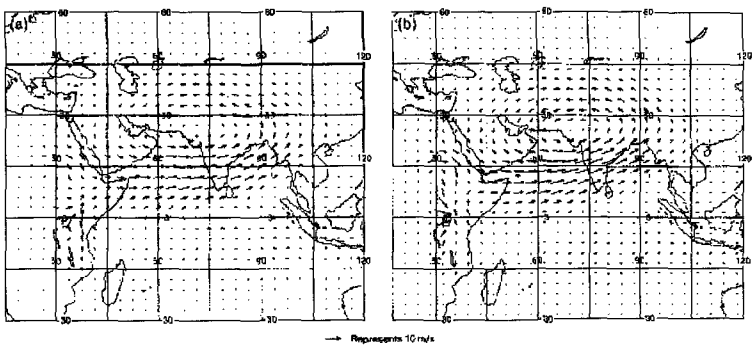

Fig. 6.28 Forecast wind vectors at the surface after 5 days integration of (a) semi-geotriptic model and (b) model as used for weather forecasting. The same frictional drag is used in both models. From [Cullen and Mawson (1992)]. ©Royal Meteorological Society, Reading, U.K.

This page is intentionally left blank

Chapter 7

Summary

In this volume we have demonstrated that the semi-geostrophic model is a mathematically well-posed approximation to the governing equations of the atmosphere and ocean on large scales. The solution can be regarded as evolution through a sequence of minimum energy states. This characterisation holds in all the cases studied,. In particular cases, this characterisation corresponds to the system being Hamiltonian, or, in more cases, that it can be written as a mass transportation problem. On present evidence, the semi-geostrophic model is the most general model which can be solved for large times and is asymptotically valid on large scales. It is thus the most general slow manifold. The large-scale assumption is quite restrictive in the atmosphere, and only allows the description of extra-tropical weather systems and sub-synoptic structure such as fronts which are large-scale in one direction. In the tropics, the only solutions described are steady state responses to spatially varying heat sources.

Validation of the results against solutions of the Navier-Stokes equations shows the expected behaviour, with differences corresponding to the error estimates. It demonstrates that the semi-geostrophic model is useful in the appropriate asymptotic regime, but is otherwise inaccurate. Observations of trajectories in the extra-tropics and of inertial (in)stability in the tropics show that the conditions for the theory to be valid are usually met in practice on scales larger than 100km. It is thus likely that the predictability of the atmosphere estimated from semi-geostrophic theory will be a useful guide to the real system.

In the extra-tropics, the theory suggests that the development of fronts will not degrade predictability, as they are essentially passive. There are no dynamically preferred two-dimensional structures, and they evolve slowly. Thus predictability should be high for 1-2 weeks, which is the time-scale

of this evolution. On the seasonal time-scale, the absence of preferred structures means that predictability may be low. Both these conclusions are consistent with current experience. In the tropics, the theory can predict the anomalous circulations due to localised heat sources. These would typically come from the ocean, so there should be high predictability on the time-scale on which ocean temperature anomalies vary. However, the theory cannot describe the convectively-coupled waves which are probably responsible for variability on shorter time-scales, so their predictability may be low. This also agrees with current experience.

There are many open mathematical questions to be addressed in the theory. Probably the uniqueness of the solutions is the most important, as it is closely linked to predictability. The potential for extending the theory in a rigorous way to include frictional drag and latent heat release would greatly widen its applicability. There are also implications for numerical modelling. Semi-geostrophic solutions are fundamentally Lagrangian, and it may be very difficult to reproduce their properties with the Eulerian methods which have to be used to make operational weather forecasting practicable. This may be a serious limitation.

Bibliography

Adams, R. A. (1975) *Sobolev spaces.* Academic Press, New York.

Allen, J. S., Barth, J. A. and Newberger, P. (1990) On intermediate models for barotropic continental shelf and slope flow fields. Part III: Comparison of numerical model solutions in periodic channels. *J. Phys. Oceanog.* **20**, pp. 1949–1973.

Ambrosio, L. (2003) Transport equation and Cauchy problem for BV vector fields. *Invent. Math.* **158**, pp. 227–260.

Angenent, S., Haker, S. and Tannenbaum, A. (2003) Minimising flows for the Monge-Kantorovich problem. *S.I.A.M. J. Math. Anal.* **359**, pp. 61–97.

Babin, A., Mahalov, A. and Nicolaenko, B. (1999), Global regularity of 3D rotating Navier-Stokes equations for resonant domains. *Indiana University Mathematics Journal* **48**, pp. 1133–1176.

Babin, A., Mahalov, A. and Nicolaenko, B. (1999) Fast singular oscillating limits of stably stratified 3-D Euler and Navier-Stokes equations and ageostrophic wave fronts. In *Large-Scale Atmosphere-Ocean Dynamics*, J. Norbury and I. Roulstone eds., Cambridge University Press, vol. I, pp. 126–201.

Benamou, J.-D. and Brenier, Y. (1997) A numerical method for the optimal time-continuous mass transport problem and related problems. In *Monge-Ampere equations: applications to geometry and optimisation. (Deerfield Beach, FL. 1997).* Contemporary Math., Amer. Math. Soc. **226**, pp. 1–11.

Benamou, J.-D. and Brenier, Y. (1998) Weak existence for the semi-geostrophic equations formulated as a coupled Monge-Ampere/transport problem. *SIAM J. Appl. Math.* **58**, pp. 1450–1461.

Bennetts, D. A. and Hoskins, B. J. (1979) Conditional symmetric instability-a possible explanation for frontal rainbands. *Quart. J. Roy. Meteor. Soc.* **105**, pp. 945–962.

Bogue, N. M., Huang, R. X. and Bryan, K. (1986) Verification experiments with an isopycnal coordinate ocean model. *J. Phys. Oceanogr.* **16**, pp. 985–990.

Bourgeois, A. J. and Beale, J. T. (1994) Validity of the quasigeostrophic model for large-scale flow in the atmosphere and ocean. *SIAM J. Math. Anal.* **25**, pp. 1023–1068.

Brenier, Y. (1991) Polar factorisation and monotone rearrangement of vector-

valued functions. *Commun. Pure Appl. Math.* **44**, pp. 375–417.
Burton, G. R. and Douglas, R. J. (1998) Rearrangements and polar factorisation of countably degenerate functions. *Proc. Roy. Soc. Edin.* **128A**, pp. 671–681.
Burton, G. R. and McLeod, J. B. (1991) Maximisation and minimisation on classes of rearrangements. *Proc. Roy. Soc. Edin.* **119A**, pp. 287–300.
Burton, G. R. and Nycander, J. (1999) Stationary vortices in three-dimensional quasi-geostrophic flow. *J. Fluid Mech.* **389**, pp. 255–274.
Caffarelli, L. A. (1992) The regularity of mappings with a convex potential. *J. A. M. S.* **5**, pp. 99–104.
Caffarelli, L. A. (1992) Boundary regularity of maps with convex potentials. *Comm. Pure Appl. Math.* **45**, pp. 1141–1151.
Caffarelli, L. A. (1996) Boundary regularity of maps with convex potentials-II. *Ann. Math.* **144**, pp. 453–496.
Charney, J. G. (1949) On the scale of atmospheric motions. *Geofys. Publ.* **17**,(2) 17pp.
Charney, J. G. (1971) Geostrophic turbulence. *J. Atmos. Sci.*, **28**, pp. 1087-1095.
Charney, J. G. and Devore, J. (1979) Multiple flow equilibria in the atmosphere and blocking. *J. Atmos. Sci.*, **36**, pp. 1205-1216.
Charney, J. G., Fjortoft, R. and von Neumann, J. (1950) Numerical integration of the barotropic vorticity equations. *Tellus* **2**, pp. 237–254.
Chemin, J-Y. Perfect incompressible fluids. Oxford University Press, 185pp.
Chynoweth, S. (1987) *The semi-geostrophic equations and the Legendre transform.* Ph. D thesis. University of Reading, Whiteknights, PO Box 220, Reading, RG6 2AX, U.K., 248pp.
Chynoweth, S. and Sewell, M. J. (1989) Dual variables in semi-geostrophic theory. *Proc. Roy. Soc. Lond.* **A424**, pp. 155–186.
Cloke, P. and Cullen, M. J. P. (1994) A semi-geostrophic ocean model with outcropping. *Dyn. Atmos. Ocean.* **21**, pp. 23–48.
Cordero-Erausquin, D. (1999) Sur le transport de mesures périodiques. *C. R. Acad. Sci. Paris Ser. I Math.* **329**, pp. 199–202.
Craig, G. C. (1991) A three-dimensional generalisation of Eliassen's balanced vortex equations derived from Hamilton's principle. *Quart. J. Roy. Meteor. Soc.* **117**, pp. 435–448.
Cullen, M. J. P. and Purser, R. J. (1984) An extended Lagrangian theory of semi-geostrophic frontogenesis. *J. Atmos. Sci.* **41**, pp. 1477–1497.
Cullen, M. J. P., Chynoweth, S. and Purser, R. J. (1987) On semi-geostrophic flow over synoptic-scale topography. *Quart. J. Roy. Meteor. Soc.* **113**, pp. 163–180.
Cullen, M. J. P. (1989) On the incorporation of atmospheric boundary layer effects into a balanced model. *Quart. J. Roy. Meteor. Soc.* **115**, pp. 1109–1131.
Cullen, M. J. P. (1989) Implicit finite difference methods for modelling discontinuous atmospheric flows. *J. Comp. Phys.* **81**, pp. 319–348.
Cullen, M. J. P. and Purser, R. J. (1989) Properties of the Lagrangian semi-geostrophic equations. *J. Atmos. Sci.* **46**, pp. 2684–2697.
Cullen, M. J. P. and Mawson, M. H. (1992) An idealised simulation of the Indian

monsoon using primitive-equation and quasi-equilibrium models. *Quart. J. Roy. Meteor. Soc.* **118**, pp. 153–164.

Cullen, M. J. P. and Roulstone, I. (1993) A geometric model of the nonlinear equilibration of two-dimensional Eady waves. *J. Atmos. Sci.* **50**, pp. 328–332.

Cullen, M. J. P. (2000) On the accuracy of the semi-geostrophic approximation. *Quart. J. Roy. Meteor. Soc.* **126**, pp. 1099–1115.

Cullen, M. J. P. and Gangbo, W. (2001) A variational approach for the 2-D semi-geostrophic shallow water equations. *Arch. Rat. Mech. Anal.* **156**, pp. 241–273.

Cullen, M. J. P. and Maroofi, H. (2003) The fully compressible semi-geostrophic system from meteorology. *Arch. Rat. Mech. Anal.* **167**, pp. 309–336.

Cullen, M. J. P. (2002) Large scale non-turbulent dynamics in the atmosphere. *Quart. J. Roy. Meteorol. Soc.* **128**, pp. 2623–2640.

Cullen, M. J. P. and Douglas, R. J. (2003) Large amplitude nonlinear stability results for atmospheric circulations. *Quart. J. Roy. Meteorol. Soc.* **129**, pp. 1969–1988.

Cullen, M. J. P. and Salmond, D. J. (2003) On the use of a predictor-corrector scheme to couple the dynamics with the physical parametrizations in the ECMWF model. *Quart. J. Roy. Meteorol. Soc.* **129**, pp. 1217–1236.

Cullen, M. J. P., Douglas, R. J., Roulstone, I. and Sewell, M. J. (2005) Generalised semi-geostrophic theory on a sphere. *J. Fluid Mech.* **531**, pp. 123–157.

Cullen, M. J. P. and Feldman, M. (2004) Lagrangian solutions of semi-geostrophic equations in physical space. *SIAM J. Math. Anal.*, to appear.

Davies, T., Cullen, M. J. P., Malcolm, A. J., Mawson, M. H., Staniforth, A., White, A. A. and Wood, N. (2005) A new dynamical core for the Met Office's global and regional modelling of the atmosphere. *Quart. J. Roy. Meteorol. Soc.* **131**, pp. 1759–1782.

DiPerna, R. J. and Lions, P. L. (1989) Ordinary differential equations, transport theory, and Sobolev spaces. *Invent. Math.* **98**, pp. 511–547.

Douglas, R. J. (1994) Rearrangements of functions on unbounded domains. *Proc. Roy. Soc. Edin.* 124A, pp. 621–644.

Douglas, R. J. (2002) Rearrangements of functions with application to meteorology and ideal fluid flow. In *Large-Scale Atmosphere-Ocean Dynamics*, J. Norbury and I. Roulstone eds., Cambridge University Press, vol. I, pp. 288–341.

Elhmaidi, D., Provencale, A. and Babiano, A. (1993) Elementary topology of two-dimensional turbulence from a Lagrangian viewpoint and single-particle dispersion. *J. Fluid Mech.* **257**, pp. 533–558.

Eliassen, A. (1949) The quasi-static equations of motion with pressure as an independent variable. *Geofys. Publ.* **17**, 44pp.

Eliassen, A. and Kleinschmidt, E. (1957) Dynamic meteorology. *Handbuch der Physik, Geophysik II.* Springer Verlag, p. 154.

Emanuel, K. A. (1983) The Lagrangian parcel dynamics of moist symmetric instability. *J. Atmos. Sci.* **40**, pp. 2368-2376.

Fincham, A. M., Maxworthy, T. and Spedding, G. R. (1996) The horizontal

and vertical structure of the vorticity field in freely-decaying stratified grid turbulence. *Dyn. Atmos. Ocean.* **23**, pp. 153–160.

Ford, R., McIntyre, M. E. and Norton, W. A. (2000) Balance and the slow quasi-manifold: some explicit results. *J. Atmos. Sci.* **57**, pp.1236–1254.

Fjortoft, R. (1946) On the frontogenesis and cyclogenesis in the atmosphere. Part I. On the stability of the stationary circular vortex. *Geofys. Publik.* **16**(5), pp. 1–28.

Fjortoft, R. (1950) Applications of integral theorems in deriving criteria of stability for laminar flows and for the baroclinic circular vortex. *Geofys. Publ.* **17(6)**.

Handbook of weather forecasting. Meteorological Office Met.O, No. 875 London, Meteorological Office, 1975.

Gangbo, W. and McCann, R. J. (1996) The geometry of optimal transportation. *Acta Math.* **177**, pp. 113–161.

Gérard, P. 1992 Résultats récents sur les fluides parfaits incompressibles bidimensionnels. *Seminaire Bourbaki* **757**, pp. 411–444.

Gill, A. E. (1982) *Atmosphere-Ocean Dynamics.* Academic Press. 662pp.

Godson, W. L. (1950) Generalised criteria for dynamic instability. *J. Meteor.* **7**, pp. 268–278.

Gordon, A., Grace, W., Schwerdtfeger, P. and Byron-Scott, R. (1998) *Dynamic Meteorology: a Basic Course.* Arnold, 325pp.

Halmos, P. R. (1950) *Measure Theory.* van Nostrand.

Haltiner, G. J. and Williams, R. T. (1980) *Numerical Prediction and Dynamic Meteorology.* John Wiley. 477pp.

Haynes, P. H. and McIntyre, M. E. (1990) On the conservation and impermeability theorems for potential vorticity. *J. Atmos. Sci.* **47**, pp. 2021–2031.

Holm, D. D. (1996) Hamiltonian balance equations. *Physica D*, **98**, pp. 379–414.

Holt, M. W. (1990) Semi-geostrophic moist frontogenesis in a Lagrangian model. *Dyn. Atmos. Ocean.* **14**, pp. 463–481.

Holt, M. W. and Thorpe, A. J. (1991) Localised forcing of slantwise motion at fronts. *Quart. J. Roy. Meteorol. Soc.* **117**, pp. 943–963.

Holton, J. R. (1992) *An Introduction to Dynamic Meteorology.* Academic Press. 511 pp.

Hoskins, B. J. and Bretherton, F. P. (1972) Atmospheric frontogenesis models: formulation and solutions. *J. Atmos. Sci.* **29**, pp. 233–242.

Hoskins, B. J. (1975) The geostrophic momentum approximation and the semi-geostrophic equations. *J. Atmos. Sci.* **32**, pp. 233–242.

Hoskins, B. J. and Draghici, I. (1977) The forcing of ageostrophic motion according to the semi-geostrophic equations and in an isentropic coordinate model. *J. Atmos. Sci.* **34**, pp. 1859–1867.

Hoskins, B. J. and West, N. V. (1979) Baroclinic waves and frontogenesis. Part II: uniform potential vorticity jet flows- cold and warm fronts. *J. Atmos. Sci.* **36**, pp. 1663–1680.

Hoskins, B. J. (1982) The mathematical-theory of frontogenesis. *Ann. Rev. Fluid Mech.* **14**, pp. 131–151.

Hoskins, B. J., McIntyre, M. E. and Robertson, A. W. (1985) On the use and

significance of isentropic potential vorticity maps. *Quart. J. Roy. Meteorol. Soc.* **111**, pp. 877–946. Also **113**, pp. 402–404.

Kantorovich, L. (1942) On the Translocation of Masses. *C.R. (Doklady) Acad. Sci. URSS (N.S.)* **37**,pp. 199–201.

Kushner, P. J. and Shepherd, T. G. (1995a) Wave-activity conservation laws and stability theorems for semi-geostrophic dynamics: Part 1. Pseudo-momentum based theory. *J. Fluid Mech.* **290**, pp. 67–104.

Kushner, P. J. and Shepherd, T. G. (1995b) Wave-activity conservation laws and stability theorems for semi-geostrophic dynamics: Part 2. Pseudo-energy based theory. *J. Fluid Mech.* **290**, pp. 105–129.

Larichev, V. D. and McWilliams, J. C. (1991) Weakly decaying turbulence in an equivalent-barotropic fluid. *Phys. Fluids* **A, 3(5)**, pp. 938–950.

Leith, C. E. and Kraichnan, R. E., (1972) Predictablity of turbulent flows. *J. Atmos. Sci.* **29**, pp. 1041–1052

Lions, J.-L., Temam, R. and Wang, S. (1992) On the equations of the large-scale ocean. *Nonlinearity* **5**, pp. 237–288.

Loeper, G. (2004) The semi-geostrophic equations. Preprint, EPFL, SB, IMA Lausanne.

Lorenz, E. N. (1963) Deterministic non-periodic flow. *J. Atmos. Sci.* **20**, pp. 131–141.

Lorenz, E. N. (1963) The slow manifold–What is it? *J. Atmos.Sci.* **49**, pp. 2449–2451.

Lynch, P. (1989) The slow equations. *Quart. J. Roy. Meteorol. Soc.* **115**, pp. 201–219.

McCann, R. J. (1995) Existence and uniqueness of monotone measure preserving maps. *Duke Math. J.*. **80**, pp. 309–323.

McCann, R. J. (1997) A convexity principle for interacting gases. *Adv. Math.* **I**, pp. 153–179.

McCann, R. J. (2001) Polar factorisation of maps on Riemannian manifolds. *Geom. Funct. Anal.* **11**, pp. 589–608.

McIntyre, M. E. and Roulstone, I. (2002) Are there higher-accuracy analogues of semi-geostrophic theory. In *Large-Scale Atmosphere-Ocean Dynamics*, J. Norbury and I. Roulstone eds., Cambridge University Press, vol. II, pp. 301–364.

McWilliams, J. C. and Yavneh, I. (1998) Fluctuation growth and instability associated with a singularity of the balance equations. *Phys. Fluids* **10**, pp. 2587–2596.

McWilliams, J. C., Yavneh, I., Cullen, M. J. P. and Gent, P. R. (1999) The breakdown of large-scale flows in rotating, stratified fluids. *Phys. Fluids* **10**, pp. 3178–3184.

Majda, A. J. (1984) *Compressible fluid flow, and systems of conservation laws in several space variables.* Applied Mathematical Sciences, **53**, Springer, New York.

Majda, A. J. (2003) *Introduction to PDEs and waves for the atmosphere and ocean.* Courant Lecture Notes, **9**, American Math. Society.

Magnusdottir, G. and Schubert, W. H. (1991) Semi-geostrophic theory on the

hemisphere. *J. Atmos. Sci.* **48**, pp. 1449–1456.

Malardel, S., Thorpe, A. J. and Joly, A. (1997) Consequences of the geostrophic momentum approximation on barotropic instability. *J. Atmos. Sci.* **54**, pp. 103–112.

Mawson, M. H. (1996) A shallow water semi-geostrophic model on a sphere. *Quart. J. Roy. Meteorol. Soc.* **122**, pp. 267–290.

Mohebalhojeh, A. R. and Dritschel, D. G. (2001) Hierarchies of balance conditions for the $f-$plane shallow water equations. *J. Atmos. Sci.*, **58**, pp. 2411–2426.

Monge, G. (1781) *Mémoire sur la théorie des déblais et de remblais.* Memoires de l'Academie des Sciences, pp. 686–704.

Muraki, D. J., Snyder C., and Rotunno R. (1999) The next-order corrections to quasigeostrophic theory. *J. Atmos. Sci.* **56**, pp. 1547-1560.

Nakamura, N. and Held, I. M. (1989) Nonlinear equilibriation of two-dimensional Eady waves. *J. Atmos. Sci.* **46**, pp. 3055–3064.

Nakamura, N. (1994) Nonlinear equilibriation of two-dimensional Eady waves: simulations with viscous geostrophic momentum equations. *J. Atmos. Sci.* **51**, pp. 1023–1035.

Neumann, C. J. (1993) 1993 Global overview. Chapter 1 in Holland, G. J. (ed.) *Global guide to tropical cyclone forecasting.* WMO/TD 560, TCP Report 31.

Norbury, J. and Roulstone, I. (2002) *Large-scale atmosphere-ocean dynamics*, Vols. I and II, Cambridge University Press, 2002.

Ostdiek, V. and Blumen, W. (1997) A dynamic trio: inertial oscillation, deformation frontogenesis, and the Ekman-Taylor boundary layer. *J. Atmos. Sci.* **54**, pp. 1490–1502.

Parsons, A. T. (1969) A two-layer model of Gulf Stream separation. *J. Fluid Mech.* **39**, pp. 511-528.

Pedder, M. A. and Thorpe, A. J. (1999) The semi-geostrophic diagnosis of vertical motion. I: Formulation and coordinate transformations. *Quart. J. Roy. Meteorol. Soc.* **125**, pp. 1231–1256.

Pedlosky, J. (1987) *Geophysical fluid dynamics.* Springer-Verlag.

Phillips, N. A. (1963) Geostrophic motion. *Rev. Geophysics*, **1**, pp. 123–176.

Phillips, N. A. (2000) The start of numerical weather prediction in the United States. *Proc. 50th Anniversary of Numerical Weather Prediction.*, Deutsche Meteorologische Gesellschaft, pp. 13–28.

Pogorelov, A. V. (1964) *Monge-Ampère equations of elliptic type.* Noordhoff, Groningen, 114pp.

Preparata, F. P., and Hong, S. J. (1977) Convex hulls of finite sets of points in two and three dimensions. *Comm. A. C. M.* **20**, pp. 87–93.

Purser, R. J. and Cullen, M. J. P. (1987) A duality principle in semi-geostrophic theory. *J. Atmos. Sci.* **44**, pp. 3449–3468.

Purser, R. J. (2002) Legendre-transformable semi-geostrophic theories. In *Large-Scale Atmosphere-Ocean Dynamics*, J. Norbury and I. Roulstone eds., Cambridge University Press, vol. II, pp. 224–250.

Rasmussen, E. (1985) A case study of a polar low development over the Barents Sea. *Tellus* **37A**, pp. 407–418.

Reed, R. J. and Albright, M. D. (1986) A case study of explosive cyclogenesis in the Eastern Pacific. *Mon. Weather Rev.* **114**, pp. 2297-2319.

Ren, S. (2000a) Finite-amplitude wave-activity invariants and nonlinear stability theorems for shallow water semi-geostrophic dynamics. *J. Atmos. Sci.* **57**, pp. 3388–3397.

Reiser, H. The development of numerical weather prediction in Deutsche Wetterdienst. *Proc. 50th Anniversary of Numerical Weather Prediction.*, Deutsche Meteorologische Gesellschaft, pp. 51–80.

Richardson, L. F. (1922) Weather prediction by numerical process. Cambridge University Press. 236pp (also from Dover Publications Inc., New York, 1965).

Robert, R. and Sommeria, J. (1991) Statistical equilibrium states for two-dimensional flows. *J. Fluid Mech.* **229**, pp. 291–310.

Rockafellar, R. T. (1970) *Convex analysis.* Princeton University Press, 451pp.

Roulstone, I. and Norbury, J. (1994) A Hamiltonian structure with contact geometry for the semi-geostrophic equations. *J. Fluid Mech.* **272**, pp. 211–233.

Roulstone, I. and Sewell, M. J. (1996) Potential vorticities in semi-geostrophic theory. *Quart. J. Roy. Meteorol. Soc.* **122**, pp. 983–992.

Roulstone, I. and Sewell, M. J. (1996) The mathematical structure of theories of semi-geostrophic type. *Phil. Trans. R. Soc. London* **A**, pp. 2489–2517.

Ryff, J. V (1970) Measure preserving transformations and rearrangements. *J. Math. Anal. and Applics.* **30**, pp. 431–437.

Salmon, R. (1985) New equations for nearly geostrophic flow. *J. Fluid Mech.* **153**, pp. 461–477.

Schar, C. and Wernli, H. (1993) Structure and evolution of an isolated semi-geostrophic cyclone. *Quart. J. Roy. Meteorol. Soc.* **119**, pp. 57–90.

Schubert, W. H. and Hack, J. J. (1985) Transformed Eliassen balanced vortex model. *J. Atmos. Sci.* **40**, pp. 1571–1583.

Schubert, W. H. (1985) Semi-geostrophic theory. *J. Atmos. Sci.* **42**, pp. 1770–1772.

Schubert, W. H., Ciesieleski, P. E., Stevens, D. E. and Kuo, H-C. (1991) Potential vorticity modelling of the ITCZ and the Hadley circulation. *J. Atmos. Sci.* **48**, pp. 1493–1509.

Schubert, W. H. and Magnusdottir, G. (1994) Vorticity coordinates, transformed primitive equations, and a canonical form for balanced models. *J. Atmos. Sci.* **51**, pp. 3309–3319.

Schwerdtfeger, W. (1975) The effects of the Antarctic peninsula on the temperature regime of the Weddell Sea. *Mon. Weath. Rev.* **103**, pp. 45–51.

Sewell, M. J. (2002) Some applications of transformation theory in mechanics. In 'Large-scale Atmosphere-Ocean Dynamics', J. Norbury and I. Roulstone eds., Cambridge University Press, vol. II, pp. 143–223.

Shapiro, M. A. and Thorpe, A. J. (2004) *Thorpex science plan.* Available from http://www.mmm.ucar.edu/uswrp/thorpex.html

Shutts, G. J. (1987) The semi-geostrophic weir: a simple model of flow over mountain barriers. *J. Atmos. Sci.* **44**, pp. 2018–2030.

Shutts, G. J. (1987) Balanced flow states resulting from penetrative, slant-wise

convection. *J. Atmos. Sci.* **44**, pp. 3363–3376.

Shutts, G. J., Booth, M. W. and Norbury, J. (1988) A geometric model of balanced, axisymmetric flow with embedded penetrative convection. *J. Atmos. Sci.* **45**, pp. 2609–2621.

Shutts, G. J. (1989) Planetary semi-geostrophic theory. *J. Fluid Mech.* **208**, pp. 545–573.

Shutts, G. J. and Cullen, M. J. P. (1987) Parcel stability and its relation to semi-geostrophic theory. *J. Atmos. Sci.* **44**, pp. 1318–1330.

Shutts, G. J. and Gray, M. E. B. (1994) A numerical modelling study of the geostrophic adjustment process following deep convection. *Quart. J. Roy. Meteorol. Soc.* **120**, pp. 1145–1178.

Shutts, G. J. (1995) An analytical model of the balanced flow created by localised convective mass transfer in a rotating fluid. *Dyn. Atmos. Oceans* **22**, pp. 1–17.

Shutts, G. J. (1998) Idealised models of the pressure drag force on mesoscale mountain ridges. *Contr. Atmos. Phys.* **71**, pp. 303–313.

Snyder, C., Skamarock, W. C. and Rotunno, R. (1991) A comparison of primitive-equation and semi-geostrophic simulations of baroclinic waves. *J. Atmos. Sci.* **48**, pp. 2179–2194.

Thomson, W. (Lord Kelvin) (1910) Maximum and minimum energy in vortex motion. *Mathematical and Physical Papers* **4**, pp. 172–183. Cambridge University Press.

Thorpe, A. J. and Pedder, M. A. (1999) The semi-geostrophic diagnosis of vertical motion. II: Results for an idealized baroclinic wave life cycle. *Quart. J. Roy. Meteorol. Soc.* **125**, pp. 1257–1276.

Thuburn, J. and Li, Y. (2000) Numerical simulations of Rossby-Haurwitz waves. *Tellus* **A 52**, pp. 181–189.

Thuburn, J., Wood, N. and Staniforth, A. (2002) Normal modes of deep atmospheres. I: spherical geometry. *Quart. J. Roy. Meteorol. Soc.* **128**, pp. 1771–1792.

Van Meighem, J. M. (1952) Hydrodynamic stability. *Compendium of meteorology* Amer. Met. Soc., pp. 434–453.

Veitch, G. and Mawson, M. H. (1993) A comparison of inertial stability conditions in the planetary semi-geostrophic and quasi-equilibrium models. U.K. Met. Office Short Range Forecasting Tech. Report no. 60.

Villani, C. (2003) *Topics in optimal transportation.* Vol. 58 of *Graduate Studies in Mathematics*, Amer. Math. Soc., Providence, RI.

Wakefield, M. A. and Cullen, M. J. P. (2005) Modelling the response of the atmosphere to equatorial forcing. *Int. J. Numer. Meth. Fluids*, **47**, pp. 1345–1351.

Wang, X.-J. (1995) Some counter-examples to the regularity of Monge-Ampère equations. *Proc. A. M. S.* **123**, pp. 841–845.

Warn, T., Bokhove, O., Shepherd, T. G. and Vallis, G. K. (1995) Rossby-number expansions, slaving principles, and balance dynamics. *Quart. J. Roy. Meteorol. Soc.* **121**, pp. 723–739.

White, A. A. (2002) The equations of meteorological dynamics and various ap-

proximations. In 'Large-scale Atmosphere-Ocean Dynamics', J. Norbury and I. Roulstone eds., Cambridge University Press, vol. I, pp. 1–100.

White, A. A., Hoskins, B. J., Roulstone, I. and Staniforth, A. (2005) Consistent approximate models of the global atmosphere: shallow, deep, hydrostatic, quasi-hydrostatic and non-hydrostatic. *Quart. J. Roy. Meteorol. Soc.*, **131**, pp. 2081–2108.

Wiin-Nielsen, A. (2000) Numerical weather prediction: the early development with emphasis on Europe. *Proc. 50th Anniversary of Numerical Weather Prediction.*, Deutsche Meteorologische Gesellschaft, pp. 29–50.

Winkler, C. R., Newman, M., Sardeshmukh, P. D. (2001) A linear model of wintertime low frequency variability, Part 1: formulation and forecast skill. *J. Climate* **14**, pp. 4474–4494.

Wood, N. and Staniforth,A. (2003) The deep atmosphere Euler equations with a mass-based vertical coordinate. *Quart. J. Roy. Meteorol. Soc.* **129**, pp. 1289–1300.

This page is intentionally left blank

Index